A GEOCHEMICAL AND MINERALOGICAL INVESTIGATION OF THE MOBILITY OF URANIUM AND OTHER LITHOPHILE ELEMENTS DURING HIGH-GRADE METAMORPHISM.

by

Michael Bradford Fowler

A thesis submitted for the degree of Doctor of Philosophy, University of London.

Department of Geology,
Imperial College of Science and Technology,
Prince Consort Road,
London SW7.

May, 1985

ABSTRACT

Two case-studies were selected for their contrasting characteristics. Regional granulite-grade element depletion was studied in an amphibolite to granulite facies transition, identified at Gruinard Bay, by adopting a comparative approach. Literature data were used for the metamorphic end members, having first established magmagenetic comparability. Despite pervasive retrogression, Gruinard Bay gneisses are thought to have suffered hornblende-granulite facies Badcallian metamorphism. The intracrustal partial melting model for granulite genesis is inappropriate for the specific conditions leading to such a hornblende-bearing residuum. K and Rb abundances at Gruinard Bay intersect those of the end members, related to the continued stability of hornblende and biotite. Radioelement abundances remain significantly higher than those of granulites, substantially due to the presence of allanite. Minor minerals exert a crucial control on U (and Th?) abundances both in Gruinard Bay gneisses and in granulites. Together with the high mineral-melt partition coefficients for radioelements of even rock-forming minerals when in equilibrium with acid melts, this suggests that partial melting would not result in the observed extensive radioelement depletion. Therefore a fluid is preferred, H_2O-rich rather than carbonic because of the advanced stage of depletion reached in rocks which retain significant hydrous minerals.

In contrast, the Glen Dessarry syenite provides a potential example of local element mobility during amphibolite-facies metamorphism/deformation. However, fractional crystallisation coupled with local crustal contamination clearly remains the first-order control on element distribution, regardless of the degree of deformation. A more rigorous study of deformation in the leucocratic syenite confirmed its isochemical and isovolumetric nature on the scale of a whole-rock

sample. Nevertheless, several styles of microscopic mobility of selected incompatible elements were detected. Most could be related to pegmatite production in the last stages of a protracted magmatic history. However, intracrystalline mobility of U, Th and possibly light REEs occured as a direct result of deformation, which adequately defines the scale within which any deformation-related mobility might be sought in this particular environment.

ACKNOWLEDGEMENTS

The author thanks especially Professor Janet Watson* and Dr Jane Plant for their supervision of this project. Dr G.F. Marriner helped with XRF analyses at Bedford College; Mr P.R. Simpson (BGS London) with facilities and advice on fission-track analysis; Dr D.I.Smith (BGS Edinburgh) with early work in the field; Dr C.T.Williams (BMNH) with identification and analysis of zirconolite, and Drs J.V.P. Long and R.W. Hinton (University of Cambridge) with ion-probe facilities. Other members of technical and academic staff in the Department of Geology at Imperial College and the Metalliferous Minerals and Applied Geochemistry Unit (BGS London) are too numerous to mention individually, but without their ready help and advice this thesis would never have been completed. Lastly, thanks to Christine for putting up with the single-minded chaos necessary for writing up, with confidence that she will get her own back one day.

*Shortly before this thesis was submitted, Professor Watson died. She will be sadly missed; this work is dedicated to her memory.

LIST OF CONTENTS

Chapter	Title	Page
Chapter 1	General Introduction	15
Chapter 2	Introduction to Gruinard Bay	24
2.1	History of Research	25
	The Lewisian Complex	25
	Amphibolite-Granulite Transitions Elsewhere	28
2.2	Geological Setting and Sample Collection	29
2.3	Approach	31
2.4	Presentation of Results	32
Chapter 3	Magmagenesis: Comparisons with Metamorphic End Members	33
3.1	Geochemical Data for "Immobile" Elements	33
	Major Elements	34
	Transition Metals	37
	"Immobile" Large-Ion Lithophile Elements	37
	High Field-Strength Elements	37
	Rare Earth Elements	39
3.2	Magmagenetic Models	42
3.2.1	A Calc-Alkaline Intrusive Suite	43
	Partial Melting of a Wet Basaltic Source Leaving an Eclogitic Residue	44
	Fractional Crystallisation from a Basaltic Parent	50
3.2.2	A Lower-Crustal Residue after the Abstraction of a Granitic Partial Melt	54
Chapter 4	The Transitional Nature of the Badcallian Metamorphism at Gruinard Bay	59
4.1	Mineralogy	59
	Granulite-Facies Mineralogy	59
	Hornblende-Granulite Facies Mineralogy	60
	Amphibolite-Facies Mineralogy	69
	Greenschist-Facies Mineralogy	71
4.2	Fission-Track Determination of the Distribution of Uranium	71
	Gruinard Bay Gneisses	72
	Granulite-Facies Gneisses	75

4.3 Large-Ion Lithophile Element Interfacies Variations....76
Data for the Whole Suite....79
A Comparison of Specific Rock Groups....85
Chapter 5 Large-Ion Lithophile Element Depletion Mechanisms....94
5.1 Rubidium and Potassium....94
5.2 Uranium and Thorium....96
5.3 The Phase Responsible for Depletion: Fluid or Melt?....98
Chapter 6 Conclusions to Gruinard Bay....105
Chapter 7 Introduction to Glen Dessarry....107
7.1 History of Research....107
7.2 Geological Setting and Sample Collection....109
7.3 Approach....112
7.4 Presentation of Results....114
Chapter 8 Mineralogy and Petrographic Variations....115
8.1 Mineralogy....115
Feldspars....115
Pyroxenes and Amphiboles....116
Biotites....118
Accessory Minerals....118
8.2 Petrographic Variations....120
Cumulates....120
Mafic Syenites....121
Leucocratic Syenites....123
Metasedimentary Xenoliths....123
Syenite-Host Rock Reactions....124
8.3 The Origin of Amphibole....125
Chemical Comparisons with Igneous and Metamorphic Amphiboles....128
Oxygen Isotopes....129
Chapter 9 Relict Magmatic Controls on Element Distribution....133
9.1 Major Element Oxides....136
9.2 Trace Elements....142
Transition Metals....144
Large-Ion Lithophile Elements Controlled by Major Mineral Phases....145

	Incompatible Elements which Enter Minor Mineral Phases	148
9.3	Incompatible Element Chondrite-Normalised Diagrams	159
	Low-level Fractionation	159
	In-situ Fractionation	161
	Crustal Contamination	163
9.4	Magmagenesis	166
9.5	Reactions with Country Rocks	170
	Fenitisation of Adjacent Moine Metasediments	170
	Syenite Vein-Xenolith Reactions	173
Chapter 10	Bulk Chemical Changes Accompanying Deformation of the Glen Dessarry Leucocratic Syenite	176
10.1	Mineralogy	177
	Feldspars	177
	Pyroxenes and Amphiboles	179
	Biotites	180
	Minor and Accessory Phases	181
10.2	Whole-Rock Chemistry	182
Chapter 11	Microscopic Mobility of Incompatible Elements	190
11.1	Sphene	192
11.2	Allanite	198
11.3	Apatite	200
11.4	Zirconium-Rich Phases	203
Chapter 12	Conclusions to Glen Dessarry	206
Chapter 13	General Discussion	208
	References	214
	Appendix	236
	A.1 Whole-Rock Data	236
	A.2 Mineral Analyses	271
	A.3 Partition Coefficients	298
	Enclosures	300

LIST OF FIGURES

Figure	Title	Page
Figure 1.1	Pressure-temperature grid illustrating metamorphic conditions of interest (after Collerson and Fryer, 1978)	17
Figure 1.2	Map showing the distribution of metamorphic grades in Northern Scotland (after Watson et al, 1982)	21
Figure 2.1	Locality map of Gruinard Bay	29
Figure 3.1	Comparative Harker diagrams for Lewisian gneisses	35
Figure 3.2	Comparative normative feldspar and AFM diagrams for Lewisian gneisses	36
Figure 3.3	Comparative trace element variation diagrams for Lewisian gneisses	38
Figure 3.4	Comparative chondrite-normalised REE plots for Lewisian gneisses from Gruinard Bay (this study), and Rhiconich (inset, Weaver and Tarney, 1981)	40
Figure 3.5	Comparative chondrite-normalised REE plots for Lewisian gneisses from the central block (this study) and Assynt (inset, Weaver and Tarney, 1980)	41
Figure 3.6	Qz-Ab-Or diagram showing field of experimental melt compositions with data from Gruinard Bay gneisses	45
Figure 3.7	Partial melting models for the generation of tonalitic-trondhjemitic gneisses from Gruinard Bay	49
Figure 3.8	Fractional crystallisation models for the generation of tonalitic-trondhjemitic gneisses from Gruinard Bay	53
Figure 3.9	Intracrustal partial melting model for residual granulites (A) and residual hornblende-granulite facies gneisses (B)	56

Figure 4.1 Diagramatic comparison of "primary" amphibole (A) and biotite (B) from Gruinard Bay gneisses with literature data for amphibolite facies and granulite facies minerals.....66
Figure 4.2 Pressure-temperature grid comparing Badcallian metamorphic conditions at Gruinard Bay with those of the granulite facies.....68
Figure 4.3 Mantle-normalised incompatible element plot comparing hornblende-granulite facies sample MJ037 with statically-retrogressed gneisses.....78
Figure 4.4 Histograms of LILE abundances in Gruinard Bay gneisses compared with granulite-facies data (this study) and literature data.....80
Figure 4.5 Logarithmic bivariate plots of K vs. Rb and U vs. Th in Gruinard Bay gneisses compared with granulite-facies data (this study) and literature data.....82
Figure 4.6 Logarithmic bivariate plot of U vs. Rb in Gruinard Bay gneisses.....85
Figure 4.7 Amphibolite-facies-normalised incompatible element plot of intermediate, tonalitic and trondhjemitic granulites.....87
Figure 4.8 Th Harker diagram for Gruinard Bay gneisses.....88
Figure 4.9 Mantle-normalised incompatible element plot comparing intermediate gneiss compositions from amphibolite-facies, Gruinard Bay, and granulite-facies regions.....90
Figure 4.10 Mantle-normalised incompatible element plot comparing tonalitic gneiss compositions from amphibolite-facies, Gruinard Bay and granulite-facies regions.....91
Figure 4.11 Mantle-normalised incompatible element plot comparing trondhjemitic gneiss compositions from amphibolite-facies, Gruinard Bay and granulite-facies regions.....92

Figure 5.1 REE model of in-situ partial melting at Gruinard Bay.....99
Figure 7.1 Locality map of Glen Dessarry.....110
Figure 8.3 Variation of $\delta^{18}O$ with SiO_2 for Glen Dessarry syenites.....131
Figure 9.1 Normative data for Glen Dessarry syenites projected onto the Qz-Ab-Or-Ne quaternary.....136
Figure 9.2 Schematic diagram illustrating interpretation of Harker diagrams in terms of in-situ and low-level fractional crystallisation.....137
Figure 9.3 Harker diagrams for Glen Dessarry syenites.....138
Figure 9.4 Schematic diagram illustrating interpretation of logarithmic, bivariate trace element plots in terms of Rayleigh fractionation.....142
Figure 9.5 Logarithmic, bivariate plot of transition metal abundances for Glen Dessarry syenites.....144
Figure 9.6 Logarithmic, bivariate plot of Rb-Ba-Sr for Glen Dessarry syenites.....146
Figure 9.7 Chondrite normalised REE plots for Glen Dessarry syenites.....150
Figure 9.8 Logarithmic, bivariate plot of Ce-Yb for Glen Dessarry syenites.....152
Figure 9.9 Chondrite-normalised REE plot for "contaminated" mafic syenite and Moine metasediments; model of assimilation via crustal anatexis.....155
Figure 9.10 Logarithmic bivariate plots of U-Th and Hf-Ta for Glen Dessarry syenites.....157
Figure 9.11 Chondrite normalised incompatible element plots of mafic and leucocratic syenite fields of analyses, and cumulates.....160
Figure 9.12 Chondrite normalised incompatible element plots of mafic and leucocratic syenite samples....162
Figure 9.13 Chondrite normalised incompatible element plots of filter-pressed pegmatite samples.....163
Figure 9.14 Chondrite normalised incompatible element plots for "contaminated" mafic syenite, Moine metasediments; model of assimilation via crustal anatexis.....165

Figure 9.15 Chondrite normalised incompatible element plot comparing mafic syenite, two examples of the Lorne Plateau lavas, and Kentallenite.....169
Figure 9.16 Chondrite normalised REE and incompatible element plot for Moine metasediments and fenitised Moine.....172
Figure 9.17 Chondrite normalised REE and incompatible element plot for syenite vein and reaction zone.....175
Figure 10.1 Variation diagram of selected major and trace elements with degree of deformation in the Glen Dessarry leucocratic syenite.....183
Figure 10.2 Multi-element plot illustrating the comparability of deformed samples with MJ008 (the least deformed).....185
Figure 10.3 Diagram of element abundance variations during deformation from MJ008 to MJ003.....188
Figure 10.4 Chondrite normalised incompatible element plot of highly-foliated sample MJ009 and the field of leucocratic syenite analyses.....189
Figure 11.1 Semi-quantitative chondrite normalised LREE plots for magmatic sphene.....194
Figure 11.2 Semi-quantitative chondrite normalised LREE plots for deformed sphene.....197
Figure 11.3 Chondrite normalised LREE plots for primary, secondary and pegmatitic allanite.....199
Figure 11.4 Chondrite normalised REE plot for zirconolite.....204

LIST OF TABLES

Table	Title	Page
Table 3.1	Partial melting models for the generation of tonalitic-trondhjemitic gneisses from Gruinard Bay	48
Table 3.2	Amphibole fractional crystallisation models for the generation of tonalitic-trondhjemitic gneisses from Gruinard Bay	52
Table 3.3	Intracrustal partial melting model for residual granulites and residual hornblende-granulites	55
Table 4.1	Comparison of pyroxenes from Gruinard Bay gneisses with literature data for granulites	61
Table 4.2	Two-pyroxene geothermometry	62
Table 4.3	Comparison of "primary" amphiboles and biotites from Gruinard Bay with literature data for amphibolite and granulite-facies minerals	65
Table 4.4	Plagioclase analyses from hornblende-granulite facies samples, and plagioclase-clinopyroxene-quartz geobarometry	67
Table 4.5	Comparison of texturally-distinct amphibole compositions from amphibolite-facies samples	70
Table 4.6	Allanite analyses from hornblende-granulite facies samples	74
Table 5.1	Comparison of zircon U contents from granulite and amphibolite-facies Lewisian gneisses	97
Table 5.2	REE model for 10% batch melting retaining a hornblende-granulite facies residue	99
Table 5.3	U and Th depletion factors from amphibolite to granulite grade, and required bulk mineral-melt distribution coefficients	100
Table 5.4	Literature data for U and Th mineral-melt partition coefficients	101
Table 8.1	Average perthite analyses from Glen Dessarry mafic and leucocratic syenites	116

Table 8.2 Average pyroxene and amphibole analyses from the Glen Dessarry syenite.....117
Table 8.3 Average biotite analyses from the Glen Dessarry syenite.....118
Table 8.4 Average analyses of minor or accessory minerals from the Glen Dessarry syenite.....119
Table 8.5 Comparison of $\delta^{18}O$ values for amphibole derived from an aqueous fluid with that precipitated from a silicate melt.....130
Table 9.1 Average whole rock analyses of Glen Dessarry syenites.....135
Table 9.2 Mass-balance calculations of low-level fractional crystallisation in the Glen Dessarry syenite.....140
Table 9.3 Incompatible element model of melts generated by Moine anatexis.....164
Table 9.4 Major element analyses of typical Moine metasediment and fenitised Moine.....171
Table 10.1 Feldspar analyses from undeformed (MJ008) and deformed (MJ003) leucocratic syenites, and modelled unmixing of alkali feldspar to give orthoclase (77%) and plagioclase (23%).....179
Table 10.2 Average analyses of pyroxene and amphibole from undeformed (MJ008) and deformed (MJ003) leucocratic syenites.....180
Table 10.3 Average analyses of biotite from undeformed (MJ008) and deformed (MJ003) leucocratic syenites.....181
Table 10.4 Whole-rock analyses of variably-deformed leucocratic syenites with comparable primary geochemistry.....184
Table 10.5 Computations of likely volume change and mass transfer during progressive deformation.....187
Table 11.1 SIMS relative count rates for "normal" and "low-U" apatite.....203

LIST OF PLATES

Plate	Title	Page
Plate 4.1	Mineral assemblages of hornblende-granulite (A), amphibolite (B and C) and greenschist facies (D) gneisses from Gruinard Bay	64
Plate 4.2	U, Th-rich minerals in Lewisian gneisses	73
Plate 8.1	Amphibole textures in the Glen Dessarry syenite	127
Plate 10.1	Fabric development in the Glen Dessarry leucocratic syenite	178
Plate 11.1	Sphene and allanite in the Glen Dessarry syenite	193
Plate 11.2	Apatite and Zr-rich minerals in the Glen Dessarry syenite	201

CHAPTER ONE

GENERAL INTRODUCTION

This thesis is concerned with the mobility of "lithophile" elements during "high-grade" metamorphism. Since both these terms are fairly broad in their application, the first few paragraphs of this introduction are devoted to defining the element group and metamorphic conditions with which the work is primarily involved. Following this is a brief selective illustration of the many types of element mobility which are common under diverse crustal conditions, so that the present study can be viewed in a broad overall context. Finally, a short introduction is given to the rock suites that have been chosen for specific study here, including the reasoning responsible for their choice.

In 1932, Goldschmidt classified elements into several fundamental groups, based on their distribution in the separate phases constituting meteorites. One of these was the "lithophile" element group, which includes those elements which concentrate in the silicate phases; the others being siderophile, chalcophile and atmophile. Although this empirical classification has strict relevance only to the conditions pertaining during meteorite formation, it has been widely used in geochemical studies of many disciplines since its inception. However, for most geochemical purposes lithophile is a rather all-embracing term, and some sub-division is required, preferably based on elemental behaviour under more pertinent conditions.

The main subject of this thesis is that sub-group of lithophile elements known as the "incompatible" elements (synonymous with the more recently-introduced terms "hygromagmatophile" and "hygromagmaphile"). This terminology is based on the elements' relative partitioning behaviour between minerals and coexisting melt during primary igneous processes, such as partial melting of mantle assemblages and subsequent crystallisation of the derived liquid. As will become

apparent in the text, such a classification is not always applicable, and breaks down even under some igneous conditions where so-called incompatible elements are demonstrably not so. Nevertheless, it forms an important basis from which to proceed since it adequately defines the group to which U belongs during most primary magmatic processes. Therefore, by studying the group as a whole, any anomalous behaviour shown by U (or other members of the group) during specifically crustal processes, will be more immediately apparent. The incompatible elements of concern to this work include the following: Ba, Rb, U, Th, K, Sr, Nb, Ta, La, Ce, Pr, Nd, Sm, Eu, Gd, Tb, Dy, Er, Yb, Lu, Zr, Hf, P, Ti, Y. These may be conveniently divided into two further groups, even though they slightly overlap, which will be referred to extensively throughout the thesis:

i) Large-Ion Lithophile Elements (LILEs) - by which is meant those elements which are incompatible by virtue of their comparatively large ionic size with respect to the common crystallographic sites into which they might substitute (e.g., Rb, Th, U and K).

ii) High Field Strength Elements (HFSEs) - by which is meant those elements which are incompatible because of a relatively high stable valence state combined with a small ionic radius (e.g., Zr, Hf, Nb and Ta).

This therefore defines those elements of principal (though by no means exclusive) interest to the following work. However, the crustal conditions of particular relevance ("high-grade metamorphism") remain to be constrained, and for this purpose all that is considered necessary here is a simple P/T grid. The particular example used (Fig. 1.1) is after Collerson and Fryer (1978), and the conditions of particular concern fall approximately within the hatched area. Clearly, a considerable range is involved such that it would be impossible to attain comprehensive coverage. Moreover, the metamorphic environment represents a continuum of systematic variation and treatment of one part in isolation risks some degree of oversimplification. This

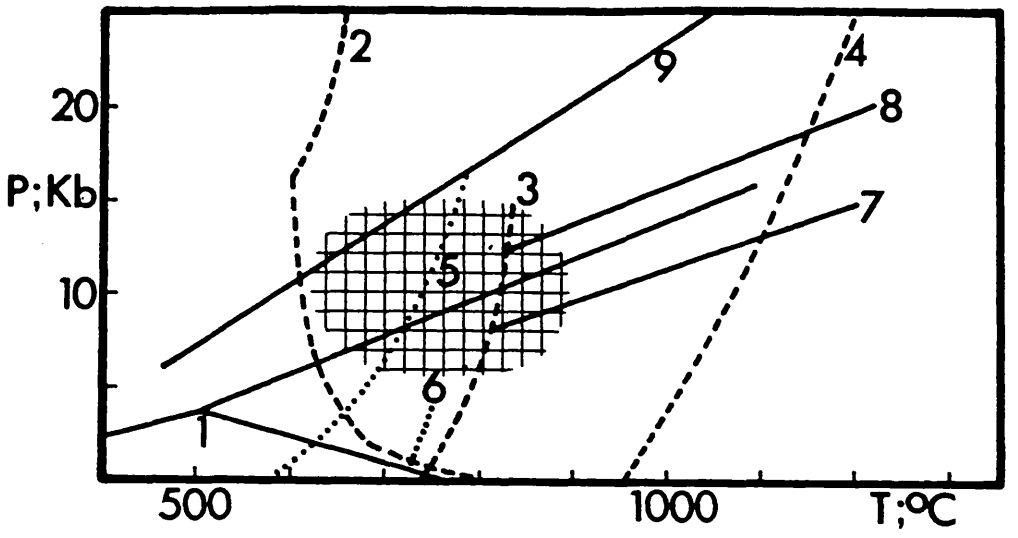


Figure 1.1: Pressure-temperature grid illustrating metamorphic conditions of interest (after Collerson and Fryer, 1978).

(1= aluminosilicate triple point, after Holdaway (1971). 2= solidus for the system Qz-Ab-Or-H_2O, after Huang and Wyllie (1975). 3= solidus for tonalite with water just sufficient to form muscovite, biotite and hornblende, after Wyllie (1977). 4= solidus for anhydrous system Qz-Ab-Or, after Huang and Wyllie (1975). 5= amphibolite/granulite boundary, after Turner (1968). 6= experimentally determined amphibolite/granulite boundary, after Spear (1976). 7= low to intermediate pressure granulite transition. 8= intermediate to high pressure granulite transition. 9= high pressure granulite to eclogite transition. 7, 8 and 9 after Green and Ringwood (1967)).

can be partly mitigated by the selection of more than one study area, with contrasting characteristics. Before introducing those areas selected here, a brief illustration of the types of element mobility in other crustal environments might help to put the present study into context.

In the low grade environment, two contrasting situations have received considerable attention in the literature. Basalt-seawater alteration has been shown to be an important process in the geochemical evolution of the crust, including its recycling into the mantle at subduction zones, and large scale mobility of LILEs is common. For example, Williams and Floyd (1981) have studied the distribution of U and other incompatible

elements in spilitic pillow lavas, and concluded that the major part of the U complement of the rocks (c. 1ppm) was introduced early during the alteration process due to interaction with sea-water, a result similar to those of MacDougall et al. (1979) and Mitchell and Aumento (1977). More specifically, the former authors used the fission track technique to determine the microdistribution of U, and identified four distinct areas: vesicle infillings; phenocrysts and medium-grained groundmass; fine-grained groundmass and vesicle rims and veinlets. These were interpreted in terms of post-enrichment redistribution during low-grade metamorphism, probably as a result of carbonate complex formation. The present U distribution was attributed to the influence of new mineral phases formed during this event, particularly the stable Ti-, P- and Zr-bearing phases. Humphris et al. (1978) have also documented the selective mobility of many incompatible elements (including the LREE) during low-grade alteration of basalts from various localities including Mull, Iceland and the Mid-Atlantic Ridge, and suggested that the dominant controlling factor was the igneous crystallisation history of the individual lavas. A reduction in the Sr^{87}/Sr^{86} ratios of the Mull lavas has also been reported (Hawkesworth and Morrison, 1978), in contrast to the more "normal" increase during such processes (Hart et al., 1974; O'Nions et al., 1978).

Similarly, element mobility during focused convective overturn of meteoric water as a result of granite intrusion is the cause of much hydrothermal, granite-related mineralisation, and as such has attracted substantial interest. Notable for a comprehensive approach to this topic are the studies of Zeilinski et al. (1981), who combined the use of whole-rock geochemistry with acid leaching experiments, the fission track method, and U-Th-Pb isotope systematics to document the distribution and mobility of U in granitic plutons, and their associated mineralisation. Bowie et al. (1973), Simpson et al.

(1979; 1982) and Plant et al. (1980; 1983) have developed a model for granite-hosted U-Sn mineralisation which involves highly-evolved felsic plutons associated with substantial fluid-rock interaction from high to low temperatures, and the mobilisation of U from stable accessory minerals into the coexisting fluid. Zeilinski (1979, 1982) has also shown that U may be readily mobilised from siliceous extrusive rocks during deuteric alteration.

Interestingly, medium-grade processes seem not to be central either to ore-forming processes, or to crustal evolution in general, and so less literature exists on element mobility under such a regime. One study with which the author is familiar is of zonal metasomatism (Read, 1934; Curtis and Brown, 1969, 1971; Koons, 1981; Sanford, 1982; Fowler et al., 1981, 1983), caused by incomplete re-equilibration of juxtaposed acid and basic protoliths. Diffusion-controlled reaction between antigorite pods and granodioritic country rock has produced a series of virtually monomineralic zones of progressive chemical adjustment, from chlorite in contact with the acid host, through hornblende, tremolite and talc to the relict antigorite core. Therefore, the mineralogical framework has been totally reconstituted during the metasomatic event, such that element mobility was virtually unavoidable. Even those trace elements which have gained the reputation of being relatively immobile during metamorphism, such as the REEs, have been mobilised (and fractionated) on the scale of several metres.

Once the high-grade (granulite facies) environment is considered, another process important in crustal evolution is apparent - that of LILE loss from the lower crust. Heat-flow studies (e.g., Birch et al., 1968; Lachenbruch, 1968; Buntebarth, 1976; Jaupart et al., 1981, 1982; Pollack, 1982) confirm that low heat production rocks similar to those in exposed crustal cross-sections (Fountain and Salisbury, 1981) are of regional extent in the lower continental crust (see also

Lambert and Heier, 1967). Therefore the pervasive removal of K, Rb, U and Th, and (possibly) Cs and Pb from "lower-crustal" lithologies such as the Scourian tonalites (e.g., Tarney et al., 1979; Weaver and Tarney, 1980, 1981), has been the subject of much debate, of which more detail will be given later. Thus, throughout the range of metamorphic conditions, elements can be mobile within their lithological framework, and often the essence of any argument about mobility is one of scale. However, within the constraints of a single piece of work all that can be hoped for is information on specific environments which might perhaps lead to more general conclusions. Two have been studied here, from the metamorphic complexes of NW Scotland. Scotland is an ideal place from which to select material, since it contains representatives of all metamorphic grades from greenschist to granulite facies, in geological settings where metamorphism can be related to contemporary tectonic and magmatic events. The following brief summary of the geological structure and distribution of metamorphic rocks in Scotland (Fig. 1.2) is modified after Watson et al. (1982).

The Hebridean Craton, exposed in the far northwest, represents an old, deeply-eroded terrain. It comprises the Lewisian basement complex of dominantly granodioritic to tonalitic gneisses, with older basic-ultrabasic units and sparse metasediments, which were metamorphosed at c. 2.7 Ga in conditions of the upper amphibolite or granulite facies. Subsequent metamorphic and tectonic reworking at lower grades continued periodically until about 1.8 Ga, spanning the intrusion of the mafic Scourie Dyke suite (Tarney, 1963) at c. 2.4 Ga. Overlying this basement complex is the undisturbed, largely fluviatile Torridonian Formation (late Proterozoic), together with younger formations. The Hebridean Craton is bounded in the east by the eastward-dipping Moine Thrust Zone, which marks the front of the Caledonian orogenic belt. Reworked Lewisian probably continues at depth as far south as the

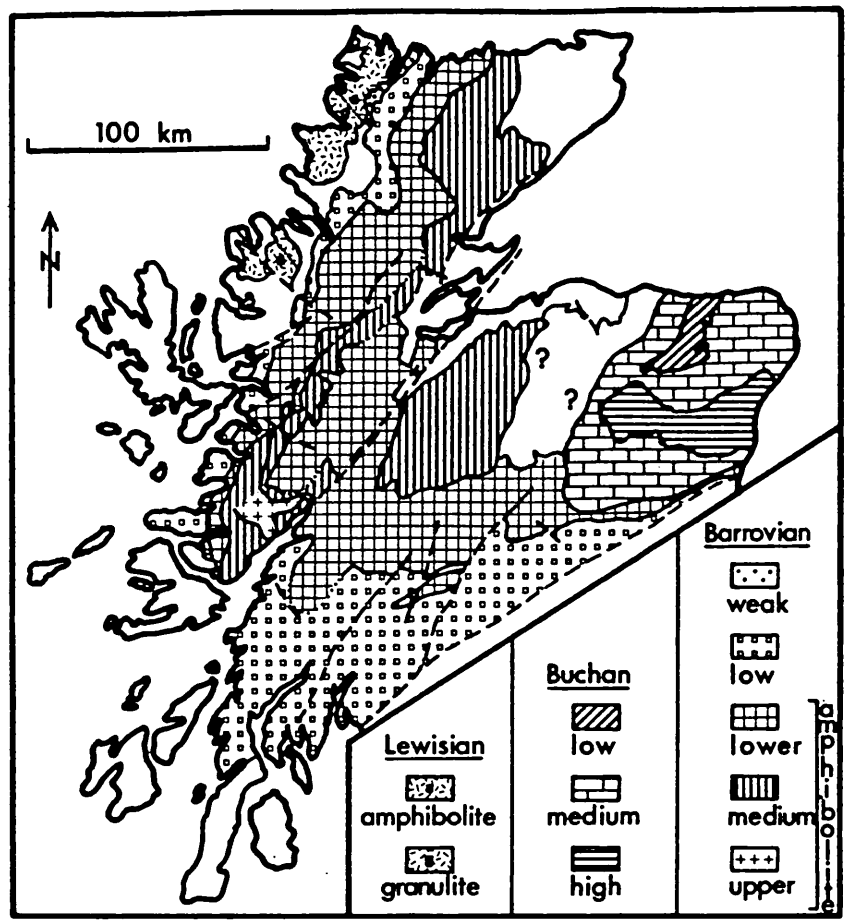


Figure 1.2: Map showing the distribution of metamorphic grades in northern Scotland (after Watson et al., 1982).

Southern Uplands Fault (Bamford et al., 1978), underlying the metamorphosed sediments and associated intrusive masses of the Caledonian cycle. During this cycle the late Proterozoic to lower Palaeozoic cover units of Moine and Dalradian groups were folded, metamorphosed and invaded by a variety of igneous rocks including the well-developed Caledonian granite suites whose origin is currently under discussion (see below). The metamorphic grade reached in the metasediments varies regionally from lower greenschist facies in the west and south, to upper amphibolite facies in parts of the interior. Migmatites are associated with the highest metamorphic grades. The areal distribution of the metamorphic zones is relatively well established (Fettes, 1979). Late- and post-orogenic uplift at the end of the Caledonian cycle resulted in rapid erosion

and deposition of a second fluviatile and lacustrine sequence in fault-bounded troughs and basins - the Old Red Sandstone (Devonian).

Watson et al. (1982) discussed the regional geochemistry of U in relation to this well-known geology, which therefore forms a good introduction to the choice of subject material for this project. Regional aspects were based on the analysis of stream sediment samples (IGS, 1979, 1982, 1984 and BGS, in press). There is good evidence that the geochemical patterns produced in this way closely follow those of the underlying geology (e.g., Plant et al., 1984). Some of the major conclusions reached include the following:

There is no doubt that the major U mobilisation event in the metamorphic environments of Scotland was related to the high pressure, granulite-facies metamorphism in the Hebridean Craton. Much literature exists on the subject, from Scotland and elsewhere, but relatively little is known about the precise mechanisms by which U is lost from the gneisses. The Lewisian Complex has been the subject of many detailed geochemical studies, notably those of Weaver and Tarney (1980, 1981) which have defined the geochemistry of the amphibolite-facies and granulite-facies end-member representatives of the exposed lithologies. However, in terms of the LILE-removal processes operating during high-grade metamorphism, the amphibolite-facies rocks are essentially unaffected, while those of the granulite facies have progressed to completion. An opportunity therefore exists for further study of the depletion processes, if a region in which they have been arrested before completion can be identified and sampled. It is now believed that Gruinard Bay represents such a region and so forms one of the areas selected for investigation here.

The Caledonian metamorphism did not reach granulite grade in any of the rocks now exposed, and the highest grades attained are in the upper amphibolite facies at the interior of the orogen. Watson et al. (1982)

demonstrated that no systematic regional trends in U distribution can be directly attributed to metamorphic grade; most being lithologically controlled and cutting across the metamorphic isograds. This is supported by the results of Atherton and Brotherton (1979), based on whole-rock analyses of radioelements in Dalradian rocks of varying metamorphic grade. Nevertheless, this does not preclude smaller scale U redistribution within specific geochemical environments, and local reactions of this type would form an interesting comparison with the regional removal of elements at the highest grades. The Glen Dessarry syenite has been chosen as a suitable subject - a pluton intruded into the high-grade core of the Caledonian Complex, and affected by amphibolite-facies deformation during or shortly after intrusion.

It is hoped that investigation of these two complementary subjects might allow some more general conclusions with respect to element mobilty during high-grade metamoprhism to be reached.

CHAPTER TWO

INTRODUCTION TO GRUINARD BAY

The first case-study chosen is therefore one of regional mobilisation of LILEs, during high-grade metamorphism of the Archaean Lewisian Complex of NW Scotland. As has been outlined above, in order to add anything of value to published detailed accounts of LILE depletion at granulite grade (Moorbath et al., 1969; Sheraton, 1970; Sheraton et al., 1973; Tarney and Windley, 1977; Rollinson and Windley, 1980a, b; Pride and Muecke, 1980, 1981, 1982; Weaver and Tarney, 1980, 1981) a transitional facies between amphibolite and granulite facies was sought on the Mainland Lewisian. Investigation of such a region, in which LILE depletion has been arrested at an intermediate stage, might provide valuable additional information for consideration with respect to the many existing genetic models and proposed depletion mechanisms. No such transition has yet been documented on the Scottish Mainland, although Drury (1980) interpreted field relationships on Barra in a similar context and has briefly documented a hornblende-granulite facies on Coll and Tiree (1973, 1974). Gruinard Bay was initially selected on the basis of a literature survey (see below) and advice from acknowledged experts on the Lewisian Complex (J.V.W.) and is now believed to represent the required prograde, amphibolite-granulite transition zone.

A crucial problem at Gruinard Bay, resulting directly from the fact that elements have been mobilised on a regional scale, is that it is impossible to determine the original element abundances and distribution in the study area, since they are not preserved. However, in order to constrain these to some extent, reference can be made to published literature on unaffected rocks from elsewhere in the Lewisian (e.g., Rhiconich). Similarly, high-quality data on the granulite-facies end-member are also available, so that a comparative approach may be adopted.

2.1 History of Research

In contrast to Glen Dessarry, the present topic is founded on an extensive literature dating from the early studies of the Lewisian Complex, by the Geological Survey (Peach et al., 1907) and Sutton and Watson (1951). It is still the focus of much active research, as is the geochemistry of the lower crust in general, but such is the extent of the literature that a comprehensive review would be too voluminous for inclusion here. The following paragraphs therefore represent only a selective summary of those features of the Lewisian Complex important to the present study, and highlight the more pertinent publications in the literature. Following this, a brief review of recent publications concerned with the amphibolite-granulite boundary in other parts of the world is included.

The Lewisian Complex.

The Lewisian basement gneisses of NW Scotland represent one of the most intensively-investigated continental lower crust terrains in the world and form a classic area in which granulite-facies LILE depletion has been studied. A fundamental tenet of this continuing investigation is the belief that such rocks, although now exposed at the surface, are representative of those which form the lower regions of the continental crust. Perhaps the most persuasive independent evidence in support of this assertion is the geothermometric and geobarometric data derived from stable Scourian mineral assemblages preserved in the rocks. For example, O'Hara and Yarwood (1978) and Rollinson (1978, 1979, 1982) have derived temperatures in excess of 1000°C and pressures of c. 15 Kb from granitic lithologies. However, it is now thought that these relate to a pre-Scourian magmagenetic episode and that more realistic estimates of temperature and pressure at the peak of metamorphism are 8-900°C and c. 11 Kb (e.g. Rollinson, 1979, 1980, 1981; Barnicoat, 1983). Such temperatures and pressures are appropriate only to the very low levels of the continental crust.

The Lewisian Complex is dominated by quartzofeldspathic gneisses which contain many relics of supracrustal metasedimentary material (Okeke et al., 1982), and early basic to ultrabasic intrusions (e.g., Savage and Sills, 1980; Sills et al., 1981). Moreover, it also contains isolated "lacunae" (Windley, 1982; Lowman, 1984) of intrusive representatives of the tonalite-trondhjemite-granite suite (Rollinson 1978, Rollinson and Windley, 1980; Rollinson and Fowler, in prep.) which are geochemically identical with their host gneisses (e.g., compare the data of Rollinson and Windley, 1980 with those of Sheraton et al., 1973). This strongly suggests that the gneisses themselves had an intrusive origin, although a metasedimentary parentage is still favoured by some (e.g., Lowman, 1984). Isotopic evidence (Hamilton et al., 1979) indicates that the igneous precursors of both the granulite and amphibolite-facies gneisses were generated from the mantle about 2.92 +/- 0.05 Ga ago. These igneous bodies became gneissose during the subsequent penetrative deformation and associated high-pressure amphibolite- to granulite-facies metamorphism (2.8 Ga to 2.6 Ga). Later Inverian deformation took place under amphibolite-facies conditions in steep NW-SE trending shear zones. These early events were followed by the emplacement of a widespread swarm of tholeiitic basic and ultrabasic minor intrusions (the Scourie dykes; e.g., Weaver and Tarney, 1981). The dykes and their host gneisses then suffered polyphase retrograde deformation under amphibolite facies conditions during the Laxfordian cycle (1.8 Ga to 1.6 Ga).

To date, detailed geochemical studies have concentrated on the amphibolite-facies and granulite-facies end-members of the high-grade metamorphic continuum, generally sampled from the northern part of the mainland outcrop (e.g., Rollinson and Windley, 1980a, b; Weaver and Tarney, 1980, 1981; Pride and Muecke, 1980, 1981, 1982). This has resulted in a clear conception of magmagenesis and of the overall

geochemical effects of the Badcallian phase of Scourian metamorphism - principally the pervasive removal of LILEs (K, Rb, Th, U and possibly also Cs and Pb), with attendant inter-element ratio variations and isotopic effects. However, the mechanisms by which such interfacies element fractionation arose remain partly unresolved, especially with respect to the radioelements, since in the end-member compositions they were either largely inoperative or had progressed to completion. Consequently, much discussion still surrounds the identity of the major process(es) responsible for LILE removal. Recent opinion has focussed on the following models:-

i) According to Weaver and Tarney (1981), LILE abstraction is directly related to the infiltration of a possibly mantle-derived, CO_2-rich fluid into the igneous complex undergoing contemporaneous metamorphism and deformation; a thesis to which considerable support has been lent by the discovery of widespread CO_2-rich fluid inclusions in diverse granulite terrains, although these do not yet include the Lewisian (Touret, 1974; Hoefs and Touret, 1975, Coolen, 1982; Touret and Dietvorst, 1983). Nevertheless, gross extensions of the fluid involvement model such as that proposed by Collerson and Fryer (1978) seem unnecessary to explain the characteristic features of the Scourian complex (Weaver and Tarney, 1981). These authors assembled a mass of data to suggest that it is theoretically possible for CO_2-dominated fluids to remove not only LILEs but also a range of other elements including the HREEs from lower crustal environments, thus giving rise to the common HREE "depletion" seen in the now-exposed remnants. As will be discussed later and has been pointed out in the literature (Weaver and Tarney, 1981), equilibration of a melt with hornblende or garnet is a more likely cause of this particular whole-rock feature.

ii) The main opposing hypothesis is that argued by Pride and Muecke (1980), that granulites represent the residua after extensive partial melting - a granitic magma being

responsible for the removal of much of the original LILE budget from the precursor, upper-crustal lithologies. Thermodynamic evidence supporting this model has been provided by Powell (1982; 1983a, b) who ascribes the preponderance of CO_2-rich fluid inclusions in granulitic residues to the preferential incorporation of H_2O into the transient silicate melt.

iii) A third, presently less-popular possibility, is that the differences in bulk LILE abundances between amphibolite- and granulite-facies extremes are primary features unrelated to subsequent metamorphic processes (Watson and Plant, 1979).

The bulk of the recent geochemical and isotopic data argue cogently against the latter, but fail to unambiguously resolve the other two alternatives.

Amphibolite-Granulite Transitions Elsewhere.

Several recent publications have considered various aspects of the boundary between amphibolite-facies and granulite-facies terrains (Phillips, 1980; Barbey and Cuney, 1982; Condie et al., 1982; Janardhan et al., 1982; Holt and Wightman, 1983; Maccarrone et al., 1983; Smalley et al., 1983; Allen et al., 1985), but most do not dwell on the trace-element geochemistry of the transition. Further, some deal with bulk compositions not strictly relevant to the orthogneiss system considered here, but may be returned to later where applicable to the controlling reaction mechanisms. However, investigations of the Archaean transition zone in Southern India (Friend, 1981; Janardhan et al., 1982; Holt and Wightman, 1983; Allen et al., 1985), which is composed of tonalitic gneisses apparently similar to those of the Lewisian Complex, suggest that the amphibolite-granulite boundary is marked by complex field relationships involving dehydration-induced charnockite "trees". Local areas of migmatisation may be interspersed with areas of banded amphibolite-facies rocks and texturally-identical granulite-facies lithologies. This is strong additional evidence to

suggest that partial melting is not everywhere the cause of granulite-facies conditions, although it may be an attendent process, and these authors prefer the CO_2-fluxing model outlined above.

2.2 Geological setting and sample collection

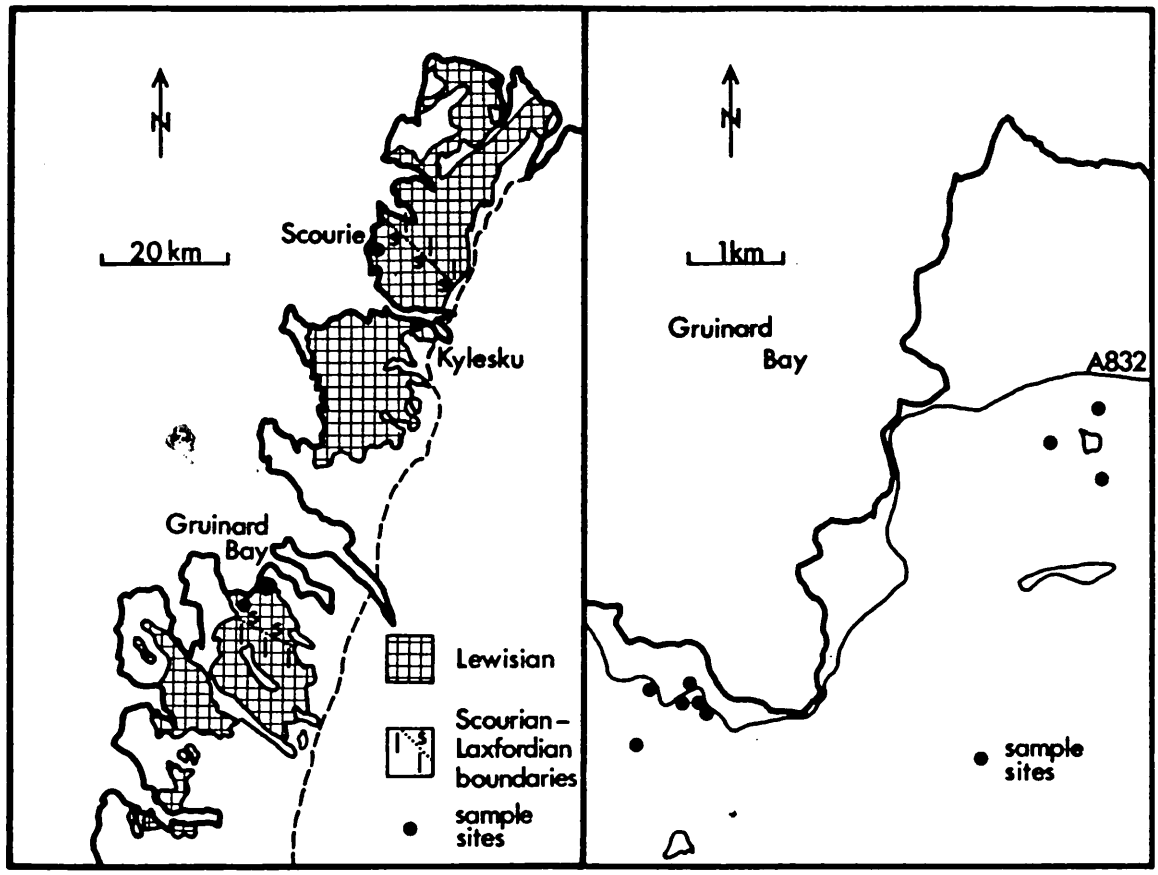


Figure 2.1: Locality map of Gruinard Bay.

Gruinard Bay lies on the NW coast of Scotland, at the south of the "central block" of the mainland Lewisian outcrop (Fig. 2.1), in the major part of which the Badcallian metamorphic episode gave rise to granulite-facies assemblages of charnockitic affinities (e.g., Sutton and Watson, 1951, and numerous publications thereafter). Peach et al. (1907) and Davies (1977) record the presence of minimal finite Laxfordian strain in the Gruinard Bay area, and the preservation of essentially Scourian structural features. Sutton and Watson (1951) identified the area as important in deciphering the metamorphic history of the Lewisian

since here "lower grade grey gneiss" was produced by the early metamorphism rather than the charnockitic rocks common north of Loch Broom. There is conflicting published evidence as to the original metamorphic grade. Davies (1977) contends that this was in the amphibolite facies, and that no evidence of a granulite-facies event is preserved. However, Field (1978) recorded the local occurrence of two-pyroxene, granulite-facies associations in the acid gneisses, for example north of the Gruinard River, and cited several other authors' observations of relict granulites in the area (Park, 1970; Moorbath and Park, 1972; Cresswell and Park, 1973; and Holland and Lambert, 1973). Also preserved locally are lithologies characterised by hornblende and/or biotite stable in association with two pyroxenes, therefore representing a hornblende-granulite subfacies (De Waard, 1966). Nevertheless, Rollinson and Windley (1980) regarded samples from Gruinard Bay as amphibolite-facies geochemical counterparts of Scourian granulites. Static retrogression during the later metamorphic episodes is probably widespread; most of the region is now characterised by hornblende- and biotite-bearing, amphibolite-facies quartzofeldspathic gneisses, and hornblende records Laxfordian K/Ar ages, (Moorbath and Park, 1972). Mineral assemblages are also locally characteristic of the greenschist facies. Such is the extent of retrogression that detailed original field relationships of the complexity described by Holt and Wightman (1983) from the transition in southern India, could not be expected to survive. For the present, two structural types of exposure might perhaps be usefully distinguished:-

i) those in which the Scourian and all later deformations show minimal effects, and the original intrusive relationships between the invading tonalitic-trondhjemitic magmas and the pre-existing basic-ultrabasic rocks, older gneisses (Davies, 1977) and supracrustal rocks are preserved (Rollinson and Fowler, in prep.).

ii) those in which the Scourian deformation has produced typical grey gneisses from these intrusive precursors, and whose structural grain is cross-cut by the later Scourie dyke suite.
The former are much less abundant than the latter, and every gradation between the two exists.

Since Rollinson (1978) has carried out a detailed study of the recognisable intrusive units, it was decided to concentrate here on the gneisses derived from these types, thereby allowing a more strictly correct comparison with published data from Lewisian gneisses of other metamorphic grades. Therefore, samples were collected from Gruinard Bay localities as marked in Fig. 2.1.

Although suitable data on the amphibolite-facies and granulite-facies extremes already exist, U and Th data are far from plentiful. A preliminary survey by gamma-ray scintillometry indicated a close comparability of total radioelement abundances at Gruinard Bay with the granulites which occupy the rest of the Mainland Central Belt (Sutton and Watson, 1951). Accordingly, a rather more detailed radioelement comparison is required with granulites than with the amphibolite-facies extreme, in order to highlight the possibly only subtle variations. Therefore, typical granulite-facies gneisses from the northern part of the central block were sampled in order to expand the U and Th data set for the granulitic end-member.

2.3 Approach

The purpose of the study is to investigate granulite-grade LILE depletion mechanisms by a consideration of geochemical data derived from the Lewisian gneisses of Gruinard Bay, having demonstrated that the mineralogical features and LILE abundances of the area are consistent with those expected in an amphibolite-granulite transition zone. The latter is achieved by a comparison with well-characterised granulites and amphibolite-facies rocks, but only having

first carefully established its validity by the use of elements thought to be "immobile" during the high-grade event. This is particularly important in view of the changing bulk chemistry of the Lewisian Complex with metamorphic grade. For example, Davies (1977) and Rollinson and Fowler (in prep.) have shown that trondhjemite dominates the Gruinard Bay lithologies, as opposed to tonalite at Scourie. Clearly, a bulk comparison should only be used as a preliminary to detailed comparison of tonalite with tonalite, trondhjemite with trondhjemite etc. Having done this, the data can be interpreted with more confidence in terms of the mechanisms and processes by which the observed pervasive element removal occurred.

2.4 Presentation of Results

The results have been dealt with below in three main chapters. The first deals with the magmagenetic processes as deduced from elements for which there is good evidence of immobility on a scale greater than that of a whole-rock sample, during the metamorphic events (principally REEs: Hamilton et al., 1979; Weaver and Tarney, 1980; 1981). The purpose of this is to demonstrate that there are no significant differences in "immobile" elements between like rocks from Gruinard Bay and from the end-member lithologies, so that the subsequent comparative method for LILEs may be considered valid. The next chapter deals with the original (Scourian) mineralogy and its relationships with that produced by retrogression, and then proceeds to demonstrate the geochemically transitional nature of Gruinard Bay by comparison of LILE abundances with published end-member data. The third then concentrates on the implications of the new data for LILE-removal processes.

CHAPTER THREE

MAGMAGENESIS: COMPARISONS WITH METAMORPHIC END MEMBERS

During the protracted history of research into the Lewisian Complex, many hypotheses concerning its ultimate origin have been advanced, some of which have been noted above. Of these, the following have perhaps been most influential:

i) As a supracrustal sequence consisting mainly of sedimentary material (Dearnley, 1962; Lowman, 1984).

ii) As an essentially volcanic sequence with calc-alkaline affinities (Sheraton, 1970; Sheraton et al., 1973).

iii) As a calc-alkaline intrusive suite generated in a crustal setting similar to a present-day Cordilleran belt (Holland and Lambert, 1975; Tarney and Windley, 1977; Weaver and Tarney, 1980, 1981).

iv) As a lower crustal residue after the generation and removal of an extensive granitic partial melt from "normal" upper crustal lithologies (e.g., Pride and Muecke, 1980, 1981, 1982).

Although the debate is still in progress, most recent literature is centred around the latter two alternatives, and so their relevance to the Gruinard Bay gneisses will be discussed below. Specific reference is made to those elements for which there is no evidence of mobility during the high-grade metamorphic event. At all stages, particularly during the presentation of the data below, comparison with amphibolite- and granulite-facies counterparts is emphasised, in order to demonstrate the magmagenetic similarity of the Lewisian orthogneisses through the range of metamorphic grades.

3.1 Geochemical data for "immobile" elements

The data are presented below in five groups: major element oxides, transition metals, "immobile" LILEs, HFSEs (excluding the REEs) and the REEs. A listing of the data set is available in the appendix.

Major Elements.

The major element data from Gruinard Bay and the author's suite of granulites are plotted as a series of Harker diagrams in Fig. 3.1. Most major elements show a continuous, smooth variation with SiO_2, a phenomenon often cited in favour of a fractional crystallisation mechanism to relate the range of chemistries observed, but not inconsistent with an origin by varying degrees of partial melting. It is clear from these diagrams that there are no systematic differences between the data from Gruinard Bay and those from the granulite-facies, charnockitic rocks. For the purpose of comparison with published data, the major element data are summarised by normative feldspar and AFM diagrams on Fig. 3.2, together with relevant comparative plots for amphibolite- and granulite-facies material taken from the literature. The gneisses of the Gruinard Bay area follow a calc-alkaline trend similar to those from other parts of the Lewisian Complex, and vary from granodioritic to trondhjemitic in the classification of O'Connor (1965). These are features common to Archaean gneiss terrains from many parts of the world (e.g., Jahn et al., 1981; Bickle et al., 1983; and Jahn et al., 1984).

It is particularly important to emphasise that there is no indication in any of the plots (K_2O will be discussed further below) that the Gruinard Bay suite differs from the granulites analysed in this study, or Lewisian gneisses of various metamorphic grades already discussed in the literature. Thus, on the basis of the major-element data there is no need to postulate special genetic conditions for the Gruinard Bay section of the Lewisian Complex.

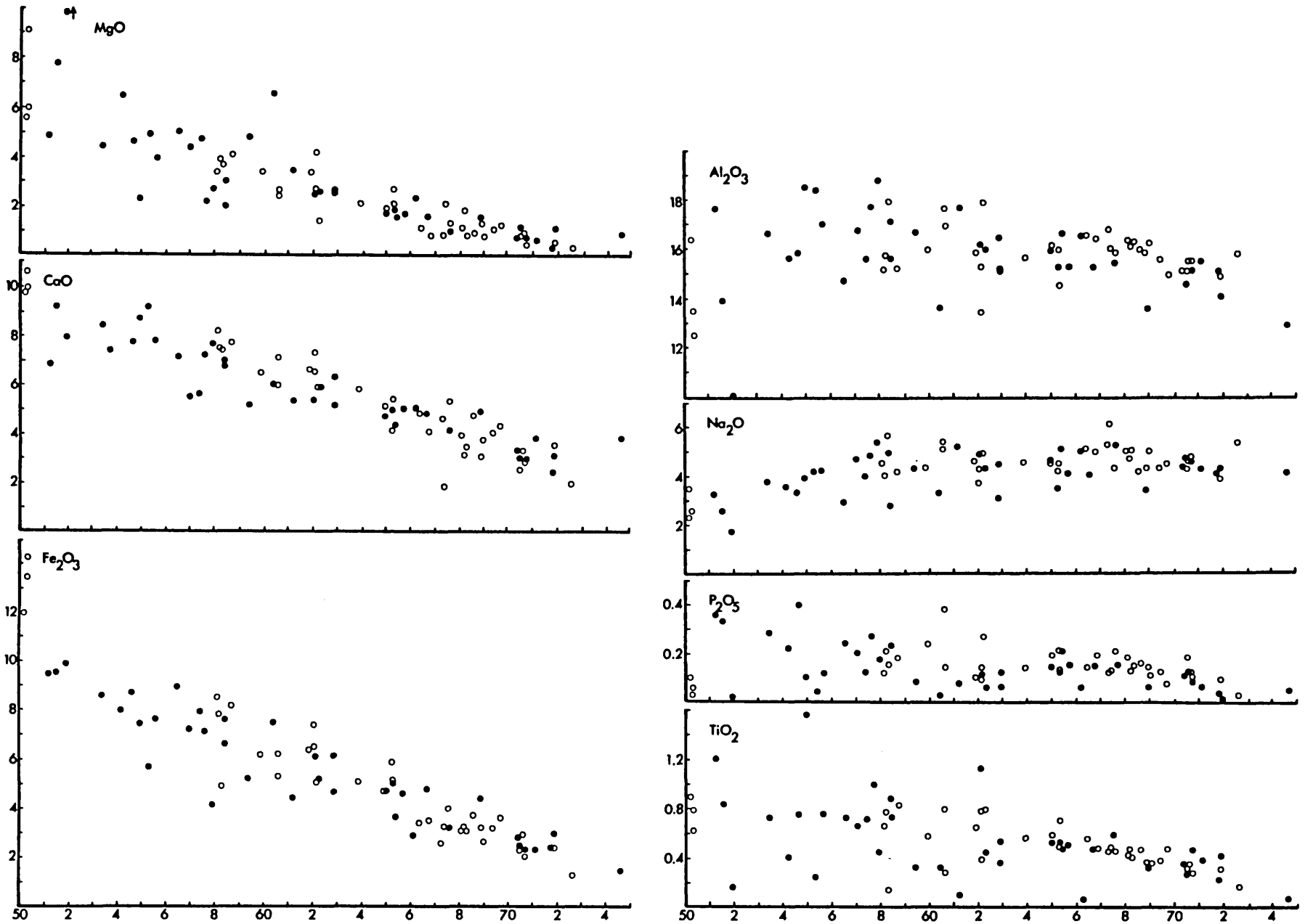


Figure 3.1: Comparative Harker diagrams for Lewisian gneisses.
(closed circles= Gruinard Bay gneisses; open circles= granulites).

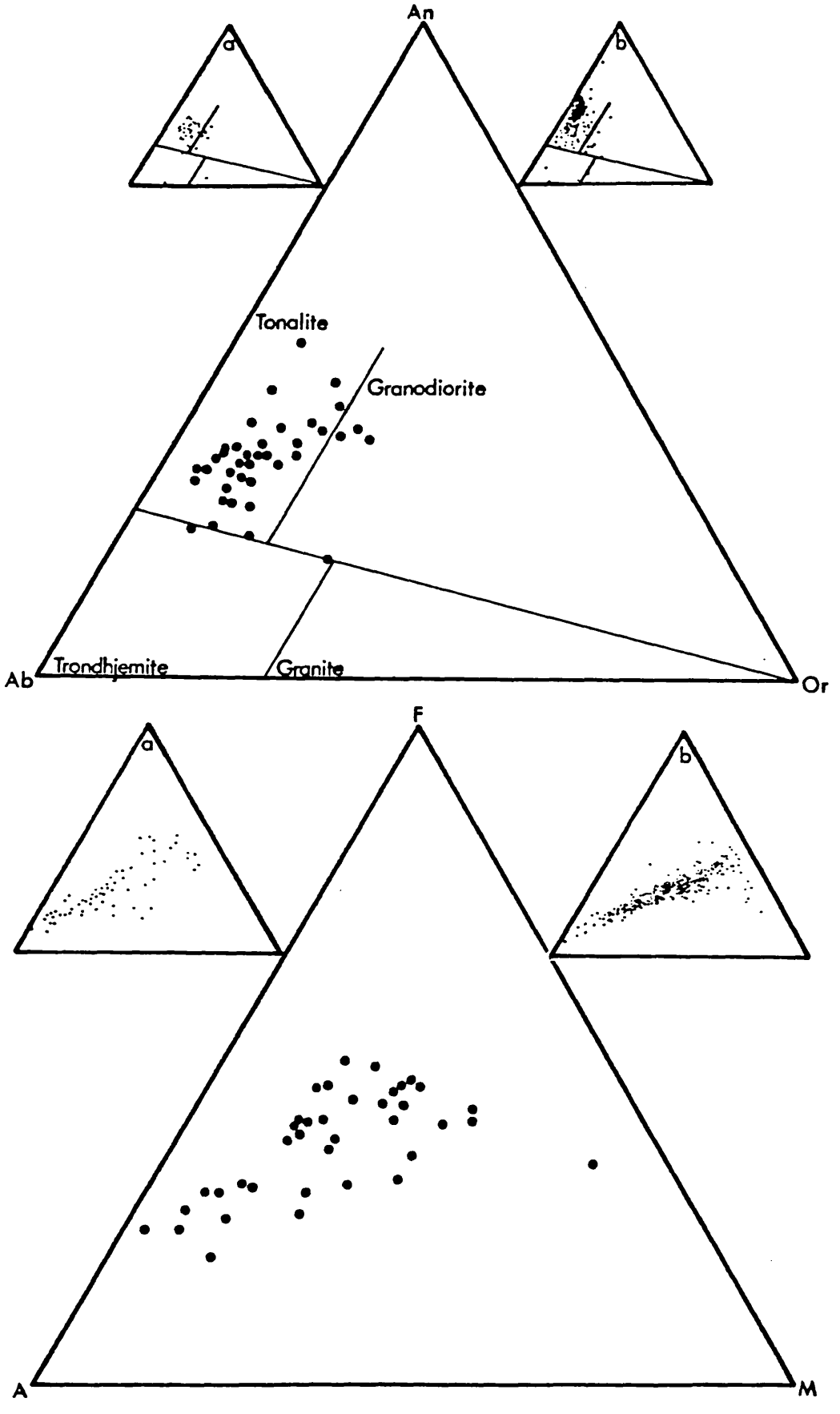


Figure 3.2: Comparative normative feldspar and AFM diagrams for Lewisian gneisses.

(a= amphibolite facies; b= granulite facies: from Tarney et al., 1979 (top) and Sheraton et al., 1973 (bottom)).

Transition Metals.

Data for Cr , Ni and V are plotted against SiO_2 in Fig. 3.3, together with data for the granulites, and published data from the amphibolite- and granulite-facies suites which will be used below for detailed LILE comparison. There is no indication of any significant difference. The transition metals all have variable abundance at given SiO_2, but generally decrease as silica increases. Weaver and Tarney (1980) have noted that their abundances fall too slowly to characterise a fractional crystallisation process dominated by mafic phases. However, Beach and Tarney (1978) postulate extensive (but probably closed-system on a large scale) adjustment of transition metal distribution during late-metamorphic retrogression, as a result of alteration of the mafic mineral assemblage from pyroxene-dominated to amphibole-dominated. This may have introduced some scatter to originally more tightly-constrained trends.

"Immobile" Large-Ion Lithophile Elements.

LILEs for which there is no evidence of open-system mobility during the high-grade event include Ba and Sr. The diagram (Fig. 3.3) also shows these plotted against SiO_2, and demonstrates the lack of any consistent trend with increasing acidity. This is also true for the granulites and amphibolite-facies gneisses, from which it is difficult to distinguish the Gruinard Bay suite.

High Field-Strength Elements.

Zr, Nb and Y are used as examples to compare HFSE abundances in the Gruinard Bay gneisses with the rest of the Lewisian Complex (Fig. 3.3). Zr values are generally high but variable, and there are no obvious differences which would require different magmagenetic interpretations. The same is true for Nb, except that abundances are generally rather low, a feature common to many calc-alkaline rock suites. This has been attributed to its retention in minor phases stable in the residue

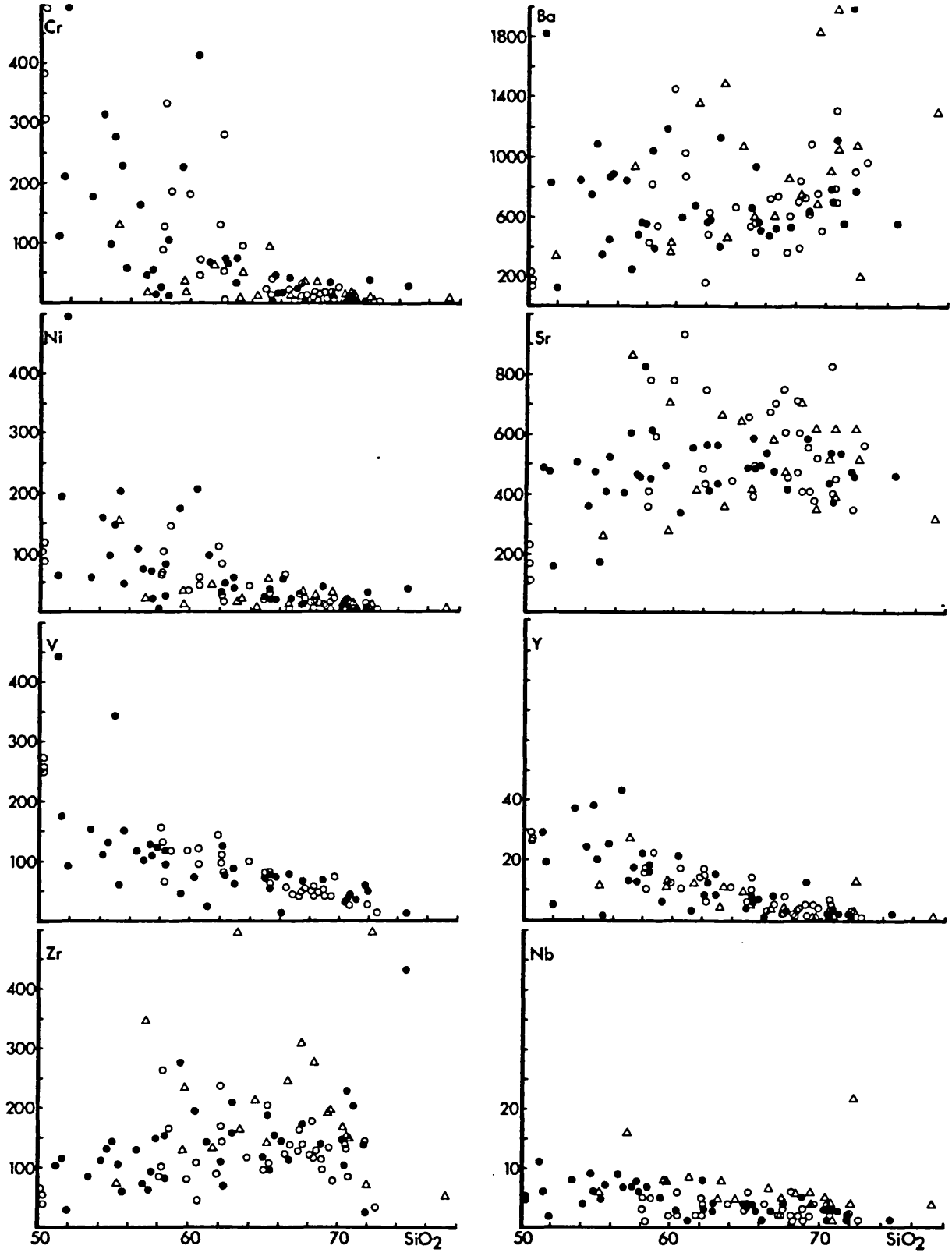


Figure 3.3: Comparative trace element variation diagrams for Lewisian gneisses.

(closed circles= Gruinard Bay gneisses; open circles= granulites; open triangles= data from Weaver and Tarney, 1980, 1981).

of their source (e.g., Saunders et al., 1979; Thompson et al., 1984), and is manifest as a trough on the mantle-normalised plots to be employed extensively below. Some samples have anomolously high or low Zr, which may be due to local zircon accumulation or fractionation, as shown by Rollinson and Fowler (in prep.). These are dealt with in more detail later, since the presence or absence of zircon might have implications for U and Th abundance variations. Y abundances are also low, but in general decrease with increasing SiO_2 from a region of relatively high scatter between 50 and 60% SiO_2. The trend shown on the diagram is precisely similar to that documented by Tarney et al. (1979), and there are no indications of significant inter-facies variation.

Rare Earth Elements.

Although the once widely-accepted premise that REEs are immobile during metamorphism has been shown to be a gross oversimplification (e.g., Alderton et al., 1980; Fowler et al., 1983 and many others), there is compelling evidence from the Lewisian to suggest that under the particular metamorphic conditions which affected the Complex, the lithochemical system remained closed to REEs on the scale of a typical whole-rock sample. This ranges from a direct comparison of granulite-facies REE data with those from lithologically similar amphibolite-facies regions (Weaver and Tarney, 1981), to discussion of the Sm-Nd isotope systematics of Lewisian gneisses of various metamorphic grades (Hamilton et al., 1979), which record a whole-rock age of 2.92 +/- 0.05 Ga with no subsequent resetting such as that which occurs in the U-Th-Pb system at c. 2.7 Ga (Moorbath et al., 1969).

REE analyses of representative samples from Gruinard Bay and the author's comparative granulite suite are presented in Figs. 3.4 and 3.5, with literature data for amphibolite-facies and granulite-facies examples (Weaver and Tarney, 1980; 1981) as insets to each, respectively.

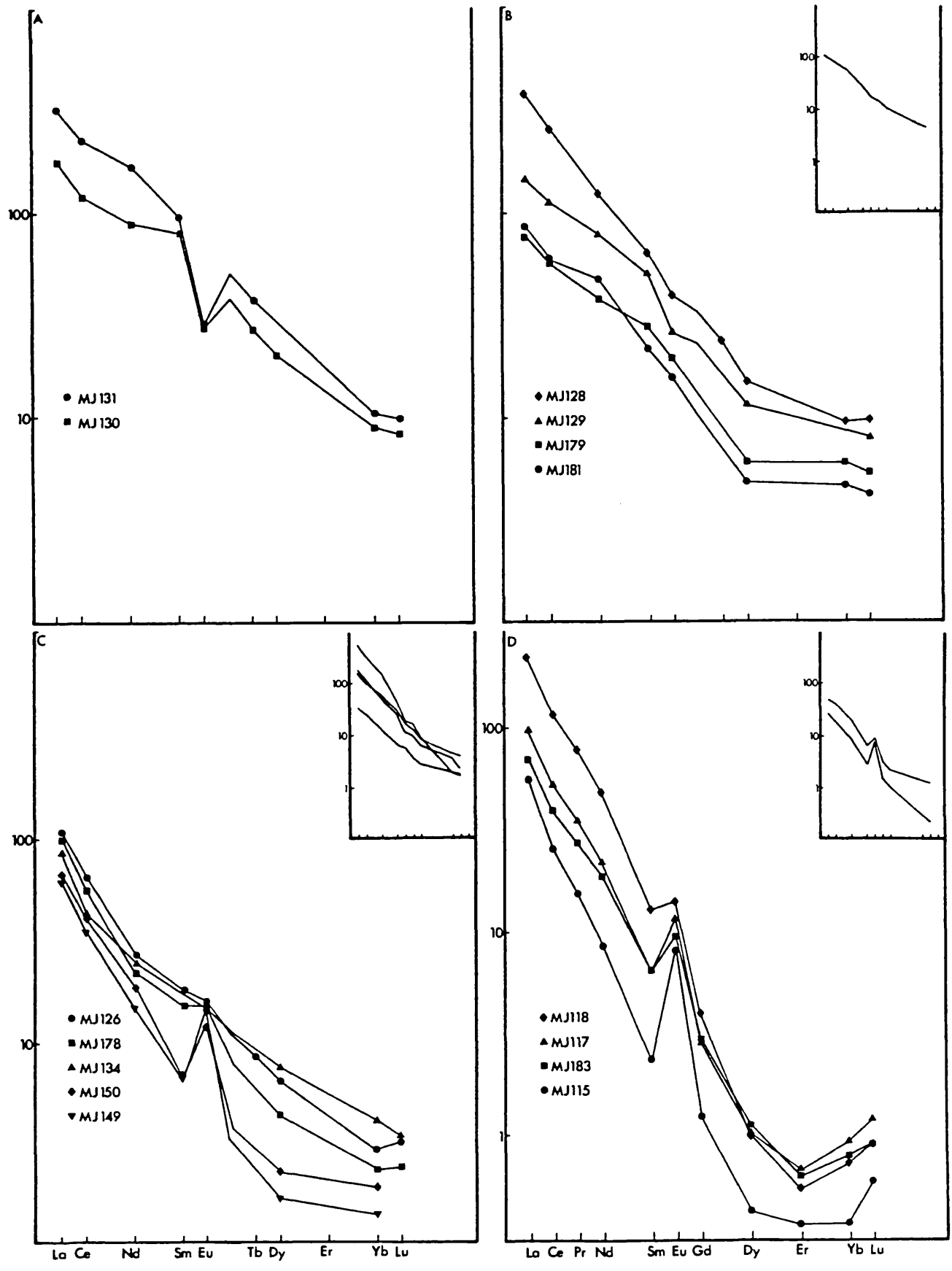


Figure 3.4: Comparative chondrite-normalised REE plots for Lewisian gneisses from Gruinard Bay (this study) and Rhiconich (inset, Weaver and Tarney, 1981).
(A, B= intermediate gneisses; C= tonalites; D= trondhjemites).

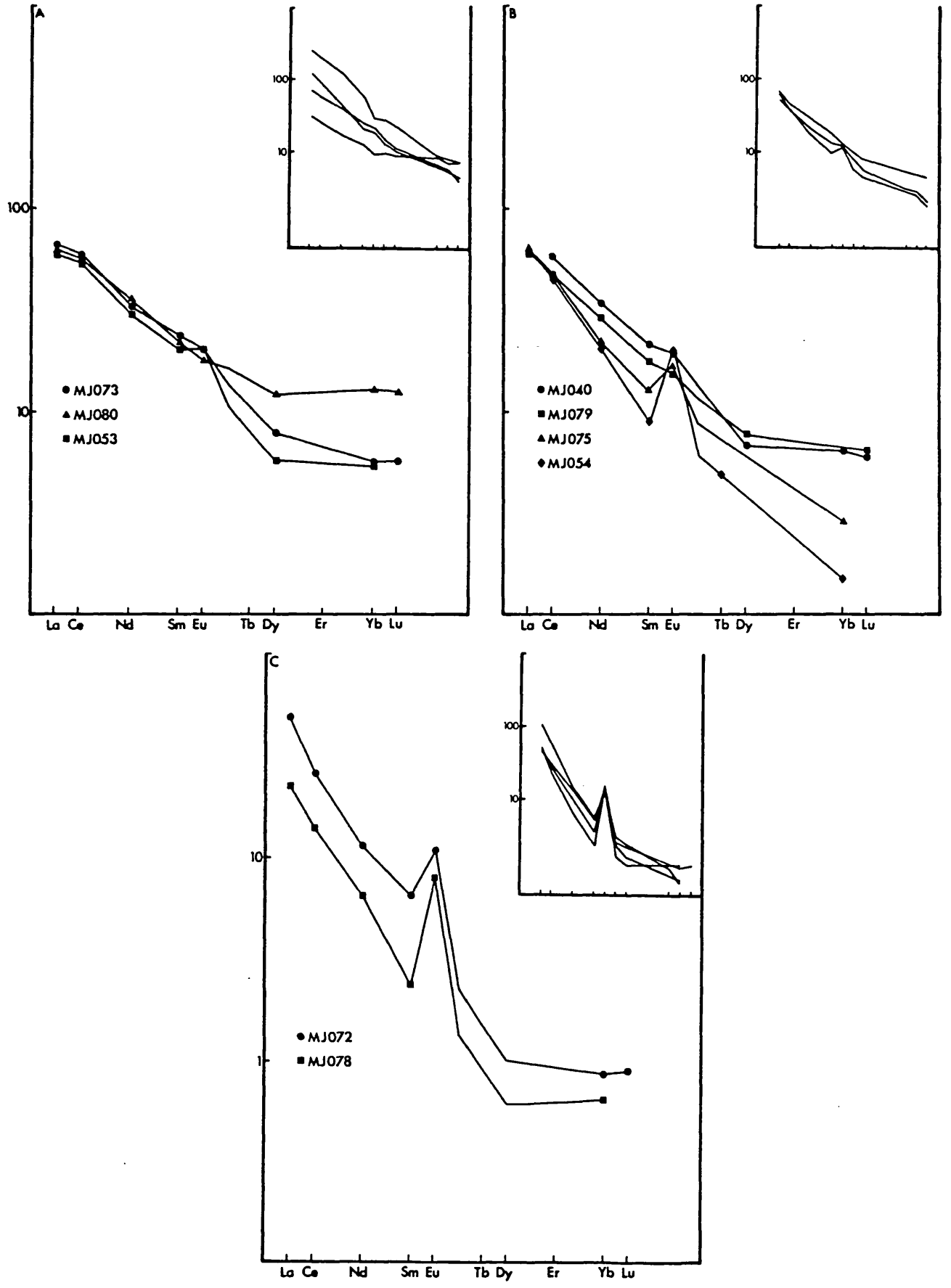


Figure 3.5: Comparative chondrite-normalised REE plots for Lewisian gneisses from the central block (this study) and Assynt (inset, Weaver and Tarney, 1980). (A= intermediate gneisses; B= tonalites; C= trondhjemites).

The general characteristics of the Gruinard Bay suite may be summarised as follows:

i) There is a good general correlation with increasing % SiO_2 although this is clearly not inviolate.

ii) The intermediate gneisses show LREE-enriched patterns, with generally small positive or negative Eu anomalies. Two samples (MJ130, 131) have large negative Eu anomalies. Importantly, there is no strong depletion of HREEs, and total REEs decrease with increasing SiO_2.

iii) The tonalitic gneisses show a range of patterns from those similar to the intermediate gneisses towards more fractionated examples with decreasing HREEs. A good correlation exists between decreasing absolute HREE abundance and increasing size of positive Eu anomaly.

iv) The trondhjemitic gneisses have highly-fractionated patterns, with the lowest HREE abundances, a marked concave-upward HREE section and very large, positive Eu anomalies.

The first point to note, and perhaps the most important for this study, is that there are once again no discernable significant differences between the Gruinard Bay suite and rocks from other parts of the Lewisian Complex. This adds considerable weight to the contention that the chosen rock suites are directly comparable in terms of their genesis and primary geochemistry, since it is now founded upon the petrogenetically important REE group.

3.2 Magmagenetic Models

The applicability of the two models outlined above, which form the focus of most modern literature and are both thought to be capable of describing the overall geochemistry of the tonalite-trondhjemite rock suite, can now be critically assessed with respect to the Gruinard Bay gneisses, by using the REEs in the familiar manner, as sensitive indicators of a rock's parentage.

3.2.1 A Calc-alkaline intrusive suite.

Several publications have considered the genesis of rocks similar to those at Gruinard Bay in terms of plutonic processes. For example, Arth et al. (1978) discussed an Archaean gabbro-diorite-tonalite-trondhjemite suite from Finland, whose REE geochemistry shows many similarities with comparable lithologies from around the world, including the Lewisian. These rocks show a systematic variation of REE patterns for gabbroic through tonalitic to trondhjemitic samples, ascribed in large part to the progressive increase of the hornblende-melt partition coefficient in an increasingly silicic melt. This may be interpreted (Arth et al., 1978) either as a result of different degrees of partial melting of a hornblende-bearing source, or as the result of extensive fractionation of hornblende from a basaltic parent melt. The rather smooth progression from gabbroic to trondhjemitic chemistries with no obvious hiatus, and the presence of cumulus lithologies, led these authors to prefer the latter option.

Weaver and Tarney (1980) noted the close similarity of Lewisian gneiss geochemistry with that of the Finnish suite and tested in detail the fractional crystallisation hypothesis, raising a number of objections:

i) Transition metal abundances do not fall rapidly enough.

ii) The volume of hypothetical early melt is too small.

iii) There are no obvious cumulates.

iv) The amount of fractionation required to produce the range of compositions observed seems unreasonably large.

In preference, they invoked varying degrees of partial melting of a compositionally heterogeneous basaltic source region; the residual mineralogy with which the melt equilibrated being dominated by garnet, rather than hornblende (see also Drury, 1978, 1980; Rollinson and Fowler, in prep.). In order to produce incompatible-element abundances observed in the Lewisian by partial melting of a primitive (mantle) source, very

small degrees of melting would be required. Bearing in mind the volume of magmas produced at about 2.9 Ga, a subduction-zone setting has been suggested, the downgoing slab supplying the required voluminous, relatively enriched source region (Tarney and Windley, 1977).

In addition, Rollinson and Windley (1980) have discussed the origin of an intrusive, granulite-grade tonalite-trondhjemite-granite suite from Scourie in terms of fractional crystallisation of hornblende and/or plagioclase with minor zircon and apatite. The parental tonalite liquid was considered to be derived from a basaltic source either by partial melting or by fractional crystallisation, with hornblende and/or garnet as residual phases.

Thus, the data from Gruinard Bay should be considered in terms of several pre-existing accounts of the intrusive magmagenesis of the gabbro-diorite-tonalite-trondhjemite suite in general, and the Lewisian gneisses in particular. Although they are not mutually exclusive, for practical purposes modelling of the observed range of variation using each process separately has been carried out, with the knowledge that this may be an oversimplification of the natural events.

Partial melting of a wet basaltic source leaving an eclogitic residue

Experimental studies by Holloway and Burnham (1972), Stern, (1974), Helz (1976), Peto and Hamilton (1976), and Spulber and Rutherford (1983) have all demonstrated the possibility of producing acidic melts, whose closest natural analogues are tonalite- trondhjemite, by melting a basaltic source under conditions of high pH_2O. Fig. 3.6 shows a Qz-Ab-Or projection of the system Qz-Ab-Or-An-H_2O on which are plotted the range of compositions produced experimentally and those of samples from Gruinard Bay. There is clearly a close correspondence between the two, especially the more-acid gneisses (SiO_2 greater than 60%).

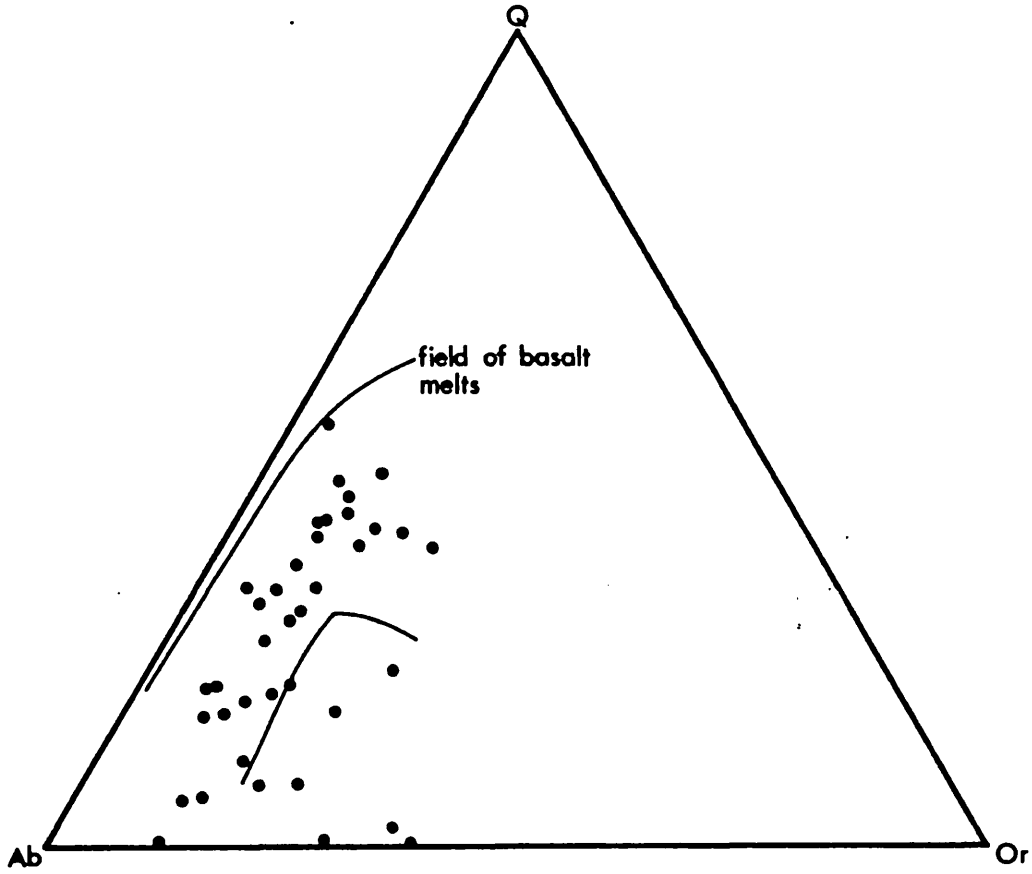


Figure 3.6: Qz-Ab-Or diagram showing field of experimental melt compositions with data from Gruinard Bay gneisses.

Intermediate gneisses

The lack of appropriate REE partition coefficient data for melts of this bulk composition make a quantitative treatment of the intermediate gneisses difficult, but Weaver and Tarney (1980) consider that corresponding rocks from Scourie could be generated by partial fusion of source rocks similar to those which, in their view, produced the tonalite-trondhjemite suite. This may well be true for the majority of samples from Gruinard Bay, although in a few cases (e.g., MJ128 and MJ129) it would require the production of a melt of higher total REE abundance by a larger degree of partial melting (since they are more basic) which at first sight seems rather unlikely. Although mineral-melt partition coefficients generally decrease with falling melt SiO_2 content, which would result in greater element enrichment in more basic

melts, it is uncertain whether this is capable of explaining the observed trend, and a more basic source might perhaps be invoked. On the other hand, samples MJ130 and MJ131 have significant negative Eu anomalies, which might suggest feldspar removal. However, these also have lower SiO_2 and higher transition metal abundances than many other intermediate gneisses, which both argue against an origin as their derivative liquids which have fractionated plagioclase. They might instead represent partial melts which have equilibrated with a significant proportion of plagioclase in their source, or liquids derived by plagioclase fractionation from an altogether more primitive parent.

Tonalites and trondhjemites

Using the partition coefficient data of Arth and Hanson (1975) for dacitic and rhyolitic rocks (see appendix), a quantitative model can be suggested for melts within this silica interval. With any partial melting model in which the source composition and residual mineralogy are speculative, a large degree of freedom is allowed in the initial assumptions. Consequently, several extremes might be envisaged, with the real situation perhaps represented by some combination of these. Nevertheless, it is instructive to consider the extremes separately, and this is done below.

i) Partial melting of a homogenous source.

Although there is no consensus on which style of melting (equilibrium or batch) is more likely to have taken place, the shapes of the patterns produced by both are similar. Therefore, after demonstrating the different degrees of melting required to produce a similar result in the first model, the remainder use batch melting only, this being perhaps more appropriate. Both equations have been applied to a source composition of 20x chondrites, approximating to an Archaean tholeiitic basalt. The melt is presumed to

have equilibrated with 55% clinopyroxene, 30% garnet and 15% quartz, after Arth and Hanson (1975). The results for steps up to 50% melting are given in Table 3.1, and plotted in Fig. 3.7a and b, showing a marked similarity in shape to those observed in the gneisses at Gruinard Bay, and indeed other parts of the Lewisian Complex (Drury, 1978, 1980; Weaver and Tarney, 1980; Pride and Muecke, 1980). However, it is also immediately apparent that a simple model such as this will not suffice, since it requires an array of REE patterns which intersect between Sm and Nd due to the change in distribution coefficients from less than to greater than one. This is not observed in the sample suite. Therefore it becomes necessary to introduce substantial source heterogeneity for the tonalitic- trondhjemitic rock types as well. Such a concept is probably valid considering the range of Archaean tholeiite compositions available (e.g., Condie, 1976), if such is to be the source. Its effects are difficult to model quantitatively, since the relationship between source REE pattern and residual mineralogy is essentially unknown. Nevertheless, some indications can be gained by divorcing the changes in source and residue.

ii) Partial melting of a heterogeneous source, with a uniform residue.

A variation in the source from say, 10x - 50x chondrites is not beyond the realms of possibility, and this will simply produce an array of parallel patterns for a given degree of melting and residual mineralogy. However, variable fractionation of the source is perhaps more likely, and will induce complementary fractionation in the derived melts (Fig. 3.7c; Table 3.1). This provides a closer approximation to the array of patterns from Gruinard Bay, especially if coupled with different degrees of melting. However, the largest likely variations in source composition are in the LREE (see Condie, 1976 for example), which would therefore produce larger variations in LREE than HREE in the derivative

Fusion with uniform residual mineralogy of 55% clinopyroxene, 30% garnet and 15% quartz.

	D	Melt/source for given % batch melting					
		10	20	30	40	50	60
Ce	0.38	2.42	2.22	2.03	1.85	1.68	1.52
Nd	0.76	1.28	1.26	1.24	1.21	1.19	1.16
Sm	1.71	0.60	0.61	0.63	0.64	0.66	0.69
Eu	1.30	0.77	0.78	0.80	0.81	0.82	0.84
Gd	4.16	0.25	0.26	0.27	0.29	0.31	0.33
Dy	9.64	0.11	0.11	0.12	0.13	0.14	0.15
Er	13.75	0.08	0.08	0.09	0.09	0.10	0.11
Yb	12.83	0.08	0.09	0.09	0.10	0.11	0.11
Lu	9.72	0.11	0.11	0.12	0.13	0.14	0.15

	D	Melt/source for given % equilibrium fusion					
		10	20	30	40	50	60
Ce	0.38	2.26	1.98	1.77	1.59	1.45	1.33
Nd	0.76	1.28	1.24	1.20	1.17	1.14	1.11
Sm	1.71	0.61	0.64	0.67	0.70	0.74	0.78
Eu	1.30	0.79	0.81	0.83	0.85	0.87	0.89
Gd	4.16	0.26	0.28	0.31	0.35	0.39	0.44
Dy	9.64	0.11	0.13	0.14	0.16	0.19	0.22
Er	13.75	0.08	0.09	0.10	0.12	0.14	0.16
Yb	12.83	0.09	0.10	0.11	0.12	0.16	0.17
Lu	9.72	0.11	0.13	0.14	0.16	0.19	0.22

Batch melting with heterogeneous residue.

	D for given residual mineralogy (cpx: gnt: qtz)				
	100:0:0	80:5:15	70:15:15	55:30:15	0:100:0
Ce	0.50	0.41	0.40	0.38	0.35
Nd	1.11	0.91	0.85	0.76	0.53
Sm	1.67	1.46	1.56	1.71	2.66
Eu	1.56	1.32	1.31	1.30	1.50
Gd	1.85	2.00	2.87	4.16	10.50
Dy	1.93	2.97	5.64	9.64	28.60
Er	1.66	3.46	7.58	13.75	42.80
Yb	1.58	3.25	7.09	12.83	39.90
Lu	1.54	2.71	5.51	9.72	29.60
	Melt/source for 20% batch melting				
Ce	1.80	2.07	2.13	2.22	2.36
Nd	0.91	1.08	1.15	1.26	1.72
Sm	0.63	0.70	0.66	0.61	0.40
Eu	0.67	0.78	0.78	0.78	0.69
Gd	0.57	0.53	0.37	0.26	0.11
Dy	0.55	0.36	0.19	0.11	0.04
Er	0.63	0.31	0.15	0.08	0.03
Yb	0.66	0.33	0.15	0.09	0.03
Lu	0.67	0.39	0.20	0.11	0.04

Table 3.1: Partial melting models for the generation of tonalitic-trondhjemitic gneisses from Gruinard Bay.

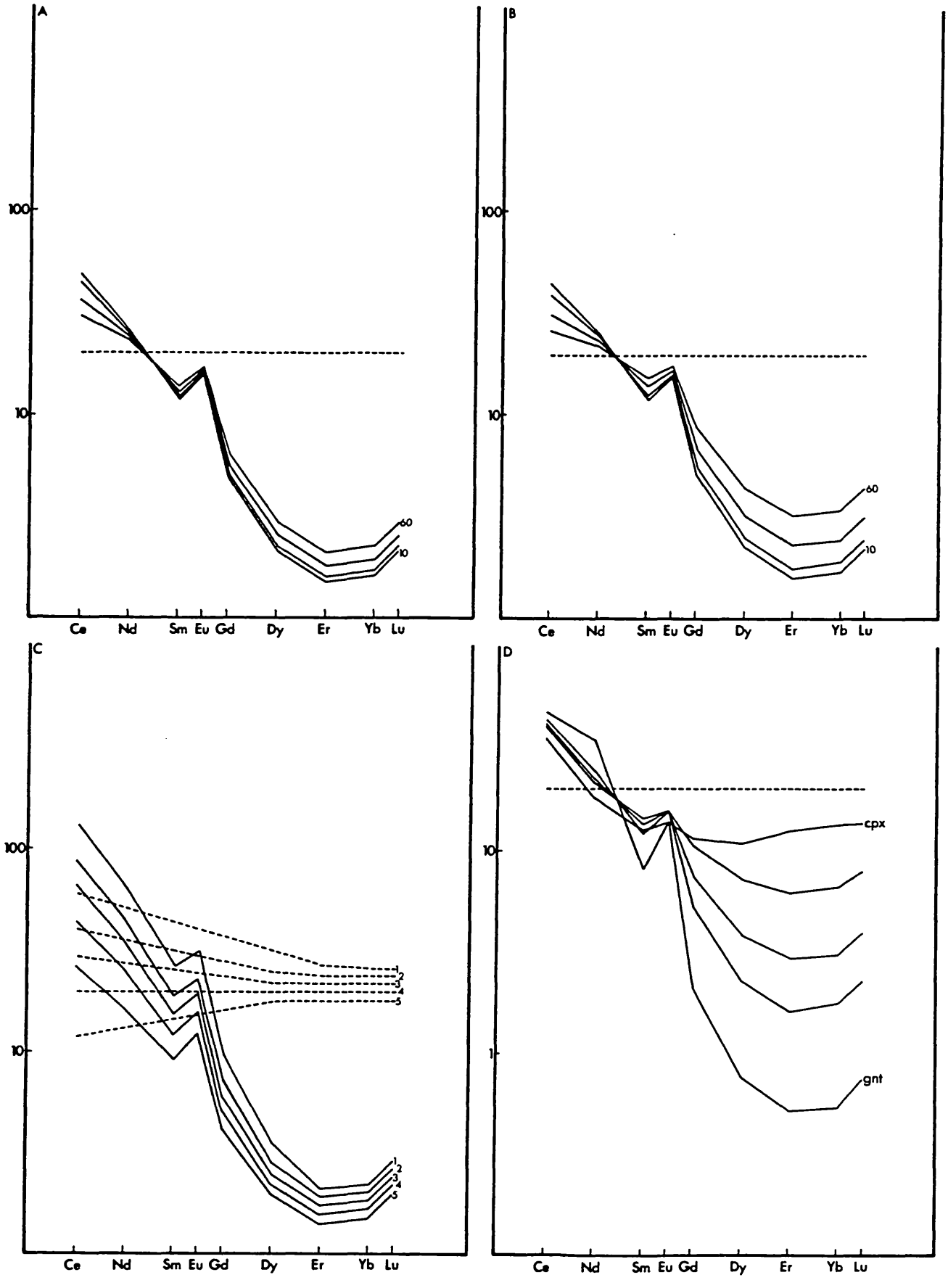


Figure 3.7: Partial melting models for the generation of tonalitic-trondhjemitic gneisses from Gruinard Bay. (A= batch melting; B= equilibrium melting; C= variation in source composition; D= variation in residual mineralogy).

melts, the opposite to what is observed in the sample analyses. Hence, variations in the mineralogy of the residue might be invoked, especially since the HREE abundances are particularly dependant on the proportion of residual garnet or hornblende.

iii) Partial melting with a heterogeneous residue.

Perhaps the most important potential variation in residue is in the proportion of garnet, which will cause large variations in the HREE complement of the melt. A limiting case of 100% garnet in the residue is illustrated in Fig. 3.7d (Table 3.1) for 20% melting of a 20x chondrite source, together with more "normal" residues such as those used above. The extreme patterns produced are similar to sample MJ115, although there are some important differences (particularly the LREE abundances), and these do seem rather unlikely genetic conditions. Nevertheless, the extensive HREE range is reproduced well and so the simultaneous alteration of the source REE content and the residual mineralogy (for example increasing the proportion of garnet in the residue as the source REE concentration falls) could conceivably produce an array of patterns similar to that observed in the Gruinard Bay Complex.

Fractional crystallisation from a basaltic parent

Fractional crystallisation is an alternative hypothesis to the partial melting models, and has been invoked by several authors, including Rollinson and Windley (1980) and therefore deserves consideration here. Both the Rayleigh fractionation equation (model a) and the equilibrium fractionation equation (model b) have been used.

Intermediate gneisses

Lack of precise partition coefficient data again precludes a quantitative assessment but simple consideration of the sample array (Fig. 3.4) leads to the conclusion that any fractionating assemblage is

required to have bulk distribution coefficients approximately equal for all the REEs and uniformly greater than one - except for a small, negative Eu anomaly. Using the partition coefficient data of Arth and Hanson (1975) for more silicic compositions as a guide, it is clear that the general shape required is difficult to generate using likely rock-forming minerals. Since the acidity of the melt affects only the magnitude of the partition coefficients and not the shape of the plot, this conclusion is probably also valid for intermediate melts. One way to generate a very approximately flat REE distribution coefficient pattern with absolute values significantly greater than one would be to invoke substantial plagioclase involvement coupled with a mineral of very high partition coefficients for HREEs, such as hornblende. However, barring unreasonably high fO_2 in order to reduce the affinity of plagioclase for Eu (Drake and Weill, 1976), this process will produce increasing negative Eu anomalies in the residual melts, as has been demonstrated by Weaver (1980) in the Madras granulites. This is generally not seen at Gruinard Bay. Furthermore, those samples (MJ130 and MJ131) which do have such large negative Eu anomalies, also have high transition metal abundances and are more basic than many intermediate gneisses, to which they therefore cannot be related by such a mechanism. Moreover, any fractional crystallisation scheme dominated by rock-forming minerals would require their removal in quantities far exceeding that allowed by the major element data. Therefore, it seems difficult to produce the desired falling REE abundances without resorting to an assemblage containing a high proportion of minor mineral phases, for which there is no petrographic evidence. Thus the intermediate gneisses apparently do not represent a series of liquid compositions related by a simple crystal fractionation scheme.

Tonalitic-trondhjemitic gneisses

In this case the parent melt composition has been taken as an average of two of the most evolved intermediate gneisses (MJ179 and 181). Since the fractionating assemblage in such systems is thought to be dominated by hornblende (Arth et al., 1978), the simplifying assumption of 100% hornblende fractionation has been adopted. Calculations are listed in Table 3.2 for 10% to 50% removal, for both fractionation equations.

Rayleigh fractionation.

	D	Melt/initial melt for given % fractionation				
		10	20	30	40	50
Ce	1.52	0.95	0.89	0.83	0.77	0.70
Nd	4.25	0.71	0.48	0.31	0.19	0.10
Sm	7.76	0.49	0.22	0.09	0.03	0.01
Eu	5.14	0.65	0.40	0.23	0.12	0.06
Gd	10.00	0.39	0.13	0.04	0.01	-
Dy	13.00	0.28	0.07	0.01	-	-
Er	12.00	0.31	0.09	0.02	-	-
Yb	8.38	0.46	0.19	0.07	0.02	0.01
Lu	5.50	0.62	0.37	0.20	0.10	0.04

Equilibrium fractionation.

	D	Melt/initial melt for given % fractionation				
		10	20	30	40	50
Ce	1.52	0.95	0.91	0.87	0.83	0.79
Nd	4.25	0.75	0.61	0.51	0.43	0.38
Sm	7.76	0.60	0.42	0.33	0.27	0.23
Eu	5.14	0.71	0.55	0.45	0.38	0.33
Gd	10.00	0.53	0.36	0.27	0.22	0.18
Dy	13.00	0.45	0.29	0.22	0.17	0.14
Er	12.00	0.48	0.31	0.23	0.19	0.15
Yb	8.38	0.58	0.40	0.31	0.25	0.21
Lu	5.50	0.69	0.53	0.43	0.36	0.31

Table 3.2: Amphibole fractional crystallisation models for the generation of tonalitic-trondhjemitic gneisses from Gruinard Bay.

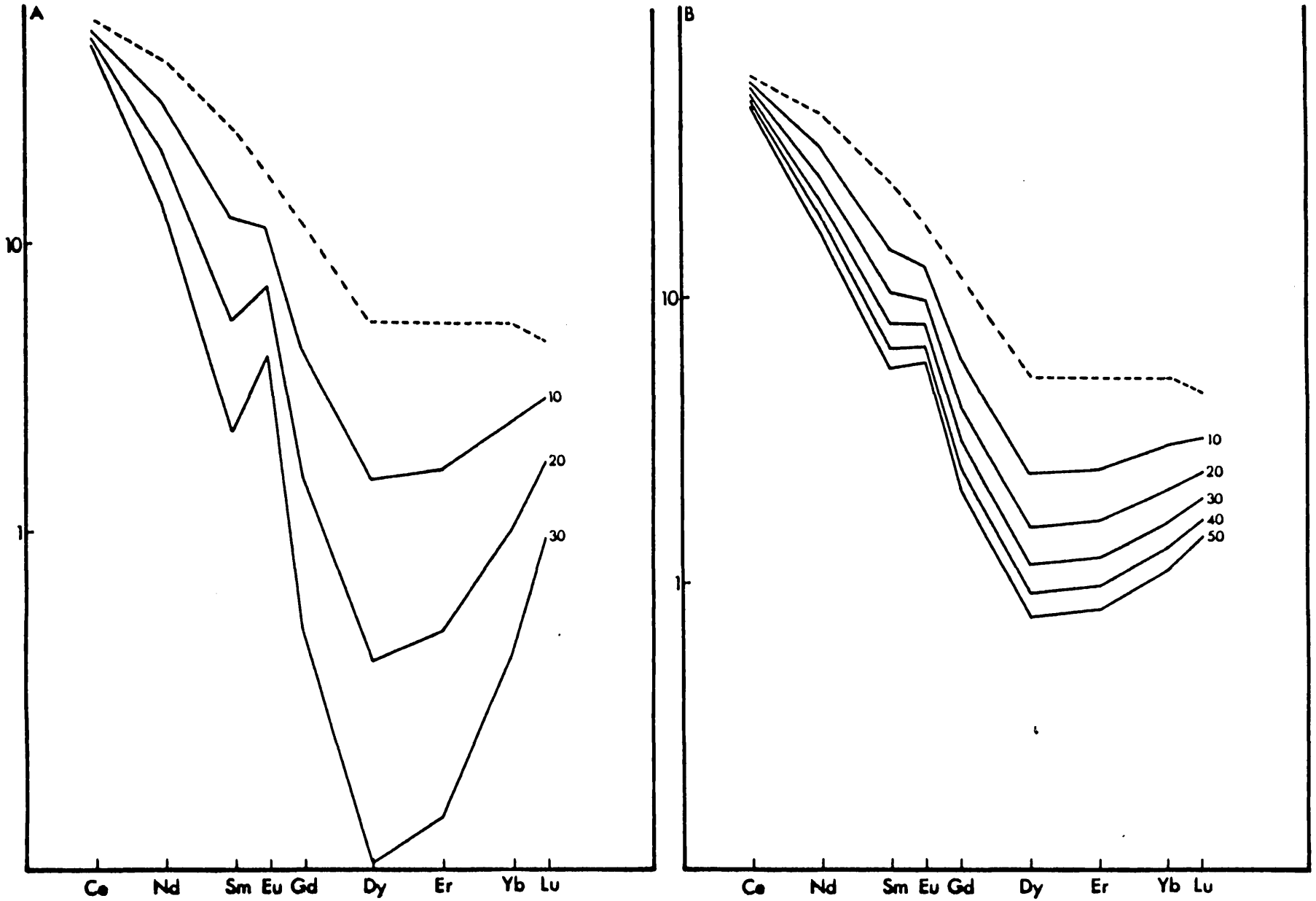


Figure 3.7: Fractional crystallisation models for the generation of tonalitic-trondhjemitic gneisses from Gruinard Bay.
(A= Rayleigh fractionation; B= equilibrium fractionation).

The resultant patterns are plotted in Fig. 3.8. Clearly, the REE pattern of the most extreme trondhjemite (see Fig. 3.4) might be approximated by c. 30% hornblende removal from the parent melt assuming surface equilibration only (a), and the patterns produced by removal of smaller amounts bear some similarity to the tonalitic samples. On the other hand, if the equilibrium fractionation equation applies (b), the range of compositions is impossible to generate with sensible degrees of crystallisation and efficient removal. Further, although the HREE range is reproduced well in the Rayleigh fractionation model, the LREE abundances do not vary sufficiently when compared to the sample suite - e.g., Ce varies from 58 to 48x chondrite in the model and 58 to 25x chondrite in the rocks studied. Thus, the involvement of a LREE-rich phase in the fractionation scheme would be required (see also Rollinson and Fowler, in prep.). However, local fractional crystallisation of hornblende cannot be ruled out, especially for the genesis of the extreme rock types, for which partial melting seems inappropriate (e.g., MJ115).

A likely model for an overall intrusive origin would therefore be as follows. Primary melt production took place by variable degrees of partial melting of a compositionally heterogeneous basaltic source, leaving a mineralogically-variable eclogitic residue, and this was followed by only local hornblende fractionation, perhaps during emplacement. This is similar to the models of Jahn and Zhang (1984), and Jahn et al. (1984) for Archaean tonalite-trondhjemite- granodiorite suites in general.

3.2.2 A lower-crustal residue after the abstraction of a granitic partial melt.

Generation and removal of a granitic partial melt from the upper crust has been applied as a genetic mechanism to the Lewisian Complex in particular by Pride and Muecke (1980; 1981) and by many other authors to crustal sequences elsewhere (e.g., Ben Othman et al., 1984). The

former authors hold the view that the precursors to the Scourian Complex were "typical" upper crustal rocks, and in their quantitative modelling exercise (1980) used a greywacke as the parent, presumably in order to gain an average upper crustal analysis. However, they point out that any reasonable starting material should produce similar trends. They contend that the presently exposed Scourian Complex represents the residuum after the genesis and removal of granitic melts, and further, that this was responsible for the observed upward concentration of incompatible elements in the continental crust.

Their trace-element model is based on REEs, Rb, Ba, and Sr and is summarised in Table 3.3, and Fig. 3.9a. It employs the following assumptions:-

i) Scourian gneisses represent the residue.

ii) Equilibrium partial melting took place.

iii) Distribution coefficients for rhyolites (Arth and Hanson, 1975) are applicable.

iv) The trace element content of the precursor is known (greywacke).

	Granulite Facies			Hornblende-granulite Facies			
%melting		20		10		20	40
	Source	Melt	Residue	Melt	Residue	Residues	
Ce	52.3	128	33.3	157	40.7	33.5	24.6
Nd	21.8	-	-	38.4	20.0	18.3	15.9
Sm	4.00	7.58	3.11	4.80	3.90	3.84	3.68
Eu	1.07	0.72	1.16	0.82	1.10	1.12	1.19
Gd	3.38	-	-	2.40	3.10	3.39	3.41
Tb	0.51	0.86	0.42	-	-	-	-
Dy	3.00	-	-	2.40	3.10	3.15	3.30
Er	1.68	-	-	1.43	1.71	1.73	1.80
Yb	1.57	2.89	1.24	1.80	1.55	1.52	1.48
Lu	0.26	0.52	0.19	0.40	0.24	0.23	0.21

Table 3.3: Intracrustal partial melting model for residual granulites, and residual hornblende granulites (values in ppm).

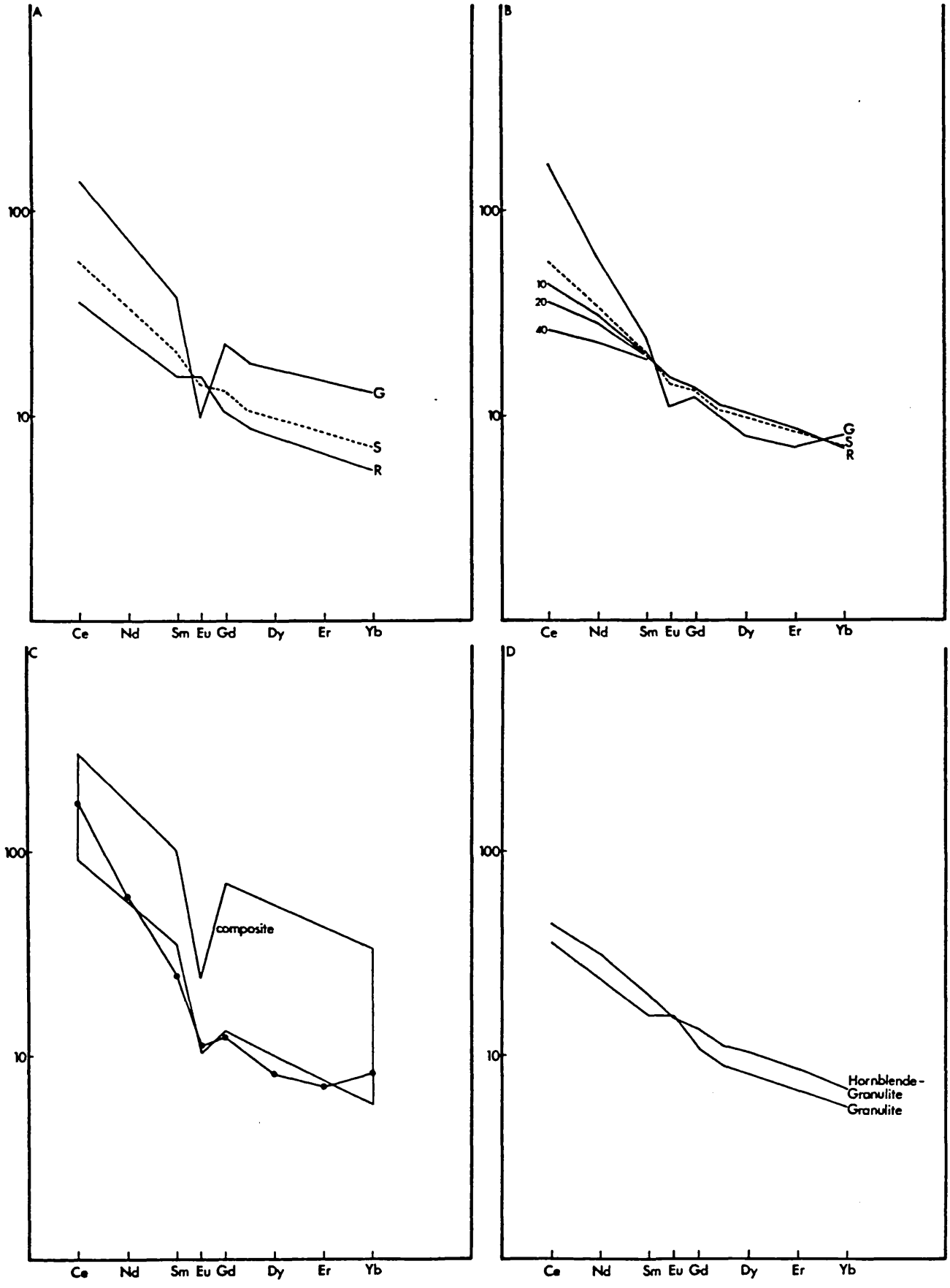


Figure 3.9: Intracrustal partial melting model for residual granulites (A) and residual hornblende-granulite facies gneisses (B).

(C= granite from B compared with granite composite; D= comparison of residues; G= granite; S= source; R= residue).

The residual mineralogy was taken to be a weighted average of the individual gneiss types which comprise the Scourian Complex, which would seemingly require equilibration over rather large distances. Nevertheless, a 20% melt produced a liquid with broadly "granitic" characteristics (LREE- enriched, negative Eu anomaly) and left a residue broadly comparable to some "average" Scourian Complex. Weaver and Tarney (1981) have criticised such a model (using a more likely starting composition - an amphibolite-facies Lewisian gneiss) and suggest that it does not fit the available data in detail.

However, it is now possible to test the intracrustal partial melting model further, by assessing its applicability to hornblende-granulite facies material. The parent composition may reasonably be held the same, as an average representative of the upper crust, but the residual mineralogy is significantly different since it contains hornblende in addition to, and stable with, two pyroxenes (see below). For the purposes of the following model it has been taken as 12% hornblende, 6% orthopyroxene, 6% clinopyroxene, 50% plagioclase and 26% quartz - a typical original metamorphic mineralogy from Gruinard Bay. Calculations for 10, 20 and 40% melting are listed in Table 3.3, and the results are plotted in Fig. 3.9b (note that for the HREEs the 20 and 40% melting values have been omitted for clarity).

The "granites" produced show a highly fractionated, concave-upward LREE pattern, only small negative Eu anomalies, and concave-upward HREE patterns. These are not typical granitic patterns, as shown when compared with Pride and Muecke's (1980) granite composite (Fig. 3.9c). The stability of hornblende also has very important conseqences for the residue: the necessary positive Eu anomaly is not developed, and both the LREE and HREE patterns are required to be increasingly concave-downwards. Comparison of this type of pattern with those derived by analysis of rocks from the Gruinard Bay area reveals that such do not exist.

This evidence strongly suggests that the intracrustal partial melting model is inappropriate to the Lewisian gneisses at Gruinard Bay. Several further points may be made in apparent opposition to the model. There is very little evidence of widespread partial melting during the granulite-facies event, even in areas of relict intrusive relationships where it should be more readily recognisable. Moreover, that which has been recorded (Pride and Muecke, 1982; Rollinson, 1983) produced granitic lithologies with a peculiar trace element composition (especially REE), particularly when compared to "normal" upper crustal granites. Furthermore, the Scourian Complex remains rich in some incompatible elements which should in theory preferentially enter a granitic melt which equilibrated with sensible residual mineralogies (e.g., Ba: Weaver and Tarney, 1980).

Therefore, the following points may be concluded from this simple modelling exercise:

i) There are no differences between Gruinard Bay grey gneisses and Lewisian intermediate-tonalite-trondhjemite lithologies from other metamorphic grades which can be related to magmatic processes.

ii) The gneisses at Gruinard Bay are not the result of the genesis and removal of a granitic melt from upper crustal lithologies.

iii) They are not the result of varying degrees of partial melting of a single homogeneous source.

iv) The intermediate gneisses are more likely to owe their origins to variable degrees of fusion of a compositionally heterogeneous source than fractionation from a more basic melt.

v) Variable degrees of partial melting of a heterogeneous source leaving a mineralogically variable residue probably provided the dominant magmagenetic mechanism for tonalites and trondhjemites, but may have been followed by local hornblende removal to generate the more extreme trondhjemitic lithologies.

CHAPTER FOUR

THE TRANSITIONAL NATURE OF THE BADCALLIAN METAMORPHISM AT GRUINARD BAY

This chapter is divided into three main sections. The first deals with the mineralogy produced during the Badcallian metamorphic phase, as far as it can be determined, and its relationships with that produced by subsequent retrogressive events. The second describes the microscopic distribution of U with respect to the mineralogy, and the third proceeds to consider the LIL element geochemistry of the area compared with that of the metamorphic end-member compositions. Chapter five will then attempt to rationalise these in the light of the controlling reaction mechanisms.

4.1 Mineralogy.

Throughout the Gruinard Bay area the effects of static retrogression are widespread, and locally reach the greenschist facies. Therefore, the preservation of samples which retain the mineralogy imparted during the Badcallian metamorphism is rare, and conflicting evidence exists as to the original metamorphic grade at Gruinard Bay (e.g., Sutton and Watson, 1951; Davies, 1977; Field, 1978; Rollinson and Windley, 1980). Nevertheless, the local preservation of granulites (ss) and hornblende-granulite facies rocks suggests that the early metamorphism may have exceeded the amphibolite facies throughout the area, and calls to mind field relationships such as those in the amphibolite-granulite transition of Southern India (Janardhan et al., 1982; Holt and Wightman, 1983; Allen et al., 1985), outlined above.

Granulite-facies mineralogy.

The granulite facies gneisses have been briefly described by Field (1978) as "typical" granulites. He gave the following modal analysis of the freshest sample: Pleochroic hypersthene (12%), diopsidic

clinopyroxene (7%), quartz (24%), plagioclase (An_{26-32} -48%), ilmenite (5%), biotite (2%), actinolitic amphibole (1%), and accessory zircon and apatite (less than 1%). K feldspar exists only as exsolution blebs in the strongly antiperthitic plagioclase. Even the freshest samples were described as incipiently-retrogressed, with clinopyroxene showing fringes of blue-green amphibole, and orthopyroxene altering marginally and along cracks and cleavage to talc, tremolite +/- opaques. Sometimes an outer rim of blue-green amphibole or biotite exists, also with or without opaques. There is no mention of primary (i.e., stable during the Badcallian metamorphism) biotite or primary amphibole in his description.

Hornblende-granulite facies mineralogy.

Also locally preserved at Gruinard Bay are samples with two pyroxenes, primary amphibole, primary biotite, quartz, and plagioclase as the rock-forming phases. This association is characteristic of the hornblende-granulite sub-facies (De Waard, 1966), and invites comparison with apparently similar rocks from Coll and Tiree (Drury, 1973, 1974). Since retrogression is so widespread, such rocks are rare and the four samples collected by the author are all from the same locality, (see Fig. 2.1). Judging from their petrography, all the samples (MJ036a, b, c and MJ037) are of intermediate- tonalitic major element chemistry, and therefore form part of the main gneiss suite. A complete analysis of one sample (MJ037) is available in the appendix, but the others were too small to give meaningful data. The rocks are medium to coarse-grained and composed essentially of clinopyroxene, orthopyroxene, plagioclase, +/- amphibole, +/- biotite, +/- quartz, with accessory apatite, zircon, allanite, sphene, and Fe-Ti oxides. Incipient later deformation has often caused grain-size reduction along original grain boundaries.

Clinopyroxenes

	MJ036		1	1	2
SiO_2	51.62	52.29	50.60	51.17	52.07
TiO_2	0.37	0.28	0.32	0.31	0.34
Al_2O_3	3.00	2.38	2.85	2.85	3.32
FeO	9.28	8.83	10.24	9.80	10.81
MnO	0.35	0.19	0.30	0.31	0.23
MgO	12.69	13.10	12.25	12.35	11.92
CaO	21.92	22.29	21.93	21.65	20.10
Na_2O	1.06	0.81	0.70	0.72	0.86
Total	100.29	100.17	99.19	99.16	99.65
Si	1.929	1.949	1.922	1.936	1.954
Al	0.071	0.051	0.078	0.064	0.046
Al	0.061	0.054	0.049	0.063	0.101
Ti	0.010	0.008	0.009	0.009	0.010
Fe	0.290	0.275	0.325	0.310	0.339
Mg	0.707	0.728	0.693	0.696	0.667
Mn	0.011	0.006	0.010	0.010	0.007
Ca	0.877	0.890	0.892	0.878	0.808
Na	0.077	0.059	0.055	0.053	0.063

Orthopyroxenes

	MJ036		1	1	2
SiO_2	51.81	52.08	51.26	51.64	51.26
TiO_2	-	-	0.07	0.07	0.12
Al_2O_3	1.30	1.36	1.68	1.68	3.29
FeO	24.81	24.46	23.99	24.38	25.91
MnO	0.49	0.55	0.77	0.68	0.49
MgO	20.49	20.65	20.42	20.39	17.62
CaO	0.50	0.39	0.46	0.54	0.97
Na_2O	0.61	0.70	-	0.03	0.15
Total	100.01	100.19	98.65	99.41	99.81
Si	1.958	1.961	1.956	1.957	1.946
Al	0.042	0.039	0.044	0.043	0.054
Al	0.016	0.021	0.032	0.032	0.093
Ti	-	-	0.002	0.002	0.003
Fe	0.784	0.770	0.766	0.773	0.823
Mg	1.154	1.159	1.161	1.152	0.997
Mn	0.016	0.018	0.025	0.022	0.016
Ca	0.020	0.016	0.019	0.022	0.039
Na	0.045	0.051	0.000	0.002	0.011

Table 4.1: Comparison of pyroxenes from Gruinard Bay gneisses (MJ036) with literature data for granulites.

(1=Rollinson, 1981; 2=Pride and Muecke, 1981)

Orthopyroxene is fresh or altered to a corona of fibrous tremolitic amphibole, giving way outwards to a more actinolitic variety, and is often shot through with veins of fine-grained "uralite", probably similar to the talc-tremolite association described by Field (1978). Electron probe analyses of the pyroxene are given in Table 4.1, from which it can be seen that it is hypersthenic and closely similar in composition to those of true Lewisian granulites.

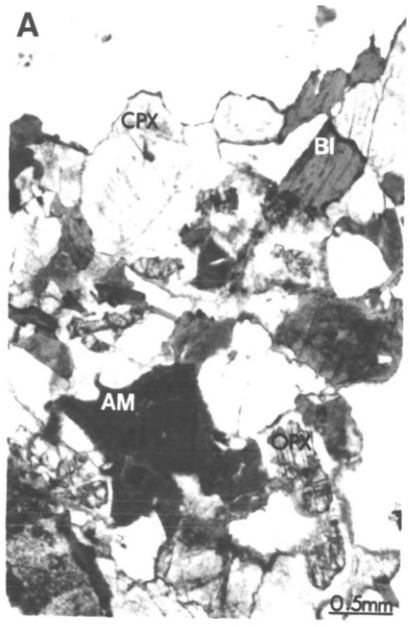
Clinopyroxene is often associated with hypersthene and is diopsidic (see Table 4.1), usually centrally fresh with a retrogressive fringe of bluish-green amphibole. The coexisting orthopyroxene- clinopyroxene pairs may be used as the familiar two-pyroxene geothermometer (Wood and Banno, 1973; Wells 1977; Wood, 1977), and Table 4.2 lists average analyses (no zoning was apparent) and temperatures calculated by both techniques. Comparison of the data with those for granulites (Rollinson, 1981) suggests that the Gruinard Bay samples equilibrated at a significantly lower temperature (700-750°C), consistent with the continued stability of hydrous minerals.

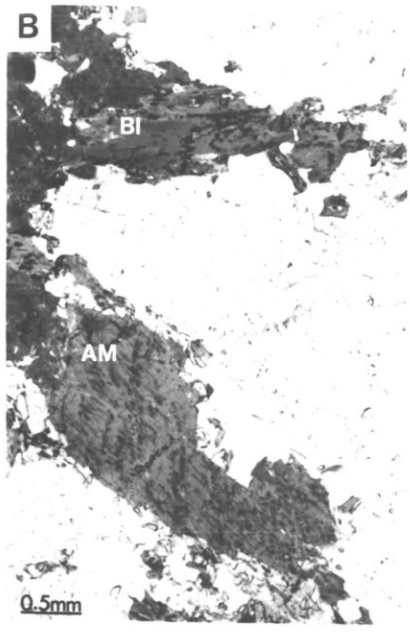
	Opx	Cpx	
SiO_2	51.93	51.78	$a^{cpx} = 0.0149$
TiO_2	-	0.23	
Al_2O_3	1.30	2.84	$a^{opx} = 0.3271$
FeO	24.39	8.76	
MnO	0.57	0.27	$X^{opx} = 0.3798$
MgO	20.61	12.90	
CaO	0.45	22.51	T_1 = 744°C (834°C)
Na_2O	0.57	0.89	
Total	99.83	100.18	T_2 = 723°C (847°C)
Si	1.962	1.933	
Al	0.038	0.067	
Al	0.020	0.058	
Ti	0.000	0.007	
Fe	0.771	0.274	
Mg	1.161	0.718	
Mn	0.018	0.008	
Ca	0.018	0.901	
Na	0.042	0.064	

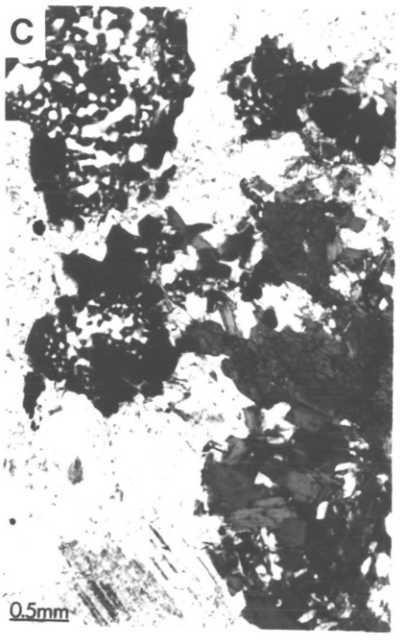
Table 4.2: Two-pyroxene geothermometry.

Opx. = average orthopyroxene; Cpx. = average clinopyroxene, T_1 uses the equation of Wood and Banno (1973), and T_2 uses that of Wells (1977). Figures in brackets are average data for the granulite facies, using the same techniques (Rollinson, 1981).

Amphibole exists as large straw-brown to green pleochroic plates in apparent equilibrium with pyroxene. The typical relationship is illustrated in Plate 4.1a (sample MJ037). The colour of the hornblende is not typical of granulite-facies hornblende, such as that described by Drury (1974) from Coll and Tiree which is brown. This distinctive colour is due to the incorporation of large amounts of Ti in the lattice structure (Stephenson, 1977), enhanced by the presence of new pyroxenes of a composition which cannot accommodate the TiO_2 content of their precursor hydrous phases. The colour of the primary amphiboles at Gruinard Bay might reflect the continued coexistence of high-TiO_2 biotite, whose presence would restrict the entry of Ti into the amphibole lattice. Biotite is not mentioned in the description of hornblende-granulites from Coll and Tiree (Drury, 1973; 1974). Amphibole might therefore retain the lower-grade colour until it becomes essentially the only major phase capable of accomodating Ti. Alternatively, the incipient retrogression which has caused exsolution of Ti-rich phases (ilmenite and/or sphene, see Plate 4.1b) may have resulted in partial loss of an original brown colour. Whatever the reason, such amphiboles are interpreted here as primary phases and mostly have the composition of ferroan pargasitic hornblende (after Leake, 1978; see Table 4.3). They are closely comarable to other hornblende-granulite and granulite-facies amphiboles, as shown by the data taken from the literature (Table 4.3). Stephenson (1977) found that the cation proportion of Ti increases in granulite-facies rocks in a manner essentially independent of whole-rock composition, and cited data of Binns (1969) and Raase (1974) in support. His data suggest that the amphibolite-granulite boundary is marked by a Ti cation proportion of approximately 0.2. This value compares well with those of amphiboles from Gruinard Bay, as illustrated on Fig. 4.1a.







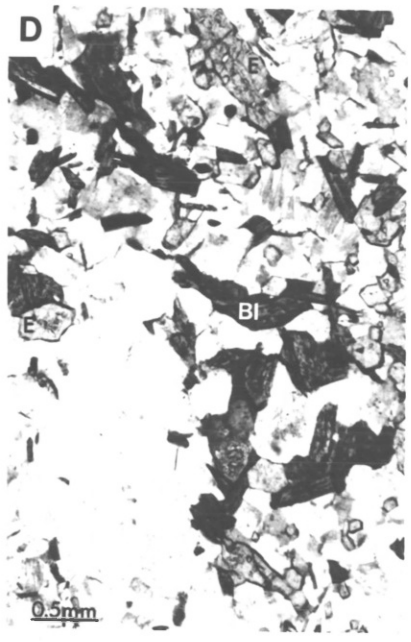


PLATE 4.1 MINERAL ASSEMBLAGES

	Amphibolite Facies[1]	MJ036			Granulite Facies[1]
		Amphiboles.			
SiO_2	42.73	42.78	42.91	42.96	43.32
Al_2O_3	10.71	11.28	11.29	11.14	10.80
FeO	16.02	13.14	12.20	12.62	17.85
Fe_2O_3	2.41	0.79	1.21	0.66	0.49
MgO	9.51	11.40	11.95	11.96	8.83
MnO	0.55	0.13	0.32	0.05	0.30
TiO_2	1.36	1.92	1.94	2.02	2.02
CaO	11.81	11.39	11.33	11.52	11.44
Na_2O	1.40	1.59	1.71	1.66	1.54
K_2O	1.37	1.72	1.71	1.67	1.64
Total	97.87	96.14	96.57	96.26	98.23
Si	6.462	6.464	6.440	6.465	6.535
Al	1.538	1.536	1.560	1.535	1.465
Al	0.372	0.473	0.438	0.441	0.456
Ti	0.155	0.218	0.219	0.229	0.229
Fe^3	0.274	0.090	0.137	0.074	0.055
Mg_2	2.143	2.567	2.673	2.682	1.985
Fe^2	2.026	1.642	1.531	1.574	2.252
Fe^2	-	0.009	-	0.015	-
Mn	0.030	-	0.002	-	0.023
Mn	0.040	0.017	0.039	0.006	0.016
Ca	1.914	1.844	1.822	1.858	1.849
Na	0.046	0.130	0.139	0.121	0.135
Na	0.364	0.335	0.359	0.363	0.315
K	0.264	0.332	0.327	0.321	0.316
		Biotites.			
SiO_2	38.42	36.59	36.81	36.49	39.12
TiO_2	3.33	4.48	4.34	4.39	4.38
Al_2O_3	14.62	14.46	14.43	14.53	14.03
FeO	18.50	16.37	16.55	16.04	19.50
MnO	0.34	0.13	-	0.17	0.14
MgO	11.63	13.03	12.57	13.05	10.56
CaO	0.38	-	-	-	0.27
Na_2O	0.24	0.33	0.15	0.26	0.26
K_2O	9.23	9.78	10.07	9.90	9.19
Total	96.69	95.17	94.92	94.83	97.45
Si	5.737	5.541	5.592	5.542	5.807
Al	2.263	2.459	2.408	2.458	2.193
Al	0.310	0.122	0.176	0.142	0.261
Ti	0.374	0.510	0.496	0.501	0.489
Fe	2.310	2.073	2.103	2.037	2.421
Mn	0.043	0.017	-	0.022	0.018
Mg	2.589	2.941	2.846	2.954	2.336
Ca	0.061	-	-	-	0.043
Na	0.069	0.097	0.044	0.077	0.075
K	1.758	1.889	1.951	1.918	1.740

Table 4.3: Comparison of "primary" amphiboles and biotites from Gruinard Bay (MJ036) with literature data for amphibolite- and granulite-facies minerals. ([1]Data from Stephenson, 1977).

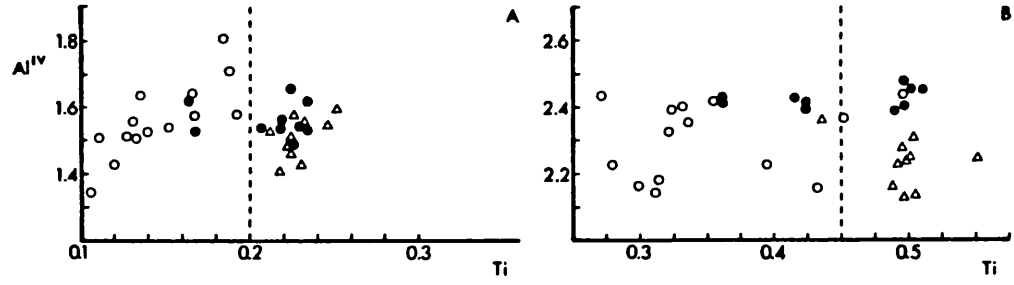


Figure 4.1: Diagramatic comparison of "primary" amphibole (A) and biotite (B) from Gruinard Bay gneisses with literature data for amphibolite-facies and granulite-facies minerals (Stephenson, 1977).
(open circles = amphibolite facies, open triangles = granulite facies, closed circles = Gruinard Bay).

Biotite exists as similar large plates, apparently perfectly stable (see Plate 4.1a), with the deep red-brown colour typical of granulite-facies biotites (e.g., Leelanandum, 1970; Stephenson, 1977). Comparison of their chemistry with that of biotites stable in other hornblende-granulite or granulite-facies regimes (Table 4.3) also reveals a close similarity, especially in the high TiO_2 concentration, which increases towards granulite-facies conditions, independant of whole-rock composition, for reasons similar to those given above for amphibole (see Fig. 4.1b). These large plates of red-brown, high TiO_2 biotite are therefore also interpreted as primary, stable in association with two pyroxenes and amphibole in hornblende-granulite facies conditions during the early metamorphism of the area.

Plagioclase is abundant, often constituting c. 50% of the rock and is a coarse-grained variety approximating to An_{40} (Table 4.4). The distribution of $CaAl_2Si_2O_6$ between plagioclase and clinopyroxene in association with quartz may be used as a geobarometer (Wells, 1977; Rollinson, 1981), which is summarised in Table 4.4. Unfortunately, the assemblage in sample MJ036 constrains the pressure only loosely. It is dependant upon the

Plagioclase analyses.

SiO_2	57.50	57.43	57.30	57.65	57.90
Al_2O_3	26.36	26.71	26.55	26.56	26.93
CaO	8.78	8.70	8.74	8.70	8.74
Na_2O	6.22	6.60	6.41	6.30	6.75
K_2O	0.16	0.25	0.13	0.00	0.12
Total	99.02	99.69	99.13	99.21	100.44
Si	10.387	10.326	10.347	10.382	10.328
Al	5.611	5.659	5.650	5.618	5.660
Al	0.000	0.000	0.000	0.018	0.000
Ca	1.699	1.676	1.691	1.679	1.670
Na	2.178	2.301	2.244	2.200	2.334
K	0.037	0.057	0.030	0.000	0.027
AB	55.65	57.03	56.60	56.72	57.90
AN	43.41	41.55	42.65	43.28	41.43
OR	0.94	1.42	0.76	0.00	0.68

Average clinopyroxene and plagioclase analyses.

SiO_2	51.78		57.56
TiO_2	0.19		-
Al_2O_3	2.53		26.62
FeO	8.76		-
MnO	0.24		-
MgO	12.98		-
CaO	22.39		8.73
Na_2O	0.85		6.46
K_2O	-		0.13
Total	99.73		99.50
Si	1.942	AB	56.79
Al	0.058	AN	42.45
Al	0.053	OR	0.76
Ti	0.005		
Fe	0.275		
Mg	0.725		
Mn	0.008		
Ca	0.900		
Na	0.062		

Pressure estimates.

a) Jadeite calculated first (minimum pressure estimate).
$a^{plag} = 0.4245$; $a^{cpx} = 0.019$
At T = 744°C, P = 6.4 Kb.
At T = 723°C, P = 6.6 Kb. Mean value = 6.5 Kb.

b) Acmite calculated first (maximum pressure estimate).
$a^{plag} = 0.4245$; $a^{cpx} = 0.05$
At T = 744°C, P = 12.0 Kb.
At T = 723°C, P = 12.0 Kb. Mean value = 12.0 Kb.

Table 4.4: Plagioclase analyses from hornblende-granulite facies samples, and plagioclase-clinopyroxene-quartz geobarometry.

order in which the pyroxene end members are calculated (essentially how much Al is assigned to the jadeite component), and limiting cases can be obtained by calculating jadeite first (after Cawthorn and Collerson, 1974) or acmite first. The pressure range generated in this way for these particular compositions is 6.5 to 12.0 Kb. The preliminary P/T data from this study is compared with the well-constrained granulite-facies metamorphism in Fig. 4.2.

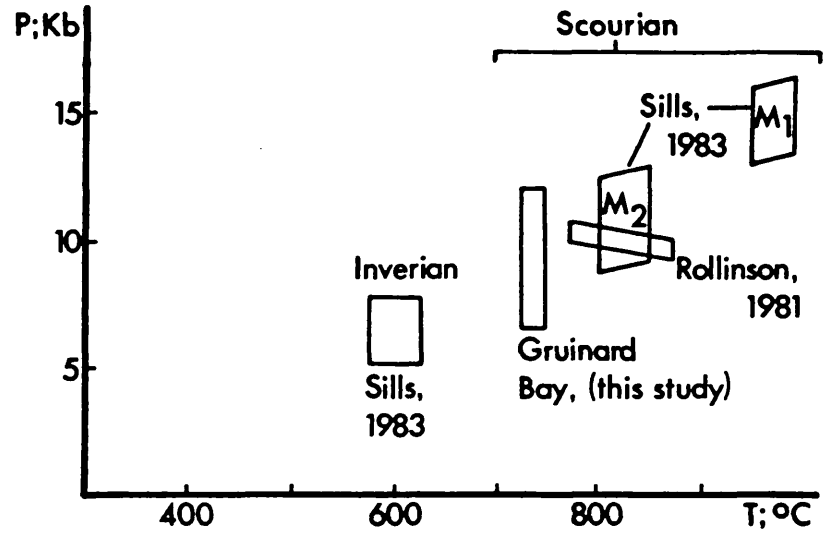


Figure 4.2: Pressure-temperature grid comparing Badcallian metamorphic conditions at Gruinard Bay with those of the granulite facies.

K-feldspar is rare, occurring only as exsolution blebs in plagioclase, except in the intermediate gneisses and trondhjemites where it occurs more commonly as discrete grains.

The grain boundaries of both feldspars are often ragged, as a result of incipient later deformation, and undulatory extinction is common. In hand specimen they show the dark grey-green colour typical in charnockitic granulites to the north.

Quartz has a dark opalescence in hand specimen, and is traversed by many minute needles in an exactly similar way to quartz from Lewisian granulites. The only

difference is the abundance of the rods, which are fewer at Gruinard Bay. If the rods are rutile (they are so small positive identification is impossible), a ready explanation of their restricted occurrence at Gruinard Bay is the continued stability of titaniferous hornblende and biotite.

Accessory phases such as apatite and zircon are also stable in the granulite facies (see below). However, small, euhedral grains of allanite are present in the primary phases at Gruinard Bay, surrounded by pleochroic haloes which provide evidence of a substantial U and/or Th content.

Although it is a large step from the recognition of local hornblende-granulite facies rocks to the assertion that this was the original metamorphic grade of the whole area, evidence that the more typical amphibolite-facies rocks also once contained pyroxenes, primary amphibole and biotite will now be presented.

Amphibolite facies mineralogy.

Pyroxene is not preserved in the amphibolite-facies rocks, but evidence of its former existence is provided by common amphibole-quartz symplectites (Plate 4.1c), similar to those which have been interpreted by other workers (Drury, 1974; Sills, 1983) as being pyroxene-derived.

Amphibole also exists as large crystals with abundant exsolved Ti-rich phases, (ilmenite, rutile or sphene; Plate 4.1b), whose presence suggests an origin as the comparatively high-TiO_2 pargasitic hornblendes described above. However, the two amphibole types are now chemically similar (Table 4.5), probably due to re-equilibration under the lower-grade conditions imposed during retrogression. Nevertheless, the common coexistence of two texturally distinct varieties may be used as a mineralogical basis for the proposal that the now-localised hornblende-granulite facies was once widespread at Gruinard Bay. Supportive geochemical evidence will be described in detail below.

	Amphibole-quartz symplectites			Amphibole, exsolved Ti-rich phases.		
SiO_2	45.03	45.20	44.78	44.07	43.78	44.56
Al_2O_3	10.78	10.83	10.71	11.48	11.48	10.82
FeO	13.80	13.35	13.17	14.63	15.27	15.16
Fe_2O_3	2.16	2.23	3.21	2.20	1.50	1.00
MgO	11.42	11.40	11.46	10.50	10.13	10.69
MnO	0.27	0.28	0.24	0.31	0.36	0.37
TiO_2	0.25	0.22	0.23	0.44	0.59	0.55
CaO	12.02	11.72	12.07	12.01	11.87	12.09
Na_2O	1.69	1.51	1.59	1.62	1.71	1.71
K_2O	0.79	0.72	0.73	0.89	0.81	0.81
Total	98.21	97.45	98.18	98.14	97.50	97.76
Si	6.650	6.696	6.615	6.551	6.560	6.644
Al	1.350	1.304	1.385	1.449	1.441	1.356
Al	0.527	0.587	0.480	0.563	0.587	0.546
Ti	0.028	0.025	0.026	0.049	0.067	0.062
Fe^3	0.240	0.248	0.356	0.246	0.170	0.112
Mg	2.513	2.517	2.523	2.326	2.262	2.375
Fe^2	1.692	1.624	1.615	1.817	1.913	1.891
Fe^2	0.012	0.030	0.012	0.002	0.002	0.015
Mn	0.034	0.035	0.030	0.039	0.044	0.032
Ca	1.902	1.860	1.911	1.913	1.906	1.932
Na	0.052	0.075	0.048	0.047	0.050	0.037
Na	0.432	0.359	0.408	0.420	0.446	0.458
K	0.149	0.136	0.138	0.169	0.155	0.154

Table 4.5: Comparison of texturally-distinct amphibole compositions from amphibolite-facies samples.

Biotite may be divided into two similar populations, one perhaps the result of retrogression of pyroxenes, and the other derived from the high-Ti primary biotite described above, and now rich in exsolved ilmenite and/or sphene (Fig. 4.1b). In some samples which have been retrogressed to a lower grade, prehnite forms along the cleavage directions.

Plagioclase responds to retrogression by forming abundant zoizitic epidote, initially as tiny inclusions which rapidly grow and dominate what was once perfectly fresh plagioclase. The extent of its development is variable, generally being greatest in lower-grade rocks of the epidote-amphibolite or greenschist facies.

Quartz is essentially inert to the retrogressive processes, locally retaining the minute rods and needles

which characterise the high-grade assemblage.

Accessory phases zircon, apatite and allanite remain stable, but an important result of retrogression already intimated is the production of abundant secondary sphene. None has been recorded in the samples with relict Scourian mineralogy.

In sample MJ118, an interesting association of retrogressive minor minerals consists of an aggregate of fine-grained apatite and allanite. This might be interpreted as a derivative assemblage from primary monazite, whose original presence has imparted a LREE, Th and U-rich character to the whole-rock geochemistry and has interesting consequences for radioelement depletion which will be discussed later.

Greenschist facies mineralogy.

These represent the most extensively retrogressed rocks in the sample suite and are relatively rare (3 samples). The best developed greenschist facies assemblage is preserved in sample MJ165 and consists of rare hornblende, epidote, chlorite, calcite and quartz. Plagioclase-derived epidote is abundant, as euhedral crystals or in aggregates, often intergrown with chlorite and calcite. A typical field of view is illustrated in Plate 4.1d. Since it is impossible to derive any meaningful information about the original mineralogy from equilibrated, low-grade rocks of this nature, they will be discussed no further, except where considering the geochemical effects of retrogression.

4.2 Fission-track determination of the distribution of uranium

Since the Lewisian Complex has been subject to a range of metamorphic conditions subsequent to that which is of particular interest to this thesis, there can be little confidence in relating subtle changes in U distribution directly to the Badcallian metamorphic episode. Nevertheless, fission-track radiography is still of particular use if judgements about mineral stability

during the early metamorphism or retrogression can be based on independant criteria. It seems reasonable to expect that identification of the uraniferous phases stable in the hornblende-granulite facies should be possible, and it is to this end that the fission-track work is directed. The comparative suite of granulites is also considered, to help define the mineralogical hosts of the increased U (and Th) complements at Gruinard Bay (see below).

Gruinard Bay gneisses.

Six uraniferous minerals have been identified in the suite of samples from Gruinard Bay, all accessory phases: monazite (or its retrogressive equivalents), zircon, apatite, allanite, sphene and epidote. This is a considerable range considering the U-depleted nature of the host rocks (see below). Allanite, retrogressed monazite and zircon are illustrated in typical habit in Plate 4.2a, b, c, and d, with associated Lexan plastic overlays where appropriate. The others are so poorly-uraniferous that photography was not attempted. Each is briefly described, in turn, below.

Monazite probably once existed in sample MJ118, but is otherwise relatively rare in the sample suite. The products of its retrogression, a fine-grained aggregate of apatite and allanite, are between them capable of accomodating all the original components (essentially LREE, U, Th and phosphate), so it is thought unlikely that the chemical microsystem was open much beyond this mineralogical scale during retrograde reaction. Nevertheless, the original presence of monazite in some of the more acidic rocks is important, since it can accomodate a substantial U, Th and LREE component, and will therefore influence the progress of radioelement depletion on its host.

Zircon is an ubiquitous uraniferous phase in the Lewisian gneisses from Gruinard Bay, and varies from euhedral or subhedral crystals with markedly heterogeneous U distribution to relatively large, ovoid

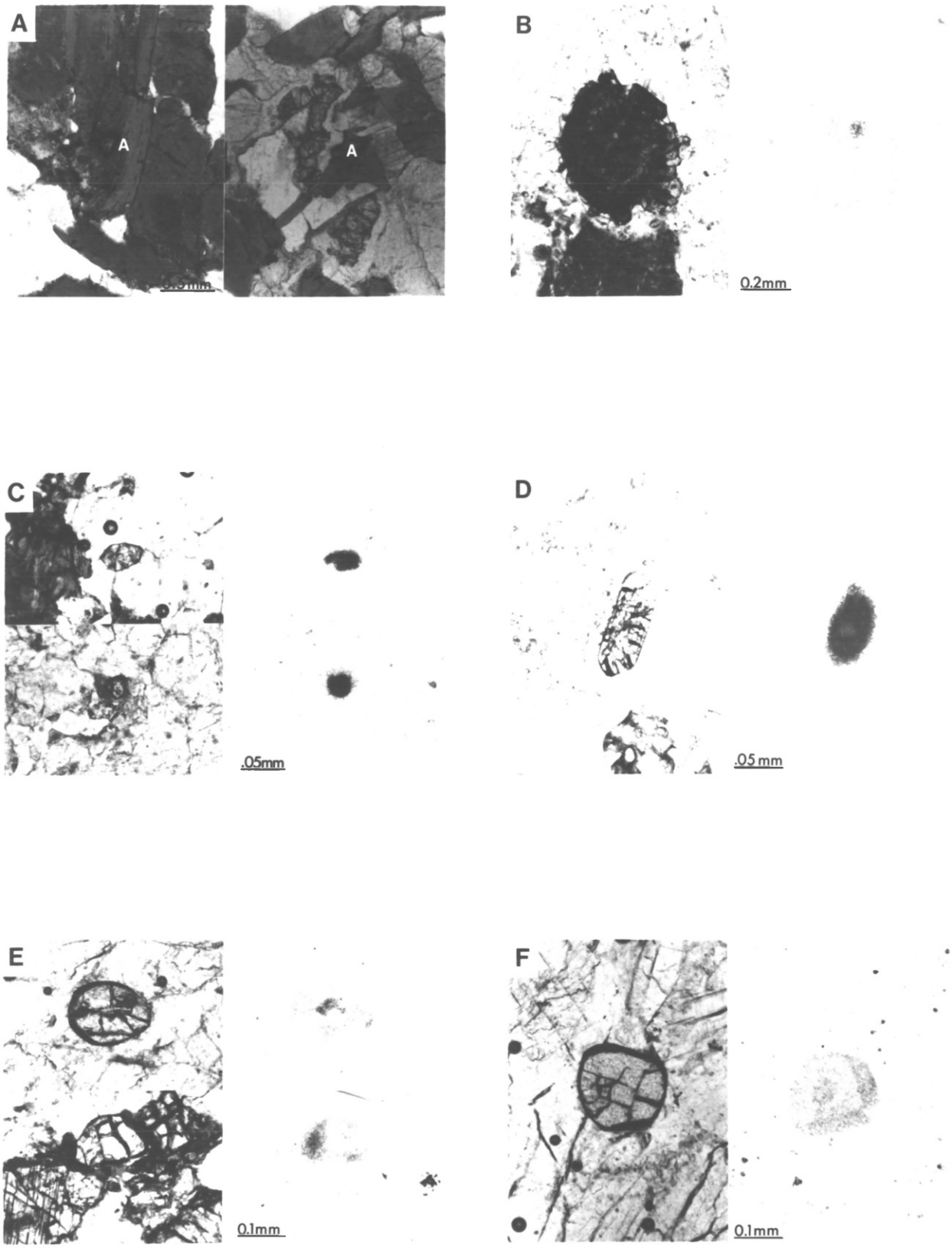


PLATE 4.2 U, Th—RICH MINERALS

varieties with a more homogeneous U distribution. The latter seem similar to the metamorphic zircons described by Pidgeon and Bowes (1972) and Lyon et al. (1973). Although it is tempting to suggest that the heterogeneous U distribution in euhedral zircons is the result of selective U removal during the high-grade metamorphism, little confidence can be assigned because of the protracted post-Badcallian metamorphic history. Nevertheless, other evidence will be presented later to suggest that U is lost from the zircon lattice structure during recrystallisation associated with the metamorphic event.

Apatite is another ubiquitous U-bearing accessory phase in the Gruinard Bay gneisses. Whole-rock geochemical evidence suggests that apatite fractionation or stability in the residua of partial melting may have been important in the generation of most samples (c.f. Rollinson and Windley, 1980b). It generally forms large, euhedral grains in which U is distributed homogeneously.

Allanite occurs in rocks at all stages of retrogression as rare inclusions in the rock-forming minerals, and is euhedral in outline and often internally zoned. In the hornblende-granulite facies rocks its host is usually either of the hydrous phases, amphibole or biotite. Electron probe analyses are given in Table 4.6. Although its modal abundance is low, it seems to have a recognisable effect on the whole-rock Th content and may be responsible for the relatively high Th contents of the Gruinard Bay gneisses when compared to equivalent granulites, in which no allanite has been detected (see below).

SiO_2	33.51	33.60	33.65	34.42
TiO_2	0.64	1.46	0.60	0.58
Al_2O_3	18.05	17.20	17.38	16.28
La_2O_3	4.35	4.69	4.33	4.36
Ce_2O_3	10.31	9.99	10.45	10.12
Nd_2O_3	2.74	2.49	2.92	2.91
FeO	11.48	12.00	11.89	11.81
MgO	2.14	2.80	2.34	3.15
CaO	12.13	11.83	11.94	10.49
H_2O*	1.62	1.63	1.62	1.60
Total	96.97	97.69	97.12	95.72

Table 4.6: Allanite analyses from hornblende-granulite facies samples.

Sphene is a widespread minor mineral phase in the Gruinard Bay suite, but occurs entirely as a product of retrogression. In the early stages it is often present as very small, exsolved grains along the cleavage directions of originally Ti-rich biotite or pargasitic hornblende. As the process proceeds, larger grains nucleate, often on an ilmenite parent. The sphene is in all cases very poorly uraniferous, often registering virtually no fission tracks from a "saturation" neutron dose, and this may be cited as evidence for the U-poor nature of the early retrogressive fluids.

Epidote is also wholly retrogressive, and is most abundant in the lowest-grade rocks. Early stages of retrogression are marked by nucleation of small grains in plagioclase, which increase in size and sometimes coalesce to form an extensive network of interlocking crystals. It is also very poorly uraniferous, and since it represents a later stage in the sequence of retrograde re-equilibration, it seems likely that the fluids responsible may have been U-poor throughout.

Granulite facies gneisses.

In all the rocks collected from the granulite facies Central Belt, only two significantly uraniferous phases have been identified: zircon (Plate 4.2e and f) and apatite, and even these generally show a rather lower U abundance than at Gruinard Bay.

Zircon has the morphology and occurrence described in detail by Pidgeon and Bowes (1972), in a study of the Pb-isotope relationships. An estimate of its bulk U content provided by these authors (50 ppm) is an order of magnitude lower than that of comparable amphibolite-facies examples (Pidgeon and Aftalion, 1972; Lyon et al., 1973) and close to U values derived from mantle zircons (5 - 40 ppm). Lewisian, granulite-facies zircon therefore represents some of the most poorly-uraniferous crustal zircon known (Watson et al., 1982). Nevertheless, the Lexan plastic overlays show a significant U content, sometimes with a weakly

heterogeneous distribution, and it is probable that zircon is the host for the bulk of the U in these rocks.

Apatite is the only other uraniferous phase which has been identified in the common granulite-facies gneisses, and generally forms large grains with a very low U content. Its rather high modal abundance relative to that of zircon suggests that it might be a significant contributor to the whole-rock U value.

Sphene and Epidote are again purely retrogressive in origin and very poorly uraniferous, attesting to the generally U-poor nature of the late, hydrous fluids.

4.3 Large-Ion Lithophile Element Interfacies Variations

It has been shown above that there are significant mineralogical differences between the primary assemblage of Gruinard Bay gneisses and comparable granulites. These might be expected to be related to sympathetic differences in whole-rock LILE content. It is implicit in the following text that the LILE abundance variations between Gruinard Bay gneisses and the metamorphic end members are a direct consequence of differing physico-chemical conditions during the Badcallian high-grade metamorphism. Therefore, it is important to present at this stage the several lines of evidence that indicate the insignificant contribution to LILE mobility made by the multiple phases of retrograde re-equilibration which have affected the Complex to varying degrees.

Although Drury (1974) has presented data which suggest retrogressive enrichment of Rb and Th in Lewisian gneisses from Coll and Tiree, there is no evidence from the mainland central block that substantial mass transfer (except for H_2O) occurred during Inverian or Laxfordian events. Indeed, evidence from a statistically large sample suite indicates that this does not occur, and that amphibolite-facies rocks generated by retrogression of granulites may be distinguished from primary amphibolite-facies samples by their relict,

minimal LILE content, high K/Rb and low Rb/Sr ratios (Tarney et al., 1972; Sheraton et al., 1973). Although some redistribution of elements will necessarily result from the substantial recrystallisation caused by hydration (Beach and Tarney, 1978), the whole-rock system apparently remained essentially closed except to H_2O, or in regions of high strain (Beach, 1976) which were avoided for the purposes of this study. Moreover, although the Pb isotope data of Moorbath et al. (1969) permit limited Laxfordian remobilisation of U, they do not allow any substantial influx into the complex.

Furthermore, if the late, lower-grade metamorphic episodes preserved in the rocks at Gruinard Bay were responsible for the detailed LILE characteristics of the area, these should show some relationship with the resultant mineralogical alteration. However, interelement bivariate plots of the four "depleteable" elements (see Fig. 4.5 below), on which are distinguished the "less-retrogressed" amphibolite-facies samples (marked 1) and the most-retrogressed samples (greenschist-facies; marked 2), show that there is no obvious relationship of LILE abundance with extent of retrogression. This strongly suggests that they may be related directly to the Badcallian high-grade metamorphism, in exactly the same way as before.

Another way of approaching the problem is to construct multi-element, comparative diagrams of retrogressed, less-retrogressed and fresh, hornblende-granulite facies lithologies. This is done in Fig. 4.3, which compares hornblende-granulite facies sample MJ037 with retrogressed equivalents of comparable "immobile" element chemistry, from which it is difficult to discern any significant LILE enhancement due to rehydration of the rocks. Moreover, retrograde minerals whose lattice structure is amenable to substantial incorporation of U, such as sphene and epidote, have been shown to be distinctly poor in this element, suggesting a similar impoverishment in the fluid with which they equilibrated. The formation of such minerals is

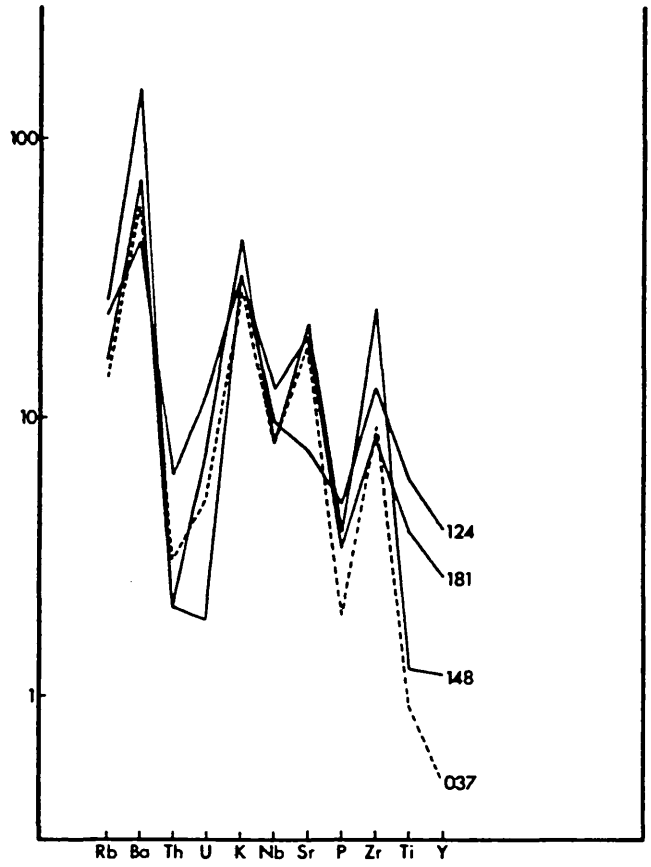


Figure 4.3: Mantle-normalised incompatible element plot comparing hornblende-granulite facies sample MJ037 with statically-retrogressed gneisses.

therefore unlikely to have caused any major perturbations in the pre-existing whole-rock U budget.

These features together argue strongly against the hypothesis that the LILE characteristics of the Gruinard Bay Lewisian gneisses are the result of retrograde processes operating on original granulites, or indeed on original amphibolite-facies rocks. In the following paragraphs they will therefore be related entirely to the Badcallian high-grade metamorphic event.

The geochemically transitional status of the Gruinard Bay area may be investigated first by consideration of data for the whole suite. Therefore, the complete LILE data are presented for comparison with Lewisian gneisses of other metamorphic grades both in histogram form and as graphical interelement plots (Figs. 4.4 and

4.5). Only broad conclusions concerning the LILE content of the area in general may be drawn from this exercise, and specific evidence regarding the mechanics of depletion will be sought from a more detailed consideration of better-constrained lithological groups. Thus, the discussion then proceeds on the basis of three whole-rock geochemical classes so that a more detailed analysis of element relationships and reaction mechanisms may be undertaken.

4.3.1 Data for the whole suite.

The LILEs are dealt with in two groups according to their mineralogical hosts - Rb and K which substitute in major rock-forming minerals; and U and Th whose distribution is controlled essentially by minor mineral phases. A complete listing of the analytical data is available in the appendix.

Rubidium and Potassium

The relationship between Rb and K depletion is of some importance since the K/Rb ratio of lower crustal lithologies is often referred to as a sensitive indicator of granulite-facies processes. Fig. 4.4 shows the data in histogram form and for comparative purposes the average values for Assynt gneisses (X^4) and amphibolite-facies gneisses (X^2) from Sheraton et al., (1973) have been used. Several points are immediately apparent. It is clear that although K_2O abundances at Gruinard Bay are quasi-granulitic, some significant differences are preserved, since Gruinard Bay does form a distinct field and has slightly higher K_2O on average.

On the other hand, Rb levels are distinct from both metamorphic end members. Of the four LILEs considered here, Rb most closely approximates to a median level and can be used definitively to distinguish Gruinard Bay from amphibolite and granulite-facies compositions. There are intriguing consequences for the K/Rb ratio at Gruinard Bay, whose average remains relatively low (c. 450) and has been quoted as a true amphibolite-

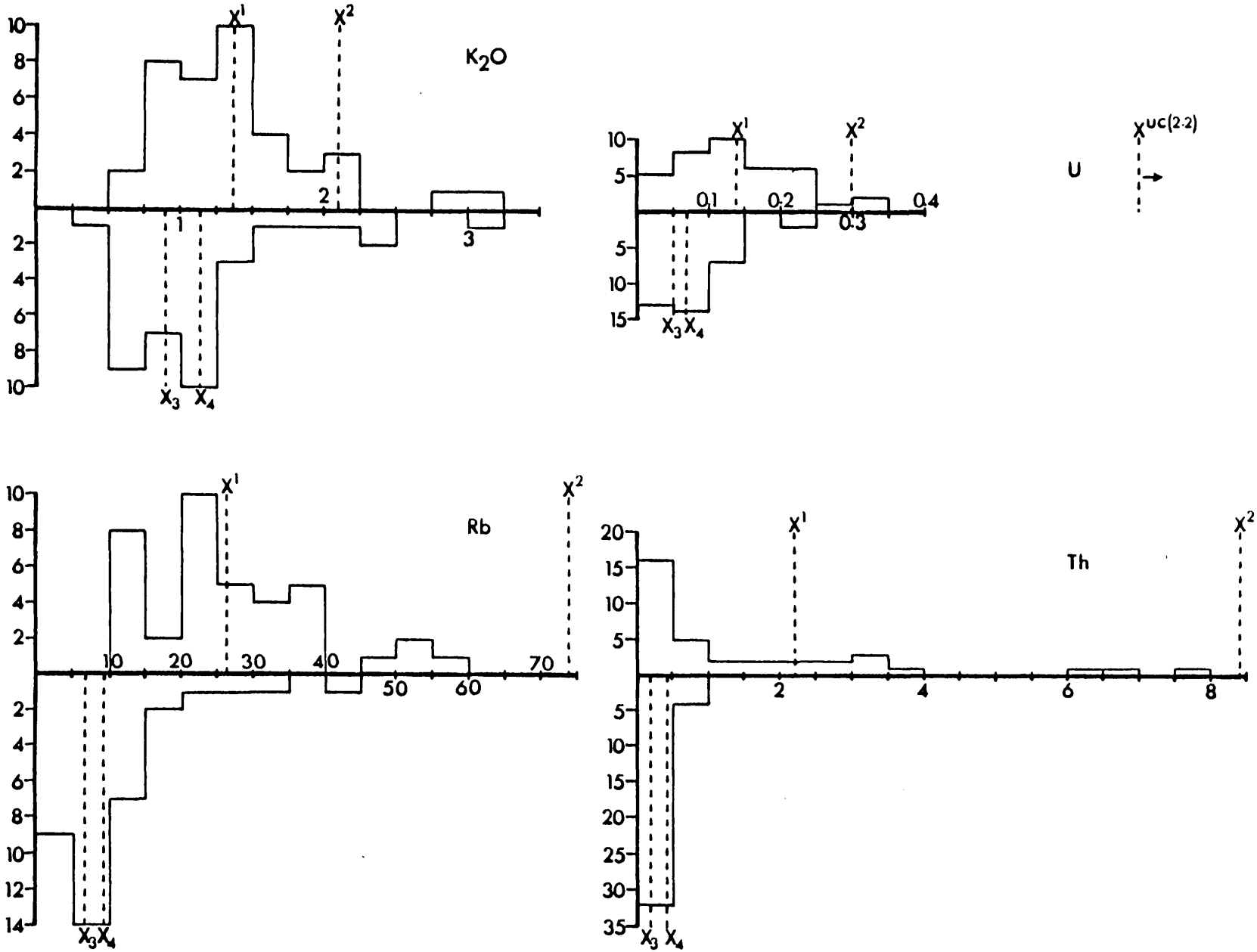


Figure 4.4: Histograms of LILE abundances in Gruinard Bay gneisses (top) compared with granulite-facies data (bottom, this study) and literature data.

(X^1= average Gruinard Bay; X^2= average literature amphibolite facies; X^3= average granulite (this study); X^4= average literature granulite; uc= upper crust average).

facies value (Rollinson and Windley, 1980). The fractionating effect of high pressure, granulite- grade metamorphism is illustrated on Fig. 4.5, a logarithmic, bivariate plot of K vs Rb abundance. Data from Gruinard Bay (both this study as plotted and from Rollinson and Windley, 1980) plot precisely between the fields of data for the metamorphic end-members. Data from hornblende-granulite-facies rocks lacking primary biotite (Drury, 1974) have an average K/Rb of 675, slightly to the high-grade side of Gruinard Bay. Clearly, the increase in K/Rb is remarkably systematic, there being a continuum of values from low in the amphibolite facies through progressively more dehydrated rocks (including the stable hornblende-granulite facies regions) to exceptionally high values in true, anhydrous granulites. The significance of mineralogy in relation to this ratio is exemplified by the difference between biotite-bearing hornblende granulites (450) and biotite-free hornblende granulites (675). Clearly, the Gruinard Bay region can no longer be regarded as typical of the amphibolite facies. Rather, the failure of the K/Rb ratio to respond significantly to demonstrable depletion can be seen as a natural consequence of the simultaneous removal of both elements. The rapid rise to K/Rb ratios characteristic of the granulite facies apparently only becomes possible when the available K reservoir has been almost exhausted, such that further removal of Rb allows the required inter-element fractionation. At Gruinard Bay, the complete granulite-facies range of K_2O has already developed (Fig. 4.5), but Rb has yet to approach its granulitic minimum. It might be envisaged, therefore, that very high K/Rb ratios would have soon been generated had the process not been prematurely arrested, as is the case on Coll and Tiree (Drury, 1974).

Uranium and Thorium

Although it has been suggested that U data for Lewisian lithologies are abundant (e.g., Rollinson and

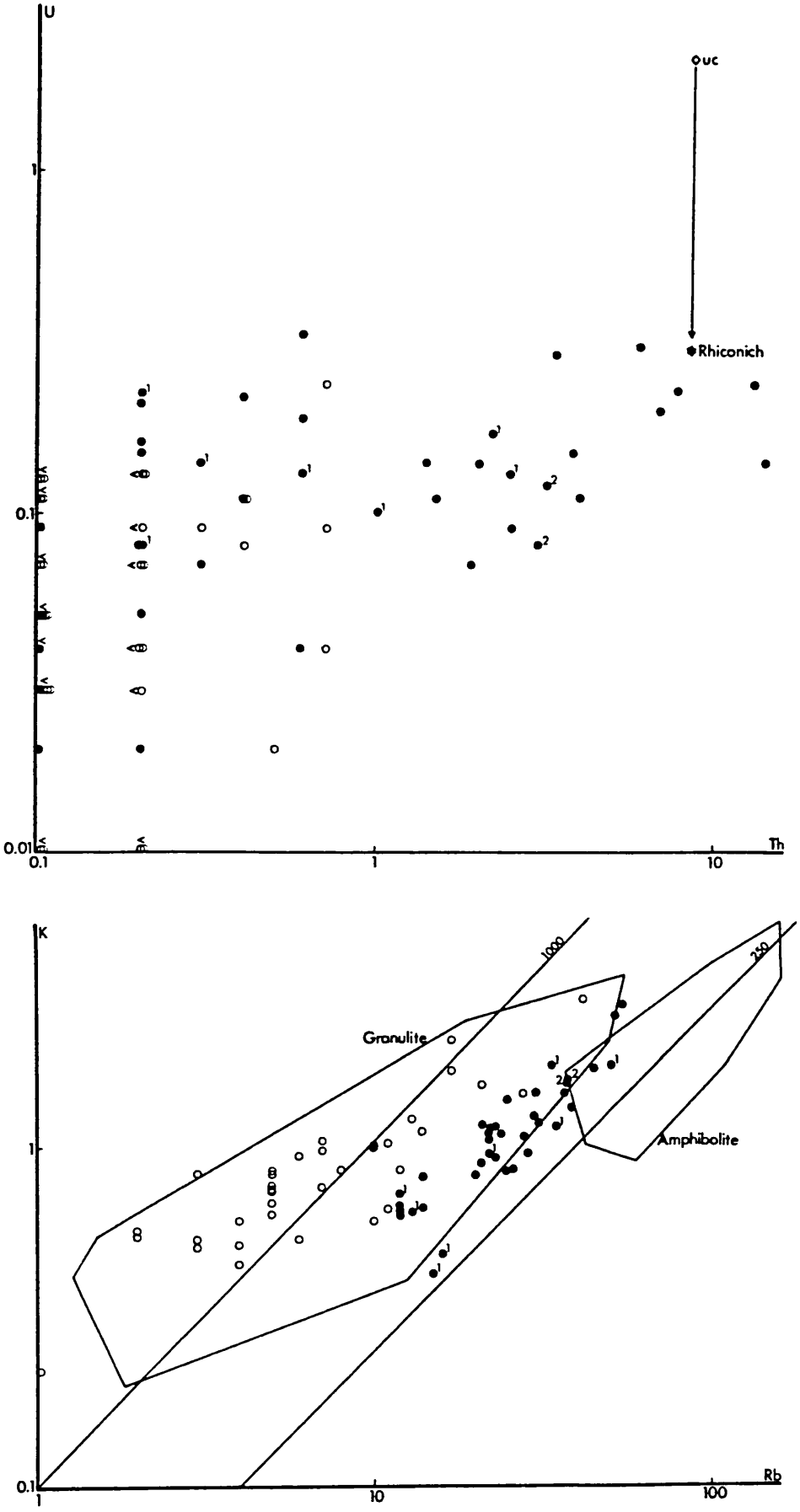


Figure 4.5: Logarithmic bivariate plots of K vs. Rb and U vs. Th in Gruinard Bay gneisses compared with granulite-facies data (this study) and literature data. (closed circles= Gruinard Bay gneisses; open circles= granulites; uc= upper crust average; fields of data from Sheraton et al., 1973).

Windley, 1980), most in fact originate in the early isotopic work of Moorbath et al. (1969), with a notable addition by Pride and Muecke (1980), and are thus still relatively scarce. Any presented here therefore represent a significant addition to the set, and for the reasons outlined in the Introduction, data for the central block granulite-facies suite are also incorporated. The comparability of the data sets can be assessed from their average values (this study: x_u granulite = 0.07 ppm, n = 38; Moorbath et al., 1969: x_u granulite = 0.05 ppm, n = 5; Pride and Muecke, 1980: x_u granulite = 0.05 ppm, n = 7). The mean U value of samples from Gruinard Bay is significantly higher (0.13 ppm) than that for the granulites (0.07 ppm) and the histogram (Fig. 4.4) clearly shows a systematic displacement towards higher values at Gruinard Bay. However, the data do not remotely approach those of the amphibolite facies, summarised by the average values of 2.2 ppm taken from Weaver and Tarney (1984), and 0.3 ppm from the Rhiconich data of Moorbath et al., (1969). 2.2 ppm is of the same order as U values in a comparable amphibolite-facies Archaean tonalite-trondhjemite-granodiorite suite studied by Bickle et al. (1983). Therefore, the amphibolite-facies rocks from Rhiconich have probably already lost part of their original U content - in accord with Pb-isotopic data (Moorbath et al., 1969). Watson et al. (1982) suggested that this fraction might represent that originally located on intergrain boundaries, which would have provided the most leachable U site within the framework of the rock.

The Th histogram reveals an interfacies relationship similar to that of U, but the data from Gruinard Bay lie closer to a median value between the metamorphic end members. It has been noted above that allanite is stable in rocks retaining hornblende-granulite facies mineralogy from Gruinard Bay, but not in true granulites. This might provide a ready explanation of the rather higher radioelement contents at Gruinard Bay, and the observed interelement differences (i.e. Th is in

general less depleted than U; allanite contains more Th than U). However, as intimated in the section on fission-track radiography and discussed in more detail later, this is only part of a complex story also involving radioelement removal from phases that are stable under both regimes. The Th vs. U plot (Fig. 4.5) exemplifies the granulite vs. Gruinard Bay discrepencies; suggests a broad equivalence of increasing U with increasing Th; and demonstrates the generally greater Gruinard Bay gneiss to granulite disparity for Th than U. It also suggests that in a few samples the radioelements are themselves fundamentally fractionated. That this can be related to whole-rock chemical and mineralogical features, and may be important in unravelling some of the mineralogical controls on depletion mechanics is also discussed in a following section.

Further general information might perhaps be derived from a consideration of the relationship between removal of the two element groups (K + Rb; U + Th). If the progress of depletion is controlled principally by the availability of the transporting medium, then a close correlation between all the affected elements would be expected. This would be the case if the rate of element release exceeded the rate of fluid supply (be it melt, aqueous or carbonic). However, Fig. 4.6 (U vs. Rb) demonstrates a general lack of correspondence between the groups, which suggests that restriction of fluid supply is not the most important factor. This being so, the rate-determining step might be either the release of LILEs, i.e., the sum of the mineralogical reactions which free U, Th, Rb and K to a sufficiency of transporting medium; or the rate at which they are stabilised in that medium. In the former case, the role of mineralogy becomes determinative, and close correlations may be expected only between elements whose residence sites are similar and which are therefore subject to the same prograde phase stability relationships. In the latter, the composition of the

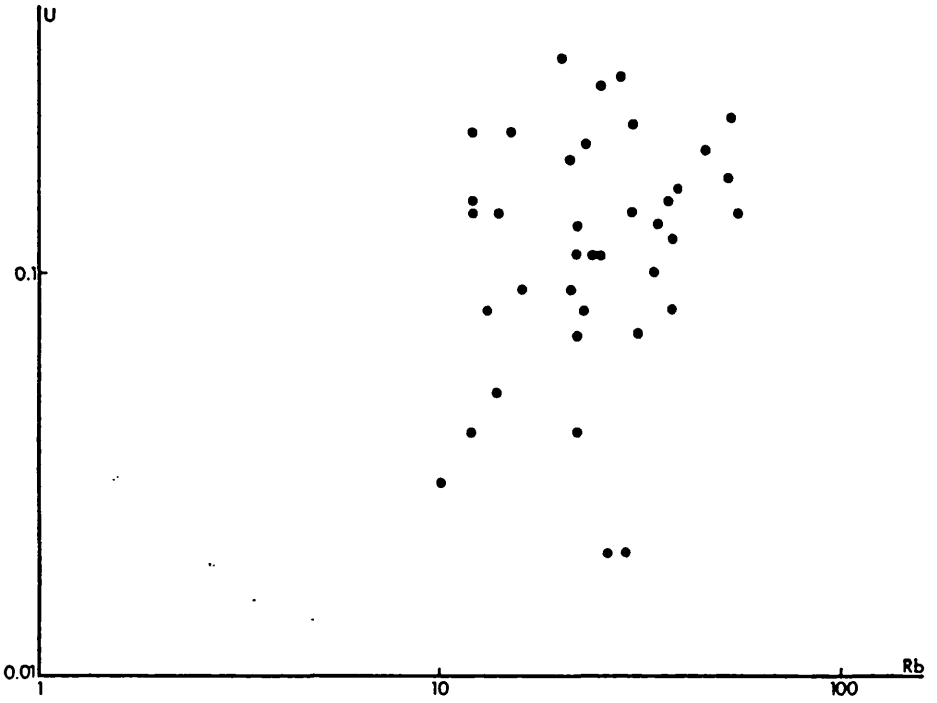


Figure 4.6: Logarithmic bivariate plot of U vs. Rb in Gruinard Bay gneisses.

fluid is vital and close relationships would be expected between elements whose stability is subject to similar factors. Either (or both) could be the case at Gruinard Bay. Moreover, recent evidence suggests that composition of metamorphic fluids may be significantly buffered by that of the local lithology, which would effectively complicate matters further. Before attempting to throw some light on these problems, it is essential to demonstrate that the transitional nature of Gruinard Bay gneisses is not the spurious result of bias towards a non-representative sample composition. Accordingly, further analysis proceeds by comparison of three rock groups with closely-comparable whole-rock "immobile element" chemistry.

4.3.2 A comparison of specific rock groups.

Rollinson and Windley (1980) introduced the concept of selective depletion by demonstrating that granitic rocks were not Rb- or K-poor, even when at granulite grade. Apart from its intrinsic theoretical attraction, it has

received support in several subsequent publications (e.g., Barbey and Cuney, 1982; Okeke et al., 1983). Further, it has been shown above that the gross characteristics of the Gruinard Bay suite also indicate a "differential" process - i.e., the progress of abstraction of each element is dependent upon its own particular set of controls, resulting in some elements more closely approaching complete removal (defined as granulite-facies levels) than others. Lastly, the very existence of hornblende-granulite facies zones at Gruinard Bay and on Coll and Tiree (Drury, 1974) with the transitional element abundances outlined above, shows that the process is progressive, and not simply a case of granulite (ss) or amphibolite facies (ss).

The identification of the zone of transitional LILE abundance offers the opportunity for a detailed assessment of the depletion process in relation to these concepts. In order that a more specific comparative assessment might be successful, it is important that the samples used are lithologically and chemically similar in respect of those elements not mobile during the high-grade metamorphic event. Three silica intervals have been chosen (50-60%; 60-70% and greater than 70% SiO_2, termed "intermediate", "tonalitic" and "trondhjemitic" respectively) for the initial screening, but similarity on the basis of immobile elements as plotted on multi-element, mantle-normalised diagrams is the requirement used for meaningful inter-facies comparison.

Selective element depletion

As stated above, this concept was specifically introduced by Rollinson and Windley (1980) who applied it to the removal of LILEs from some rock types, but not from others. They studied a granulite-grade tonalite-trondhjemite-granodiorite-granite suite from the type granulite area near Scourie, concluding that the granite sheets were not depleted in any way, or had lost the same fixed proportion of Rb and K such that original,

magmatic differences remained discernable. In contrast,the tonalites and trondhjemites were found to be strongly LILE-depleted. The relevance of the term "selective" to the intermediate-tonalite-trondhjemite suite of this study may be tested by careful comparison of selected end-member rock types representing the three silica intervals. Fig. 4.7 shows a series of multi-element plots of average granulite-facies rocks from each class normalised to equivalent amphibolite-facies representatives, designed to highlight any differences between the absolute fraction of the original LILE complement lost during the high-grade metamorphism. The data sources are Weaver and Tarney (1980, 1981).

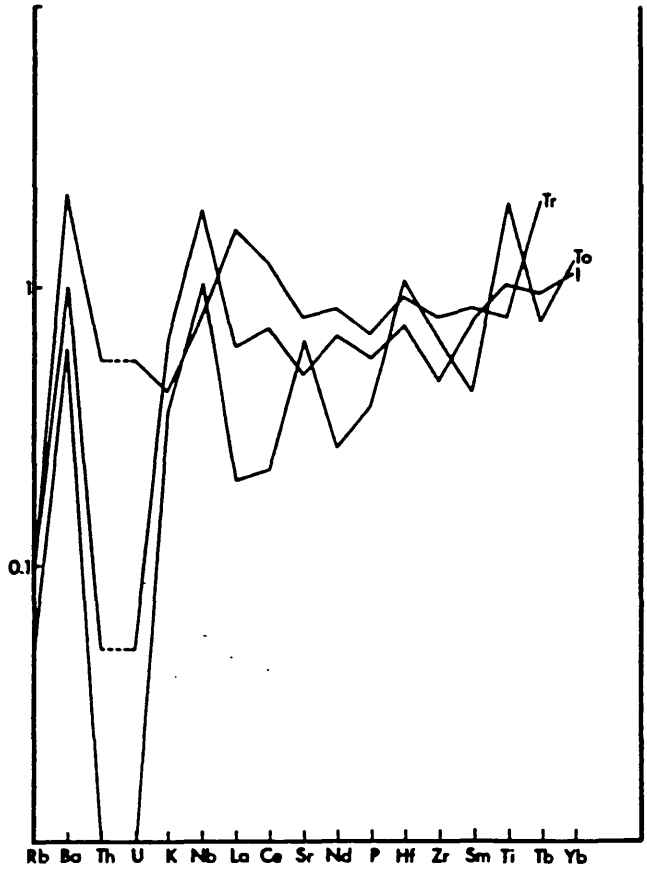


Figure 4.7: Amphibolite-facies-normalised incompatible element plot of intermediate, tonalitic and trondhjemitic granulites.

This diagram shows that the major fractionation resulting from granulite-facies metamorphism is specific

to Rb, Th, U and K (although the latter is much better shown by larger data sets above). Rb is removed to a fairly constant one tenth of its original value in all three rock groups. Selective depletion is best shown by Th (and U?). The tonalites appear to have lost the largest fraction (about 0.98) of their original budget, intermediate rocks are the next most severely affected (about 0.95) and trondhjemites least of all (about 0.45). It should be pointed out that the high average values of Th (and U?) for granulite-facies trondhjemites are imparted by a single sample (16Y) but this nevertheless suggests the local presence of anomalously high Th (and U?) abundance in rocks of trondhjemitic chemistry, also reflected in the data set for rocks from Gruinard Bay (see below). However, as far as samples of granulite-facies, intermediate to trondhjemitic rocks are concerned, although some selective element removal is indicated, perhaps the most striking feature is the essential similarity of the three lithochemical groups. Another way of investigating the selective nature of the depletion process is to consider the bulk element data from Gruinard Bay plotted against silica percentage, in order to distinguish isolated samples with high LILE values. Only Th suggests a significant selective effect (Fig. 4.8), apparently confirming that the extremes of the compositional range retain isolated examples with high Th (eg., sample MJ128 with 13ppm Th at 51% SiO_2 and sample MJ118 with 14ppm Th at 71.8% SiO_2).

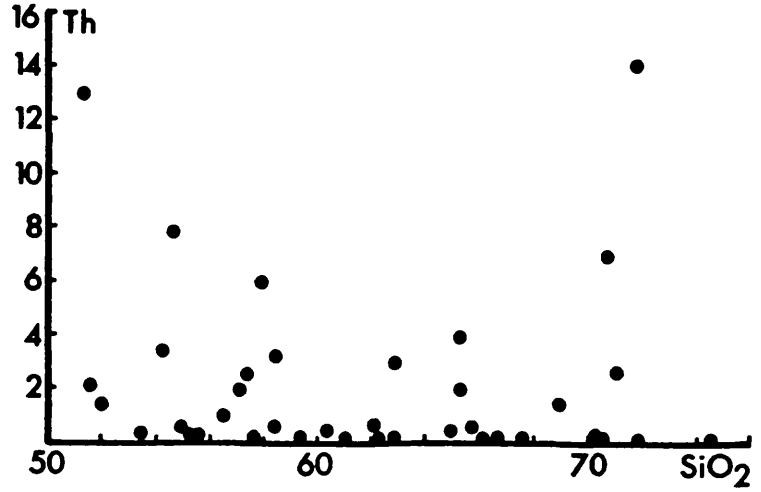


Figure 4.8: Th Harker diagram for Gruinard Bay gneisses.

Differential element depletion

Just as selective depletion indicates differences in behaviour of rock types, this term is intended to describe the differences in behaviour of individual elements as a result of the depletion process(es). For example, in the context of complete extraction at granulite grade differences exist in the absolute fraction of the original element budgets removed. In tonalites, Rb loses about 0.95x its original abundance; U and Th about 0.99 and K about 0.65 on average (Fig. 4.7). A direct result of this "differential depletion" is the increasing K/Rb ratio, due to the fractionation of Rb from K.

Progressive element depletion

The selective and differential nature of the depletion process that has been demonstrated above is perfectly clear from a close study of the literature, and indeed published data have been used extensively in order to emphasise their importance. The significance of a distinct hornblende-granulite subfacies with transitional element abundances is that these features of element depletion can also be shown to be progressive in their operation. Moreover, it is now possible to define one further stage in the removal of the LILEs and thus to place additional constraints on the mechanisms involved.

It has been shown on the basis of data for the whole suite, that the imposition of anhydrous conditions is gradual and systematic, as exemplified by the regular increase in K/Rb ratios from amphibolite facies through biotite-bearing hornblende-granulites (Gruinard Bay) and biotite-free hornblende-granulites (Coll and Tiree) to genuine granulite-facies lithologies. In order to assess this and other "progressive" features in more detail, reference can be made to mantle-normalised multi-element diagrams (Figs. 4.9 to 4.11), for intermediate, tonalitic and trondhjemitic samples. Each is itself divided into four - a,b,c and d. Part a shows the patterns of the available literature analyses for the

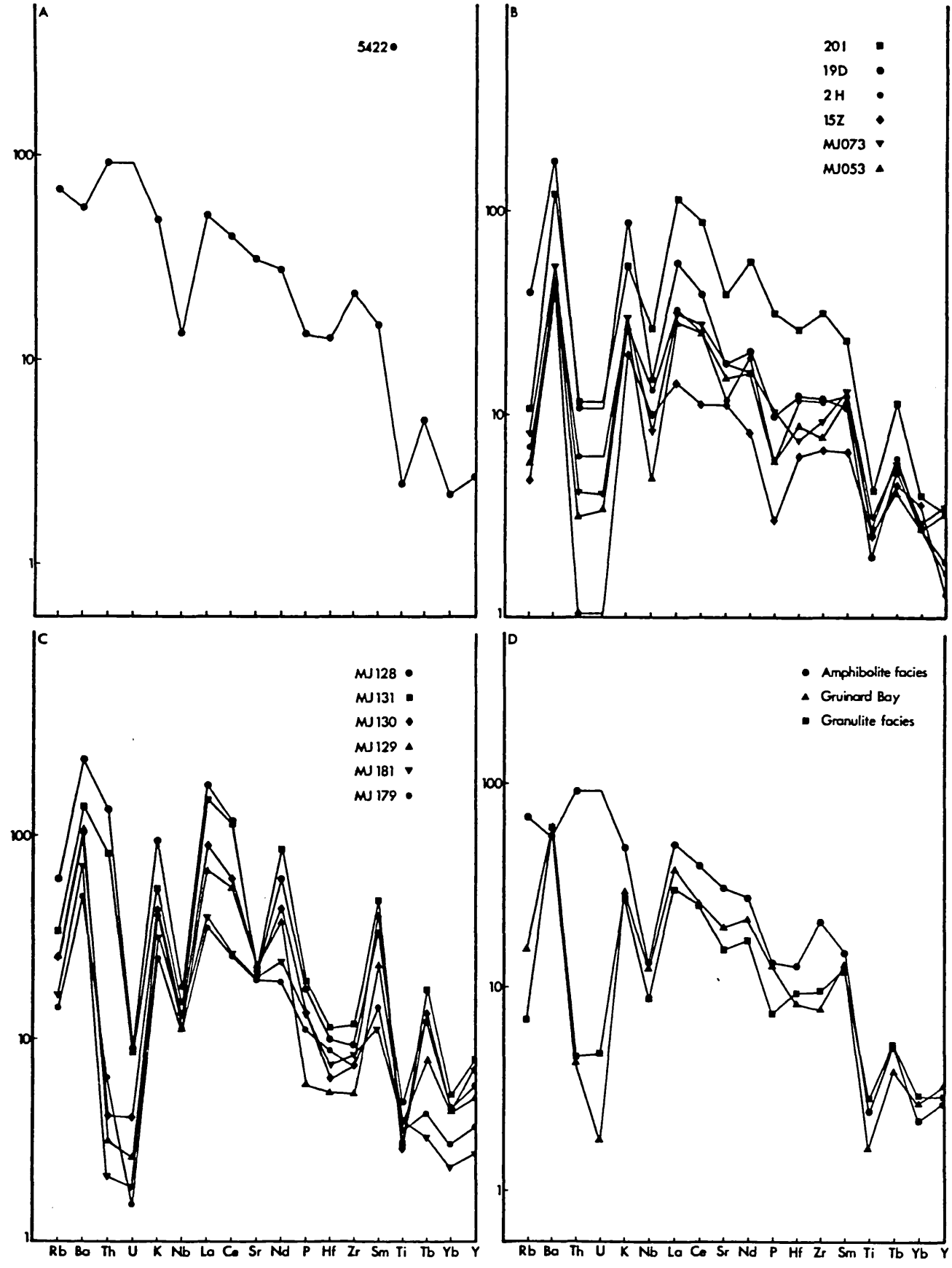


Figure 4.9: Mantle-normalised incompatible element plot comparing intermediate gneiss compositions from amphibolite facies, Gruinard Bay, and granulite facies. (D= 5422 vs. ave. 2H, MJ073, MJ053 vs. ave. MJ181, MJ129).

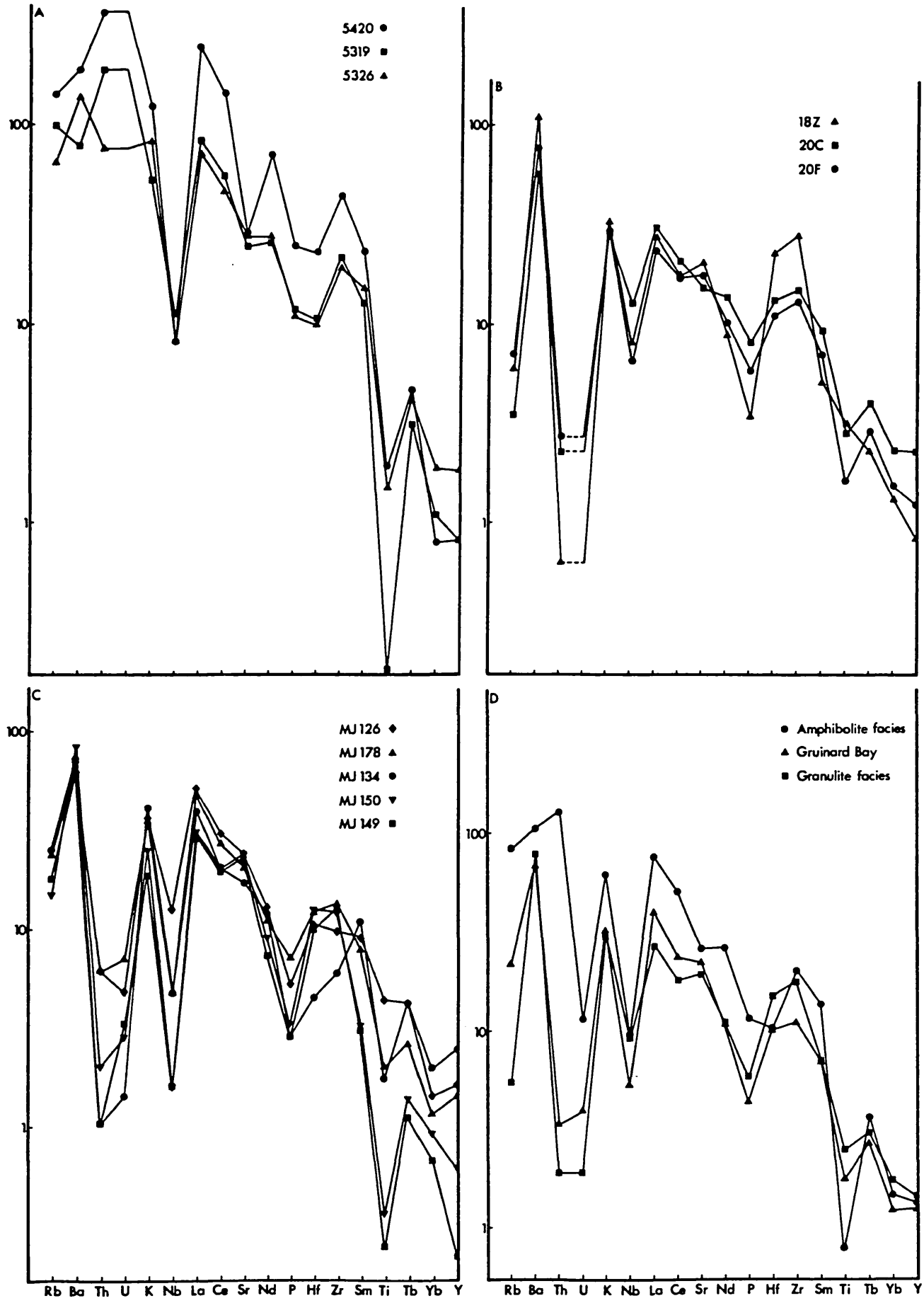


Figure 4.10: Mantle-normalised incompatible element plot comparing tonalitic gneiss compositions from amphibolite facies, Gruinard Bay, and granulite facies.

(D= ave. 5420, 5319, 5326 vs. ave. 18Z, 20C, 20F vs. ave. MJ126, MJ178, MJ134, MJ150, MJ149).

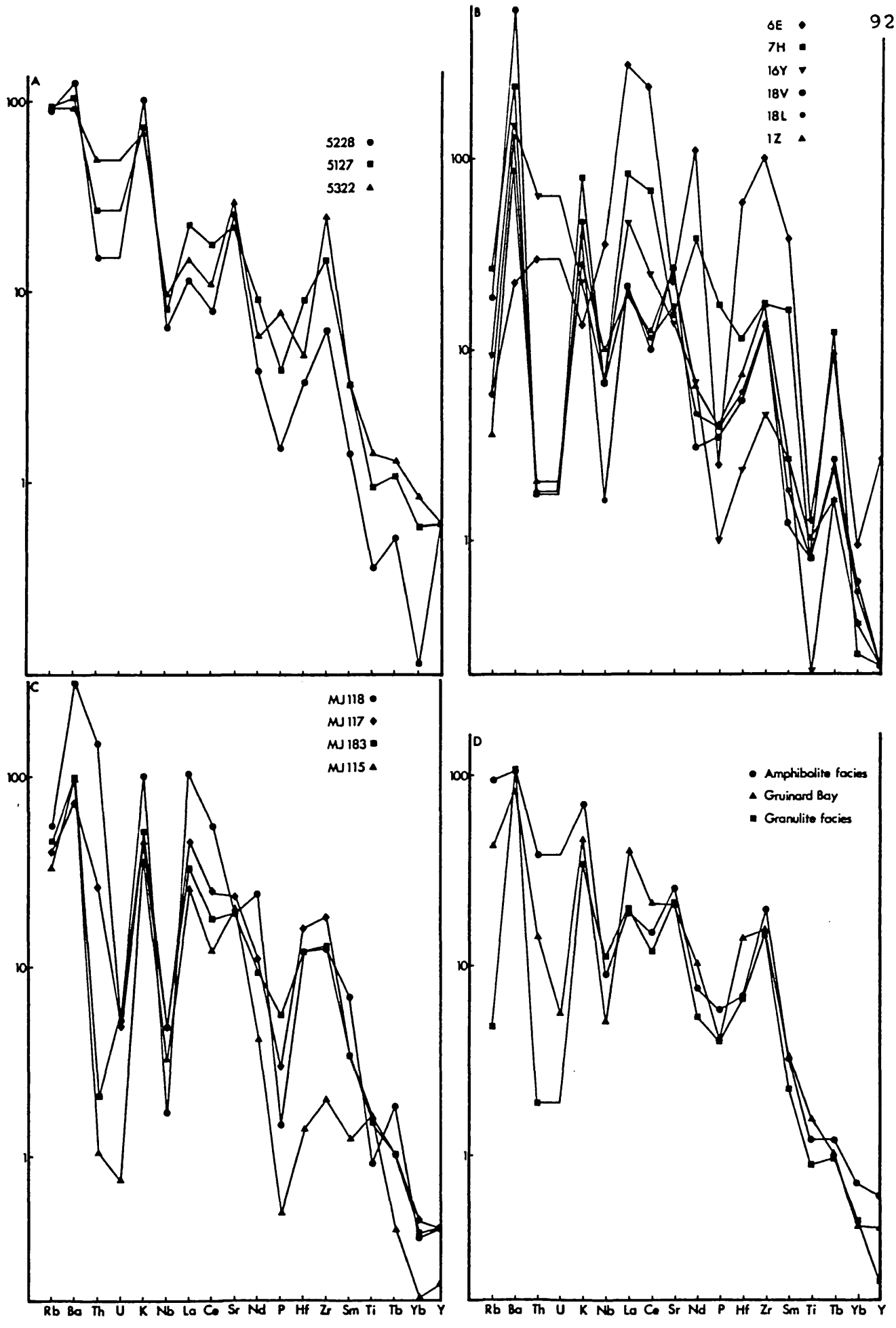


Figure 4.11: Mantle-normalised incompatible element plot comparing trondhjemitic gneiss compositions from amphibolite facies, Gruinard Bay, and granulite facies.
(D= ave. 5322, 5127 vs. 1Z, 18V vs. MJ183, MJ117).

amphibolite-facies end-member; part b the same for the granulite-facies and part c for the present rock suite from Gruinard Bay. Finally, part d plots average values for each, rejecting any obviously anomalous samples (which may be either of fundamentally different origin to the rest or extreme members of the class, and which it would, therefore, be unwise to include in the comparison). Normalisation values and element order are those of Wood (1979), after Weaver and Tarney (1981), and although the samples which are used are noted on the diagram, some explanation might be useful here.

The intermediate gneiss composition is restricted by the only available amphibolite-facies sample (5422), so that samples from Gruinard Bay and the granulite facies must be chosen which have similar "immobile" element abundance and patterns. Gneisses MJ181 and MJ129 fulfill this requirement from Gruinard Bay, but only one granulite from the literature (2H). Therefore, two samples of the author's granulites have been included, and are also plotted on Fig. 4.9b. Since the tonalites form a well-constrained group, no samples have been omitted. In contrast, the trondhjemites are more variable, and the most meaningful comparison is between granulites 1Z and 18V; Gruinard Bay samples MJ183 and MJ117; and amphibolite-facies gneisses 5322 and 5127.

The validity of this comparative approach may be judged from the close fit for the "immobile" trace elements. The diagrams confirm inferences drawn from data for the whole suite in a more specific way, based on closely-comparable, tightly-constrained rock groups. Rb and K abundances at Gruinard Bay without fail intersect those of the end members. Although the radioelements are severely depleted, significant differences remain in the tonalites and trondhjemites.

These features of the Gruinard Bay gneisses, based on a comparison of similar rock types from three points in the high-grade metamorphic continuum, may now be considered in terms of the proceeding mineralogical reactions involved in the depletion process, and the phase(s) responsible for LILE-loss.

CHAPTER FIVE

LARGE-ION LITHOPHILE ELEMENT DEPLETION MECHANISMS

It is perhaps now defensible to be somewhat more specific about element abundances and their derived ratios in terms of the mineralogical control of element abstraction, since the general trends described above have been confirmed on the basis of these more tightly constrained chemical classes. Clearly, any genetic model which requires gradual and uniform depletion of all LILEs has become untenable, in favour of a rather complex, probably multi-stage process partially dependent on original rock mineralogy.

It has been shown above that K and Rb tend to behave together, as do U and Th, but that there is little correlation between the groups. This is explicable in terms of a common residence(s) for K and Rb and a different, common residence for Th and U. The former is probably represented by K-feldspar, biotite and hornblende, and the latter by members of the accessory mineral suite; as has been demonstrated by fission-track radiography.

5.1 Rubidium and Potassium

Sheraton et al. (1973) documented the likely mineralogical reactions which release Rb and - to a lesser extent - K, summarised as follows:

$$Bi = 6Hy + Al_2O_3 + K_2O + 2H_2O$$

$$2Hb + Al_2O_3 + SiO_2 = 2An + 5Hy + H_2O$$

or

$$Di + Al_2O_3 + SiO_2 = An + Hy$$

and

$$Di + Or = An + Hy + 5Qz + K_2O$$

Where Bi= biotite, Hb= hornblende, An= anorthite, Or= orthoclase, Hy= hypersthene, Di= diopside, and Qz= quartz.

Thus, K-feldspar is stable in rocks which are not

diopside normative, and this adequately explains why granites are not extensively depleted in K or Rb (Rollinson and Windley, 1980). The results presented here require no substantial modifications to these conclusions, but they do suggest that the depletion of K and Rb proceeds only initially as a coupled abstraction, causing a gradual rise in K/Rb, until the "depleteable" K reservoir is exhausted. Subsequent interelement fractionation occurs during prolonged Rb removal which raises K/Rb to characteristically high granulitic values. Assuming that the pre-Badcallian minerals equilibrated with a melt (as has been suggested in the magmagenesis section and in references cited therein) and that the major K and Rb accepting phases were K-feldspar, hornblende and biotite, it is possible to estimate from partition coefficient data the relative contributions of each phase to the whole-rock elemental budgets. Thus, biotite would contain a proportionately much larger fraction of the Rb budget than it would of the K budget (c. 3x) and vice versa for hornblende (Henderson, 1982). The extended stability of biotite in the hornblende-granulite facies at Gruinard Bay will cause the retention of more Rb than K, and the rapid rise in K/Rb will be delayed until biotite instability becomes an important factor. This might explain the relatively large difference between K/Rb ratios in hornblende-granulite facies rocks at Gruinard Bay (biotite-bearing, average 450) and on Coll and Tiree (biotite-free, average 675- Drury, 1974).

Further, there are some discrepancies between individual rock classes at Gruinard Bay which are perhaps explicable in terms of mineralogy. For example, the intermediate rocks in general have relatively high K/Rb ratios compared with the rest of the suite. Since in the more basic samples the proportions of biotite and particularly hornblende increase, so will their importance in controlling the K and Rb distribution (compared to that of K-feldspar). Therefore, the K/Rb ratio in these more basic rocks might reflect that of

hornblende, which is also relatively high. Conversely, the trondhjemites still have relatively low K/Rb ratios, which might be due to the increasing stability of K feldspar as the proportion of normative diopside decreases. Therefore, the competing influences of hornblende, biotite and K feldspar on the K and Rb content of their host can explain the overall evolution of the K/Rb ratios from amphibolite to granulite facies, as well as compositionally-controlled variations within the Gruinard Bay suite itself.

5.2 Uranium and Thorium

The removal of U will be particularly sensitive to the proportions resident in each distinct whole-rock site: in solid solution in the rock-forming silicates; in discrete, high-U accessory minerals; or adsorbed onto grain boundaries and in crystal defects. Clearly, each fraction will have a different susceptibility to depletion. Fission-track analysis of ^{235}U (presented above) allowed determination of its microdistribution, and hence the relative contribution of each site to the total depletable U has been investigated. Previous studies of U microdistribution in relation to high-grade metamorphism (Dostal and Capedri, 1978; Ahmad and Wilson, 1981) concluded that depletion is confined to the grain boundary fraction of the U budget, and that U distribution in granulite-facies rocks is governed by the presence or absence of accessory phases. Similar conclusions have been reached on the basis of whole-rock geochemistry and mineralogy, by Windrim et al. (1984) and Iyer et al. (1982). In the Gruinard Bay gneisses, which show an advanced stage of radioelement depletion, there are 5 major uraniferous phases: monazite, zircon, allanite, sphene and apatite, but virtually no grain-boundary U. It is conceivable that the earlier, major phase of Scourian U loss was achieved by the removal of U on grain boundaries, perhaps at the onset of dehydration reactions (the Pb-isotope system records some depletion of U even in amphibolite-facies terrains:

Moorbath et al. (1969) and the U abundance at Rhiconich is only 0.14 x upper crustal average) but detailed consideration of the U distribution suggests that this is only part of a more complex story.

Fission-track radiography has shown zircon to be the most important uraniferous phase in Lewisian granulite-facies tonalites, reflected in the near co-incidence of the average U:Zr ratio for granulite-facies whole-rock samples with that of zircons derived from granulite-facies rocks (c. 1.67×10^{-4} and 1.43×10^{-4} respectively). In contrast, amphibolite-facies samples have nearly an order of magnitude divergence between the respective ratios (c. 6.67×10^{-3} and 1.25×10^{-3}), which is probably related to the increasing importance of U located in other minor phases such as allanite (see also Watson et al., 1982). Instability of such minerals under the newly-imposed, granulite-facies conditions may therefore be important in reducing the U concentration to the background granulite levels. The breakdown of allanite in particular has consequences for the potential mobility of the light REEs for example, although the Nd isotope data of Hamilton et al. (1979) seem to preclude any open system behaviour.

On the other hand, apatite and zircon remain stable in granulites from Scourie but contain markedly less U than at Gruinard Bay (e.g., Plate 4.2). Whether U is leached from the apatite lattice (e.g., Fowler, 1981) or lost during a more complex process of mineral breakdown and re-precipitation is unclear, but a process similar to the latter may affect zircon.

Metamorphic Grade	U content in Zircon
Amphibolite facies	659 - 780ppm[1]
	382 - 452ppm[2]
Granulite facies	44.3 - 56.9ppm[3]
	33.3 - 55.2ppm[3]

Table 5.1: Comparison of zircon U contents from granulite- and amphibolite-facies Lewisian gneisses. (1 = Pidgeon and Aftalion, 1972; 2 = Lyon et al., 1973; 3 = Pidgeon and Bowes, 1972).

Table 5.1 lists published U abundances of Lewisian amphibolite- and granulite-facies zircons and records approximately an order of magnitude variation between these extremes. The zircons are large and have the typical ovoid habit generated during the high-grade event (Pidgeon and Bowes, 1972), but their former existence in the undeformed protoliths is recorded by the presence of sparse, U-rich premetamorphic cores. It might be inferred that the major phase of U loss from the zircon structure occurred during recrystallisation and new zircon growth at granulite grade, which was accompanied by resetting of the U-Pb isotopic system.

Some individual samples from Gruinard Bay retain evidence for the dominating influence of one particular phase. For example, sample MJ118 has anomolously high Th and Th/U, and high light REEs, which has been correlated with the former presence of monazite in the rock. Alternatively, some samples show the opposite U/Th fractionation such that U remains high, (e.g., MJ144). These commonly have high Zr and Hf, which might suggest local zircon accumulation (see also Rollinson and Fowler, in prep.).

Thus, after the initial loss of easily-leachable (grain-boundary?) U, radioelement depletion apparently proceeds as a function of the combined, varied responses of the host minor minerals to the newly-imposed conditions. This involves not only radioelement release due to mineral breakdown, but also their loss from phases which are still stable in the granulite facies. Samples which are rich in one particular minor phase, for whatever reason, may retain anomalous radioelement abundances.

5.3 The phase responsible for depletion: fluid or melt?

Whole-rock REE geochemical modelling has suggested that the intracrustal partial melting model for granulite genesis, as advocated particularly by Pride and Muecke (1980, 1981, 1982) is inappropriate as a genetic mechanism for the Gruinard Bay gneisses.

However, this does not necessarily mean that partial melting has not occurred, merely that it was not responsible for the overall genesis of the suite.

	D	Residue / Source	Melt / Source
Ce	0.26	0.74	3.33
Nd	0.52	0.91	1.83
Sm	0.82	0.98	1.21
Eu	1.33	1.03	0.76
Gd	1.02	1.00	0.98
Dy	1.28	1.02	0.79
Er	1.19	1.02	0.79
Yb	0.87	0.98	1.14
Lu	0.61	0.94	1.59

Table 5.2: REE model for 10% batch melting retaining a hornblende-granulite facies residue.

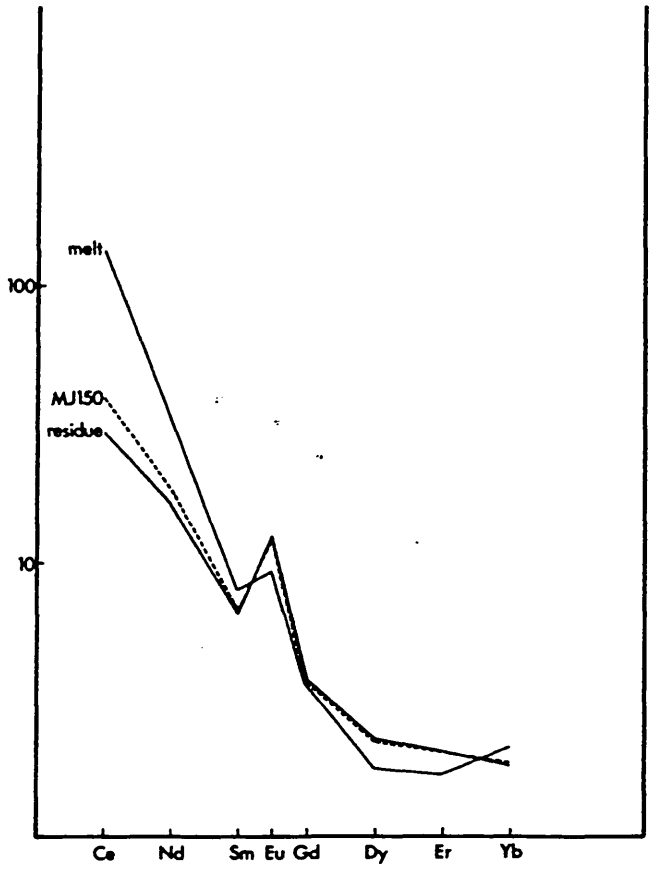


Figure 5.1: REE model of in-situ partial melting at Gruinard Bay.

Fig. 5.1 and Table 5.2 show that REE patterns typical of the tonalitic- trondhjemitic rock types are "robust" to the extraction of a small-degree partial melt in equilibrium with the observed residual mineralogy, and therefore that partial melting may go unnoticed as far as this particular element group is concerned (although note Weaver and Tarney's (1980, 1981) objections based on Ba abundances). Therefore it deserves further consideration here.

It has recently become clear that increasing the acidity of the melt phase results in a rapid increase in mineral-melt partition coefficients for most incompatible elements (Mahood and Hildreth, 1983, Villemant et al., 1981). In the light of this it is instructive to consider the partition coefficients required by the observed U and Th depletion factors from amphibolite to granulite grade; as shown in Table 5.3.

"undepleted" amphibolite facies: U = 2.7ppm, Th = 10ppm.

"depleted" granulite facies: U = 0.05ppm, Th = 2ppm.

Interfacies fractionation ("depletion factor") for both elements = 0.02x original value.

For EQUILIBRIUM PARTIAL MELTING, this requires a bulk distribution coefficient of 0.004, at 20% melting.

For FRACTIONAL MELTING, it requires a bulk distribution coefficient of 0.055, again at 20% melting.

Table 5.3: U and Th depletion factors from amphibolite to granulite grade, and required bulk mineral-melt distribution coefficients.

Clearly, for sensible degrees (i.e., less than 50%) of either equilibrium partial melting or fractional melting partition coefficients for the radioelements required to effect the observed fractionation are comparable with those for basaltic melts under upper mantle conditions. That this appears unlikely is demonstrated by Table 5.4, which is a compilation of available U and Th partition coefficient data for rock-forming minerals with acidic melts.

	U				Th			
Rock-forming minerals								
Feldspar	0.008 0.027	0.021 0.022	0.018 0.037	0.014	0.0095 0.0253 0.0149 0.088	0.0173 0.0225 0.033 0.059	0.0208 0.0158 0.065	0.076
Clinopyroxene	0.07	0.35	0.031	0.084	5.41	6.56	0.013	0.035
Orthopyroxene	0.25	0.31			7.76	5.30		
Biotite	0.131	0.19	0.18		0.511	1.74	1.43	0.31
Accessory minerals								
Zircon	383	298			91.2	62.4		
Apatite					1.2			
Sphene	0.58	2.1			1.74	8.0		
Allanite	17	14			548	420		

Sources:

Nagasawa and Wakita (1968)

Higuchi and Nagasawa (1969)

Dudas et al. (1971)

Mahood and Hildreth (1983)

Worner et al. (1983)

Table 5.4: Literature data for U and Th mineral-melt partition coefficient data.

Moreover, the above discussion has not given sufficient weight to the role of accessory phases in the residue (e.g., Harrison and Watson, 1984). It has been demonstrated above that the bulk of the U (and Th?) complements of hornblende-granulite and granulite facies, Lewisian gneisses resides in zircon, apatite and allanite. Available U and Th partition coefficient data for these phases are also listed in Table 5.4. The range is considerable and depends on many factors, but it obviously requires only a very small modal abundance of such phases to make the required interfacies radioelement fractionation inconceivable, if based on equilibrium or fractional melting. Therefore, it appears that even if partial melting did occur, if it was controlled by currently accepted theories of melt/crystal equilibration, it would not have been capable of removing sufficient U or Th from original amphibolite-facies lithologies to generate the highly-impoverished hornblende granulites (Gruinard Bay) or granulites (Scourie).

This implicates some sort of non-silicate fluid, as has been advocated extensively in the literature (e.g., Tarney and Windley, 1977; Weaver and Tarney, 1980, 1981; Rollinson and Windley, 1980a, b). Current knowledge on the partitioning behaviour of the radioelements into fluids under pertinent crustal conditions is almost nonexistent, and appeal has to be made to experimental results either on other (comparable?) elements, or under different (generally lower P, T) conditions.

Since the REEs have become so extensively used in petrogenetic discussions, most data exist for this group of elements. A CO_2-rich fluid has been widely proposed as the phase in which LILEs are lost during granulite-grade metamorphism (although see the note of caution by Lamb and Valley, 1984; who suggest that graphite should be precipitated if substantial CO_2 fluxing has taken place). However, Wendlandt and Harrison (1979) have shown that under the P/T conditions of interest (8 - 12 Kb and 700 - 800°C), a CO_2 vapour

would very strongly partition REEs and cause substantial REE mobility, which is not seen.

The advanced stage of depletion reached at Gruinard Bay in gneisses which still retain a partly hydrous mineral association suggests that the fluids in which LILEs were removed from the system were also H_2O-rich rather than purely carbonic. This accords with other studies of the amphibolite to granulite facies transition (e.g., Holt and Wightman, 1982) which propose an advancing front of mantle-derived CO_2 flushing before it a LILE-charged H_2O-dominated fluid generated by dehydration reactions. In contrast to the experimental results for CO_2, those for aqueous liquids suggest that no strong partitioning of REEs into the fluid would occur under crustal P/T conditions (Cullers et al. 1973; Zeilinski and Frey, 1974; Flynn and Burnham, 1978; and Wendlandt and Harrison, 1979). However, available evidence (Beswick, 1973 and Shaw, 1978) indicates that Rb and K could be removed from plagioclase (the dominant mineral in the Lewisian gneisses), in equilibrium with an aqueous fluid. Rollinson and Windley (1980) estimated a bulk mineral-fluid distribution coefficient of 0.024 for Rb, which would cause its entry into the fluid. However, this requires that the proportion of CO_2 be relatively low, and other ligands with which to complex and stabilise radioelement cations might be sought. Several studies (e.g. Leelanandum, 1970; Blattner and Black, 1980) have shown that specific hornblende-granulite and granulite-facies minerals are Cl- and F-rich (apatite, amphibole, biotite, scapolite), providing direct evidence for their significant presence in the coexisting fluid. Others have demonstrated the ability of halide anions to form complex species with high-ionic-potential cations in aqueous media (Bandurkin, 1961; MacDonald et al., 1973; Alderton et al., 1980). Thus it is possible that those mobile LILEs with high ionic potential (i.e. U and Th) may be stabilised in the fluid by halides, as well as the more-often quoted CO_3^{2-} anion.

It seems likely to the present author that the radioelements were removed from the Lewisian gneisses during hornblende-granulite facies metamorphism, in a fluid charged with halides and some CO_2, but with a still-significant aqueous component, shortly before inversion to the CO_2-dominated conditions recorded in granulites from many parts of the world (e.g., Newton et al., 1980).

CHAPTER SIX

CONCLUSIONS TO GRUINARD BAY

The following conclusions may be derived from this study of regional LILE mobility at granulite-grade.

i) The geochemistry of the Lewisian grey gneiss at Gruinard Bay shows many similarities with that of other parts of the Lewisian Complex in terms of elements "immobile" during the LILE depletion event.

ii) This can be traced to comparable processes of magma genesis which established many of the main geochemical characteristics of the Complex as a whole.

iii) Intracrustal partial melting is not a suitable model for the generation of the range of lithologies exposed at Gruinard Bay. These are more likely to be the result of variable degrees of partial melting of a compositionally heterogeneous basaltic source leaving a variably garnet-bearing residue. Local hornblende fractionation may have been important in the genesis of some of the more "extreme" trondhjemites. Removal of LILEs was not a direct result of the magmagenetic processes.

iv) In terms of LILE abundances and "primary" mineralogy, Gruinard Bay gneisses represent an intermediate stage in the depletion process, probably characterised by hornblende-granulite facies conditions during the Badcallian metamorphism.

v) Rb, K, Th and U are all depleted to some extent, relative to comparable amphibolite-facies rocks, but not in a uniform manner: the radioelements have reached an advanced stage of depletion while K and Rb "lag behind", such that K/Rb ratios remain relatively low.

vi) The processes which together constitute the depletion event are complex, probably beginning in the amphibolite facies (U-loss) and proceeding as a function of mineralogy and bulk geochemistry along with other factors. Depletion can be shown to be "selective", "differential" and "progressive" in its operation.

vii) The late stages of radioelement loss, as represented by Gruinard Bay gneisses, are critically dependent on the reaction of minor mineral phases to the imposed conditions. Allanite appears to be crucial in maintaining significantly higher U and Th abundances in the hornblende-granulite facies lithologies.

viii) Loss of K and Rb proceeds initially as a coupled abstraction, during which the K/Rb ratio responds sluggishly but further Rb loss during later stages (biotite and hornblende breakdown?) causes a rapid increase in K/Rb as granulite-facies (ss) conditions are approached.

ix) The importance of accessory minerals in hornblende-granulite and granulite-grade gneisses as their main hosts of the U (and Th?) complement, renders it unlikely that the extreme radioelement incompatibility required by partial melting models for depletion would be met.

x) The recently documented rapid rise in mineral-melt partition coefficients for highly silicic rock types also argues against the efficient removal of LILEs in a granitic melt, even if the influence of accessory minerals is ignored.

xi) The advanced stage of depletion reached in rocks which are still demonstrably hydrous suggests that the fluid responsible for LILE transport out of the lithochemical system may also have been hydrous, not CO_2-rich.

xii) A CO_2-rich phase may have been the cause of the dehydration reactions, driving before it a flux of LILE-charged hydrous fluids. These may have caused partial melting at higher levels in the crust, similar to documented high-grade transitional terrains elsewhere in the world.

CHAPTER SEVEN

INTRODUCTION TO GLEN DESSARRY

The Glen Dessarry syenite is the second subject studied in detail here, and was chosen to illustrate local element migrations at amphibolite grade, as a complement to the regional mobility discussed above. It was thought to be of potential interest for the following reasons:-

i) It is a product of deep-seated processes, probably representing a primary crustal addition from the mantle (van Breemen et al., 1979), and therefore bears directly on the mechanisms of incompatible element addition to the crust.

ii) Intrusion occurred at a low crustal level under the metamorphic conditions pertinent to this thesis, and local reactions with the envelope occured during consolidation.

iii) Amphibolite-facies metamorphism and deformation pene-contemporaneous with intrusion affected the Complex to varying degrees, whose effects on the primary element distribution may therefore be studied.

iv) Uranium is concentrated in a limited number of accessory minerals, some of which occur commonly in the lower crust, and a study of their response to metamorphism and deformation might therefore have a broad relevance to crustal regimes in general.

Hence, the syenite may be used to study the behaviour of the incompatible element group from melt generation in the mantle, through the fractionation processes which gave rise to the parent melts of the presently-exposed variants, to localisation as a result of magmatic influences, and finally redistribution occurring during deformation in the amphibolite-facies metamorphic event.

7.1 History of Research

In contrast to the Lewisian rocks, the chapters concerning which were founded on an extensive literature, the alkaline plutons of the NW Highlands

have received the attention of only a relatively few publications.

The early descriptions of the Glen Dessarry area were those of Harry (1951, 1952) who described the core of a sharp "anticline" in the Moine psammites as a gneissic Lewisian inlier of subsequently feldspathised pyroxene-amphibole rocks, marble and paraschist. He proposed that a phase of porphyroblastesis occurred during the decline of an episode of migmatisation, resulting in a rock "almost wholly composed of randomly-orientated, large, grey alkali-felspars", and called it "felspar-porphyroblast rock".

Remapping of the area by Geological Survey of Great Britain was undertaken between 1956 and 1961, and the findings summarised briefly in Summ. Progr. geol. Surv. UK (1957, 1958, 1960, 1961, 1962). During this time the previously used term "Inlier" was replaced by the less-committal "Complex", since the fold was now seen to close downwards rather than upwards. Lambert et al. (1964) divided the Complex into two types of syenite; provided Rb-Sr isotopic evidence for a post-Lewisian age; reported the presence of kyanite, sillimanite, staurolite and mica in the "paraschists" of Harry (1952); and proposed a magmatic history for the syenites which were thought to have been emplaced during or before an early phase of Moinian metamorphism. The results of further research by Richardson were published shortly afterwards (Richardson, 1968). These broadly confirmed and extended the more recent ideas on the genesis of the Complex, recording the presence of two types of syenite "which were intruded before or during a phase of almandine-amphibolite facies regional metamorphism". The magmatic history was envisaged as involving low-level crystal fractionation in a magma chamber at depth, of aegerine-augite, biotite and magnetite to relate the parental compositions of the two syenite types. Metamorphism and deformation caused unmixing of mesoperthite into granular orthoclase and sodic plagioclase, contemporaneous (according to

Richardson) with generation of disequilibrium pyroxene-hornblende associations by a reducing (H_2-H_2O) fluid entering the Complex from the surrounding metasediments. A comprehensive account of the major mineralogy of the syenites and some major-element geochemistry was included.

Van Breemen et al. (1979) reported U-Pb, Rb-Sr and K-Ar data for rocks selected from the Complex; and suggested a crystallisation age of 456 +/- 5 Ma; that amphibolite-facies conditions persisted until about 430 Ma; and that the area cooled from 500°C to the K-Ar blocking temperature (about 300°C) in about 20 Ma. Importantly, an initial $^{87}Sr/^{86}Sr$ isotopic ratio of 0.7041, combined with a feldspar Pb-isotope composition too radiogenic to be derived from a U-depleted source (i.e., granulite facies Lewisian basement - which is also capable of producing low $^{87}Sr/^{86}Sr$ ratios), were taken to strongly suggest a mantle derivation. Van Breemen et al. (1979b) proposed that Glen Dessarry and the other alkaline plutons of the NW Highlands were generated during tensional tectonics at depth related to doming due to the compressive tectonics of subduction, thus providing classic conditions for the generation of "within-plate" alkaline magmas. It should perhaps be noted here that the geochemical data to follow indicate that Glen Dessarry is not a typical "within plate" alkaline melt (Thompson and Fowler, in prep.).

Most recently, Fowler (1981) briefly described the distribution of U within the syenites and discussed its implications. This formed a basis for the present work and will be considered in full and expanded upon below.

Geological Setting and Sample Collection

The Glen Dessarry syenite is one of four major alkaline plutons exposed in NW Scotland. The other three (Loch Loyal, Loch Ailsh and Loch Borrolan; see Parsons, 1965, 1979) are all significantly younger than Glen Dessarry and are exposed on or near the foreland. All have to date escaped a concerted geochemical

investigation, although pertinent isotopic data are available (van Breemen et al., 1979a, 1979b). Glen Dessarry has been dated at 456 +/- 5 Ma (van Breemen et al., 1979a), and is a composite pluton comprising two tracts of leucocratic syenite intruding an earlier, mafic syenite (Fig. 7.1).

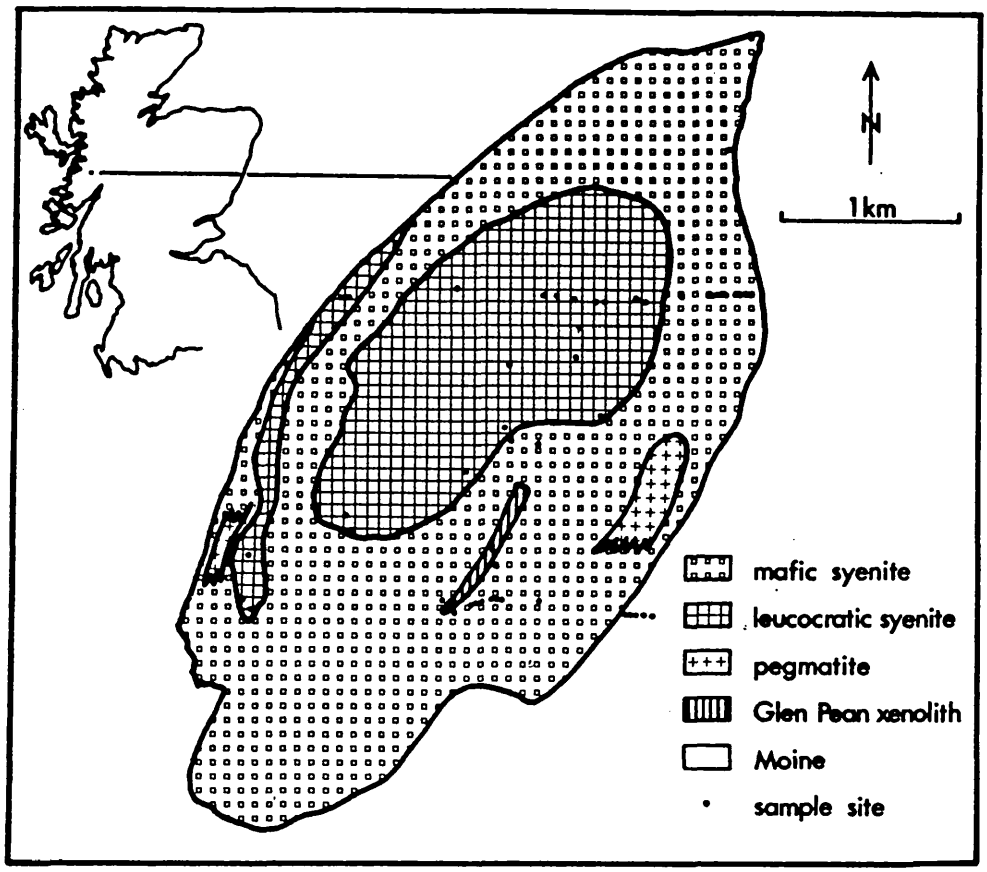


Figure 7.1: Locality map of Glen Dessarry.

The relationships of the two leucocratic syenite tracts are obscured by drift in the valley of the river Dessarry, but have been interpreted both as one continuous body of leucocratic syenite (van Breemen et al., 1979) and as two separate occurrences (Lambert et al., 1964). The contact between the mafic and leucocratic syenite types is intrusive, which implies that two magma pulses occurred (Richardson, 1968), rather than some extreme form of in-situ differentiation. Sheets of leucocratic syenite cut mafic syenite confirming the expected age relationships; that the former post-dates the latter. The two massive

granitic pegmatites may be members of a regional Caledonian pegmatite swarm, whereas more numerous, rather nebulous patches within the syenites themselves are probably the result of local filter pressing action. Xenoliths of ultramafic rock up to about 4m across are most common in the mafic syenite, and have been interpreted as fragments of early cumulates derived from a magma chamber at depth (Richardson, 1968). Metasedimentary material ranging in size from about 500m (the Glen Pean Xenolith) to patches visible only under the microscope, is present in the mafic syenite, and this includes the three marble bodies described by Harry (1952).

The country rocks are Moinian psammites to semi-psammites which commonly develop a glassy texture adjacent to the contact. In places rheomorphism has given rise to the autobrecciated rock of Lambert et al. (1964). Locally, very close to the contact (within about 3m), a pervasive reddening of the metasediments occurs, in response to interaction with the crystallising syenite (see later).

The whole Complex has been affected by deformation, and while its macroscopic effects remain conjectural and a matter for discussion (e.g., van Breemen et al., 1979a; Roberts et al., 1984), there is no doubt that the local development of a pronounced planar fabric in the syenites is directly related to this process, rather than to flow differentiation during consolidation as has been suggested for the Loch Loyal syenite (Robertson and Parsons, 1974). Most of the syenites are affected to some extent, but the centre of the intrusion preserves textures which may be more easily related to crystallisation from a magma. More detail on the microscopic effects of deformation are given later. The lineation developed within the syenites is coincident with that in the surrounding metasediments, which was produced during the second phase of metamorphism in the area (Lambert et al., 1964). This suggests that dating of the syenite by the U-Pb methods used gives a maximum

age for the second fold movements (van Breemen et al., 1979a).

Samples were collected of all the main variants of the Complex - ultrabasic rocks, mafic syenites, leucocratic syenites and pegmatites, in varying states of deformation. In addition, samples of reddened marginal metasediments, unaltered Moine country rock and reaction rocks associated with syenite veins were collected with a view to consideration of their effects on the localisation of U and other elements, initially indicated by gamma-ray scintillometry (see below). Sample localities are marked on Fig. 7.1.

7.3 Approach

The features of the Glen Dessarry syenite which make it an attractive intrusion to study for the purposes of this thesis have been outlined above. However, the best approach to the investigation of metamorphic and/or deformational element mobility was not immediately apparent, since it could have been misleading to simply assume that all the present chemical variations are of metamorphic origin. Nevertheless, some preliminary pointers do exist.

It is clear from the field relationships that the overall form and structure of the Complex (Fig. 7.1) retain much of their original intrusive character, which immediately suggests that magmatic factors may still exert a strong influence on rock chemistry. Supportive evidence for this point of view was derived from the use of a total gamma-ray scintillometer in the field (see appendix), which allowed a qualitative assessment of the major features controlling radioelement distribution on the scale of an outcrop. These factors include the following:

i) Differences between leucocratic syenite, mafic syenite and pegmatite.

ii) Magmatic assimilation of metasedimentary material.

iii) Local reactions of intrusive syenite veins invading metasedimentary rafts.

iv) Local metasomatism of the country rock host immediately adjacent to the contact with the syenite. These are all of magmatic rather than metamorphic origin and no obvious correlation of radioelement abundance with degree of deformation was detected. Nevertheless, the intense local deformation which produced strongly-foliated, metamorphic rocks from the precursor igneous lithologies may have profoundly modified the original element distribution within the whole-rock system.

Accordingly, an early "pilot" study was directed solely at a consideration of the abundance and distribution of U in variably-deformed samples of the leucocratic syenite (Fowler, 1981). This used fission-track and delayed neutron analytical techniques for U, combined with textural interpretation of some of the uraniferous accessory minerals, to provide evidence for the existence of U and REE-bearing fluids within the syenites, which were shown to have modified the primary distribution of these elements. However, several further questions were raised:

"(i) The extent to which processes demonstrated by fission-track radiography result directly from amphibolite-facies metamorphism. (ii) The source of the secondary uranium and its possible transport by an intergranular fluid phase. (iii) The chemical composition of the fluid and speciation of the uranium. (iv) The extent to which the development of high uranium zones in sphene was an isochemical process."

The following chapters describe results of the work undertaken by the author in pursuit of the answers. In the light of the preliminary evidence, it was decided that the best approach would be to delineate any remaining magmatic controls on element abundances and distribution, before embarking on a study of subsequent metamorphic or deformational redistribution.

7.4 Presentation of Results

In accord with the approach detailed above, the results are presented in the following manner. The next chapter deals in some detail with the construction of a magmagenetic scheme involving fractional crystallisation, crustal contamination and reactions with country rocks during emplacement, so that the extent to which element abundance variations might still reflect such magmatic factors can be ascertained. Since this involves modelling trace-element variations in terms of theoretical mineral-melt partitioning behaviour, if the magmatic scheme proves viable, it provides an estimate of the primary mineralogical distribution of incompatible elements. Any subsequent remobilisation can then be studied by analysis of samples exhibiting profound secondary textures, and this falls within the scope of the following two chapters. The first deals with bulk (i.e., whole-rock) chemical changes accompanying deformation, and the second with microscopic element mobility and its relationships with magmatic and deformational processes as previously described.

CHAPTER EIGHT

MINERALOGY AND PETROGRAPHIC VARIATIONS

8.1 Mineralogy

Richardson (1968) gave a comprehensive and detailed account of the major mineral phases in the syenites which clearly forms an important basis for this study. Accordingly, a summary of his findings is included below, with additional new mineral-chemical data which will be required to assess the viability of fractional crystallisation as an evolutionary mechanism. Of equal importance to the present study, and not dealt with in such detail by Richardson (1968), are the minor and accessory mineral phases which provide lattice sites for many of the elements considered in this thesis.

Feldspars.

The feldspars from the Complex display varying degrees of unmixing from a single hypersolvus perthite to separate orthoclase and plagioclase members. This proceeds through broadening of the lamellae and a tendency towards patchy development of a twinned plagioclase guest in a homogeneous K-feldspar host. Further unmixing results in rather ragged K-feldspar enclosing scattered areas of plagioclase still in optical continuity. Untwinned, granular K-feldspar eventually forms equant grains associated with plagioclase of similar texture but often twinned. Richardson (1968) provided a contoured map of the proportion of large perthite crystals, which suggests a generally increasing percentage towards the leucocratic syenite core of the intrusion, and was interpreted as a metamorphic effect related to the present form of the pluton, imposed after crystallisation of the igneous rocks. New electron-probe analyses of the perthitic feldspars from mafic and leucocratic syenites are given in Table 8.1.

	GD30 (6)	MJ008 (6)
SiO_2	64.27	63.81
Al_2O_3	20.03	19.69
CaO	0.79	0.51
BaO	0.38	0.72
Na_2O	5.66	3.76
K_2O	8.28	11.12
Total	99.43	99.60
Si	11.703	11.735
Al	4.297	4.265
Al	0.002	0.002
Ca	0.154	0.100
Ba	0.027	0.052
Na	2.000	1.341
K	1.923	2.609
AB	48.73	32.69
AN	3.75	2.43
OR	47.53	64.87

Table 8.1: Average perthite analyses from Glen Dessarry mafic and leucocratic syenites.
(GD30= mafic syenite, MJ008= leucocratic syenite).

Pyroxenes and Amphiboles.

Pyroxene occurs with and without amphibole in both syenite variants and is a pale green, sometimes zoned aegerine-augite. Electron-probe analyses from euhedral crystals are given in Table 8.2. They are clearly magmatic and are often intergrown with biotite. In many of the syenite samples pyroxenes show varying degrees of replacement by a dark green edenitic amphibole, often along the cleavage directions and edges, and sharing the z crystallographic orientation (Richardson, 1968). Typical electron-probe analyses of the amphiboles are also presented in Table 8.2.

Richardson (1968) provided a distribution map of modal pyroxene/(pyroxene + hornblende) which, like the feldspar exsolution data, suggests a broad correlation with the present outcrop morphology. He therefore advanced the hypothesis that the igneous pyroxenes were replaced by metamorphic hornblende due to the influx of a reducing, hydrous fluid phase from the surrounding

	Pyroxenes				Amphiboles		
	GD48 (8)	GD30 (8)	MJ008 (8)		GD48 (5)	GD30 (8)	MJ008 (8)
SiO_2	50.74	52.06	51.85	SiO_2	45.43	43.22	42.27
TiO_2	0.72	0.00	0.00	Al_2O_3	8.34	9.11	9.33
Al_2O_3	3.18	1.24	1.06	FeO	10.90	16.23	17.17
FeO	7.70	11.17	13.01	Fe_2O_3	2.45	3.08	2.86
MnO	0.25	0.61	0.94	MgO	14.06	10.03	9.17
MgO	12.94	11.08	9.65	MnO	0.34	0.48	0.71
CaO	22.57	22.20	20.62	TiO_2	0.60	0.59	0.59
Na_2O	1.45	1.62	2.24	CaO	11.87	11.31	11.07
Total	99.56	99.97	99.37	Na_2O	2.10	2.04	2.20
				K_2O	0.85	1.27	1.38
				Total	96.94	97.35	96.74
Si	1.906	1.977		Si	6.745	6.595	6.542
Al	0.094	0.023		Al	1.255	1.405	1.458
Al	0.047	0.032		Al	0.204	0.234	0.244
Ti	0.020	-		Ti	0.067	0.068	0.069
Fe	0.242	0.355		Fe^3	0.271	0.345	0.320
Mn	0.008	0.020		Mg	3.111	2.281	2.115
Mg	0.725	0.627		Fe^2	1.347	2.072	2.236
Ca	0.908	0.903		Fe^2	0.009	0.008	-
Na	0.105	0.120		Mn	-	-	0.017
				Mn	0.043	0.062	0.076
				Ca	1.888	1.849	1.836
				Na	0.060	0.081	0.088
				Na	0.545	0.523	0.572
				K	0.161	0.274	0.273

Table 8.2: Average pyroxene and amphibole analyses from the Glen Dessarry syenite.
(GD48= ultramafic cumulate, GD30= mafic syenite, MJ008= leucocratic syenite.)

metasedimentary envelope. An investigation of Mg, Ti and Mn distribution between the phases suggested that the pyroxene-amphibole intergrowths represent a disequilibrium assemblage. The requirement for an external fluid to bring about the observed pyroxene/hornblende association will be discussed at several places in the following text, since there are other possibilities which the present author finds difficult to dismiss. For example, the source of hydrating postmagmatic fluids may have been internal; alternatively amphibole may have crystallised directly from a magma with pH_2O progressively increasing during crystallisation, with the fluid distribution constrained by the physical morphology of the magma reservoir. The origin of the amphiboles clearly affects an

understanding of the metamorphism of the pluton, but a more detailed discussion will be deferred until a later section.

Biotites.

Biotite is common in all the syenite variants - from accessory amounts in some ultrabasic cumulates and pegmatites, to common magmatic intergrowths with pyroxene (with perpendicular c axes; Richardson, 1968) in the leucocratic and mafic syenite types. Electron-probe analyses are given in Table 8.3. Rarely, it is altered to chlorite and opaques.

	GD48 (6)	GD30 (6)	MJ008 (6)
SiO_2	36.81	37.03	36.88
TiO_2	2.06	2.24	2.17
Al_2O_3	14.12	13.75	13.13
FeO	14.53	19.11	19.08
MnO	0.18	0.32	0.49
MgO	16.34	12.38	12.54
CaO	0.16	0.28	0.05
Na_2O	0.53	0.51	0.46
K_2O	9.82	8.95	9.81
H_2O	3.96	3.89	3.87
Total	98.51	98.46	98.47
Si	5.573	5.699	5.712
Al	2.427	2.301	2.288
Al	0.092	0.193	0.109
Ti	0.235	0.259	0.252
Fe	1.840	2.459	2.471
Mn	0.023	0.041	0.064
Mg	3.687	2.840	2.894
Ca	0.027	0.046	0.009
Na	0.154	0.151	0.138
K	1.897	1.756	1.937

Table 8.3: Average biotite analyses from the Glen Dessarry syenite.

(GD48= ultramafic cumulate, GD30= mafic syenite, MJ008= leucocratic syenite).

Accessory Minerals.

Fission track investigations (Fowler, 1981) have shown that the diverse suite of accessory minerals in the syenites is important in controlling the abundance of U, and further work has indicated that this is also true of many other elements with which this thesis is

particularly concerned. Accordingly, a detailed study of the accessory suite has been conducted the importance of which is such that it will be treated at length later. For the present, only a few brief comments are made.

The opaque minerals present in the syenites comprise essentially magnetite and local pyrite (e.g., syenite-vein/xenolith reactions). Apatite is a common minor phase, as are sphene and allanite with both primary and secondary relationships. Zircon is an ubiquitous accessory as partially resorbed igneous crystals (van Breemen et al., 1979) and monazite, epidote, quartz, calcite and strontianite have a more localised occurrence (see Richardson, 1968). An additional, widely distributed accessory often found as inclusions in perthite crystals is a rarely reported Zr-Ti oxide - zirconolite, identified as a result of

Zirconolite	
	(4)
ZrO_2	31.53
TiO_2	28.80
CaO	9.05
FeO	7.70
ThO_2	8.22
UO_2	2.86
La_2O_3	0.91
Ce_2O_3	3.25
Pr_2O_3	0.28
Nd_2O_3	1.36
Sm_2O_3	0.39
Eu_2O_3	0.15
Gd_2O_3	0.47
Yb_2O_3	0.09
Y_2O_3	0.67
Ta_2O_5	0.26
Nb_2O_5	2.71
HfO_2	0.31
PbO_2	0.29
BaO	0.54
Total	99.84

Allanite		
	LS 1^{γ}	MS 1^{γ}
	(3)	(8)
SiO_2	32.81	33.39
TiO_2	0.57	0.46
Al_2O_3	15.01	17.97
La_2O_3	7.30	5.45
Ce_2O_3	8.87	8.02
Nd_2O_3	1.27	0.61
FeO	15.36	14.66
MnO	0.47	-
MgO	0.87	0.78
CaO	13.29	14.67
H_2O	1.57	1.63
Total	97.40	97.65

Monazite	
	(5)
La_2O_3	15.42
Ce_2O_3	26.86
Pr_2O_3	2.87
Nd_2O_3	9.28
Y_2O_3	1.43
ThO_2	11.22
UO_2	0.60
CaO	1.76
P_2O_5	29.79
Total	99.23

Sphene	
	(6)
SiO_2	29.72
TiO_2	35.73
CaO	27.54
Ce_2O_3	1.47
Nd_2O_3	0.75
Al_2O_3	1.18
FeO	1.95
Na_2O	0.20
Total	98.54

Apatite	
	(3)
CaO	54.00
P_2O_5	41.03
SiO_2	0.57
Na_2O	0.24
SrO	0.82
SO_2	0.92
Total	97.58

Table 8.4: Average analyses of minor or accessory minerals from the Glen Dessarry syenite.
(LS= leucocratic syenite, MS= mafic syenite.)

fission-track analysis (Fowler, 1981 and see below). Of particular importance to this study are those common accessory phases which provide lattice sites for many HFSEs: zirconolite, sphene, allanite, apatite, zircon and monazite, and Table 8.4 lists representative analyses (except for zircon).

8.2 Petrographic Variations

This section is not intended to be a comprehensive description of all the petrographic variations that exist within the Complex, but rather to briefly describe those variations within the author's sample suite, which was collected specifically for geochemical analysis along two traverses across the Complex. Therefore its purpose is to set the petrographic framework within which the geochemical variations should be interpreted. The samples specifically described here have been chosen for their relatively low degree of strain, since the processes of deformation are discussed later. The variations of concern to this section may therefore be related to a pre-deformation episode.

Cumulates.

Richardson (1968) notes the presence of ultramafic rocks which are virtually feldspar-free (although some poorly feldspar-bearing examples occur) and interprets them as fragments of cumulate bodies caught up in the mafic syenites during intrusion. Several samples of such ultramafic bodies were collected for this study, to illustrate the range in their composition and mineralogy. Two (GD15 and GD49) are pyroxene-rich, composed of large, interlocking subhedral pyroxenes which show incipient intergrowth with amphibole and contain small inclusions of sphene and rare magnetite. Marginal to pyroxene, large subhedral to euhedral apatites are common, not infrequently associated with a thin, discontinuous mantle of allanite. Biotite is rare and feldspar generally absent.

An interesting (and perhaps important) feature of sample GD49 is a "pocket" of amphibole- and feldspar-rich material several centimetres across. As this is approached, the proportion of amphibole relative to pyroxene rapidly increases, until amphibole is the main ferromagnesian phase. A concomitant increase occurs in the proportion of incompatible-element-rich accessory phases, sphene, apatite, zircon and allanite. The latter now exists as independent, euhedral crystals, not necessarily associated with apatite, which itself shows abundant, large and apparently primary fluid inclusions. Feldspars form a matrix into which the amphiboles appear to have grown. One interpretation of this association is as the crystallised products of trapped interstitial melt, with pH_2O high enough to cause the crystallisation of amphibole instead of pyroxene. The incompatible elements, which have been concentrated in the melt as a result of earlier mafic phase crystallisation, are thus forced to enter or form the abundant accessory phases. It is tempting to view this as an isolated mimic of the crystallisation trends of the syenites themselves, which may also have crystallised amphibole when pH_2O had risen sufficiently.

The second type of cumulate is represented by sample GD48, which is essentially a polymineralic aggregate of pyroxene, biotite, apatite, Fe-Ti oxides, sphene, zircon and amphibole; and might be related to a later stage in the low-level evolution of the parent melt.

Mafic syenites.

There are considerable variations in the petrography of the mafic syenites, in addition to those due to the superimposed deformation. They are essentially the result of varying the constituent amounts of the major and minor mineral phases described above. For example, samples MJ012 and MJ025 are pyroxene and biotite-rich, with a consequently lower modal abundance of feldspars. The pyroxenes are euhedral to subhedral and often slightly zoned, at the

edges, with inclusions of biotite, magnetite, apatite and rare zircon, allanite and sphene. Amphibole is minor. Large plates of green to brown pleochroic biotite are associated with abundant accessory sphene, apatite and allanite. Only a few relict braid- or patch-perthites are present.

On the other hand, some samples have many large phenocrysts of now-perthitic alkali-feldspar (e.g., GD30 and GD44), suggesting that feldspar accumulation may have been locally important. These two samples show extensive (although not complete) replacement and/or overgrowth of pyroxene by amphibole. Biotite is common as are accessory sphene, apatite, allanite, zircon and magnetite.

The coarsest-grained of the author's sample suite are mafic syenites in which amphibole is the dominant (sometimes sole) ferromagnesian phase. These commonly contain large tablets of partially exsolved alkali feldspar, little biotite but much sphene, allanite and apatite, with accessory zircon and magnetite. The association of more than 90% mafics as amphibole with large feldspar tablets suggests that there is little correlation between amphibole abundance and the degree of deformation (c.f., Richardson, 1968).

Lastly, finer-grained, amphibole-rich mafic syenites exist which show no obvious evidence of once containing large alkali-feldspar phenocrysts (e.g., MJ026). Little pyroxene remains and the feldspars are nearly all K-feldspar or plagioclase. Biotite plates are common and epidote forms euhedral to subhedral rims on allanite or larger grains of its own. Apatite is now relatively rare, but sphene and zircon are still abundant. Rarely, quartz forms a myrmekitic intergrowth with feldspar.

The pegmatites ought perhaps to be dealt with here, since they represent the residual fluids from local filter-press action (Richardson, 1968) in the mafic syenites. They are intrinsically rather variable, but essentially consist of an aggregate of feldspar and quartz, with minor mafic phases (pyroxenes or sometimes-

fibrous sodic amphibole, of which the latter is more normal (Harry, 1952), sparse chlorite and biotite) and locally abundant accessories such as sphene, zircon, allanite and epidote. Richardson (1968) has given an account of their distribution, field relationships and mineralogy. He suggests that pegmatitic material was available until the final stages of deformation.

Leucocratic syenites.

There is apparently somewhat less variation within the leucocratic syenites, and none of the author's suite reaches the grain-size of the coarsest mafic syenites. Some have large alkali-feldspar phenocrysts (e.g., MJ010 and MJ011) associated with mafic phases dominated by pyroxene, but with some amphibole replacement and/or overgrowth. The accessory phases are similar to those found in the mafic syenite.

The samples forming the westernmost tract of leucocratic syenite (e.g., MJ001 and MJ002) are apparently distinctive, having amphibole as the main ferromagnesian phase, with minor biotite and little pyroxene. Pyroxene may once have been more abundant since some of the amphiboles form symplectites with quartz which may represent the products of a pyroxene hydration reaction. Other amphiboles are dusted with opaques, which also sometimes form at the rims of sphene. Relict perthite is rare, and large plates of sometimes euhedral K-feldspar and plagioclase are more common, often granulated at the edges.

Metasedimentary xenoliths.

As has been stated above, these exist in the mafic syenite in a range of sizes. Those described below are from the smallest, visible in hand specimen and under the microscope. They form generally rounded inclusions of psammitic - semipsammitic material, and the larger examples are petrographically similar to the surrounding Moine metasediments. The latter have been described by Lambert et al. (1964) and form medium-grained foliated

rocks composed essentially of quartz, feldspar and biotite with accessory sphene, zircon, Fe-Ti oxides. Muscovite is locally important. Some xenoliths (e.g., in samples GD17, GD43) retain a similar mineralogy, but sillimanite and staurolite are also important, perhaps indicative of desilication. Accessory sphene and zircon are still present. At the junction with the syenite, a biotitic rind is often formed, and feldspars contain inclusion trails similar to those seen in the syenite itself. As the xenoliths become progressively incorporated into the magma, only clots of Fe-Al silicates, biotite and Fe-Ti oxides remain. Accessory phases such as zircon and sphene disappear fairly early in the process, which might have important consequences for the incorporation of specific trace elements into the melt, such as the REEs, U and Th. The substantial effects on the chemistry of the magma will be outlined later, but the mineralogy of the associated syenites remains essentially the same, as would be theoretically predicted and as has been recorded during metasediment assimilation elsewhere (e.g., Kitchen, 1984). Nevertheless, some mineral-chemical variations might be induced, which could form a legitimate study of their own, and will not be pursued here.

Syenite - host rock reactions.

Two types of reaction cause observable perturbations in radioelement abundance (as indicated by gamma-ray scintillometry): marginal fenitisation of Moine and local reaction of syenite veins with the Glen Pean Xenolith.

The term "fenite" has been used in the literature to describe a multitude of metasomatic alterations of country rocks into which alkaline igneous rocks have been emplaced, related to its original definition (Brogger, 1921). McKie (1966) suggested that fenitisation accompanies carbonatite intrusion more frequently than that of alkaline silicate plutons, so those at Glen Dessarry form examples of the latter,

rather rarer association. In fact they are much more easily comparable with the restricted fenitisation effects around the Monchique alkaline complex, as desribed by Rock (1976) rather than the classic localities such as Fen. Recently, fenitisation related to (?) carbonatite intrusion deep into the Great Glen Fault has been descibed (Garson et al., 1984) approximately coeval with the emplacement of the Glen Dessarry pluton.

Samples of the fenites were collected on the southern Forestry road at the eastern contact of the intrusion with the Moine, from a narrow zone (less than 2m) of pink, altered metasediment which shows a distinctly patchy development in the field. Fenitisation proceeds by feldspathisation of quartz; development of alkali amphiboles and locally epidote and chlorite; and the introduction of a varied suite of minor and accessory minerals dominated by sphene and allanite, similar to that of the syenite itself.

Veins of mafic syenite intrude the Glen Pean Xenolith (Fig 7.1) and give rise to a characteristic pegmatoid reaction zone between the two. Due to difficulties in sampling, a complete traverse across a single reaction zone was not possible, but a composite of two is thought to provide a close approximation. Mineralogically, the reaction zone is a coarse-grained, variable aggregate of quartz, feldspar and biotite with accessory allanite, zircon, monazite and pyrite, the latter locally haematised. Chemical aspects of these local features will be described later.

8.3 The Origin of Amphibole

At several places in the preceeding text the metamorphic origin of amphibole proposed by Richardson (1968) has been questioned. The obvious importance of its status to an understanding of the metamorphism of the Complex requires that the problem now be addressed more specifically.

Richardson (1968) advanced the metamorphic-origin hypothesis on the textural grounds that amphibole replaces pyroxene with a distribution apparently controlled by the present shape of the outcrop. As has been intimated above, the time at which this occured and the processes which controlled it are open to alternative interpretation. The difficulties of textural interpretations in such systems have recently been emphasised by Otten (1984) and are manifest by the opposite views on feldspar exsolution or porphyroblastesis of Richardson (1968) and Harry (1952). In many of the author's sample collection amphibole mantles pyroxene in perfect optical continuity throughout, and often this extends to intergrown amphibole within the pyroxene itself. Alternatively, pyroxene has clearly been replaced by a symplectic intergrowth of amphibole and quartz (Plate 8.1a and b). Such relationships may be derived either by crystallisation from a melt or by epitaxial overgrowth and reaction due to sub-solidus hydration, as suggested by Richardson (1968). Many samples show no obvious sign of reaction (Plate 8.1c), or even no sign of the former presence of pyroxene (Plate 8.1d) and a few samples (e.g., GD43 and GD45) have rare amphibole crystals which are euhedral (Plate 8.1e and f). However, in most samples they are anhedral, but even in undeformed plutons the latter has been regarded as not out of context with a magmatic origin (Jones, 1984). As will become apparent below, magmatic reaction relationships in varying degrees of complexity are by no means uncommon between amphiboles and other mafic silicates in alkaline or sub-alkaline plutonic complexes (e.g., Stephenson, 1972; Robertson and Parsons, 1974; Larsen, 1975; Powell, 1978; Mitchell and Platt, 1978; Sylvester et al., 1978; Anderson, 1980; Parsons, 1981; Wilson et al., 1981; Rock, 1982; Stephenson and Upton, 1982; Anderson, 1984 and Jones, 1984). Perhaps the most complete description of amphibole reaction rims around pyroxene from the above authors, is given by Stephenson

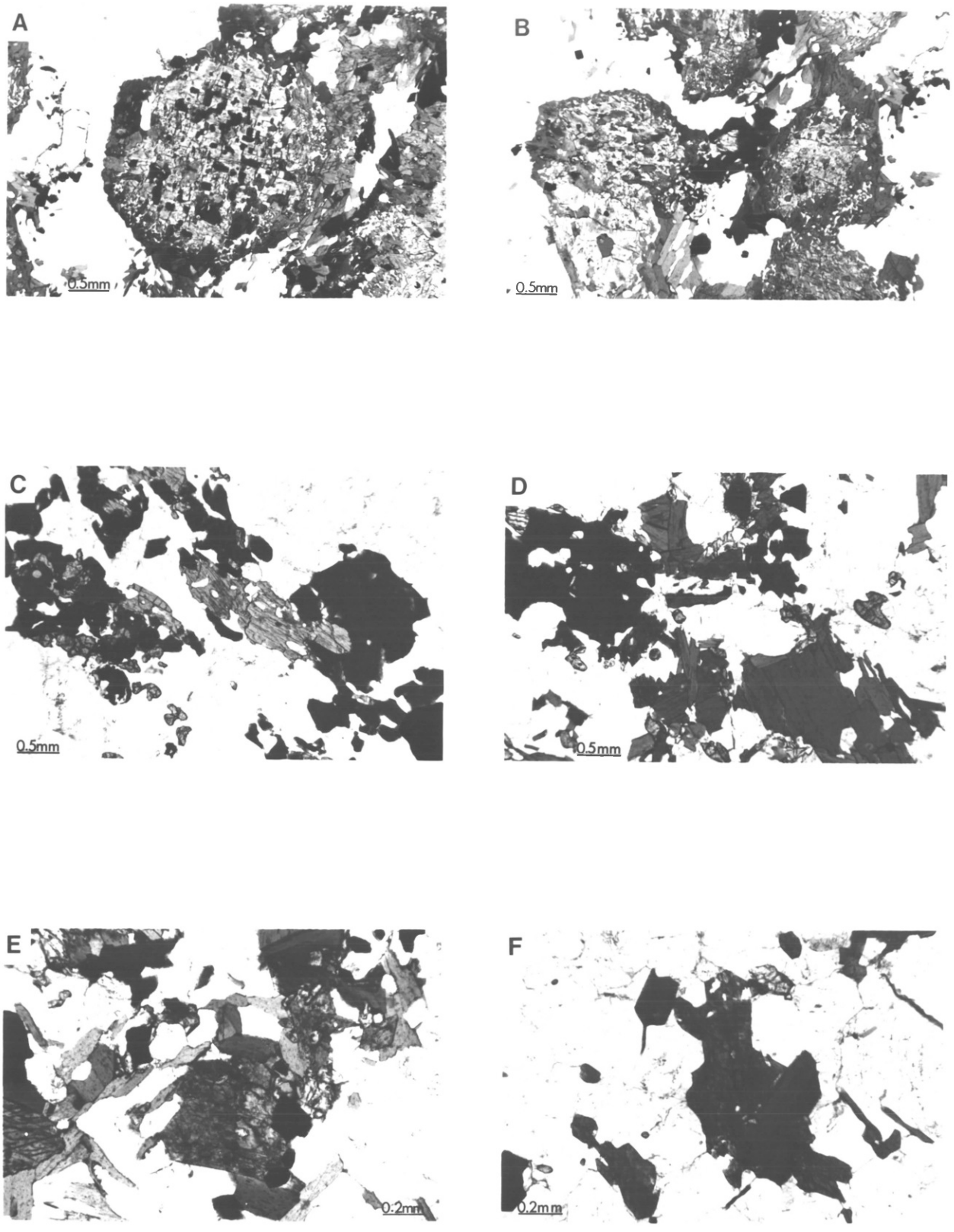


PLATE 8.1 AMPHIBOLE TEXTURES

and Upton (1982), from the Kungnat Fjeld gabbro-syenite complex. Indeed, plutons from the Gardar Province generally show such relationships (Stephenson, 1972; Larsen, 1976), perhaps due to falling temperature and fO_2 combined with increasing pH_2O in the melt (Stephenson and Upton, 1982).

Chemical comparisons with igneous and metamorphic amphiboles.

A recent review of amphiboles in the igneous environment was given by Wones and Gilbert (1981). They are represented by a range of compositions from iron-magnesium rich varieties such as cummingtonite (Kuno, 1938) through much more common calcic types to alkaline varieties in evolved rocks. The Glen Dessarry amphibole compositions are generally magnesio-hastingsitic hornblende, edenitic hornblende, ferroedenite and edenite. Speer et al. (1980) documented variations in "plutonic" amphibole compositions from a single tectonic province (often the amphiboles mantled pyroxene), which were mostly edenites and edenitic hornblendes, also showing a close similarity with those from Glen Dessarry.

Many more-specific studies of amphibole chemistry have appeared in the recent literature, in addition to those already mentioned. The Monchique alkaline complex (Rock, 1982) shows a trend through kaersutite and pargasite to hastingsite, edenite or katophorite, often exhibiting complex reaction relationships with other mafic phases. He suggests that lower Mg / Mg+Fe and higher Na / Na+Ca in amphiboles relative to their pyroxenic cores may suggest local reaction of early-formed pyroxenes with later, more volatile-rich interstitial liquids. Such elemental relationships are also found between Glen Dessarry amphiboles and pyroxenes. The Motzfeldt Centre nepheline syenites (Jones, 1984) contain pyroxenes mantled by anhedral amphiboles, from hastingsite through ferroedenite to arvedsonite in composition. The Klokken layered gabbro-syenite complex, a good example of

in-situ differentiation, contains amphiboles of ferroedenitic composition, and hastingsite replacing pyroxene in the laminated syenite (Parsons, 1981). Finally, the Wolf River monzonite (Anderson, 1980) also has amphibole displaying the obviously common replacement relationships with pyroxene, of edenitic to ferroedenitic composition. It seems clear, even from this necessarily brief summary, that amphiboles showing closely similar compositions and textures to those at Glen Dessarry are not uncommon in plutonic rocks elsewhere, and that many authors have not felt it necessary to invoke special, metamorphic conditions for their genesis, preferring instead a magmatic origin.

On the other hand, accounts of metamorphic amphiboles in originally intrusive rocks also exist, recently that of Otten (1984) for example, recording hydration of pyroxene in a gabbro during metamorphism. Amphiboles formed by retrograde re-equilibration of Lewisian metatonalites may also be edenitic or ferroedenitic (see above) or of closely similar composition (Sills, 1983). Thus, although a simple chemical comparison provides evidence which is inconclusive in itself, it does demonstrate the feasibility of an igneous origin.

Oxygen isotopes.

Since the inception of oxygen-isotope analysis in the early 1960s, it has been amply demonstrated that the $\delta^{18}O$ values of rocks and their constituent minerals are sensitive indicators of interactions with hydrous or carbonic fluids (e.g., Taylor and Forrester, 1971; Coleman et al., 1982). For this reason, a brief oxygen isotope study of the Glen Dessarry syenites was initiated in order to test the hypothesis (Richardson, 1968) that the Complex has partially equilibrated with reducing fluids derived from the Moinian host rocks. An unambiguous result reached simply by analysis of amphibole would rely on the existence of a significant difference between the oxygen isotope composition of metamorphic amphibole derived from a fluid originally in

equilibrium with the Moine metasediments, and that precipitated directly from a silicate melt. Unfortunately, even a cursory inspection of the sparse literature data for oxygen isotopic compositions of igneous and metamorphic amphiboles (e.g., Foland and Friedman, 1977; Taylor and Epstein, 1962), suggests that a resolvable difference might not exist (Table 8.5). For the record, analyses of two amphibole seperates from mafic syenite samples GD29 and MJ015 give an average value of +6.4‰ (range 0.27). This lies at the upper end of the range for igneous amphiboles but is also theoretically compatible with a metamorphic origin.

Igneous		Metamorphic
+6.4[1]	+3.1[2]	+7.0[1]
+6.5[1]	+5.2[2]	+6.8[1]
+6.6[1]	+5.0[2]	+8.3[1]
+6.9[1]	+5.1[2]	+9.0[1]
+6.9[1]	+5.6[2]	+10.8[1]
+5.9[1]		

Table 8.5: Comparison of $\delta^{18}O$ values for amphibole derived from an aqueous fluid with that precipitated from a silicate melt.
(1= Taylor and Epstein, 1962; 2= Foland and Friedman, 1977).

However, another approach which might provide useful information is the analysis of whole-rock samples. Data for representatives spanning the compositional range observed (see below) are plotted against SiO_2 in Fig. 8.3. Average values are as follows: cumulus pyroxenite +7.1; mafic syenite +8.1; leucocratic syenite +8.5; and pegmatite +8.9‰. An approximate early melt composition can be calculated from that of the cumulus pyroxenite, using a suitable pyroxene-melt fractionation factor

(+0.25, after Turi and Taylor, 1976; Taylor et al., 1979; Kyser et al., 1982 and Taylor et al., 1984). This gives an estimate of +7.35‰, towards the top of the range of accepted mantle values (+5.5 to +7.5 according to Taylor et al., 1984), and thence there appears to be a gradual increase in $\delta^{18}O$ correlated with melt

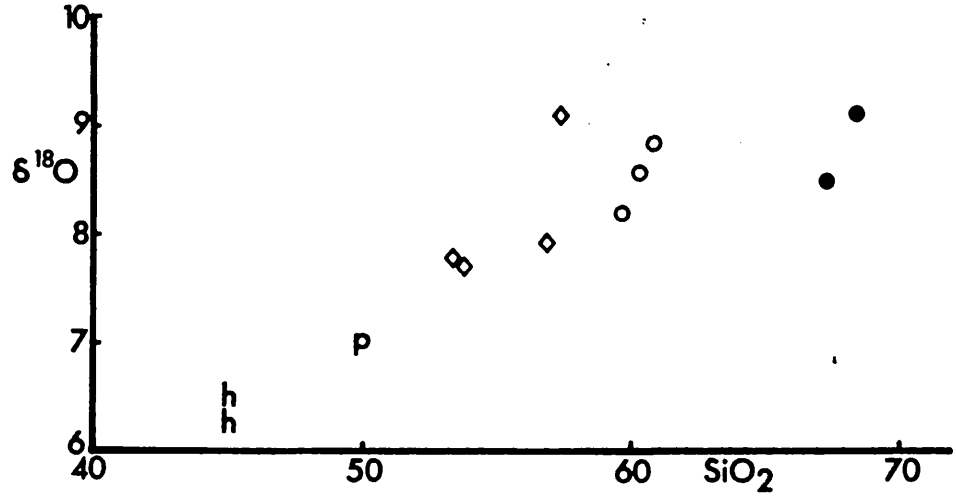


Figure 8.1: Variation of $\delta^{18}O$ with SiO_2 for Glen Dessarry syenites.

(h= amphibole, p= cumulate pyroxenite GD49, open diamonds= mafic syenites, open circles= leucocratic syenites, closed circles= pegmatites.)

evolution. Fractional crystallisation involving ^{18}O-poor mafic phases such as biotite, magnetite and amphibole could generate such a trend and range (1.5 to 2.0‰), in which case it is difficult to envisage how a subsequent influx of large volumes of high ^{18}O-metamorphic fluid could cause no obvious disturbance of the observed relationship. An oxygen isotope study of the alkaline plutons of the Red Hill Complex, New Hampshire (Foland and Friedman, 1977), in which the syenites show apparently similar amphibole-pyroxene relationships to those at Glen Dessarry, has demonstrated a similar total range of whole-rock values (+6.2 to +9.3‰), and a similar whole-rock / amphibole fractionation of 2.4, compared with 1.7 at Glen Dessarry. Furthermore, Chivas et al. (1982) and Matsuhisa (1979) have documented significant oxygen isotope fractionation as a result of

fractional crystallisation; producing a $\delta^{18}O$ range of 1.8‰ with a slope of 0.06‰ / $\%SiO_2$. Although these obviously depend on the crystallising mineral assemblage and temperature, they are comparable with the range and slope at Glen Dessarry (1.5 - 2.0‰, c., 0.08 respectively).

However, Fig. 8.1 is not so readily explicable in terms of a partial or complete re-equilibration with relatively high $\delta^{18}O$ fluids. Such a process would be required to be peculiarly selective with respect to rock type, such that isotopic exchange took place with the pegmatites and the leucocratic syenites, in preference to the mafic syenites and ultrabasic rocks. In view of the fact that a Moine-derived fluid would need to pass through the mafic syenite envelope to reach the leucocratic syenite, this seems inherently unlikely.

CHAPTER NINE

RELICT MAGMATIC CONTROLS ON ELEMENT DISTRIBUTION

The previous chapter has briefly demonstrated the considerable petrographic (and therefore chemical) diversity within the exposed syenites, over and above that obviously caused by the varying state of strain in the Complex. This chapter is intended to test the degree to which these differences might be the relict results of magmatic processes.

Any magmatic model for the crystallisation of the Complex must take into account the following features:

i) The intrusive relationships between leucocratic syenite and mafic syenite.

ii) Locally important crustal contamination, revealed by partly-digested metasedimentary xenoliths.

iii) Xenoliths of early, possibly comagmatic cumulates.

iv) Late-stage, filter-pressed pegmatites.

These favour the emplacement of two magma pulses whose original compositions may be linked by fractional crystallisation of the early (low-level) cumulates. Once emplaced, the petrographic and chemical diversity referred to above may have been caused by in-situ crystal-liquid separation at the magmatic stage, coupled with local crustal contamination.

Previous work on in-situ fractionation processes has highlighted several potential problems (McCarthy and Hasty, 1976; McCarthy and Groves, 1979 and Tindle and Pearce, 1981). Clear distinction between "cumulate" and "melt" rock types becomes progressively more difficult as melt acidity and viscosity increase. "Crystal mush" might be a more accurate term with which to describe the samples, comprising various combinations of cumulus crystals and variably evolved interstitial melt. Only rarely does good textural evidence allow an accurate assessment of the amount of cumulus minerals (e.g., Tindle and Pearce, 1981), even when the intrusion has not been subjected to later deformation as at Glen Dessarry. Neither of the two extreme mathematical

models of crystal fractionation are entirely applicable, since the rate of equilibration of crystal with melt would not have been so slow as to restrict equilibrium to the surface only (Rayleigh crystallisation), or so fast as to allow complete equilibrium at all times (equilibrium crystallisation). Some indeterminable combination of the two would probably have controlled the compositional evolution of the melt/crystal system. Further, the partition coefficients required by the equations have been shown to vary regularly with melt composition, temperature and perhaps pressure (e.g., Watson, 1976; Green and Pearson, 1983; Mahood and Hildreth, 1983), so that assumption of a unique value is undoubtedly an oversimplification. Finally, the influence of accessory minerals (in which Glen Dessarry is particularly rich) is difficult to assess quantitatively due to the lack of precise knowledge of their partition coefficients, coupled with their low modal abundance.

Bearing all these difficulties in mind, the following account attempts to assess the geochemistry of the Glen Dessarry syenites in order to test whether crystal-melt equilibria involving their constituent mineral phases could have caused the observed chemical diversity. This has been undertaken in terms of the following element groups:

i) Major element oxides whose abundances (except P_2O_5 and TiO_2) are controlled by the relative involvement of the major rock-forming minerals.

ii) Transition metals (Cr, Ni, V) which are enriched in early-formed mafic mineral phases.

iii) Large-ion lithophile elements of trace abundance whose microchemical distribution is governed by diadochic exchange with major element cations in rock-forming mineral phases (Rb, Ba and Sr).

iv) High field-strength elements and other LILEs (REE, Zr, Hf, U, Th, Nb, Ta) whose behaviour in part reflects the role of crystallisation of minor mineral phases such as those which have been observed in the syenites (e.g., zircon, allanite, apatite and sphene).

Having established the possible trends of fractionation and contamination, selected samples are used for the construction of multi-element, chondrite-normalised diagrams in order to summarise the response of the incompatible element group to low-level and in-situ fractionation; to the local processes of xenolith digestion; and to magma-related metasomatic reaction.

Full major and trace element whole-rock data for 50 samples are available in the appendix, together with derived CIPW norms, and average analyses are presented in Table 9.1.

	Leucocratic (21)	Mafic (22)
SiO_2	60.62	54.82
TiO_2	0.65	1.08
Al_2O_3	17.45	15.03
Fe_2O_3	4.56	8.19
MnO	0.09	0.15
MgO	1.12	3.86
CaO	2.80	6.03
Na_2O	5.00	3.90
K_2O	6.25	5.12
P_2O_5	0.30	0.64
Total	98.84	98.82
Cr	9	67
Ni	9	34
V	88	172
U	1.66	3.44
Th	9.1	14.8
Sr	4824	3465
Ba	3857	3099
Rb	105	105
Nb	19	22
Zr	84	190
Y	29	38

Table 9.1: Average whole-rock analyses of Glen Dessarry syenites.

Normative data are shown in Fig. 9.1, projected onto the Qz-Ab-Or-Ne quaternary. They closely resemble monzonitic plutons from temporally and tectonically diverse settings; both in terms of mineralogy and of geochemistry (Miller, 1977, 1978; Simmons and Hedge, 1978; Sylvester et al., 1978; Harris et al., 1983).

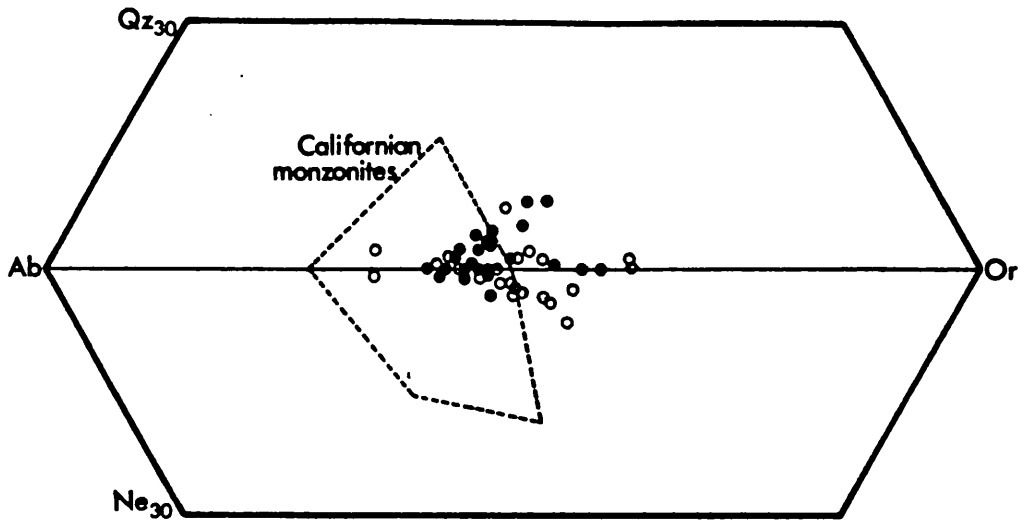


Figure 9.1: Normative data for Glen Dessarry syenites projected onto the Qz-Ab-Or-Ne quaternary.
(open circles= mafic syenite, closed circles= leucocratic syenite).

9.1 Major Element Oxides

Figure 9.2 is a schematic diagram designed to show how major element oxide, bivariate diagrams can be interpreted within the constraints already set on a possible magmatic evolutionary scheme; that is, in terms of low-level and in-situ differentiation. The low-level trend is required to drive the primary melt composition (P) through that of the mafic syenite (MS), which is intruded first, to that of the leucocratic syenite which follows (LS), by removal of some combination of cumulus mineral phases (Cp). The in-situ trends, which are due to incomplete separation of crystallising solids and evolving liquid, diverge from these parent compositions (MS and LS) according to whether the samples represent an excess of cumulates (Cms and Cls) or liquid (Mms and Mls). Note that in this simplified diagram it has been assumed that the crystallising assemblage remains the same within each evolutionary step. Should new minerals enter the assemblage once it has been established, or old minerals leave it, the trends would change direction according to its new bulk composition. Figure 9.3 shows the series of Harker (oxide vs SiO_2) diagrams for the

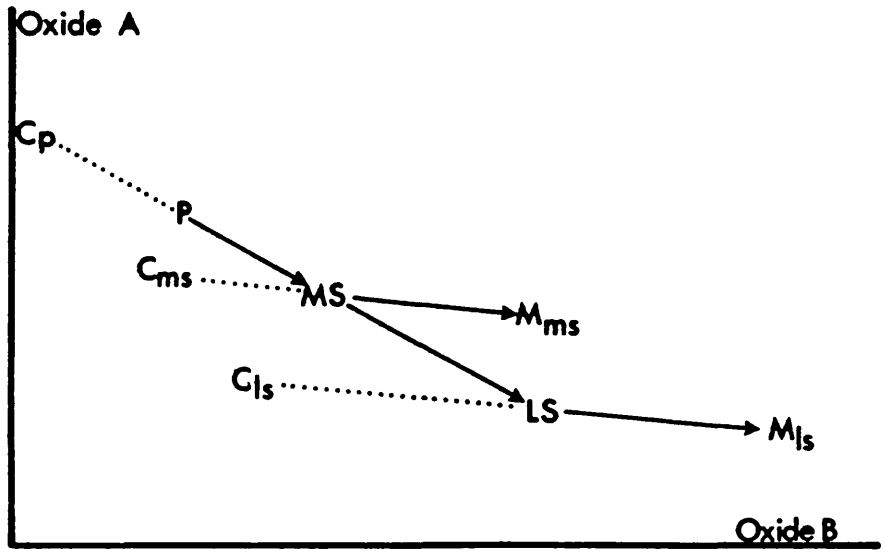


Figure 9.2: Schematic diagram illustrating interpretation of Harker diagrams in terms of in-situ and low-level fractional crystallisation.

whole-rock, major-element analyses, upon which are also plotted the fields of analyses of the major minerals likely to be involved in the fractionation processes. These are derived from euhedral crystals in samples of syenite which preserve an igneous texture (marked i), and the major mineral phases of the associated cumulate fragments (marked c); data for which have been provided in the previous section, and the appendix.

The first group of oxides discussed is MgO, Fe_2O_3 and CaO - all of which are preferentially concentrated in early-formed mafic minerals and which are therefore particularly important in constraining the relative roles of olivines, pyroxenes, amphiboles and biotites. Not surprisingly, therefore, these three oxides show many common features:

i) Rapidly falling concentration with increasing SiO_2.

ii) Good correlations with SiO_2, and between each other.

iii) A relatively restricted field for leucocratic syenites compared to the extensive mafic syenite trend.

iv) Colinearity of the mafic and leucocratic syenite regression lines.

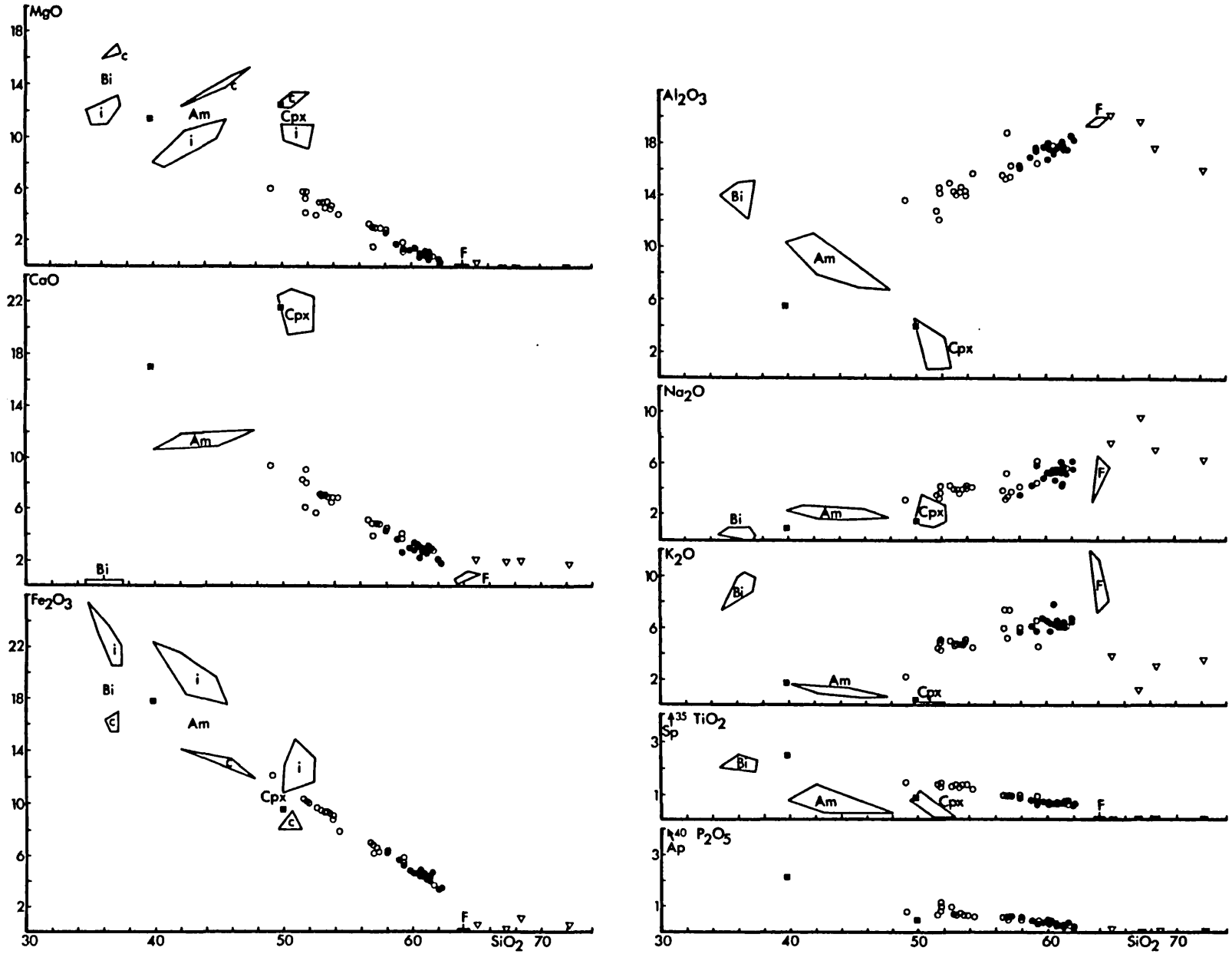


Figure 9.3: Harker diagrams for Glen Dessarry syenites.

(closed squares= ultramafic inclusions; open circles= mafic syenites; closed circles= leucocratic syenites; open inverted triangles= pegmatites; data fields: Bi= biotite; Cpx= clinopyroxene; Am= amphibole; F= alkali feldspar; Sp= sphene; Ap= apatite).

v) Ultramafic sample GD48 lies on, or close to, the extrapolation to lower SiO_2 of the mafic syenite correlation.

Assuming that to a first approximation the system as a whole remained closed, the parent "liquids" of mafic syenite and leucocratic syenite composition should lie somewhere near the average of the observed in-situ trends. Thus, an estimate of the low-level trend may be obtained from a vector connecting these two average compositions. Since amphibole analyses lie on an extrapolation of this trend to lower SiO_2, its removal could drive the liquid composition in the required direction. However, the preservation of polymineralic cumulates in preference to amphibolites suggests that a combination of other mafic phases, not necessarily involving amphibole, is more likely. For example, GD48 (which is essentially a combination of pyroxene, biotite, magnetite, sphene, apatite, and perhaps some amphibole) also falls on the correct extrapolation. Therefore, it seems reasonable (on the basis of CaO, MgO and Fe_2O_3) to suppose that the separation of a mineral assemblage equivalent to that found in some of the exposed cumulates was responsible for the mafic-leucocratic syenite evolutionary phase. Mass-balance calculations based on an assemblage represented by GD48 show that approximately 26% removal will drive an average (parent) mafic syenite composition to an average (parent) leucocratic syenite composition (Table 9.2).

The in-situ fractionation trends for this group of oxides are essentially colinear with those derived for low-level fractionation, which suggests either that no alteration to the assemblage took place upon intrusion and further evolution, or that any new minerals entering the crystallising assemblage themselves fall on the existing trend. Petrographic evidence also suggests that the mafic minerals which crystallised in the high level magma-chamber are similar to those that separated from the parent melt in the low-level

SiO_2	TiO_2	Al_2O_3	Fe_2O_3	MnO	MgO	CaO	Na_2O	K_2O	P_2O_5
Reactants (LS top, GD48 bottom)									
60.62	0.65	17.45	4.56	0.09	1.12	2.80	5.00	6.25	0.30
39.80	2.39	5.52	17.75	0.28	11.43	16.99	0.85	1.75	2.12
Estimated mafic syenite (74.34% LS + 25.66% GD48)									
55.28	1.10	14.39	7.94	0.14	3.77	6.44	3.93	5.10	0.77
Mafic syenite									
54.82	1.08	15.03	8.19	0.15	3.86	6.03	3.90	5.12	0.64
Differences									
0.46	0.02	-0.64	-0.25	-0.01	-0.09	0.41	0.03	-0.02	0.13

Residual sum of squares = 0.8772

Table 9.2: Mass-balance calculations of low-level fractional crystallisation in the Glen Dessarry syenite.

chamber. However, the importance of feldspar in the exposed lithologies and its frequent phenocryst habit, suggest that it soon became an important crystallising phase. Moreover, it is not possible to accurately model the compositions of evolved mafic or leucocratic syenites by continuation of the "GD48-assemblage" fractionation. Large errors in K_2O, Na_2O, CaO and Al_2O_3 suggest significant feldspar involvement. The position of analysed feldspars on the variation diagrams shows why its crystallisation would cause little offset to the established evolutionary paths, merely restricting the progression to high-SiO_2 lithologies. The preservation of contiguous pyroxene-biotite-rich rocks in the mafic syenite (e.g., MJ012; see Petrographic Variations, above) might nevertheless indicate that mafic phases dominated in the early stages of crystallisation. It is interesting to note that the in-situ fractionation has caused an overlap between the more-mafic leucocratic syenites and more-leucocratic mafic syenites. Extensive local filter-pressing gave rise to the nebulous pegmatites, four samples of which from the mafic syenite outcrop have been analysed in order to give some idea of the composition of the evolved melt. These lie on an

extension of the in-situ trends, in accord with their assumed origin as late-stage melts squeezed out of their nearly-crystalline mafic syenite hosts.

The second group of major elements to be considered comprises K_2O, Na_2O and Al_2O_3 (Fig. 9.3), which should provide more information on the proposed involvement of feldspars during in-situ evolution. As before, the leucocratic syenites exhibit a more restricted field than do the mafic syenites. In general terms, all three elements increase with increasing SiO_2, in response to the early removal of K_2O, Na_2O and Al_2O_3-poor mafic phases, but there is considerably more scatter than for the previous three elements. Calculations for the low-level phase (Table 9.2) confirm that approximately 26% removal of an assemblage represented by sample GD48 is compatible with the observed evolution from "parent" mafic to "parent" leucocratic syenite. The scatter on the in-situ trends may be a result of the new participation of feldspar causing large variations in the cumulus assemblage, depending upon its precise composition and crystallising proportion. The pegmatites have clearly had a relatively potassic feldspar removed, and the resultant "cumulates" may well be represented by potassic mafic syenites GD27, GD28 and GD29. It may be significant that these are all amphibole-rich (see below).

Finally in this brief consideration of the major elements, the variations in the abundances of P_2O_5 and TiO_2 should be described. These are useful petrogenetic indicators of the involvement of phosphate and Ti-bearing phases respectively, and at Glen Dessarry these are likely to be dominated by apatite and sphene. In both cases there is a very rapid fall with increasing SiO_2, indicating quantitative removal of both phases from the melts during in-situ and low-level fractionation.

Thus the new whole-rock and mineral chemical data discussed above, and the mineralogy of the cumulate samples, require no substantial modifications to the

conclusions of Richardson (1968) that the mafic and leucocratic syenites are related by fractional crystallisation of aegerine-augite, biotite and magnetite, save perhaps for the addition of sphene and apatite as important constituents, for which there is also considerable trace element evidence, to be discussed below.

9.2 Trace Elements

The three groups of trace elements (i.e., transition metals, LILEs and HFSEs) are all dealt with in a similar way below, based on comparison of the trends inherent in the analytical data with those theoretically predicted by the equations controlling fractional crystallisation. This approach is similar to that used by McCarthy and Hasty (1976), McCarthy and Groves (1979) and Tindle and Pearce (1981). In view of the common zoning preserved in most minerals which constitute the syenites, Rayleigh fractionation is thought to be more applicable than equilibrium fractionation, and so has been used throughout. Figure 9.4 (after McCarthy and Hasty, 1976) shows, in a schematic way, the method of modelling trace element variations in plutons which have suffered in-situ crystal-liquid separation.

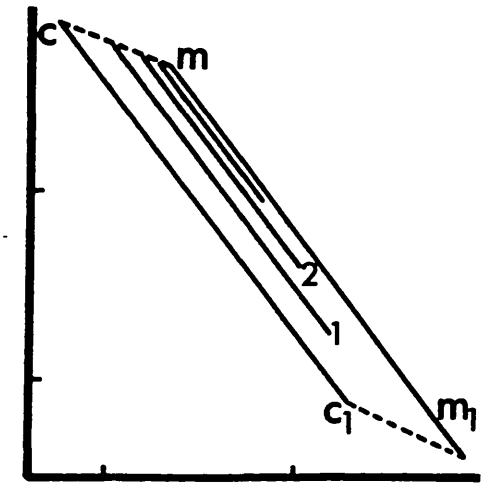


Figure 9.4: Schematic diagram illustrating interpretation of logarithmic, bivariate trace element plots in terms of Rayleigh fractionation.

When plotted on logarithmic, bivariate diagrams, Rayleigh fractionation produces straight-line vectors for evolving liquid compositions (m to m_1), and parallel vectors for equivalent cumulate compositions (c to c_1, assuming that the crystallising assemblage and relevant partition coefficients remain constant). Crystal mushes, which most rocks of the Complex probably represent, lie on mixing lines between these extremes (liquid and cumulate). The range of cumulate compositions decreases with separation efficiency, such that 20% trapped intercumulus melt produces line 1, 40% produces line 2, and so on. Melt evolution is concomitantly restricted, resulting in an overall contraction of the parallelogram with increasing amounts of trapped intercumulus melt. Thus, real data controlled by crystal-liquid equilibria should approximate to a parallelogram. Bearing in mind all the inherent inaccuracies in partition coefficients, assumptions of perfect adherence to the Rayleigh crystallisation equation, constancy of crystallising assemblage and partition coefficient, such diagrams can only be expected to reveal general trends - it is virtually impossible to define the proportion of cumulate phases versus crystallised melt in any particular sample. On each diagram are plotted mineral vectors, showing the effect on melt composition of their removal and annotated with proportion of melt remaining. These allow a semi-quantitative assessment of the mineral assemblages capable of controlling any trends observed in the data.

Choice of partition coefficients is obviously important, but their scarcity imparts an error about which little can be done. Those used here are from Villemant et al. (1981), and seem to be most applicable to the bulk composition of the Glen Dessarry samples (they are derived from an alkali basalt to trachyte suite), as well as being a more comprehensive set than most available in literature. They are listed for easy reference in the Appendix.

Transition Metals

The Cr versus Ni bivariate plot is shown in Fig. 9.5. The data for mafic and leucocratic syenite form two sub-parallel, linear arrays, compatible with a strong magmatic control during in-situ differentiation. The mineral vectors suggest tht the dominant influence for both variants is clinopyroxene - some feldspar is permissible since this would merely restrict the

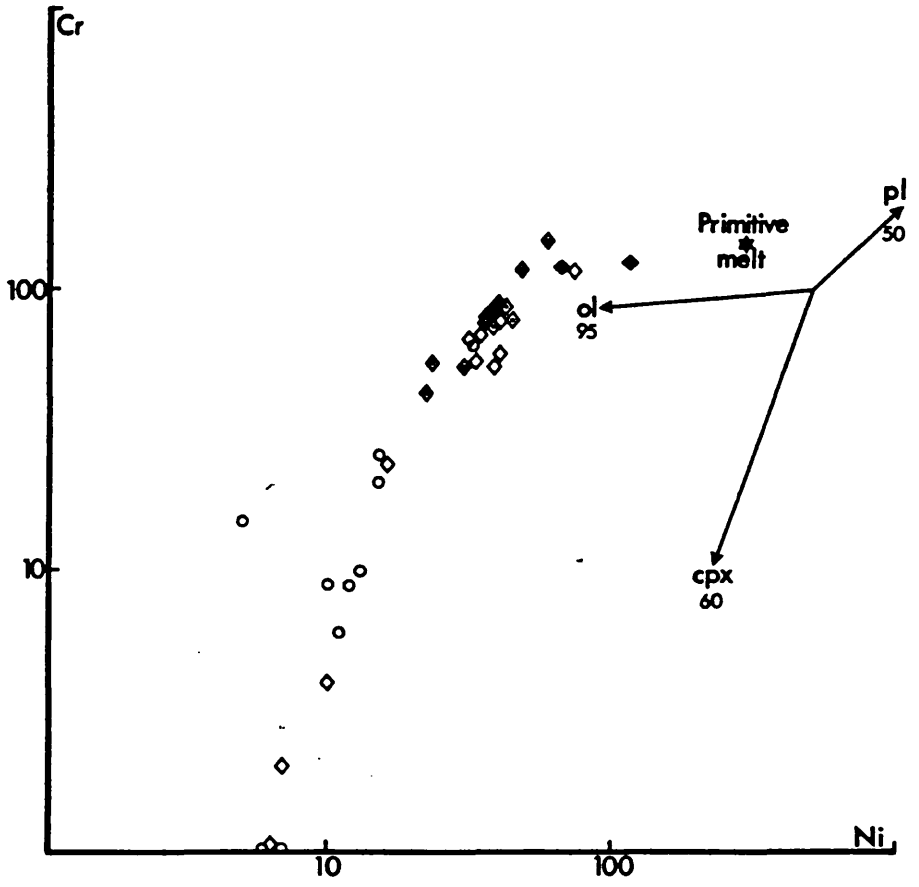


Figure 9.5: Logarithmic, bivariate plot of transition metal abundances for Glen Dessarry syenites.
(closed diamonds= cumulates, open diamonds= mafic syenites, dotted open diamonds= "contaminated" mafic syenites, open circles= leucocratic syenites).

development of the array. This confirms inferences made from the petrographic and major element evidence above. It also confirms that olivine fractionation was not important during in-situ evolution or in the mafic to leucocratic syenite low-level phase. Determination of

the latter is difficult, since it relies on identification of original liquid compositions, which are not preserved, but there seems little reason to doubt that it was also substantially influenced by pyroxene crystalisation. However, the position of primitive mantle melts on the diagram (data from Thirlwall, 1982) suggests that if the syenites were derived from such a parent (this will be discussed below), some olivine fractionation must have occurred during an early phase of the low-level differentiation. The amount of olivine removed is restricted to less than about 10% by Ni abundances in the Glen Dessarry samples, and must have been associated with substantial pyroxene separation, in order to reduce Cr to sensible levels.

Large-Ion-Lithophile Elements Controlled by Major Mineral Phases.

This group includes Rb, Sr and Ba, which may be used to derive information about biotite, amphibole and the hypersolvus alkali feldspar. The Ba-Sr relationships of both variants approximate to linearity, which implies the importance of crystal-liquid equilibria (Fig. 9.6). The mafic syenite field overlaps that of the leucocratic syenites, but extends to samples with lower Ba and Sr. The pegmatites all have very low abundances of both elements. The mafic syenite group with high Ba and Sr defines a broad trend which, by comparison with the mineral vectors illustrated, could be controlled by pyroxenes and feldspars - in accord with the previous results. On the basis of this diagram alone, the low Ba, Sr group could apparently be the result of alkali-feldspar, biotite and amphibole removal (approximately 10%) from a comparable parent melt. However, this group of samples contains those with high radioelement abundances and distinctive REE patterns which could not be generated by this hypothetical process alone (see below); and those in which there is field and petrographic evidence for contamination with metasediment. Analyses of the country rock have

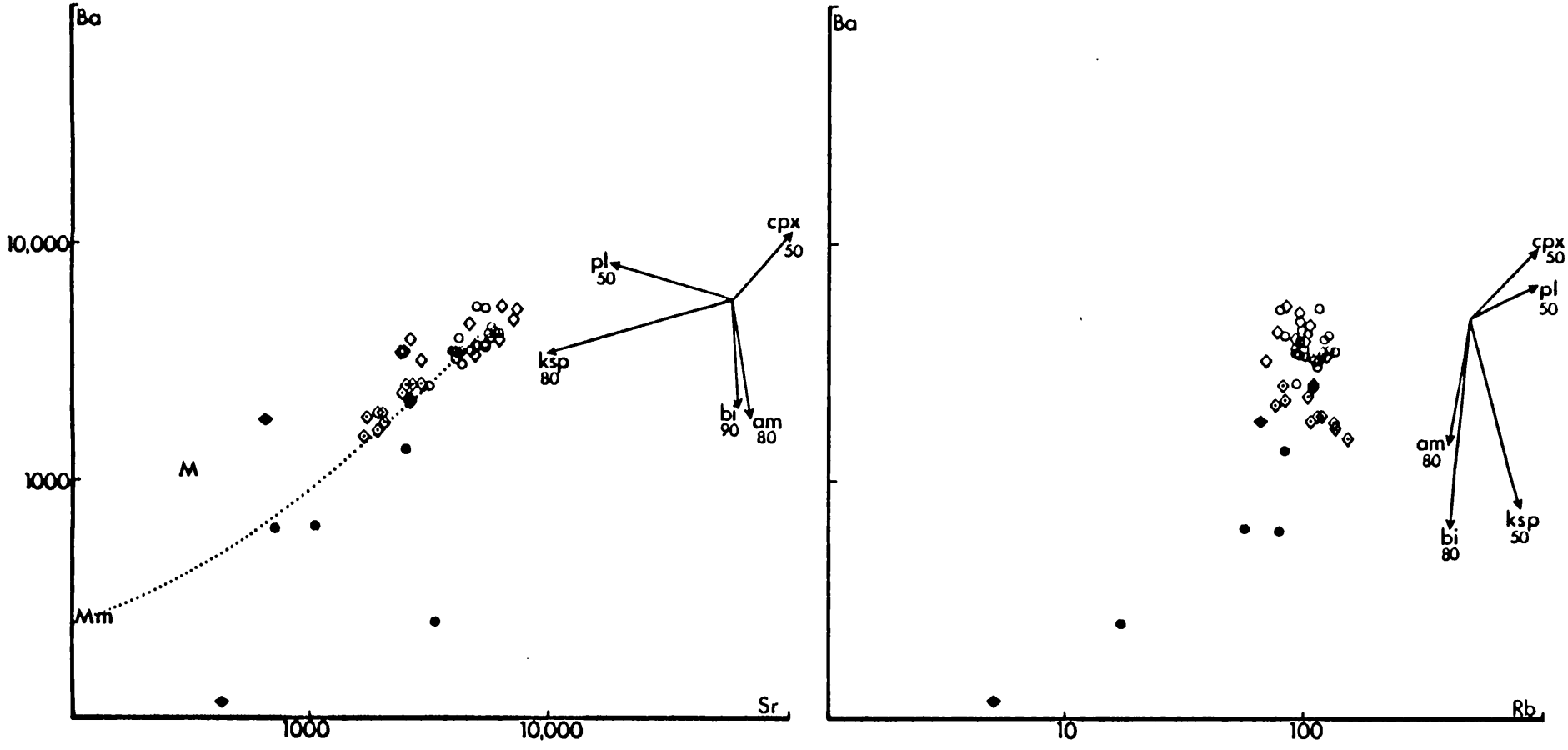


Figure 9.6: Logarithmic, bivariate plots of Rb-Ba-Sr for Glen Dessarry syenites.
(closed diamonds= cumulates; open diamonds= mafic syenites; dotted open diamonds= "contaminated" mafic syenites; open circles= leucocratic syenites; closed circles= pegmatites; M= Moine; Mm= Moine melt).

therefore been added to the diagram, with a view to assessing the ability of crustal contamination to produce this distinctive group. DePaulo (1981) has developed a model for assimilation coupled with fractional crystallisation, but in this particular environment it seems sensible to start with simple binary mixing. A mixing curve between the samples of Moine metasediment and an average high Ba-Sr mafic syenite (therefore equated with syenite uncontaminated with Moine) does not intersect the low Ba-Sr group, and small variations in the end-member compositions do not ease the problem significantly. A lower Ba-Sr end member would be required. It is not unlikely that the contamination process involved some partial melting, leaving residual assemblages similar to those found in the metasedimentary xenoliths (essentially biotite, feldspar and staurolite). Any melt phase which equilibrated with this assemblage would have considerably lower Ba and Sr abundances than their source (Table 9.3, below), and would allow a simple mixing process to model the low Ba-Sr mafic syenites more successfully, as shown.

The last stages of evolution of the mafic syenites are recorded in the pegmatite compositions. These all lie to the Ba- and Sr-poor side of their hosts, to which they cannot be related by the removal of only pyroxene and feldspar. An additional phase with a high affinity for Ba, but not Sr is required, such as biotite or amphibole. It is possible to postulate an increased importance for biotite crystallisation during the last stages of consolidation, but there is no petrographic evidence to confirm this. Indeed, biotite is an early crystallising phase, often as intergrowths with pyroxene. On the other hand, amphibole invariably shows textural relationships which are compatible with late crystallisation (although they have also been interpreted as metamorphic - see Richardson, 1968), and those samples tentatively identified as the "cumulates" of pegmatite genesis on the K_2O Harker diagram are

invariably amphibole-rich. It therefore seems possible that the pegmatite compositions record the influence of late amphibole separation from the magma, which is additional evidence for its magmatic origin.

The leucocratic syenite field overlaps that of the "uncontaminated" mafic syenites, which suggests that the low-level evolution caused no great alteration in the abundance of either element. The figure of about 26% mafic phase removal suggested above is not inconceivable, although the proportion of biotite is severely restricted by relative Ba abundances.

The Ba vs. Rb diagram shows relatively little variation between the leucocratic syenites and the "uncontaminated" mafic syenites. If interpreted in terms of fractional crystallisation, this would require a bulk mineral-melt distribution coefficient approximating to unity for the cumulus assemblage responsible for the low-level evolution. Cumulate sample GD48 lies close enough to the data for these two groups to be compatible with this hypothesis. Moreover, the vectors for the main fractionating minerals (pyroxene and biotite) lie in almost opposite directions, such that a combination of the two would have little overall effect on melt Ba/Rb relationships. The "contaminated" mafic syenites define a separate field at lower Ba abundance, again explicable in terms of mixing of mafic syenite with a Moine partial melt. The small ranges produced by in-situ differentiation show no consistent trends, but could be explained by the cumulate-melt incomplete separation scheme already postulated. The pegmatites show the clear influence of alkali-feldspar extraction, but again require the involvement of biotite and/or amphibole. The reasons for preferring amphibole have been given above.

Incompatible Elements which Enter Minor Mineral Phases.

Minor minerals may be studied by reference to those trace elements whose physical and chemical characteristics cause their partial exclusion from the major mineral phases, and which therefore tend to either

remain in the melt or, if in sufficient abundance, form minor or accessory minerals of their own. At Glen Dessarry, this category includes the REEs, one of the most intensively-investigated and "well-understood" groups of trace elements, for which partition coefficient data are particulary abundant. These are therefore treated first, and followed by consideration of the extent to which the abundances and distribution of other incompatible elements (e.g., U, Th, Zr, Hf, Ta, Nb, etc.) may be explained by magmatic influences.

Rare earth elements

Although the logarithmic, bivariate diagram approach is employed for the REEs later, it is conventional and instructive to consider variations within the group as a whole in terms of chondrite-normalised plots (Fig. 9.7). The absolute abundance of the REEs is high, up to about 300x chondrites for La, and 20x chondrites for Yb. All samples are LREE-rich and HREE-poor, from cumulates through to pegmatites. Eu anomalies are generally small, but both positive and negative anomalies are represented.

The plots for the cumulate samples (GD48 and GD49) are sub-parallel, LREE-enriched with a steep trend to relatively low HREE. Both have a small negative Eu anomaly and a marked enhancement of the Ce to Sm section of the plot.

The mafic syenites also define a consistent trend of LREE-enrichment. However, there appear to be two groups: those with small positive Eu anomalies, with steep patterns and relatively low HREE values; and those with negative Eu anomalies and enhanced HREE abundance (see Fig. 9.9). The latter correspond to the low Ba, Sr group, regarded as being due to metasediment assimilation and will be dealt with in more detail later. Within the former, "uncontaminated" variety there appear to be two sub-groups: those with slightly higher LREE, and higher HREE (GD27 and GD28) as opposed to GD30 and GD44. The small, negative Ce anomaly persists through most syenitic rocks of the Complex.

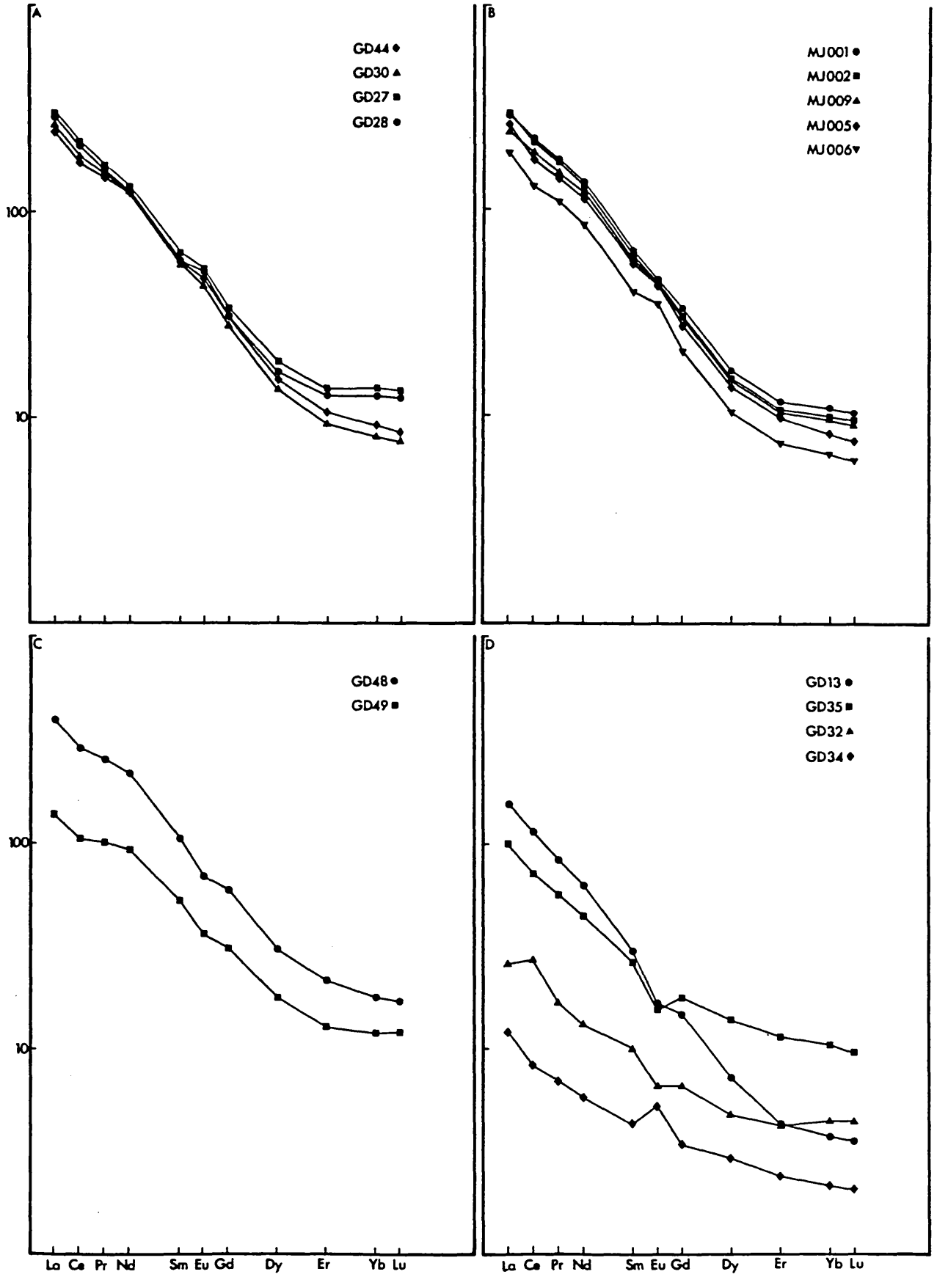


Figure 9.7: Chondrite-normalised REE plots for Glen Dessarry syenites.

(A= "uncontaminated" mafic syenites; B= leucocratic syenites; C= cumulates; D= pegmatites).

All the analysed leucocratic syenites comprise a series of systematically decreasing sub-parallel trends similar in shape to the uncontaminated mafic syenites. With increasing total REE, the small positive Eu anomaly inverts to a slight negative anomaly. The ubiquitous small, negative Ce anomaly is again present.

The pegmatites are rather variable in total REE content, but do show some common features. They all have much lower total REE than any of the syenites, but are still LREE-enriched. Three samples have a negative Eu anomaly, and one a positive Eu anomaly. Two samples (GD32 and GD34) have a trough in the Ce-Sm region, but the other two are flat in this part of the plot. Only one sample (GD13) is not sub-parallel to the others, having a more-fractionated slope (LREE-rich), and this shows abundant allanite in hand specimen and thin section.

Several points pertinent to the evolution of the magmas are immediately apparent from the shapes and positions of the plots alone. The general similarity between the mafic and leucocratic syenites (neglecting the postulated contamination effects for the present), suggests that the low-level fractionation (about 26% mafic phases) had a relatively small effect on REE abundances. Thus, the REE bulk distribution coefficients must have approximated to unity during this interval, indicating the presence of a significant component of REE-rich minerals in the separating cumulates. This is consistent with the mineralogy and geochemistry of the ultramafic xenoliths, whose REE patterns are similar in shape and abundance to those of the syenites themselves.

The variations produced by in-situ processes are significant and similar in both variants. The largest concentration range is in the HREEs, with which the LREEs vary sympathetically, but to a lesser extent. The size of the positive Eu anomaly is also variable, and may be controlled by feldspar accumulation. Its ubiquitous nature may be the result either of the early removal of Eu-poor cumulates, or some accumulation of

feldspar before intrusion. The extreme results of in-situ crystal fractionation are the local filter-pressed pegmatites. These have a consistent REE-poor character, which suggests that the later stages of in-situ melt evolution involved the quantitative removal of REE-bearing minor phases, in which some of the syenites are particularly rich.

Ce and Yb data are plotted on Fig. 9.8, representing only those samples on which it was practicable to carry out full REE analyses. The low-level evolution can perhaps be approximated by the relationship of an average leucocratic syenite with an average uncontaminated mafic syenite. This could be acheived by the suggested fractional crystallisation of a mafic

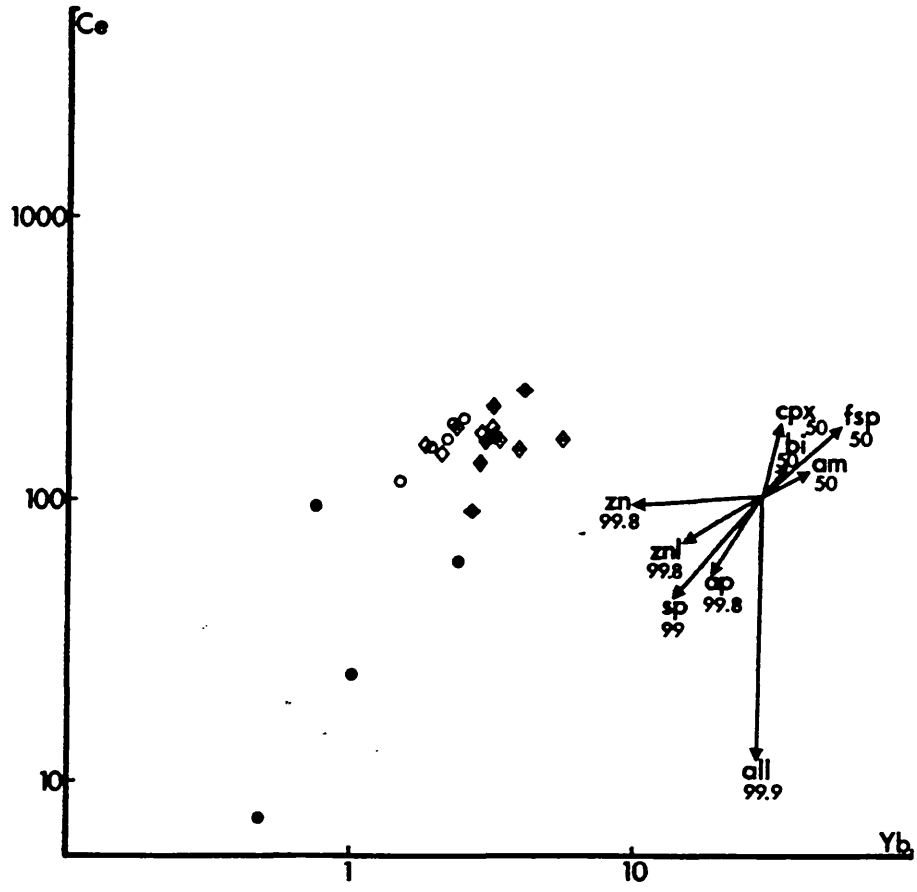


Figure 9.8: Logarithmic, bivariate plot of Ce-Yb for Glen Dessarry syenites.

(closed diamonds= cumulates, open diamonds= mafic syenites, dotted open diamonds= "contaminated" mafic syenites, open circles= leucocratic syenites, closed circles= pegmatites.)

assemblage with important minor constituents, such as sphene, zircon and apatite, which is consistent with the mineralogy of the ultramafic xenoliths.

The leucocratic syenites form an essentially linear in-situ trend, and therefore conform to control by crystal-liquid equilibria. Although the four "uncontaminated" mafic syenites do not plot entirely separately from their contaminated counterparts, they do lie at the Yb-poor side of the array, and themselves define an in-situ trend sub-parallel to that of the leucocratic syenites. Rock-forming phases undoubtedly had a strong influence, but the extent of both trends would require excessive crystallisation and removal. Minor phases are therefore implicated, whose theoretical effects are depicted by the vectors shown. Their importance is exemplified in the late evolutionary phase, by the relationship of the mafic syenite trend with that of the pegmatite analyses. The REE values for the latter can only be generated by quantitative removal of minor phases rich in REEs. All of the accessory phases documented above (Chapter eight: zircon, zirconolite, allanite, apatite and sphene) may have been involved, but there are petrographic reasons for supposing that allanite and sphene were particularly important. These two minerals commonly form overgrowths on pre-existing minerals, and may therefore have been precipitated from a late-stage fluid (see Chapter eleven).

The contaminated mafic syenites tend towards higher HREE abundances, sometimes (GD43) to an extent unlikely to be the result of sensible amounts of major phase crystallisation. Local accumulation of REE-rich accessory phases seems unlikely, since this could not produce the associated low Ba and Sr, and negative Eu anomalies. A process capable of explaining both observations is required. Although large-scale crustal contamination would not be allowed by published isotope systematics (van Breemen et al., 1979), this does not preclude local assimilation of the surrounding

metasediments. Petrographic evidence for the progressive assimilation of quartzofeldspathic metasedimentary material has been provided above, indicating that extensive desilication occured, and gave rise to aluminosilicate-rich assemblages in the more advanced stages. The details of the processes by which this occurs are at present unknown, although it seems likely that a melt phase may have been quantitatively extracted from the partly-assimilated xenoliths (e.g., Tindle and Pearce, 1983). What is more important to establish for the purposes of this thesis, is the magnitude of the control that assimilation exerts on radioelement and other incompatible-element abundances. It has been suggested in the petrographic descriptions that Moinian metasediments are likely to represent the type of material extensively assimilated, and so several samples of the adjacent Moine, collected far enough away from the contact to preclude metasomatic activity from the syenite (see below) have been analysed to provide data for the metasedimentary end-member of the assimilation process. Chondrite-normalised REE plots of the "contaminated" mafic syenites and their postulated contaminant are shown in Fig. 9.9. However, it has been intimated at several places above, that bulk assimilation of Moine metasediment will not fulfill the trace-element constraints which have been established on the contamination process, and that incorporation of a partial melt might be more appropriate. This is similar to the model presented by Bender et al. (1983) for the classic contamination of alkali-basalts in the Cortlandt Complex. Fig. 9.9 and Table 9.3 (see Page 164) show an example of how the REE patterns of the "contaminated" mafic syenites may be modelled by extracting a partial melt from a Moinian source, with a residual mineralogy representing that retained by the xenoliths within the mafic syenite. Partition coefficients used are those listed in Bender et al. (1983). If the melt is mixed with uncontaminated mafic syenite in the proportions noted on the diagram, the correspondence between "modelled" and "actual" contaminated syenite is good.

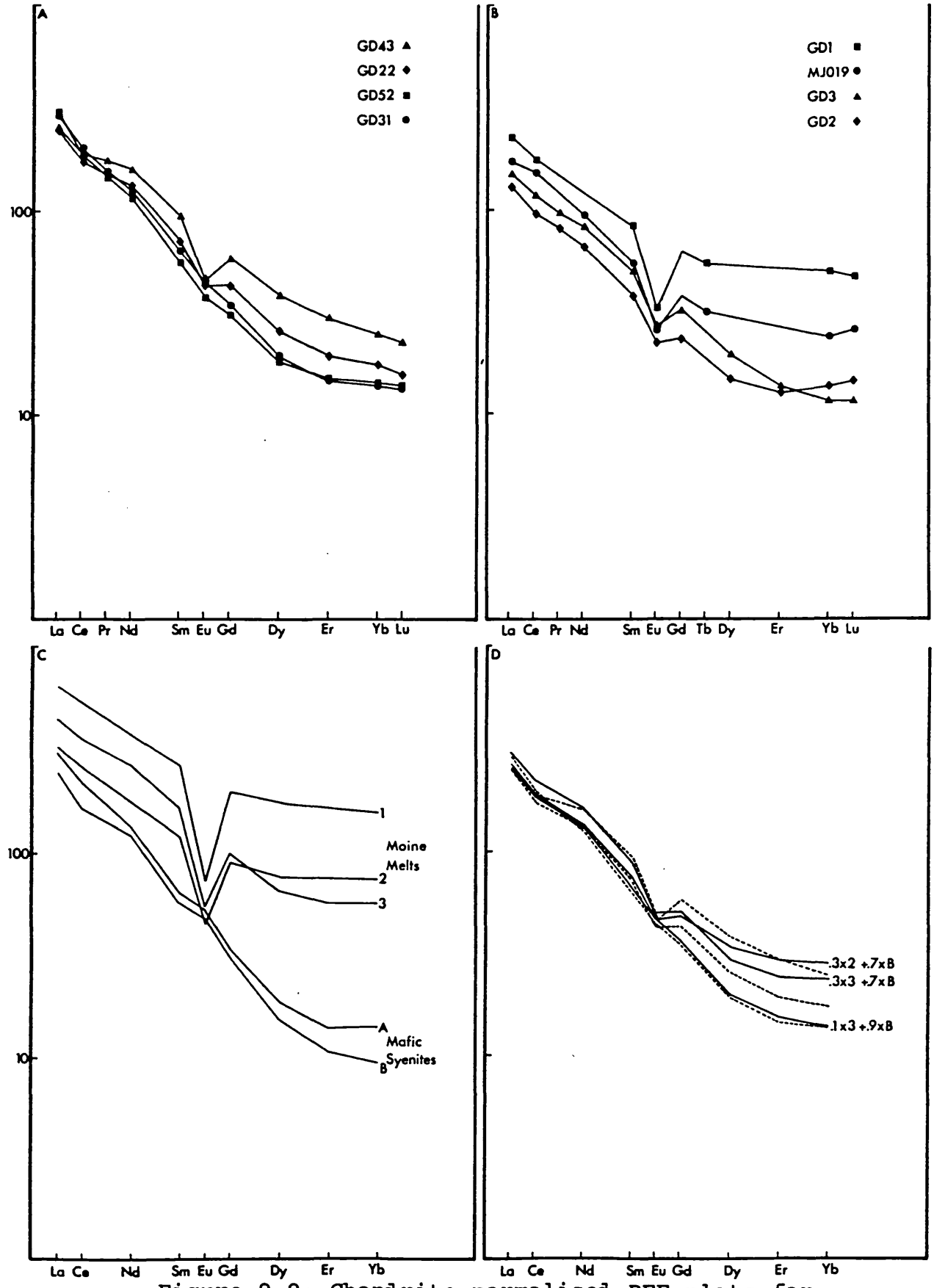


Figure 9.9: Chondrite-normalised REE plots for "contaminated" mafic syenite (A) and Moine (B); model of assimilation via crustal anatexis.

(C= end members for model; D= two-component mixtures compared to "contaminated" mafic syenites (dashed)).

Uranium and thorium

When dealing with the radioelements and the remaining trace elements (below), problems over the choice of partition coefficients become severe, especially with respect to minor phases, for which they are often non-existent. Those used here are listed in the Appendix, with their sources and comments on their applicability.

Fig. 9.10 shows that the mafic syenites can again be separated into the two sub-groups already defined. Those which correspond to the low Ba-Sr group of "contaminated" syenites tend towards higher values of U and Th (see also Fountain and Hodge, 1981), sometimes reaching very high values (e.g., GD43). On the other hand, the "uncontaminated" samples invariably have low radioelement concentrations, comparable to those of the leucocratic syenites. The overlap between the latter two groups is more pronounced than on the Ce vs Yb plot, but this may simply be due to the rather larger data set. Otherwise the data disposition closely resembles that of the REE diagram, and the interpretation is accordingly similar, dominated by magmatic influences.

Since the low-level evolutionary phase which relates the parental mafic and parental leucocratic syenite compositions had apparently little effect on U or Th abundance, the bulk distribution coefficients between the cumulus assemblage and the supernatent melt must have approximated unity. This is consistent with the high U and Th content of the exposed ultramafic rocks (GD48 = 2.3 and 6.5ppm; GD49 = 1.3 and 5.8ppm respectively), probably due to the importance of early sphene and apatite. The in-situ evolution of both variants follows similar trends, controlled by the competing influences of major and minor phases, and complicated by incomplete crystal-melt separation. However, it is clear that in the later stages of melt evolution (represented by the pegmatites), the radioelements fall rapidly in response to minor phase crystallisation and removal. Crystal-melt equilibria

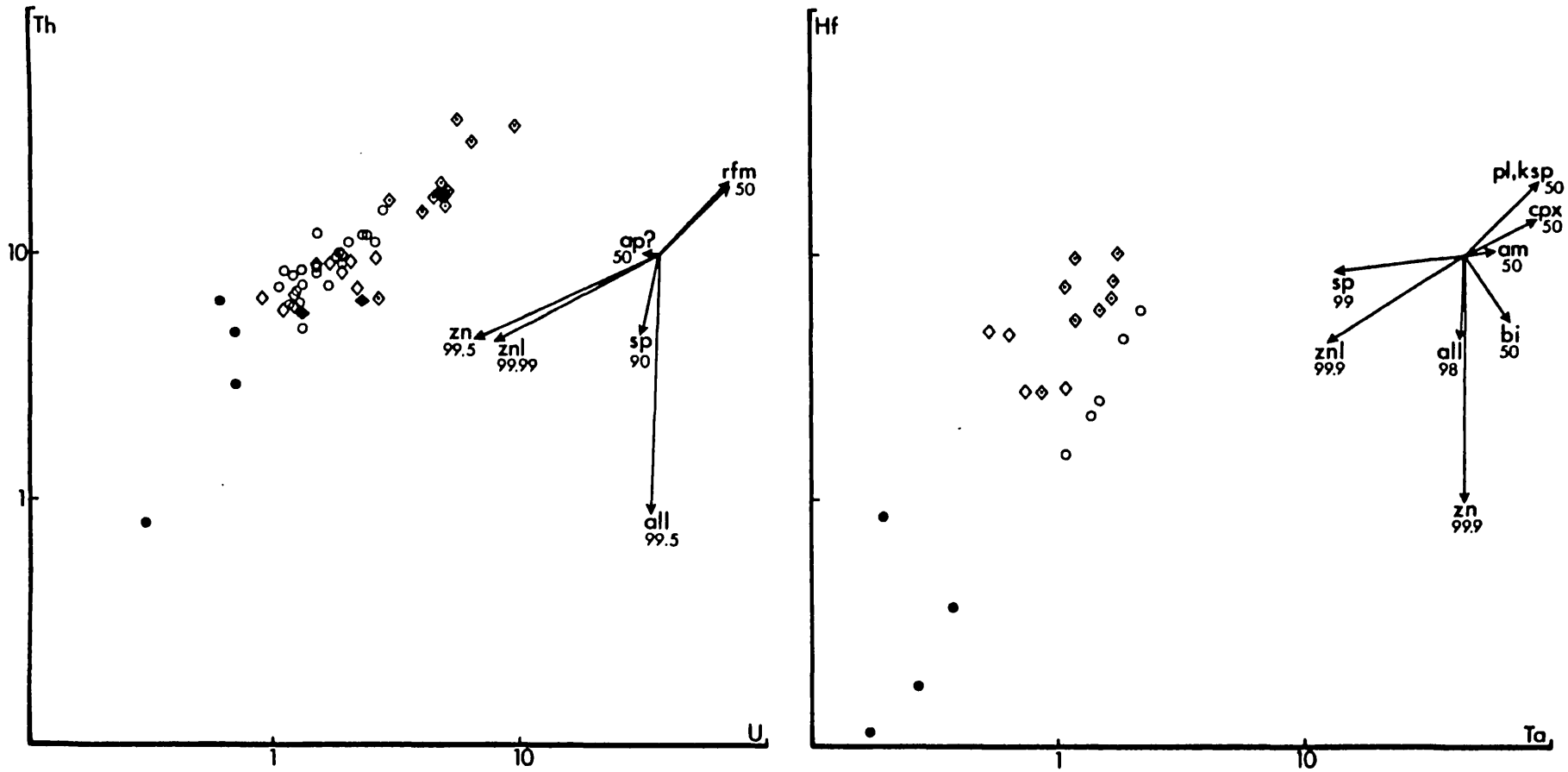


Figure 9.10: Logarithmic bivariate plots of U-Th and Hf-Ta for Glen Dessarry syenites.
(closed diamonds= cumulates; open diamonds= mafic syenites; dotted open diamonds= "contaminated" mafic syenites; open circles= leucocratic syenites; closed circles= pegmatites).

involving a combination of the accessory phases outlined above are capable of producing the required trend.

The remaining group of samples comprises those with anomalously high radioelement abundances. The mineral vectors suggest that they are unlikely to have been generated by sensible degrees of fractional crystallisation of major mineral phases, but that some accumulation of minor minerals might be responsible. As has been stated before, this alone could not explain the negative Eu anomalies and low Ba, Sr abundances with which they are associated, and the contamination model is preferred for the group as a whole.

Zirconium, hafnium, niobium and tantalum

The geochemical coherence between Zr and Hf, Nb and Ta has been adequately demonstrated, and although fractionation of the elements has been recorded in special cicumstances (eg. Wolff, 1984, Thompson et al., 1984), it seems reasonable to summarise their behaviour in terms of a Hf vs Ta plot (Fig. 9.10). Linearity implies the dominance of crystal-liquid equilibria, but the range of values is too large to be explained on the basis of rock-forming minerals alone, except for the low-level phase. The latter is consistent with the removal of an assemblage including a significant proportion of biotite. The in-situ trends, especially of the leucocratic syenite and the late stages of mafic syenite evolution which gave rise to the pegmatites, almost certainly involved minor phases. Their precise effect is difficult to constrain because of the lack of reliable partition coefficient data for the relevant melt chemistry, but the data which are available, plus some intuitive guesses, suggest that a combination of those accessories present in the syenites could well be responsible for the observed data distribution. The "contaminated" mafic syenites are again distinctive, suggesting that the contaminant had relatively high Ta and Hf abundances.

9.3 Incompatible-Element, Chondrite-Normalised Diagrams

It seems clear that much of the observed lithochemical variation may be attributed to crystal-liquid equilibria, locally modified by crustal contamination. The response of the incompatible element group as a whole to these processes may be summarised and their interrelationships clarified by the use of multi-element, chondrite-normalised diagrams of the type now becoming familiar in the literature. They are presented in three groups, dealing first with low-level fractionation, then in-situ fractionation and finally crustal contamination. The normalisation values and element order are those of Thompson, 1982.

Low-level fractionation.

Perhaps the most striking feature of the mafic and leucocratic syenite fields of analyses (Fig. 9.11) is their essential similarity. This confirms that to a first approximation, low-level fractionation caused rather little in the way of modification of the incompatible element abundances or their interelement ratios. However, there are one or two meaningful discrepancies. Nb and Ta are consistently higher in the leucocratic syenite than in the mafic syenite, indicating their continued incompatability within this crystallisation interval. P is consistently lower in the leucocratic syenites as a result of apatite fractionation, and Ti is generally lower, probably as a result of sphene removal.

The diagram also shows analyses for cumulate samples GD48 and GD49, which have been used as examples of assemblages capable of relating the parental syenite compositions by approximately 26% removal. Although it is clear that GD48 will not satisfy the trace-element constraints as well as it does those of the major elements, there is little doubt that some combination of the cumulus assemblages caught up in the melt during emplacement would be capable of reproducing the observed mafic-leucocratic syenite incompatible-element evolution.

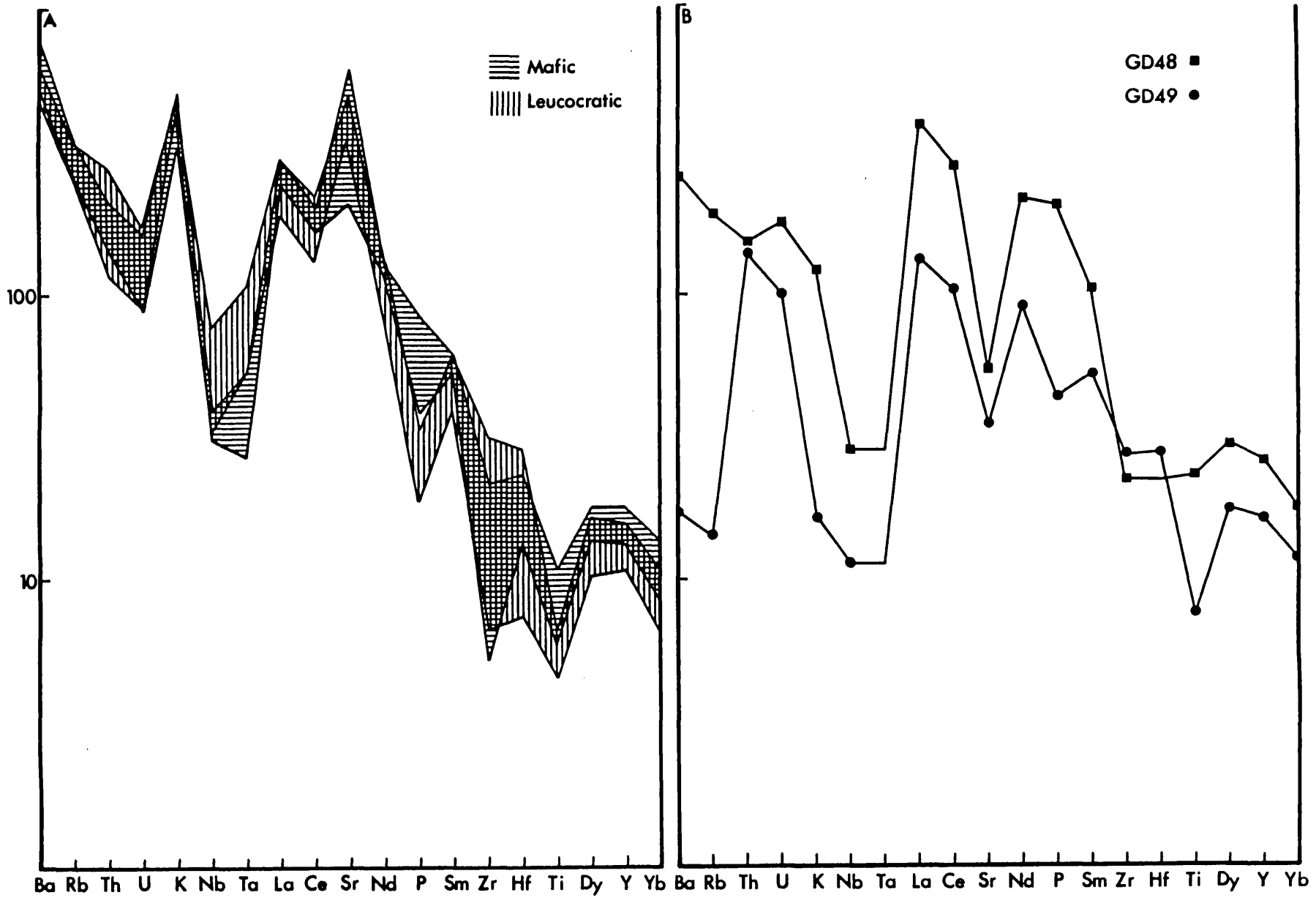


Figure 9.11: Chondrite normalised incompatible element plots of mafic and leucocratic syenite fields of analyses (A), and cumulates (B).

In-situ fractionation.

The individual patterns for uncontaminated mafic syenites and leucocratic syenites are shown in Fig. 9.12, displaying considerable variation although retaining the same characteristic shape at all times. Treating the mafic syenites first, perhaps the most spectacular in-situ effects are the large peaks for Ba and Sr in GD30 and GD44, which can probably be attributed to feldspar accumulation, as was intimated above. GD44 may also have accumulated some apatite, to judge by the rather high P value. A progressive fall in Zr and Hf abundances is correlated with a rapid decrease in the Zr/Hf ratio, and must be due to the incorporation of Zr into a phase which contains Hf in non-chondritic proportions. Zircon and zirconolite are the most likely suspects at Glen Dessarry, although Thompson et al. (1984) have also suggested garnet. Similar features can be seen on the leucocratic syenite plot, for which there are well behaved, systematic relationships between all the incompatible elements considered here. For example, MJ005 and MJ006 have accumulated feldspar, giving rise to high Ba and Sr (and positive Eu anomalies).

The four pegmatites analysed to provide an indication of the most evolved melt generated by in-situ processes within the Complex were all taken from the mafic syenite outcrop. Their incompatible-element, chondrite-normalised diagrams are shown in Fig. 9.13. The fidelity with which the pegmatite patterns retain the overall shape of their parent is remarkable, suggesting that late-stage crystallisation rapidly and uniformly depleted the evolving melt in incompatible elements. Nevertheless, even in the pegmatites there appears to be some scope for feldspar accumulation, implied by the peaks at Ba and Sr, associated with a distinct positive Eu anomaly for sample GD34. The very extensive Ti depletion is further evidence of the importance of sphene removal in the production of the pegmatite compositions, to add to the characteristic concave-upward REE pattern (see above).

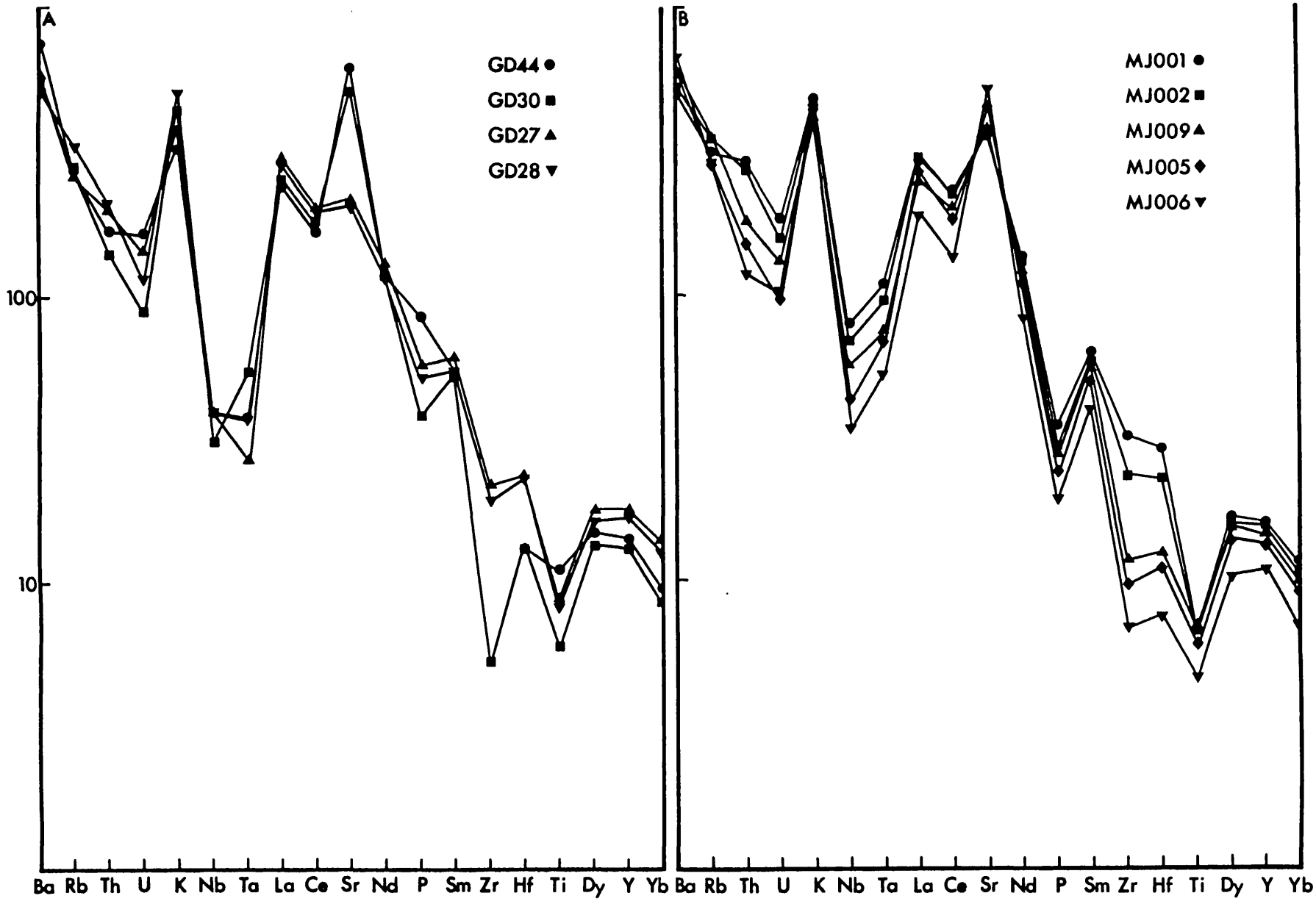


Figure 9.12: Chondrite normalised incompatible element plots of mafic (A) and leucocratic (B) syenite samples.

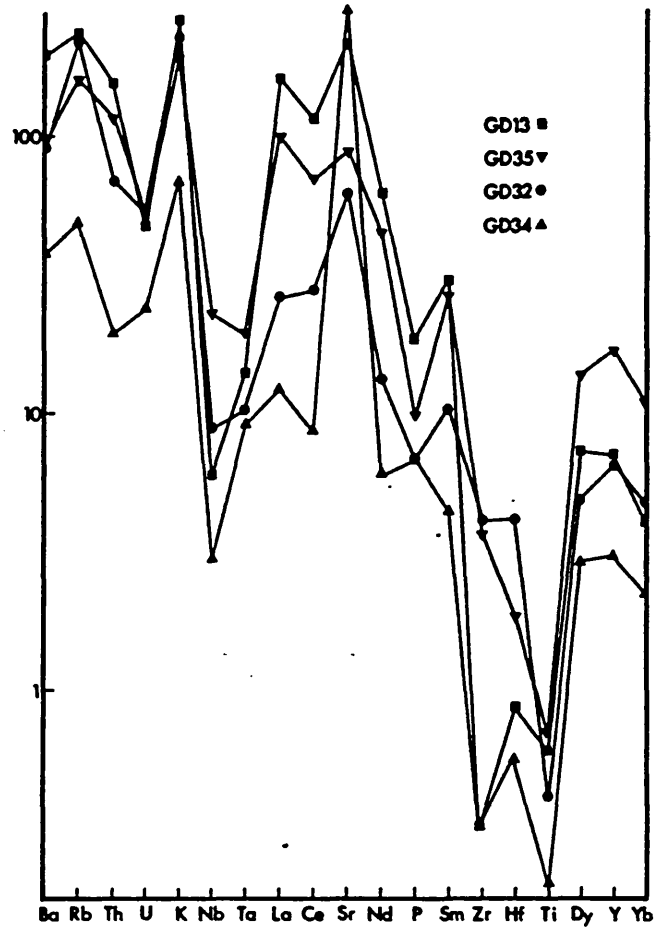


Figure 9.13: Chondrite normalised incompatible element plots of filter-pressed pegmatite samples.

Crustal Contamination.

Normalised plots for the contaminated mafic syenites and postulated contaminant are shown in Fig. 9.14. Most of the features of the metasediments can be related to their derivation from a moderately-evolved continental igneous source; such as the negative Ba, Sr, P and Ti anomalies associated with negative Eu anomalies on chondrite-normalised REE plots (Fig. 9.9), and characteristically low Nb and Ta values. It seems unlikely that they could have been derived from a source of typical Lewisian composition (Winchester et al., 1981). An attempt can now be made to extend the crustal contamination model to the whole incompatible element group by supplementing the REE partition coefficients of Bender et al. (1984) with those given by Villemant et al. (1981) for the other elements. The

Batch melting with residue of 0.55 plagioclase, 0.25 boitite and 0.2 Fe-Al silicate.

	D	Melt/Source for given % melting			
		5%	20%	30%	70%
Ba	3.13	0.33	0.34	0.36	0.46
Rb	0.79	1.26	1.23	1.21	1.12
Th	0.057	11.87	4.90	3.33	1.43
U	0.066	10.81	4.83	3.32	1.43
K	0.561	1.75	1.64	1.57	1.26
Nb	?0.16	5.49	3.76	2.96	1.43
Ta	0.162	5.49	3.76	2.96	1.43
La	0.195	4.63	3.41	2.80	1.43
Ce	0.163	5.40	3.73	2.96	1.43
Sr	1.83	0.55	0.57	0.59	0.69
Nd	0.139	6.17	4.00	3.08	1.43
P	?0.05	12.80	4.94	3.33	1.43
Sm	0.115	7.20	4.28	3.18	1.43
Eu	0.34	2.80	2.41	2.18	1.39
Gd	0.11	7.45	4.34	3.16	1.43
Zr	0.70	1.41	1.36	1.33	1.17
Hf	0.48	2.03	1.86	1.75	1.31
Ti	3.31	0.31	0.33	0.34	0.44
Dy	0.106	7.67	4.39	3.22	1.43
Y	?0.12	6.96	4.22	3.16	1.43
Er	0.12	6.96	4.22	3.16	1.43
Yb	0.132	6.44	4.08	3.11	1.43

Table 9.3: Incompatible element model of melts generated by Moine anatexis.

results of simple models are shown in Table 9.3 and Fig. 9.14. Part a shows patterns for contaminated mafic syenites, and b those for the Moine metasediments. Part c illustrates the syenitic and metasedimentary melt compositions, and d an example of the correspondence between a two component mix (0.3 x 30% melt of sample GD2 with 0.7 x GD44) and one of the contaminated mafic syenites (GD52). In the author's opinion, crustal contamination via metasediment anatexis provides a more reasonable explanation of these distinctive mafic syenites than either a rather contrived fractional crystallisation hypothesis, or one of superimposed metamorphic element mobility.

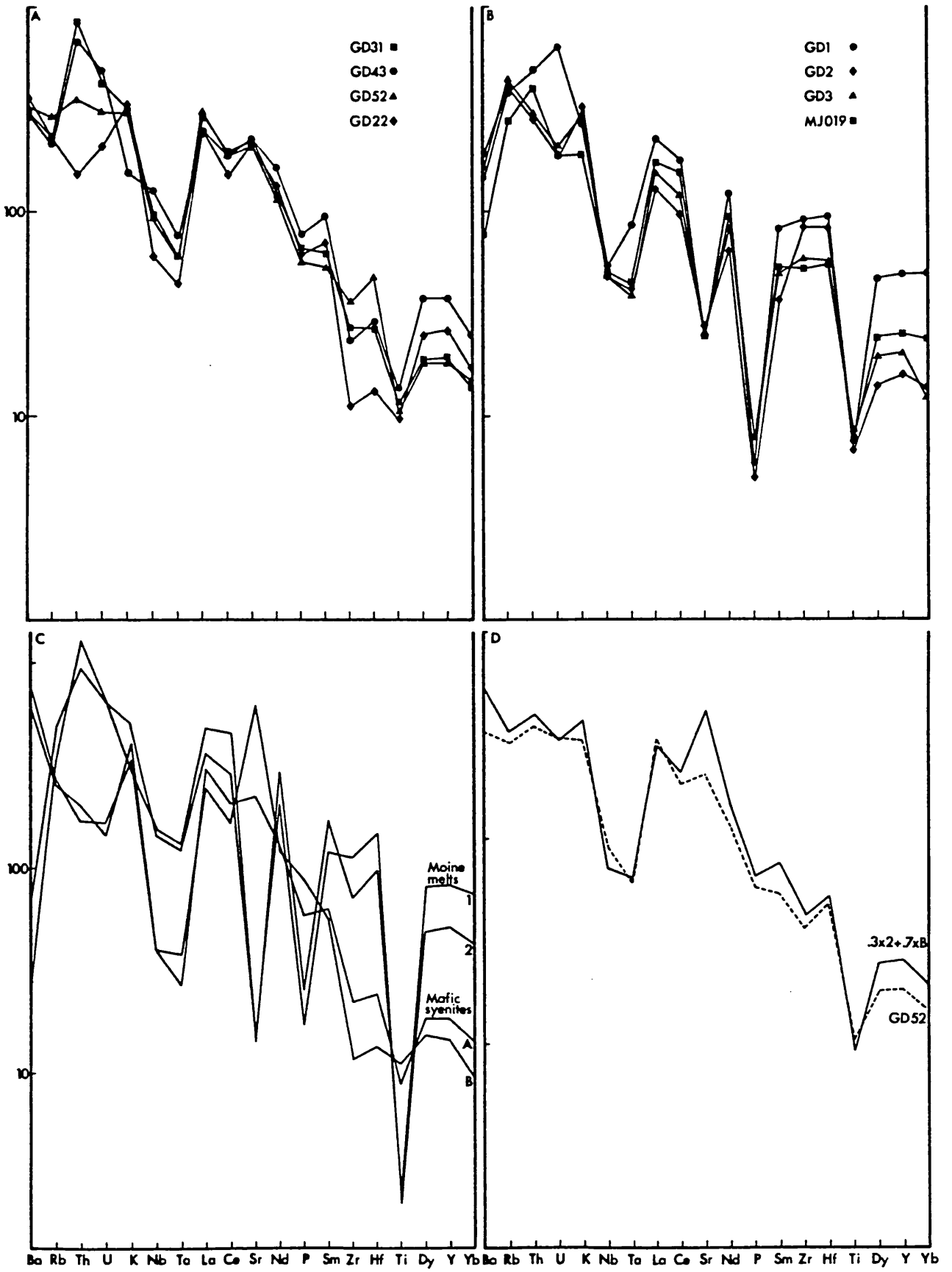


Figure 9.14: Chondrite-normalised incompatible element plots for "contaminated" mafic syenite (A) and Moine (B); model of assimilation via crustal anatexis. (C= end members for model; D= two-component mixture compared to "contaminated" mafic syenite (dashed)).

9.4 Magmagenesis

Although strictly superfluous to the needs of this thesis, a few brief comments might be addressed to the genesis of the melts. Considerable debate still surrounds the formation of those intrusions collectively known as the Caledonian granites. It is not the intention here to enter into the discussion at any length, especially since it seems perhaps overly simplistic to assume a common genesis for the suite as a whole, given that each intrusion will have been subject to its own particular set of the many possible variables both during magmagenesis and subsequent ascent, emplacement and consolidation. However, a brief review of the current literature is followed by a more detailed assessment of the Glen Dessarry melts.

Modern thought on the generation of the Caledonian granites is in a state of semi-permanent flux, especially since the advent of accurate and precise trace-element or isotopic determinations on individual plutons in the late 1970s. Pankhurst (1979) argued on the basis of REE abundances in the Foyers and Strontian intrusions that the rocks of each complex were related by fractional crystallisation, similar to the early hypothesis of Nockolds (1941). However, differences in Ce/Yb (for example) were taken to indicate differences in the evolution of the magmas. Many Caledonian granites have mixed zircon populations, one fraction being generated from the melt and the other "inherited" from pre-existing crustal rocks, particularly in those north of the Highland Boundary Fault. Pidgeon and Aftalion (1978) therefore proposed that the Highland granites represent melts of reworked Lewisian, and that the Southern Uplands and Lake District plutons are derived from Lower Palaeozoic sediments. The presence of inherited zircons is not perhaps the best indicator of melt provenance, since other mechanisms of incorporation than directly at source are possible (for example, assimilation during ascent), and the solubility of zircon in granitic melts is known to increase with

alkalinity (e.g., Bowden, 1966), so that more alkaline melts will not necessarily retain evidence of crustal incorporation in the form of an inherited zircon suite. Pb-isotope analyses (Blaxland et al., 1979; Pankhurst, 1979) seem to rule out a simple melted Lewisian source for Highland granites, suggesting an isotopically juvenile source. Hamilton et al. (1980) considered the Nd-Sr isotope geochemistry of a selection of Caledonian granites on the basis of a MORB-like sub-continental mantle, and therefore required a substantial crustal input to all the analysed samples. However, clear evidence of an "enriched" Scottish sub-continental mantle has been provided by Thirlwall (1982), which allows substantial reassessment (e.g., Plant et al., 1983) of the amount of crustal involvement necessary. Further, Clayburn et al. (1983) demonstrated the importance of a LILE-enriched mantle in the genesis of the Etive granite complex, as first proposed for uraniferous granites by Simpson et al. (1979). However, Halliday (1984) has recently challenged Thirlwall's interpretation, preferring contamination with different crustal segments as the source of the observed isotopic diversity. Recently, Brown et al. (1984) proposed a simple model of Caledonian granite genesis in terms of mantle-derived magmas in an increasingly mature arc setting. This involved the derivation of an increasing fraction of the magma from an intra-plate mantle source, reliant on a proposed, rather simple geographical distribution of granite type related to distance from the subduction zone. However, various mechanisms of fractional crystallisation in highly-evolved acid magmas are neglected in their dependence upon the abundance of HFSEs for classification (Mittlefeldt and Miller, 1983; Michael, 1983, 1984; Miller and Mittlefeldt, 1984; Thompson et al., 1984; Watson et al., in press).

Derivation of the Glen Dessarry magmas.

It can be inferred from the lack of or very small Eu anomalies in most of the syenites that the source of the

magmas must have been a feldspar-free environment, which immediately excludes most crustal rocks, including the Lewisian basement. Independent evidence for the exclusion of the Lewisian is the Pb^{207}/Pb^{204} isotope ratio of Glen Dessarry K-feldspar (van Breemen et al., 1979) which is too radiogenic to have been derived from a granulite-facies Lewisian source. An amphibolite-facies (Rb-rich) Lewisian source is also effectively ruled out by the initial Sr^{87}/Sr^{86} isotopic ratio of 0.7041 (van Breemen et al., 1979). The O-isotope data produced for this study (see above) are compatible with a juvenile source, with later enrichment due to fractional crystallisation of low ^{18}O minerals. Thus the available isotopic data provide strong evidence for derivation from within the mantle. This is consistent with the chemical data which require that the melt evolved in a low-level magma chamber from a more-basic composition by fractional crystallisation essentially of mafic phases. It is unlikely that such a basic melt could be derived from partial melting of typical crustal sources.

Supportive evidence for a mantle origin may be derived from the incompatible-element, chondrite-normalised diagrams, which can be compared to isotopically well-characterised primitive melts of probable mantle derivation - the Lorne Plateau Lavas (Thirlwall, 1981, 1982) and other chemically well-known picritic melts such as Kentallenite (Thompson et al., 1984). Fig. 9.15 shows a comparative diagram of Glen Dessarry samples, with high Ni Lorne lavas and Kentallenite from the above literature sources. The similarity is striking, and those differences which do exist can be related to the subtleties of fractional crystallisation. However, although the most potassic and incompatible-element-rich lavas (e.g., L54) have absolute element abundances close to those of Glen Dessarry, it is not suggested that these were similar to the primitive Glen Dessarry melt, since the low transition metal abundances of the latter precludes this. Nevertheless, the parental syenite

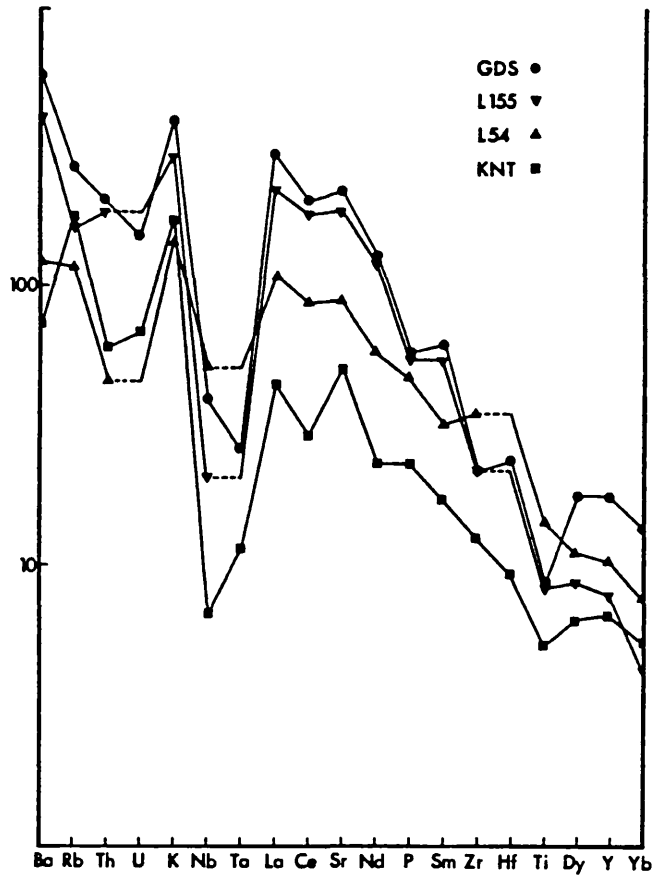


Figure 9.15: Chondrite normalised incompatible element plot comparing mafic syenite, two examples of the Lorne Plateau lavas, and Kentallenite.

liquids could well have evolved from a more-basic melt of lower incompatible element abundances (e.g., L155), by the suggested fractionation of mafic minerals such as olivine and pyroxene, the net effect of whose removal would be to enhance the incompatible element values with minimal interelement fractionation, but reduce the transition metal abundances.

The present author's preferred interpretation of the genesis of the Glen Dessarry syenites might be summarised as follows:

The parent melt was generated within the mantle (see also Thompson et al., 1984; Miller, 1978) and accumulated in a "low-level" magma chamber in which fractionation began with olivine and pyroxenes, to be superceded by clinopyroxene, biotite and perhaps a

little feldspar. Some small degree of feldspar accumulation may have taken place before intrusion of the mafic syenite pulse (quite possibly as a crystal mush). This was followed in the low-level chamber by approximately 26% separation of a clinopyroxene, biotite, magnetite, sphene and apatite-dominated cumulus assemblage before intrusion of the leucocratic syenite. In-situ crystallisation continued the already established trend with the addition of feldspar and late amphibole, involving substantial minor-mineral removal in the later stages. Contamination with a partial melt of the surrounding Moine metasediments was important only locally. This scheme is capable of explaining most of the observed element relationships in the sample suite, at least to a first approximation, without recourse to metamorphic phenomena.

9.5 Reactions with Country Rocks

The preceeding account was intended to demonstrate that factors related to magmatism can be used to explain the gross distribution of incompatible elements within the bulk of the Complex. However, gamma-ray scintillometry suggested that there are two further "local" effects which must be taken into consideration, and these may also be related to magmatism rather than metamorphism: small-scale "fenitisation" of juxtaposed Moine metasediments, and reaction relationships between syenite veins intruded into a xenolithic raft and their host (the Glen Pean Xenolith). These are briefly described, in turn, below.

Fenitisation of adjacent Moine metasediments.

The mineralogical effects of fenitisation have been outlined in Chapter eight. Major element and normative data are available in the appendix, but Table 9.4 provides analyses of a typical fenite and an unaltered metasediment for comparison.

	Moine GD6	Fenite GD8
SiO_2	72.24	64.45
TiO_2	0.74	0.72
Al_2O_3	13.31	17.96
Fe_2O_3	3.45	2.60
MnO	0.02	0.03
MgO	0.84	0.53
CaO	1.94	1.28
Na_2O	2.56	6.82
K_2O	3.69	5.38
P_2O_5	0.08	0.14
LOI	0.73	0.30
Total	99.60	100.21

Table 9.4: Major element analyses of typical Moine metasediment and fenitised Moine.

The only obvious effects on the major element chemistry are introduction of the alkali metal oxides, Na_2O and K_2O, and apparent desilication. However, it is in terms of trace elements that the fenitisation becomes particularly interesting (Fig. 9.16). Clearly, all of the fenites have suffered substantial modification of their REE contents and relative abundances, such that some now have pronounced positive Eu anomalies (c.f., Wooley et al., 1972; Martin et al., 1978). Most appear to have undergone some REE fractionation such that Ce/Yb_{cn} ranges from 14 to 7.1 as compared with a range of 9.1 to 3.4 for unaltered Moine. Although some enrichment in LREE is apparent in one sample (MJ018), the general fractionation appears to be more related to a pervasive HREE loss. Further, the regularity of the incompatible-element patterns (Fig. 9.16) for the unaltered metasediments has been lost. Enrichment of Nb and Ta in the more altered samples can probably be related to the nucleation of sphene. Three of the fenites (GD7, GD39 and GD40) may have lost U and Th, and GD39 further suggests a marked depletion in Zr, Hf, Y and Yb, perhaps related to zircon instability. It appears, therefore, that the fenitisation processes at Glen Dessarry do not merely involve element addition,

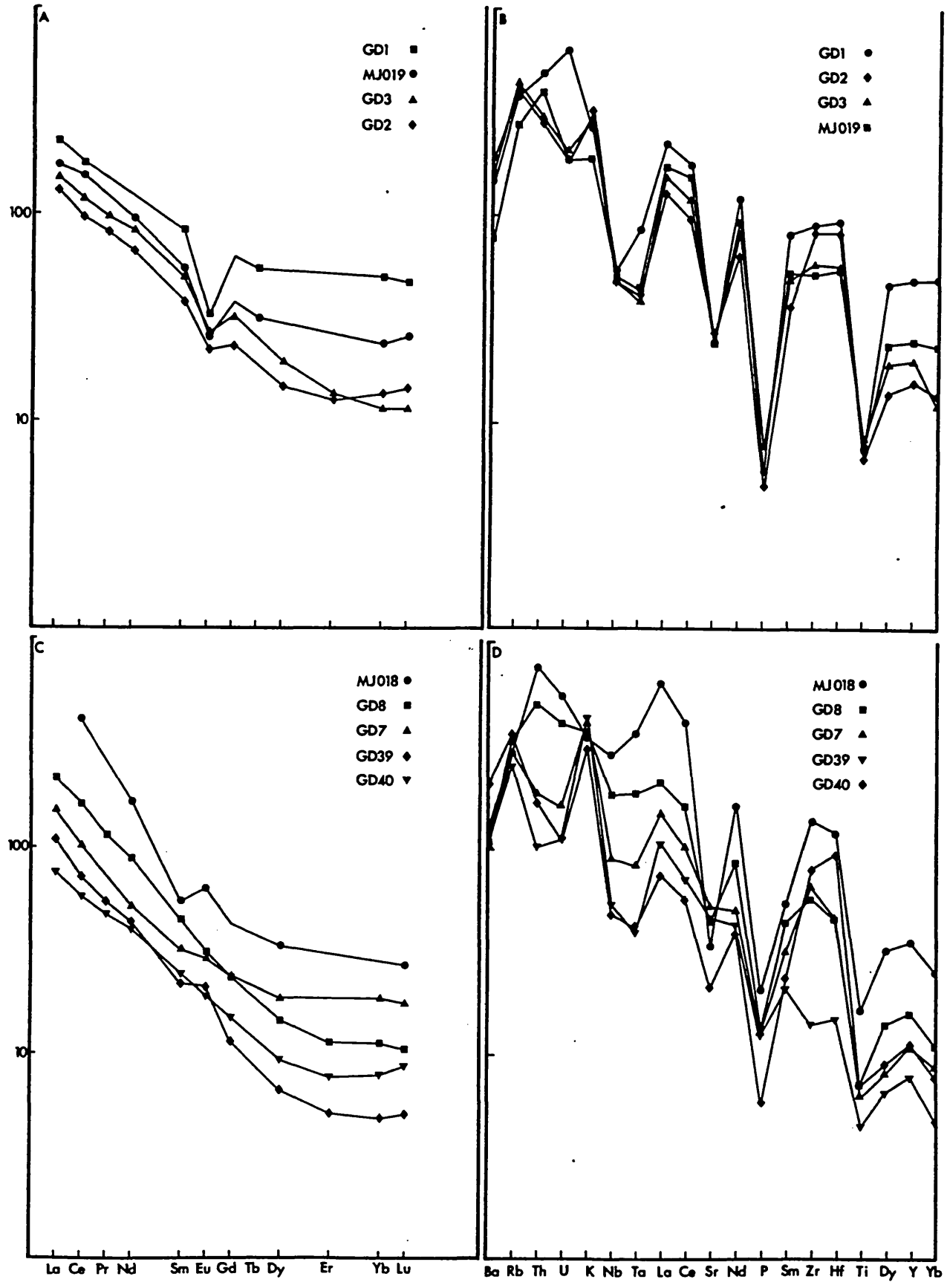


Figure 9.16: Chondrite normalised REE and incompatible element plots for Moine metasediments (A and B) and fenitised Moine (C and D).

but might be better characterised by a complex array of element redistributions in response to chemical potential gradients established as a result of intrusion. A more detailed analysis of the genetic processes is not pertinent here, since it is again sufficient to note the presence of a further magmatic influence on the abundance and distribution of incompatible elements within the Glen Dessarry Complex.

Syenite-vein / xenolith reactions.

The mineralogy of the reaction zones has been outlined above. Two samples of syenite vein were taken for chemical analysis (GD20 and GD24), and one of the "pegmatitic" reaction zone (IGS45642), necessarily from a different locality. Some small samples of the reaction zone adjacent to the analysed vein were collected, which are petrographically similar to sample IGS45642. The reaction zone has a distinctive, strongly-fractionated REE pattern (Fig. 9.17) and a small negative Eu anomaly. Evidence that this reflects the presence of abundant monazite is derived from electron probe analysis of the monazite crystals themselves. Data are listed in the appendix, and are also shown on the chondrite-normalised plot (note the change of scale required to accomodate the monazite abundances). The shapes of monazite patterns mirror those in the whole-rock sample, as do the high levels of Th and U.

The chondrite-normalised incompatible-element diagram (Fig. 9.17) shows a pattern quite unlike anything else sampled from the Complex. A considerable enrichment in Th accompanies an inordinate Th/U fractionation (Th/U_{cn}=5.4). However, the diagram does retain a few clues to the origin of this distinctive rock type. The high values of Ba and Sr leave little room for doubt that the reaction zone is syenite-derived, since this is one of the more obvious characteristics of the syenite which serve to distinguish it from the Moine metasediments. That the fractionated REE pattern and high radioelement abundances can be directly attributed

to the presence of monazite is also clear, but quite why it nucleated in the first place is not. The mineralogy and geochemistry of the reaction zone do not resemble those of the pegmatites analysed, rendering it unlikely that it was produced by a simple pegmatitic segregation, localised against the contact with the country-rock host.

Although their genesis remains equivocal, it is clear that the syenite-vein/xenolith reaction zones, produced during the magmatic phase, locally exert one of the most powerful controls on incompatible element localisation within the Complex as a whole.

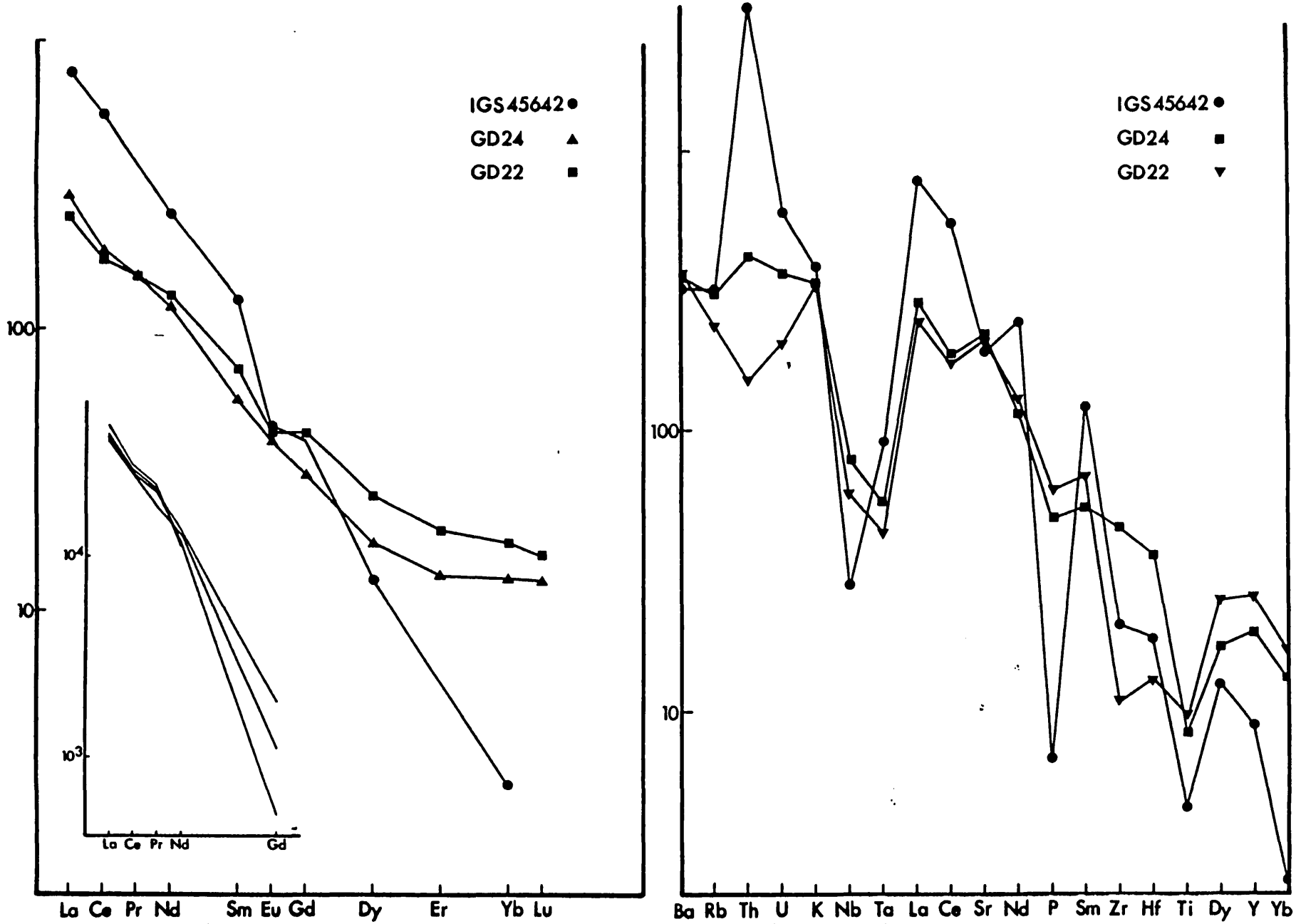


Figure 9.17: Chondrite normalised REE and incompatible element plots for syenite vein and reaction zone.
(inset= monazite analyses).

CHAPTER TEN

BULK CHEMICAL CHANGES ACCOMPANYING DEFORMATION OF THE GLEN DESSARRY LEUCOCRATIC SYENITE

The data discussed above provide a preliminary indication that deformation may have occurred in an essentially closed system. Literature studies have also shown that deformation in high temperature (amphibolite grade) regimes is essentially isochemical on a whole-rock scale (Kerrich et al., 1977), due to the nature of the dominant deformation mechanism. Details of the latter are beyond the scope of this thesis, but in view of the importance of deformation in the metamorphic processes at Glen Dessarry, it seems sensible to attempt a more careful assessment of its influence on whole-rock and mineral chemistry.

This chapter first briefly describes and illustrates the mineralogical changes associated with the development of the penetrative fabric, by comparing progressively deformed samples of leucocratic syenite. The leucocratic syenite mass is used exclusively, since primary textures are locally better preserved than in the mafic syenite. This account is followed by a consideration of whether the extent of deformation in the samples correlates with any variation in their major and trace-element geochemistry. The selection of samples is designed to minimise complications due to the demonstrable effects of in-situ crystal-liquid separation, so that a detailed assessment of element mobility during deformation can then be undertaken, based on the approaches of Gresens (1967), Babcock (1973), Kerrich et al. (1977) and Rubie (1982).

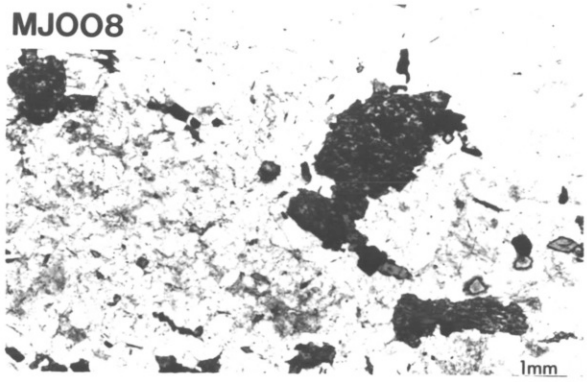
Although the deformation suffered by the Complex is extensive on a local scale, it has by no means obliterated the intrusive features, such as the sharp intervariant contacts, and the outlines of the Glen Pean metasedimentary raft, and of the local filter-pressed pegmatites (see Fig. 7.1). This effectively places the first constraint on the role of deformation processes,

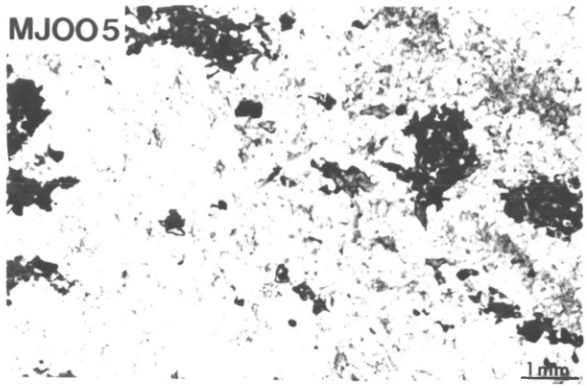
and was partly responsible for the "magmatism first" approach adopted above. Nevertheless, a fabric is developed in almost all rocks from the Complex, stages in whose development are illustrated in Plate 10.1, from "undeformed" MJ008 through to intensely-foliated MJ009.

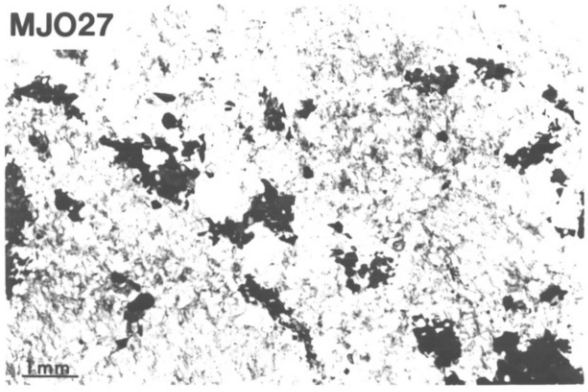
10.1 Mineralogy

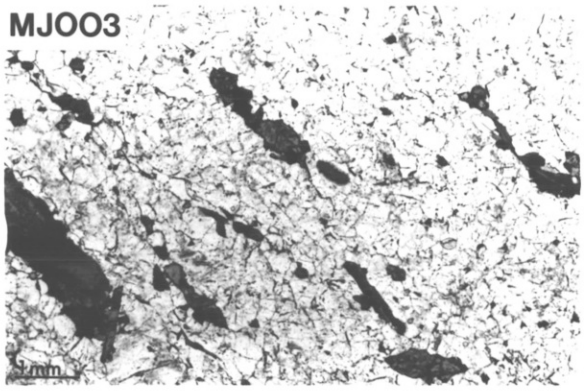
Feldspars.

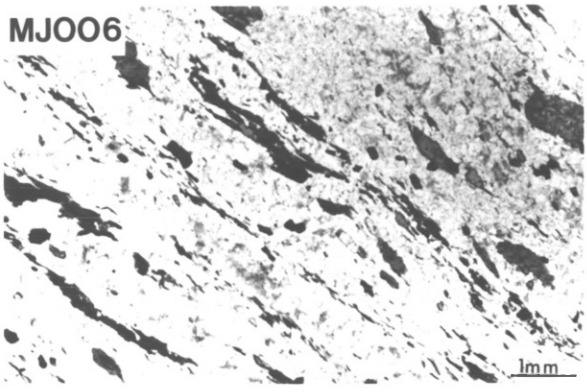
In rocks which show only the effects of low degrees of deformation, the dominant feldspar is usually a hypersolvus alkali feldspar of the type described in detail by Richardson (1968), and summarised above. Unmixing through patch perthite to large, discrete grains of orthoclase and plagioclase occurs with increasing deformation. Even in relatively undeformed samples (e.g., MJ008) unmixing is already advanced. Undulatory extinction of the exsolved orthoclase and plagioclase end-members is common, and may be related to sub-grain development. The exsolved plagioclase and K-feldspars lack the abundant and varied inclusion suite present in their parent perthites. The end result of the deformation process, as exemplified by sample MJ009 which has a pronounced planar foliation, is an approximately equigranular mosaic of medium-grained orthoclase and plagioclase. Isolated elongate pools of coarser-grained material may remain parallel to the foliation, but these invariably display undulatory extinction indicative of the continuing grain-size-reduction process. Clearly, those components - major and minor - which together form the parent and "daughter" feldspar compositions must have been mobile, albeit perhaps on a local scale only. Table 10.1 lists analyses of the parent alkali feldspar and the products of its unmixing. The least-squares calculation shows that the reaction could have occurred isochemically, with no need for any addition or removal of components.











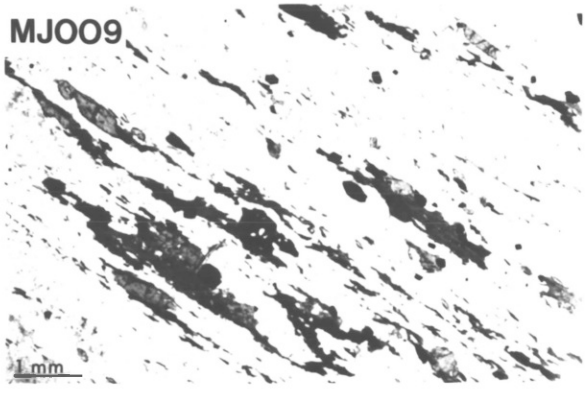


PLATE 10.1 FABRIC DEVELOPMENT

	Perthite (MJ008)	Kspar (MJ003)	Plag (MJ003)
SiO_2	63.81	63.30	66.00
Al_2O_3	19.69	19.24	21.21
CaO	0.51	-	-
BaO	0.72	1.08	-
Na_2O	3.76	1.68	10.74
K_2O	11.12	14.28	0.34
Total	99.60	99.58	99.76
Si	11.735	11.792	11.623
Al	4.265	4.208	4.377
Al	0.002	0.015	0.025
Ca	0.100	-	-
Ba	0.052	0.079	-
Na	1.341	0.607	3.668
K	2.609	3.392	0.075
AB	32.69	14.88	91.23
AN	2.43	-	6.89
OR	64.87	85.12	1.88

	Amount	SiO_2	Al_2O_3	CaO	BaO	Na_2O	K_2O
Kspar	77.21	63.30	19.24	-	1.08	1.68	14.28
Plag	22.79	66.00	21.21	1.47	-	10.74	0.34
Estimate		63.92	19.69	0.34	0.83	3.74	11.10
Perthite		63.81	19.69	0.51	0.72	3.76	11.12
Differences		0.11	0.00	-0.17	0.11	-0.02	-0.02

Residual sum of squares = 0.0552

Table 10.1: Feldspar analyses from undeformed (MJ008) and deformed (MJ003) leucocratic syenites, and modelled unmixing of alkali feldspar to give orthoclase (77%) and plagioclase (23%).

Pyroxenes and amphiboles.

Pyroxenes in less-deformed rocks are generally euhedral to subhedral and are intergrown with biotite, and/or show reaction relationships with amphibole. In the leucocratic syenites sampled for this study there is no correlation between degree of deformation and amphibole abundance, and a similar conclusion was reached for the mafic syenites, above. With progressive deformation pyroxene grains rotate into concordance with the developing fabric, but appear to be most resistant to the deformation process. Even in sample MJ009, relatively large, surprisingly equant grains remain,

although the majority have become somewhat elongate and lie parallel to the planar foliation (Plate 10.1). The grain size appears to have been reduced by disaggregation of larger parents. Amphibole often forms composite grains with length greatly exceeding width. There is little apparent change of composition of either phase (see Table 10.2), since those in deformed sample MJ003 are chemically closely comparable with those in sample MJ008, whose texture is dominantly igneous.

Pyroxenes			Amphiboles		
	MJ008 (8)	MJ003 (9)		MJ008 (8)	MJ003 (8)
SiO_2	51.69	51.86	SiO_2	42.01	42.27
TiO_2	0.03	0.09	Al_2O_3	9.40	9.33
Al_2O_3	1.14	1.84	FeO	17.85	17.17
FeO	12.51	11.87	Fe_2O_3	3.19	2.86
MnO	0.77	0.65	MgO	8.70	9.17
MgO	10.25	10.54	MnO	0.62	0.71
CaO	21.10	21.07	TiO_2	0.66	0.59
Na_2O	2.09	2.25	CaO	11.02	11.07
Total	99.58	100.18	Na_2O	2.19	2.20
			K_2O	1.33	1.38
			Total	96.98	96.74
Si	1.982	1.969	Si	6.509	6.542
Al	0.018	0.031	Al	1.491	1.458
Al	0.034	0.051	Al	0.226	0.244
Ti	0.001	0.003	Ti	0.077	0.069
Fe	0.401	0.377	Fe^3	0.372	0.320
Mn	0.025	0.021	Mg	2.009	2.115
Mg	0.586	0.596	Fe^2	2.314	2.236
Ca	0.867	0.857	Fe^2	-	-
Na	0.155	0.166	Mn	0.002	0.017
			Mn	0.079	0.076
			Ca	1.830	1.836
			Na	0.091	0.088
			Na	0.567	0.572
			K	0.263	0.273

Table 10.2: Average analyses of pyroxene and amphibole from undeformed (MJ008) and deformed (MJ003) leucocratic syenites.

Biotites.

Biotite responds to deformation by bend-gliding, kinking and fracturing. Small flakes appear to "peel" off larger parent grains, or recrystallise into fractures and along grain boundaries. In the most highly

deformed samples biotite occurs as discrete, fine-grained plates set within the feldspathic matrix. Parent and "daughter" biotites are also chemically comparable (Table 10.3), although there is an indication of some cation deficiency in the interlayer sites of the highly-deformed samples.

	MJ008 (5)	MJ003 (7)
SiO_2	36.88	35.66
TiO_2	2.17	2.26
Al_2O_3	13.13	13.69
FeO	19.08	21.84
MnO	0.49	0.46
MgO	12.54	11.36
CaO	0.05	0.26
Na_2O	0.46	0.47
K_2O	9.81	8.52
H_2O	3.87	3.83
Total	98.47	98.34
Si	5.712	5.577
Al	2.288	2.423
Al	0.109	0.100
Ti	0.252	0.266
Fe	2.471	2.856
Mn	0.064	0.061
Mg	2.894	2.647
Ca	0.009	0.043
Na	0.138	0.143
K	1.937	1.699

Table 10.3: Average analyses of biotite from undeformed (MJ008) and deformed (MJ003) leucocratic syenites.

Minor and accessory phases.

The response of the varied suite of minor and accessory phases to deformation is important, since they act as hosts for many of those elements with which this thesis is most concerned. Instability would necessarily result in element release and mobility. Various "secondary" processes have been identified, primarily by fission-track radiography (Fowler, 1981) and follow-up ion probe and electron probe microanalysis, and such is their inferred importance that they are treated in a separate chapter below, after the large-scale movement of elements has been more closely constrained.

10.2 Whole-rock chemistry

Two approaches have been adopted in assessing the nature of bulk chemical changes due to deformation. The first is a simple graphical analysis of the correlation of element abundances with approximate degree of deformation in twenty one leucocratic syenite samples. This should reveal any gross chemical changes which may have occurred. The second is similar to the method employed by Kerrich et al. (1982), whereby analyses of fewer samples of regularly increasing state of strain are considered in the light of possible volume changes by the use of volume factors (Gresens, 1966) and specific gravity measurements. This second approach requires careful selection of samples since it might easily produce spurious results if the effects of fractional crystallisation are not taken into account.

Figure 10.1 shows the relationship of element abundances with increasing deformation, and demonstrates a general lack of correlation between any major element and degree of deformation. Similarly, trace element variations display a general lack of correlation with increasing deformation, for LILEs (e.g., Rb, Ba, Sr, U, Th), HFSEs (Nb, Zr, Y) and the more compatible elements (Cr, Ni, V). All the observed variations may more easily be explained in terms of an in-situ magmatic fractional crystallisation scheme (see above).

However, in order to try and throw more detailed light on the significance of deformation during metamorphism, an attempt has been made to screen the data for the effects of in-situ fractional crystallisation. It has been shown above that Zr produces perhaps the most extreme in-situ fractionation range, with a concomitant fall in the Zr/Hf ratio. The presence of abundant zircon and some zirconolite in the syenites suggests that the whole-rock Zr is controlled essentially by these two phases. Zircon is probably more important because of its higher modal abundance and larger Zr content (c. 60% compared to about 32% in zirconolite). The grain-size reduction effects of deformation have

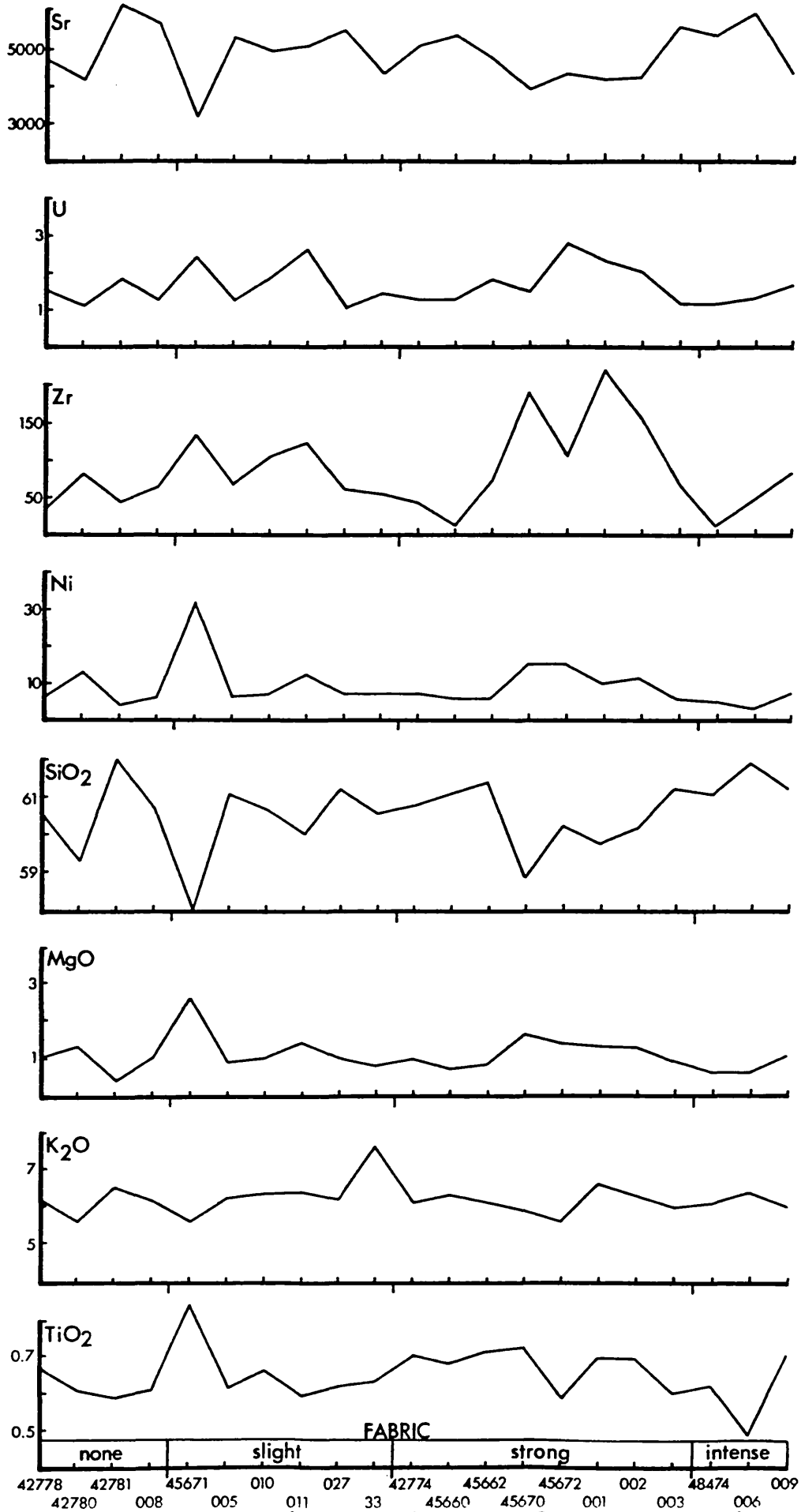


Figure 10.1: Variation diagram of selected major and trace elements with degree of deformation in the Glen Dessarry leucocratic syenite.

little effect on zircon, since the crystals are already small and can remain essentially inert throughout the process. Thus, as well as showing a large concentration range due to in-situ differentiation, Zr can be empirically considered on a mineralogical basis to be relatively immobile during deformation. It can therefore be used as a monitor of the degree of fractionation of individual samples independent of the degree of deformation. The overall Zr concentration range in the leucocratic syenites is 222ppm to 12ppm - more than an order of magnitude.

	MJ008	MJ005	MJ027	MJ003
SiO_2	60.78	61.14	61.24	61.28
TiO_2	0.61	0.61	0.62	0.60
Al_2O_3	17.55	17.68	17.78	17.73
Fe_2O_3	4.18	4.09	4.24	4.03
MnO	0.08	0.08	0.08	0.10
MgO	1.02	0.93	1.03	0.99
CaO	2.77	2.70	2.71	2.96
Na_2O	5.39	5.85	4.86	5.59
K_2O	6.22	6.27	6.25	6.00
P_2O_5	0.30	0.25	0.27	0.26
LOI	0.20	0.16	0.12	0.17
Total	99.10	99.76	99.23	99.71
Sr	5718	5281	5465	5530
Ba	4417	4093	5451	4189
Rb	98	97	79	81
U	1.26	1.27	1.06	1.18
Th	7.0	6.3	7.3	6.2
Zr	64	66	60	67
Nb	15	15	15	15
Y	27	27	25	31
Ni	6	6	7	6
V	78	81	86	80
SG	2.75	2.75	2.75	2.76

Table 10.4: Whole-rock analyses of variably-deformed leucocratic syenites with comparable primary geochemistry.

Four samples have been selected (MJ003, 005, 008 and 027) which lie in the interval 60-70ppm Zr (about 5% of the total range observed): i.e., they are very closely similar in terms of magmatic evolution. Although none of the samples has the intense foliation of, for

example, MJ009, they do show a range of deformation features, from a "massive" MJ008 through to the more deformed MJ003. The development of the fabric in these four rocks has already been illustrated in Plate 10.1. Complete whole-rock analyses together with specific gravity measurements are presented in Table 10.4. A cursory inspection of the table reveals a very close similarity between all of the samples, but as noted by Kerrich et al. (1982) and many other authors, this is not sufficient to rule out element mobility.

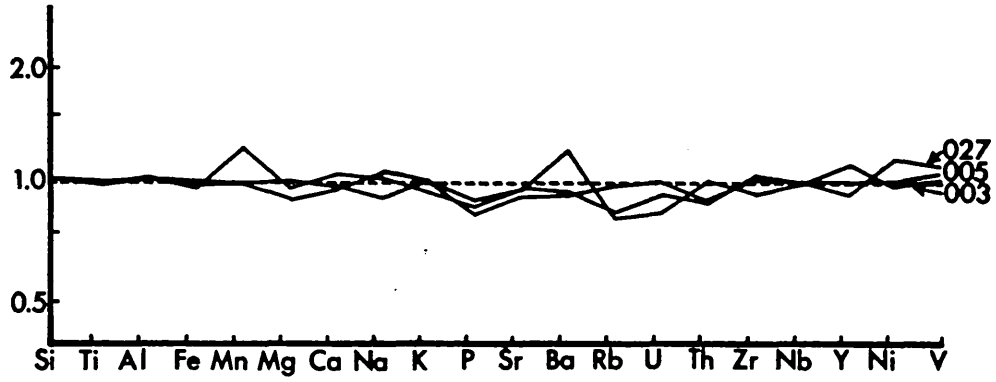


Figure 10.2: Multi-element plot illustrating the comparability of deformed samples with MJ008 (the least deformed).

In Fig. 10.2, data for the more deformed samples have been normalised to the values of the least deformed (MJ008), effectively demonstrating the similarity of the analyses for the sample sub-suite. This suggests that little obvious chemical modification has taken place during deformation. However, possible volume changes during deformation often obscure significant open-system behaviour, and these have not yet been considered.

Therefore the second, more rigorous approach is based on the technique of Gresens (1966), incorporating specific gravity data into mass balance calculations. Volume factors (fv) may be computed which correspond to the isochemical behaviour of each component, from the following equation:

$$dX_n = 100(fv \cdot X_{nb} \cdot p_b/p_a - X_{na}) \quad g / 100g \text{ of original rock}$$

dX_n=loss or gain of element n in prodution of rock B from rock A

fv=volume factor (the ratio of the final to initial volumes of the rock)

p=specific gravity

$X_{na\ b}$=weight fraction of element n in the rock (after Gresens, 1967 and Babcock, 1973).

Computation of such volume factors for all the major components in a rock suite may lead to clustering of values for elements which are empirically known to be relatively immobile in that particular system. If so, such clustering would provide a rational basis on which to assess the volume change of the reaction as a whole by using an average fv value for these "immobile" elements (Kerrich et al., 1982). In this way, a quantitative estimate of the volume change for each stage of the deformation process can be produced. For example, the "immobile" elements Al_2O_3, MgO, V, Cr, Ni, Zr and Nb could be used. Alternatively, the total immobility of one element could be assumed (e.g., Al_2O_3, or Zr) and an estimate of the overall volume change produced on this basis. Lastly, constant volume might be assumed.

The approximation to unity of fvs for all the elements listed in Table 10.5 (A) suggests that little change in chemical composition occurred during deformation. Since virtually all the values cluster near to unity, the first approach outlined above is redundant. However, immobile Zr has already been suggested, and constant volume does not seem unreasonable - there being no mineralogical changes which would induce significant density variations. Therefore, volume factors appropriate to these two assumptions have been used to calculate compositional changes for the reactions MJ008 = MJ005, MJ005 = MJ027, MJ027 = MJ003, and the overall

A. Values of fv for isochemical behaviour.

	008=005	005=027	027=003
SiO_2	0.994	0.998	0.996
TiO_2	1.000	0.984	1.030
Al_2O_3	0.993	0.994	0.999
Fe_2O_3	1.022	0.965	1.048
MnO	1.000	1.000	0.797
MgO	1.097	0.903	1.037
CaO	1.026	0.996	0.912
Na_2O	0.921	1.204	0.866
K_2O	0.992	1.003	1.038
P_2O_5	1.200	0.926	1.035
Sr	1.083	0.967	0.985
Ba	1.079	0.751	1.297
Rb	1.010	1.228	0.972
U	0.992	1.198	0.895
Th	1.111	0.863	1.173
Zr	0.970	1.100	0.892
Nb	1.000	1.000	0.996
Y	1.000	1.080	0.804
Ni	1.000	0.857	1.162
V	0.963	0.942	1.071

B. Constant volume (fv =1.000).

C. Immobile Zr.

	008=005	005=027	027=003	008=003	008=005	005=027	027=003	008=003
SiO_2	+0.59	+0.16	+0.43	+1.19	-2.43	+10.18	-10.74	-3.87
TiO_2	0.00	+1.64	-2.87	-1.28	-3.00	+11.80	-13.68	-6.22
Al_2O_3	+0.74	+0.57	+0.08	+1.39	-2.28	+10.62	-11.05	-3.68
Fe_2O_3	-2.15	+3.67	-4.61	-3.24	-5.09	+14.03	-15.22	-8.08
MnO	0.00	0.00	+25.45	+25.45	-3.00	+10.00	+11.50	+19.18
MgO	-8.82	+10.75	-3.53	-2.59	-11.56	+21.83	-14.26	-7.46
CaO	-2.53	+0.37	+9.62	+7.25	-5.45	+10.41	-2.57	+1.89
Na_2O	+8.53	-16.92	+15.44	+4.09	+5.28	-8.62	+2.60	-1.12
K_2O	+0.80	-0.32	-3.65	-3.19	-2.22	+9.65	-14.37	-8.03
P_2O_5	-16.67	+7.41	-3.35	-13.02	-19.17	+18.80	-14.10	-17.37
Sr	-7.64	+3.37	+1.56	-2.94	-10.41	+13.83	-9.74	-7.79
Ba	-7.34	+33.18	-22.87	-4.82	-10.12	+46.50	-31.45	-9.58
Rb	-1.02	-18.56	+2.90	-17.05	-3.99	-10.41	-8.54	-21.19
U	+0.79	-16.54	+11.73	-6.01	-2.23	-8.19	-0.70	-10.71
Th	-10.00	+15.87	-14.76	-11.11	-12.70	+27.46	-24.24	-15.55
Zr	+3.13	-10.00	+12.07	+5.07	-	-	-	-
Nb	0.00	0.00	+0.36	+0.36	-3.00	+10.00	-10.80	-4.65
Y	0.00	-7.41	+24.45	+15.23	-3.00	+1.85	+10.61	+9.47
Ni	0.00	+16.67	-13.97	+0.36	-3.00	+28.33	-23.54	-4.65
V	+3.85	+6.17	-6.64	+2.94	+0.73	+16.79	-17.02	-2.21

Table 10.5: Computations of likely volume change and mass transfer during progressive deformation.

reaction MJ008 = MJ003. The results are also listed in Table 10.5 (B and C). Composition - volume variation diagrams can be plotted on the basis of the data, and these are shown in Fig. 10.3.

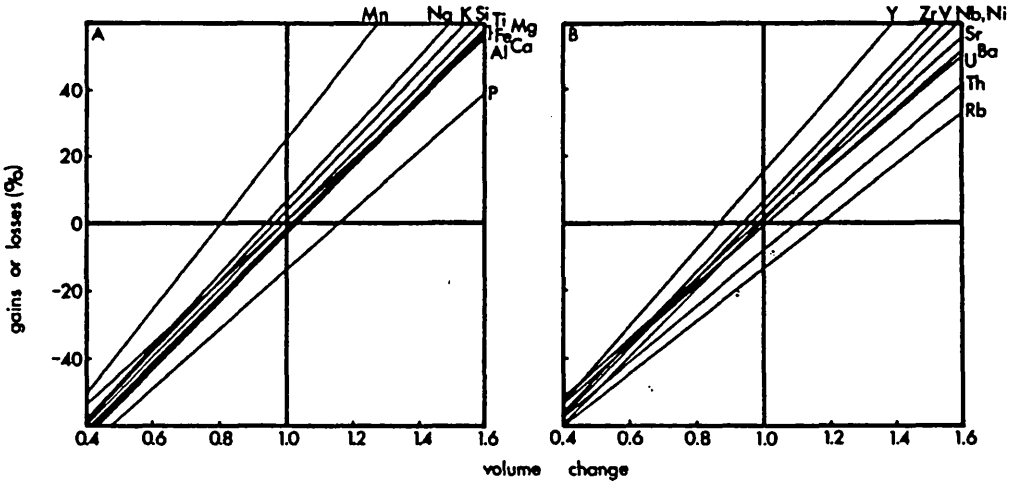


Figure 10.3: Diagram of element abundance variations during deformation from MJ008 to MJ003.

The elements define a broad band passing through the origin at about 45°. Thus, if the assumption of constant volume is correct, the reaction must have been essentially isochemical. At volume factors appropriate to Zr immobility, compositional changes are also generally less than +/- 15%. These features confirm the essentially minor and non-systematic changes in rock chemistry during deformation, and since no obvious correlations with progressive deformation exist, these may themselves be due to other factors.

Finally, in this section on whole-rock chemistry it might be instructive to consider the most deformed sample in the suite, MJ009. This shows an intense planar foliation and if any open system chemical changes occurred during deformation they should be evident in this rock. The problem of what to compare it with is tackled by using a chondrite-normalised trace element plot and showing also the field of analyses produced by

fractional crystallisation (Fig. 10.4). There is no feature of the geochemistry of sample MJ009 which cannot be explained by the fractional crystallisation model.

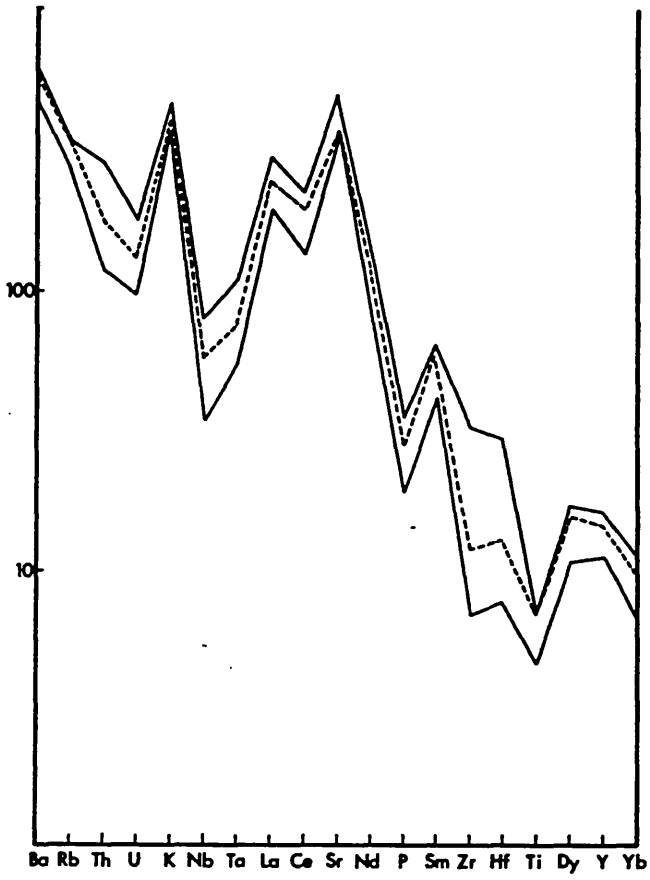


Figure 10.4: Chondrite normalised incompatible element plot of highly-foliated sample MJ009 and the field of leucocratic syenite analyses.
(MJ009= dashed line).

Apparently all that progressive deformation has done at Glen Dessarry is to re-equilibrate the mineralogical texture, causing little change in mineral chemistry, and therefore leaving whole-rock geochemistry essentially inert. The unavoidable conclusion seems to be that deformation at Glen Dessarry operated in an essentially isovolumetric and isochemical fashion on the scale of a whole-rock sample.

CHAPTER ELEVEN

MICROSCOPIC MOBILITY OF INCOMPATIBLE ELEMENTS

Although the evidence cited above does not require a total lack of element redistribution, it does constrain such effects in three ways:

i) To be on a scale smaller than that of a standard whole-rock sample (1-2 kg), and/or

ii) To be of a small enough magnitude to remain undetected during modelling of the extensive chemical changes resulting from crystal fractionation, and/or

iii) To follow a trend identical to that produced by such fractionation.

It is the purpose of the present chapter to make a detailed investigation of the extent to which the microscopic distribution of some key incompatible elements (including U) has been modified during the history of the rocks. It is based on the early fission-track study (Fowler, 1981) which demonstrated several styles of U mobility and raised the possibility that these were of metamorphic origin, contemporaneous with what was then thought to be post-igneous hydration of the syenites. The causes and mechanisms of such elemental remobilisation can now be considered and constrained in the light of the more detailed knowledge of the magmatic and metamorphic/ deformational processes outlined above.

The determination of the microscopic distribution of trace elements within the mineralogical framework of a given rock sample is no trivial task, but greatly facilitates any discussion of element mobility. However, the techniques available are generally both specialised and time-consuming (Burnett and Woolum, 1983), and the range of suitable elements is further limited by the facilities accessible to the author. Three are employed here: fission-track analysis; electron probe microanalysis and ion-probe microanalysis; (see the appendix for brief procedural details). A combination of these methods allows useful information to be

gathered on several key elements of those with which this thesis is concerned; for example, U, Th, selected REEs and Zr.

It has been shown above, on the basis of whole-rock data, that the abundance and distribution of many of the HFSEs and some of the LILEs (including U) are strongly influenced by the minor mineral phases sphene, zircon, zirconolite, allanite and apatite, particularly in the later stages of consolidation. Particle-track work has confirmed that these five mineral phases contain the major part (estimated at more than 95%) of the whole-rock U budget; with that attributable to rock-forming minerals or grain-boundary adsorption almost negligible by comparison (Fowler, 1981). This is in stark contrast to many other igneous rocks (generally granites), where a substantial fraction of the whole-rock U is resident in readily-leachable sites on grain boundaries or in crystal defects (e.g., Tieh and Ledger, 1981). However, detailed mineralogical studies, notably by Gromet and Silver (1983), have also drawn attention to the influence of minor phases such as sphene and allanite in controlling the behaviour of the lanthanide rare-earth elements, for example, in granitic (s.l.) systems. Because of their obvious importance to the geochemistry of U at Glen Dessarry, the following paragraphs record more detailed descriptions of each of the accessory minerals; their abundance, distribution, content of U and selected other elements and their individual responses to and relationships with the processes of deformation. In particular, any interaction with fluids present during the late-magmatic or sub-solidus history of the rocks is highlighted.

It should be stated at the outset that the distribution of U is complex, and there are apparent anomalies and exceptions to the simple scheme devised below. Nevertheless, it is believed to offer the best explanation for the majority of the features observed and is essentially in accord with the constraints imposed by the whole-rock chemistry.

11.1 Sphene

Sphene occurs throughout the range of magmatic rocks at Glen Dessarry, from cumulate samples GD48 and GD49 through mafic and leucocratic syenites to the filter-pressed pegmatites, though its modal abundance is greatest in the mafic and leucocratic syenites. The lack of ilmenite in the syenites (Richardson, 1968) suggests that sphene might be the major influence on TiO_2 abundance during magmatic differentiation. This is consistent with the whole-rock geochemistry above which records progressively falling TiO_2 with increasing silica percentage. Its presence in the cumulates confirms that it was a liquidus phase during fractionation in the low-level magma chamber and variations in its abundance due to in-situ processes are reflected in the array of whole-rock, chondrite-normalised REE diagrams (Fig. 9.7). Crystallisation of the two pulses of syenite melt at the higher level, gave rise to euhedral sphene grains with U distributions such as those illustrated in Plate 11.1a and b. These have been selected from leucocratic rocks which retain original igneous textures, so that the distribution of U may be considered to be relatively unmodified by secondary processes. Sphenes may be empirically divided into two populations; those in which U is homogeneously distributed throughout the crystal, and a small proportion in which it is regularly zoned-generally with increasing U abundance towards the perimeter, but sometimes with the opposite trend (especially in the mafic syenites). This is somewhat paradoxical, since the magmatic trend during the in-situ crystallisation of the syenite has been shown to be towards lower U concentrations, at least during the later stages represented by the filter-pressed pegmatites. One possible explanation is the progressive increase in mineral/melt partition coefficients of highly-charged elements related to the silica saturation of the melt (for example, compare the data given by Arth and Hanson, 1975 with that of Mahood and Hildreth, 1983; Sawka et

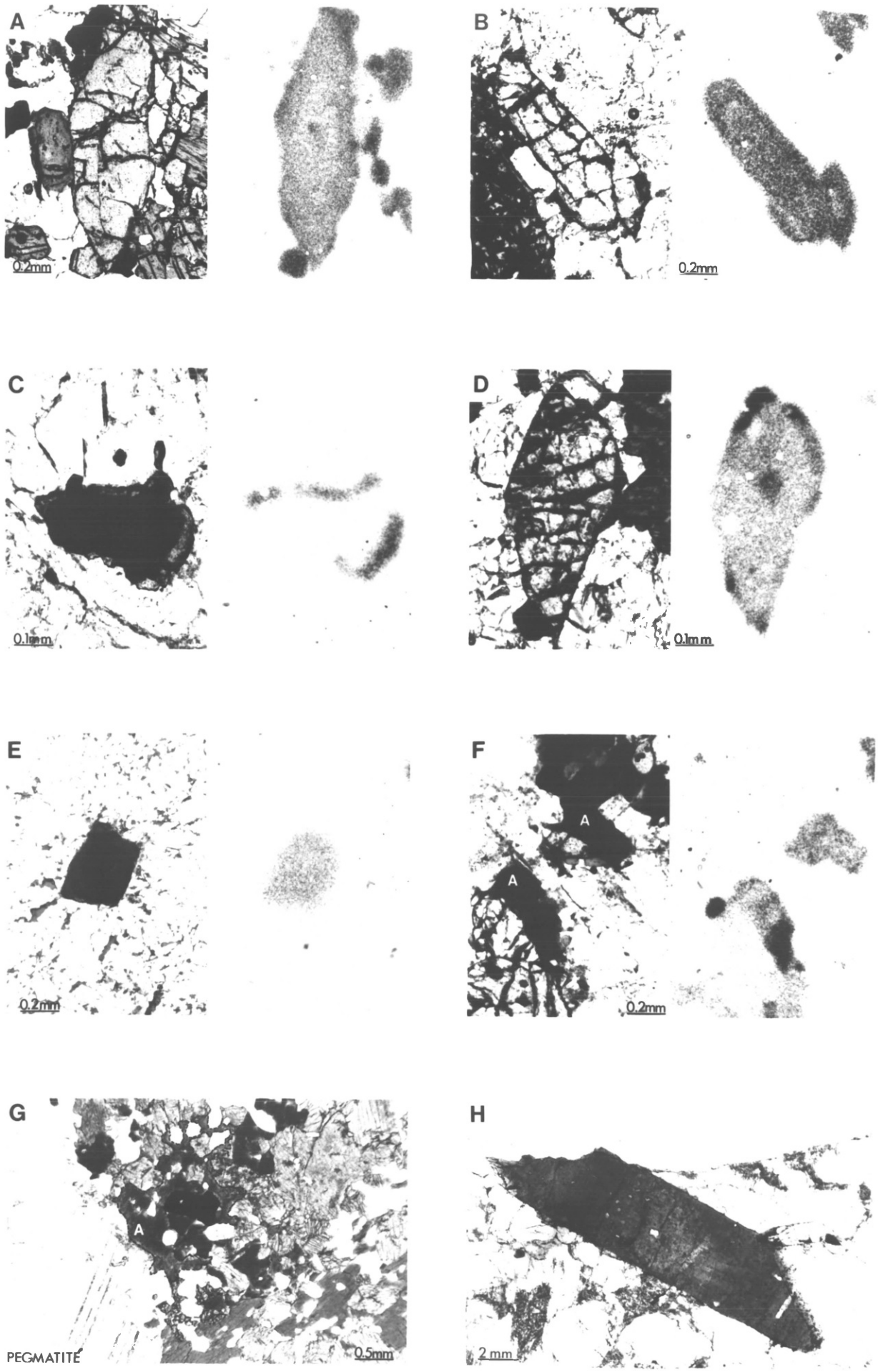


PLATE 11.1 SPHENE AND ALLANITE

al., 1984). However, it is doubtful whether the relatively small silica variations at Glen Dessarry could be responsible for such a drastic effect. A more likely possibility is that those sphene crystals zoned towards higher U concentration date from a period when U concentration in the melt was also increasing, perhaps during fractionation of early, mafic phases.

Ion-probe microanalysis (SIMS) has been used to investigate the extent to which other elements (e.g., LREEs and Th) behave in a similar manner. Quantification at such low levels is difficult, but semi-quantitative results may be obtained using the procedure detailed in the appendix. Unfortunately, HREE abundance determination is rendered impossible at present by the interferences of complex molecular ions, although extensive developmental work may partly overcome these difficulties in the future (Metson et al., 1984).

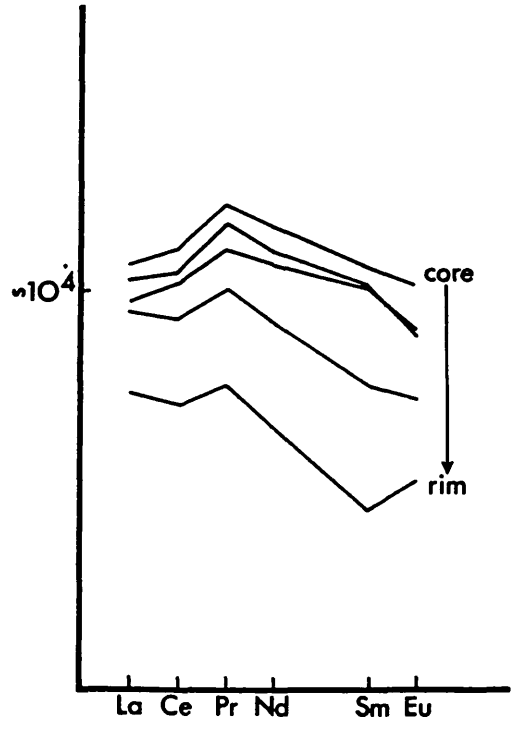


Figure 11.1: Semi-quantitative chondrite normalised LREE plots for magmatic sphene.

Only one "magmatic" sphene crystal could be investigated in the time available, and is shown in Plate 11.1a, from leucocratic syenite sample IGS42778, with the corresponding fission-track overlay clearly showing the zonation towards higher U abundance. Fig. 11.1 shows semi-quantitative, chondrite-normalised LREE plots for a traverse from the centre of the crystal to the edge. The data are available in the appendix. There is a clear, consistent trend towards lower LREE (and Th) abundances at the edge of the crystal, the reverse of the recorded U zonation, but precisely similar to that recognised by Sawka et al. (1984). There are several possible explanations. It might be supposed that the falling REEs in sphene are due to local, kinetically-induced depletion at the interface between growing crystal and melt. However, the time required for diffusive transport over millimetres in the melt is probably rapid compared to the growth rate of the mineral (Gromet and Silver, 1983). Further, U diffusion rates are probably of a similar order of magnitude and these were evidently large enough to allow increasing concentration with growth. Alternatively, Sawka et al. (1984) attributed falling REEs to rising F in the melt increasing the available coordination sites for highly-charged cations and thus reducing the mineral-melt partition coefficients. The decoupling of U and REE again argues against this, although it remains a possibility. Lastly, but in the author's opinion most likely, LREE abundance in the melt may have begun to fall while the U content was still increasing, probably due to the particular combination of crystallising phases and their relative partition coefficients.

A second and quite distinct habit shown by sphene has not yet been described - reaction rims around Fe-Ti oxides. A good example is illustrated in Plate 11.1c, and the corresponding fission-track overlays demonstrate that such secondary sphene is detectably uraniferous. Since this does not apply to either of the parent minerals, the required U must have been introduced from

an outside source. Since solid state diffusion rates are prohibitively low, the presence of a fluid phase may be inferred. These secondary phenomena, though not rare within the syenites (both mafic and leucocratic) are rather variable and localised in their occurrence. They nevertheless provide clear petrographic evidence of the circulation within the syenites of a fluid capable of transporting U and other incompatible elements.

Sphene behaves in a characteristic manner towards progressive deformation and the development of a penetrative fabric within the rocks. Stages in the transformation of large euhedral crystals to elliptical, finer-grained sphene concordant with the newly-formed planar fabric can be seen in Plate 10.1, and a good example of the recrystallised end product and its corresponding fission-track overlay in Plate 11.1d. The internal distribution of U is no longer either homogeneous or regularly zoned; it has become grossly heterogeneous and the conclusion that internal U mobility has occurred with or without addition of U from an intergranular fluid is unavoidable. Thus the microchemistry of sphene also records evidence of local mobility of U in direct response to the processes of deformation.

The extent to which other elements are affected can again be investigated by use of the ion-probe. The distribution of LREEs and Th (and U) has been investigated in one sphene crystal (from sample IGS45662 - Plate 11.1d). The resultant semi-quantitative LREE chondrite-normalised patterns are also shown in Fig. 11.2. Th values are noted in the appendix and show an antipathetic relationship with U. The LREE values of the high-U zone are considerably lower than for the body of the sphene crystal. Since this is similar to the previously determined magmatic trend, it is difficult to be certain whether it is a relict magmatic feature, or caused by an antipathetic loss of LREE during U enrichment. However, the facts that at no other place around the perimeter of the crystal did analyses

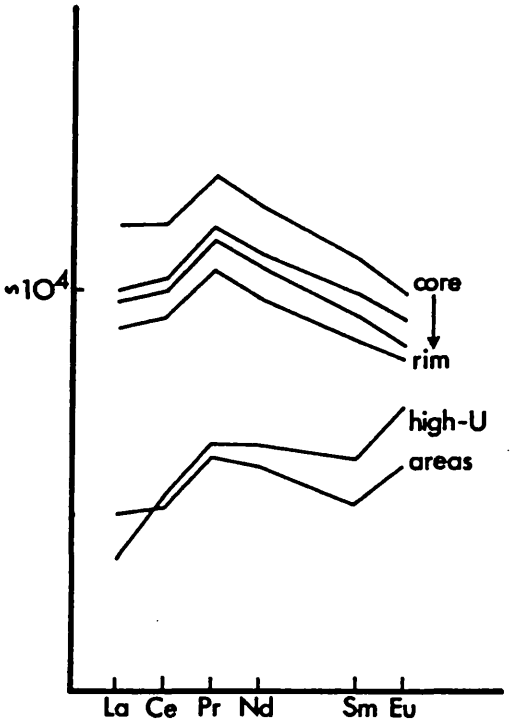


Figure 11.2: Semi-quantitative chondrite normalised LREE plots for deformed sphene.

approach these very low values, and that the shape of the pattern is different from the otherwise consistent magmatic patterns, perhaps lend support to the second alternative, and suggest that LREE may have been lost from the micro-system (see also apatite data below).

In summary, three separate aspects of trace element distribution in sphene may be recognised:

i) Primary solid-solution with homogeneous or regularly zoned distribution.

ii) Secondary, uraniferous sphene recording fluid circulation within the rocks.

iii) Intragranular U redistribution as a result of deformation and recrystallisation of primary sphene.

It is perhaps appropriate to note that the U-Pb isotopic age determination on a sphene separate by van Breemen et al. (1979) records an age about 20Ma younger than that of zircon, and that these authors suggest that this might be due to post-igneous recrystallisation.

11.2 Allanite

Allanite is also ubiquitous throughout the Glen Dessarry rocks, from cumulates through mafic and leucocratic syenites to the pegmatites. Its abundance is least in the cumulates, in which it is equivocal whether the allanite is primary or secondary. Its substantial influence has already been recorded in the section on whole-rock geochemistry, particularly with respect to petrogenetic aspects since the incorporation of large amounts of LREEs is possible, through coupled substitution with Al^{3+} and Fe^{3+} (Ribbe, 1980). Its distribution and habit show many similarities with those of sphene. Plate 11.1e and f show examples of euhedral allanite crystals which are considered to have crystallised directly from the melt. The even dispersion of U clearly indicates solid solution within the lattice structure, probably in the REE site. Gromet and Silver (1983) suggest a charge-balancing substitution for Th (also U?) as follows:

$$Ca^{2+} + Th^{4+} = 2REE^{3+}$$

Zoning towards higher U concentrations at the periphery is not uncommon, as for sphene, but in many cases high-U allanite has the appearance of an overgrowth on a low-U core (c.f., Sawka et al., 1984).

The results of electron-probe microanalysis for LREE on euhedral crystals from mafic and leucocratic syenites are plotted as chondrite-normalised LREE patterns in Fig. 11.3, and show extreme LREE/HREE fractionation. However, like sphene, allanite also exists throughout the syenite variants (except perhaps, the pegmatites), in a form which suggests it had a secondary origin as reaction rims to various minerals, but most often around apatite where juxtaposed against biotite. An example of this mode of occurrence is illustrated in Plate 11.1g. Electron-probe microanalytical data from secondary allanites are illustrated as chondrite-normalised LREE plots also in Fig. 11.3, and show a relatively LREE-poor and less-fractionated trend compared to their primary analogues. This calls to mind the magmatic evolution

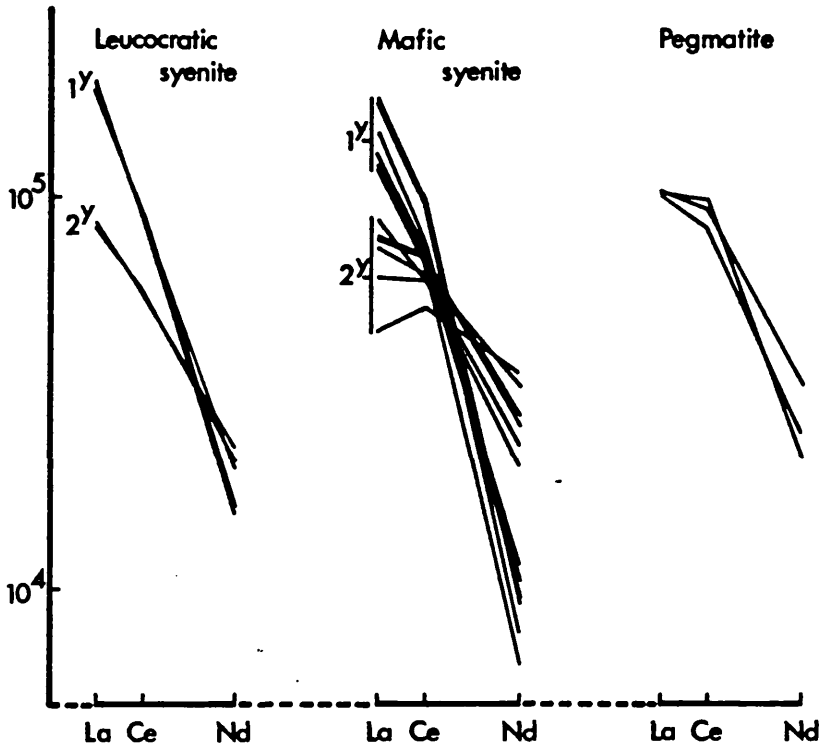


Figure 11.3: Chondrite normalised LREE plots for primary, secondary and pegmatitic allanite.

towards lower, less-fractionated REEs in the residual pegmatitic melts. Indeed, it is often the case that the most extensive development of secondary allanite is within samples collected adjacent to the nebulous filter-pressed pegmatite bodies (as shown in Plate 11.1g, from sample MJ016 which contains the junction of mafic syenite and a pegmatite), and there is no obvious relationship of its distribution with deformation. Thus the possibility of a genetic link between secondary REE- and U-bearing minerals and pegmatite production (see Fowler, 1981) has been raised both on petrographic and microchemical grounds. It would be strengthened by the demonstration of the equivalence of secondary allanite within the syenites with that crystallised directly in the pegmatites. Therefore, euhedral allanite from one of the pegmatites (GD35) has been analysed for comparison (illustrated in Plate 11.1h). Chondrite-normalised LREE

plots are presented in Fig. 11.3, and clearly show a close comparability with the analysed secondary allanites. Both are much less fractionated than the primary variety (La/Nd_{cn} about 3 to 5 for pegmatitic allanite, 1 to 4 for secondary allanite, and 10 to 20 for primary allanite). This lends considerable support to the notion that secondary allanite was itself precipitated by pegmatitic fluids pervading the already established mineral framework, during a late stage of magmatic evolution.

11.3 Apatite

Apatite has a similarly widespread distribution to sphene, occurring as obviously primary crystals in both cumulate samples, the mafic and leucocratic syenites and to a lesser extent in the pegmatites. As the only phosphate present in most rocks of the Complex (although monazite has been found in vein/xenolith reaction products), it exerts a controlling influence on the abundance and distribution of P. The multi-element, chondrite- normalised plots (Fig. 9.12), and P_2O_5 Harker diagram (Fig. 9.3) clearly show a progressive depletion of P with evolution which can be directly attributed to apatite fractionation. Plate 11.2a, b and c show the typical habit of apatite within relatively undeformed syenites, together with the associated fission-track overlays. U is homogeneously distributed through the apatite crystals, sometimes showing zoning towards lower values at the rims. In contrast to both sphene and allanite, apatite is nowhere found showing obvious secondary textural relationships. Nevertheless, several examples of U distributions which might be attributable to reactions during deformation are illustrated in Plate 11.2a and b. These show a cluster of sphene, apatite, allanite and biotite. The apatite above the allanite is clearly composed of several sub-grains. That below the biotite has a single internal grain boundary traversing NE to SW. All these internal grain boundaries correspond to areas of anomalously low fission-track

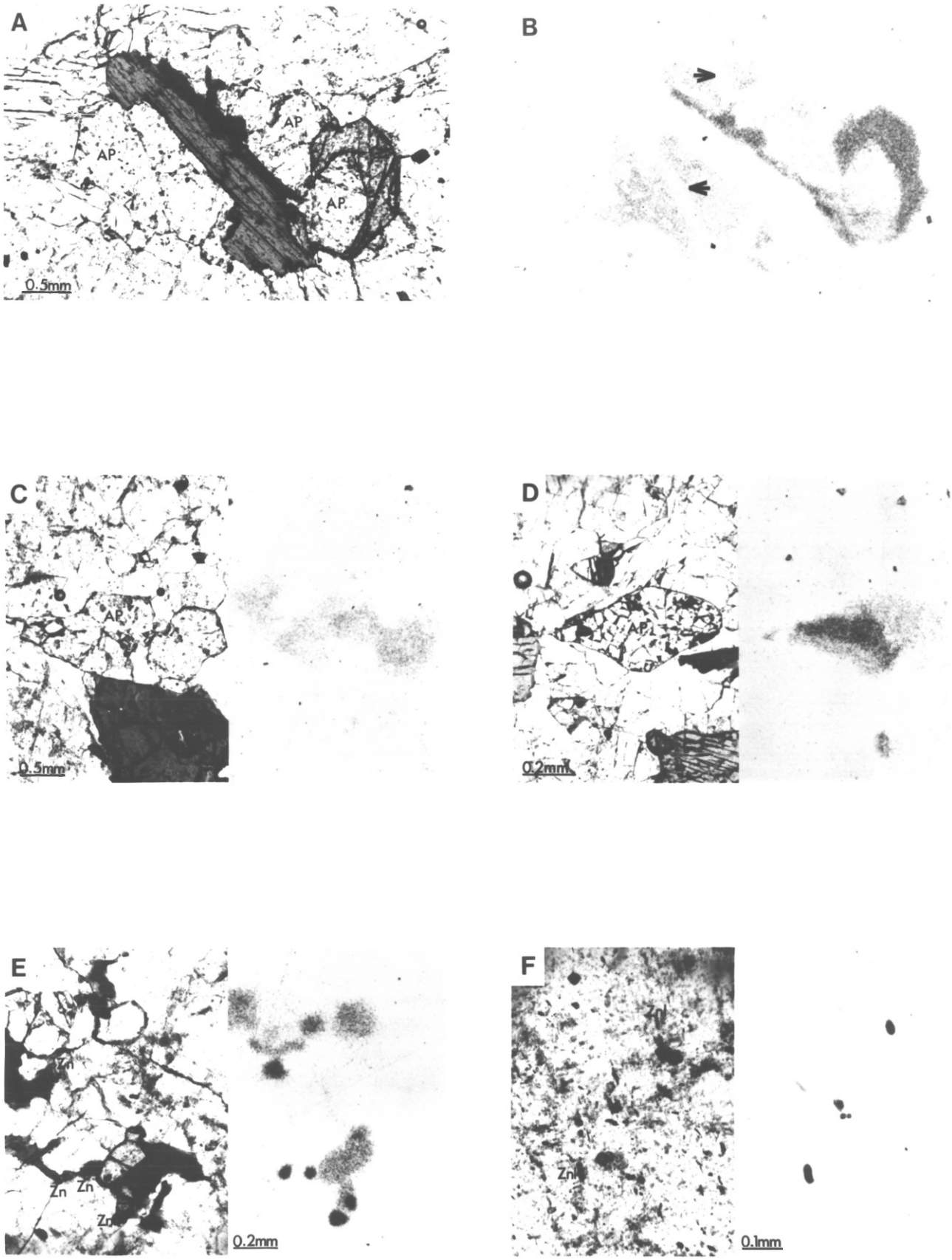


PLATE 11.2 APATITE AND Zr—RICH MINERALS

density on the associated Lexan overlay, and are not matched by corresponding areas of low track density at the external contacts with other minerals (alkali feldspar, biotite, sphene and allanite). This renders the possibility that they are related to zoning during in-situ crystallisation unlikely, barring fortuitous growth directions such that the last areas to crystallise were only those now traversed by internal grain boundaries. The preferred explanation (Fowler, 1981) is that they represent areas within the apatite crystals which underwent local U-loss to an intergranular fluid phase, during incipient deformation, since the lowermost grain boundary at least has the appearance of a fracture across a once intact single crystal. Interestingly, allanite clearly postdates the formation of the upper grain boundaries (since it appears to have grown along them), and assuming that all the internal grain boundaries are coeval, this places an important constraint on the temporal relationship between incipient deformation and the circulation of the REE- and U-bearing pegmatitic fluids probably responsible for secondary allanite growth. It is not impossible that this fluid was also responsible for U leaching from the apatite lattice, and if so its composition must have been such that the resultant chemical potential gradient encouraged U diffusion out of the apatite lattice framework. Many other examples of falling U abundance in apatite (e.g., Plate 11.2d) show such relationships with the development of the secondary fabric as to argue against a magmatic zonation cause. Thus, consideration of the detailed distribution of U in apatite has revealed a further response to the presence of fluids within the Complex, namely the solution of U without the necessity for mineral breakdown.

LREE and Th have again been investigated by use of the ion-probe. The study was concentrated on apatite in the vicinity of the internal grain boundaries discussed above. The results are presented in Table 11.1, and

	"Normal" apatite				"Low-U" area		
La	2.78	3.12	3.14	4.49	0.44	0.52	0.82
Ce	3.88	4.49	5.33	5.47	0.66	0.77	1.19
Pr	0.67	0.77	1.18	0.99	0.18	0.17	0.26
Nd*	1.01	1.05	1.35	1.19	0.67	0.74	0.73
Sm	0.28	0.31	0.36	0.29	0.18	0.21	0.20
Eu*	1.99	2.01	1.92	2.03	1.75	1.71	1.80
Th	0.17	0.12	0.34	0.19	0.001	-	0.01
U	0.03	0.07	0.06	0.09	0.01	0.02	0.01

* interferences by complex molecular ions.

Table 11.1: SIMS relative count rates for "normal" and "low-U" apatite.

clearly Th is also lost, if anything to a greater degree. Similarly, the abundance of the LREEs - especially La and Ce, drops dramatically in sympathy with the U count. This is another example of multi-element mobilisation and selective leaching by an active intergranular fluid after at least partial consolidation of the magma.

11.4 Zirconium-rich phases

Zircon is a very common phase in the Glen Dessarry Complex and despite its low modal abundance relative to sphene, allanite and apatite, its rather higher U content (c. 500 ppm; van Breemen et al., 1979) indicates its importance to the overall U budget. Plate 11.2e illustrates its typical habit and the associated Lexan plastic overlays demonstrate the high U abundance. Van Breemen et al. (1979) consider, on the basis of the optical zonation and frequent solution embayments, that zircon crystals now present in the syenite are the remnants of partially-dissolved igneous zircons. It is quite likely that crystal resorption occurred as a result of increasing melt alkalinity. There is no evidence from the leucocratic syenite or mafic syenite for an inherited zircon suite (c.f., Pidgeon and Aftalion, 1978). Since its original grain size is so small, zircon is resistant to the effects of progressive deformation, and no features compatible with secondary mobilisation have been observed.

Zirconolite is found most frequently as microscopic inclusions in hypersolvus alkali-feldspar phenocrysts, associated with intense fission-track "stars" (Plate 11.2f). Quantitative electron-probe analyses have been given above (Chapter eight, Table 8.4) showing a U content of c. 2.5% by weight UO_2. REEs are also high (total approximately 7%) and up to 8.5% ThO_2 is present. An average chondrite-normalised plot is shown in Fig. 11.4, recording a moderate LREE enrichment and small positive Ce anomaly. Despite its very low modal abundance, zirconolite is important to the radioelement and REE complement of the syenite. It is inevitably affected during the common feldspar exsolution processes, but there is no obvious change in abundance. Its small grain size renders zirconolite relatively inert to the processes of deformation.

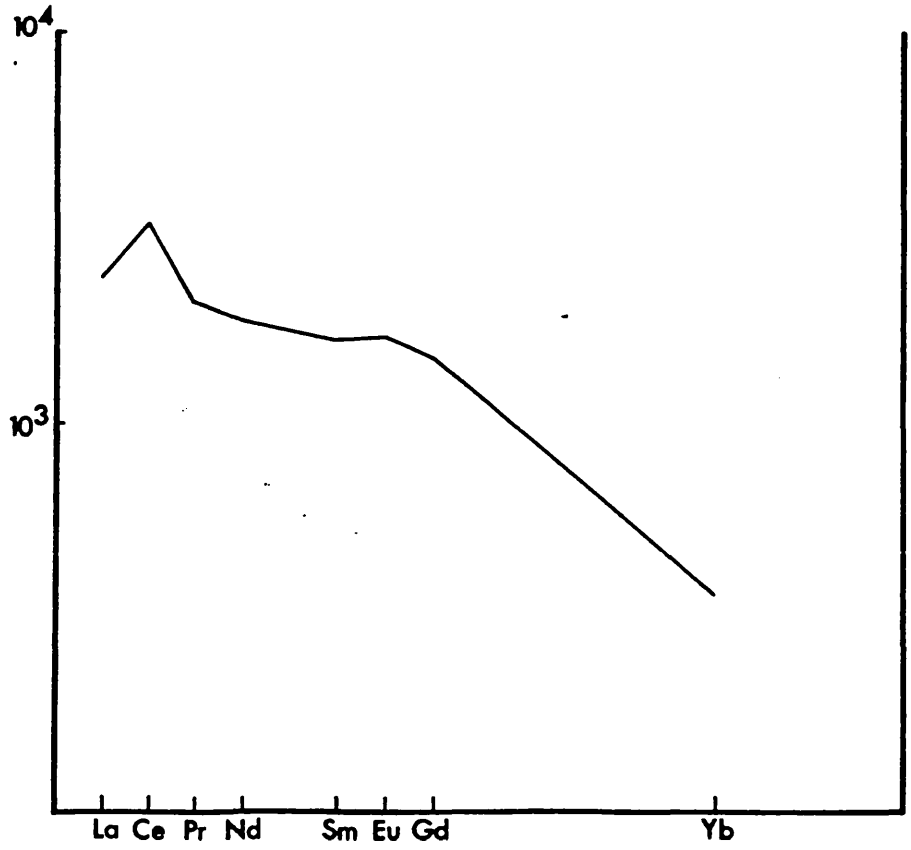


Figure 11.4: Chondrite normalised REE plot for zirconolite.

Therefore, through a consideration of the microscopic distribution of U as revealed by fission-track radiography and follow-up analyses of other critical elements such as Th and the REEs, much useful information has been gathered on the extent of their mobility within the mineralogical framework of the rock which was not apparent by consideration of whole-rock data alone. There is abundant evidence for the circulation of a fluid within the rocks, giving rise to secondary allanite and sphene, and causing element removal from apatite. This phase has been related on textural and mineral-chemical grounds to the filter-pressed pegmatite bodies. Recalling for a moment the whole-rock REE data, it was shown that the REE patterns of the pegmatites could be related to the composition of their host syenites by quantitative removal of allanite and sphene. It seems reasonable to connect the two observations and propose that the secondary mineral phases ("often...most extensive... adjacent to nebulous, filter-pressed pegmatite bodies" - above) precipitated from pegmatitic fluids present during the final phases of consolidation of the magma. Such a process probably operated in a manner similar to a modified version of "zone-refining", such that the small amounts of secondary phases precipitated in any given whole-rock sample caused no substantial elevation of the already very high REE content (for example), but contributed to the progressive evolution of the REE-depleted chemistry of the fluid itself, which finally crystallised as the exposed pegmatite bodies.

Two features may be directly related to deformation: the formation of high-U zones in sphene, perhaps associated with LREE and Th loss, and U-LREE-Th removal from some apatite grains. Considering the profound effects of deformation on the mineralogical framework of the syenites, these may be seen as rather minor perturbations in what is essentially an isochemical process.

CHAPTER TWELVE

CONCLUSIONS TO GLEN DESSARRY

The following conclusions may be derived from the study of the Glen Dessarry syenite:

i) Systematic variations in whole-rock geochemistry do exist within the exposed syenites (c.f., Richardson, 1968).

ii) Most major- and trace-element whole-rock abundance variations can be explained by reference to magmatic processes involving crystal-liquid equilibria.

iii) The parental compositions of the mafic and leucocratic syenite magma pulses evolved in a low-level magma chamber by early separation of olivine and pyroxene, to be dominated later by clinopyroxene, biotite, sphene, apatite and a little feldspar.

iv) After emplacement to the presently exposed level, in-situ crystal-liquid separation continued the already established trend, but feldspar became an increasingly important fractionating phase, to be joined by amphibole in the later stages of crystallisation.

v) Minor and accessory mineral phases exercised a substantial influence on the distribution of many "incompatible" elements.

vi) Local magma contamination with Moine metasediments caused large perturbations in the distribution of selected trace elements.

vii) Magmatic reactions with juxtaposed country rock also strongly influenced trace-element variations within the Complex.

viii) All these above conclusions severely constrain the extent of "metamorphic" element redistribution during deformation.

ix) Close study of selected samples of progressively deformed leucocratic syenite confirm that deformation caused little open-system element migration.

x) The chemistry of most rock-forming mineral phases remained unchanged during deformation, and feldspar exsolution was an isochemical process.

xi) Several types of microscopic mobility of incompatible elements have been detected by methods of in-situ trace-element analysis, mostly related to late-stage magmatic processes.

xii) Nevertheless, U culminations in sphene, related to LREE and Th depletion, are probably the result of recrystallisation during deformation. This need not have involved extensive open-system behaviour, although it cannot be definitively ruled out.

xiii) Areas of extensive U, LREE and Th depletion in apatite often show such a relationship with deformation structures as to argue against a purely magmatic origin. This presumably involved a coexisting grain-boundary fluid which removed these elements from the local lithochemical system.

CHAPTER THIRTEEN

GENERAL DISCUSSION

Detailed geochemical studies of the type attempted here cannot possibly be representative of the range of conditions and environments encompassed by high-grade metamorphism. Therefore, specific conclusions drawn from this approach are necessarily restricted and require careful thought before they can be applied to other crustal environments. Nevertheless, the examples discussed above were chosen for their contrasting characteristics so that some tentative, broader-ranging conclusions might be possible. It is the purpose of this final chapter to summarise these and the other main conclusions of the work, discuss them briefly in the light of published data and to highlight areas in which further work might prove instructive.

The purpose of the study was to derive new information - however little - about the ways in which elements are mobilised and transported within the local lithogeochemical system during metamorphism. The Glen Dessarry syenite provided a relatively small, well-defined intrusion deformed during an amphibolite-facies metamorphic event, whose effect on U distribution could therefore be studied. An early investigation of the microdistribution of U within the mineralogical framework of the leucocratic syenite revealed several features of secondary U (also LREE and Th) movement and raised multiple possibilities for their cause (Fowler, 1981). Subsequent work reported above consistently indicated the dominance of magmatic controls on the chemistry of the sample suite, and suggested that a conventional magmatic, rather than metamorphic origin for amphibole (c.f., Richardson, 1968) should be considered. This removed the requirement for a fluid phase to enter the syenite after consolidation, and made it easier to explain the lack of correlation between the proportion of amphibole relative to pyroxene and the state of strain in the

Complex. Whole-rock geochemical evidence demonstrated that filter-pressed pegmatites generated within the mafic syenites could be chemically related to them by removal of sphene, allanite, feldspar and amphibole. Sphene and allanite are precisely those REE-rich phases shown to have secondary textural relationships in the early fission-track study. Secondary allanite is now known to be closely similar to pegmatitic allanite in terms of its REE chemistry. This was taken as strong evidence that the observed mobility of U, LREE and Th was an autometamorphic effect produced during the later stages of a complex magmatic history.

Further evidence for the dominance of magmatic controls was provided by the importance of crustal contamination, metasediment fenitisation and syenite vein/xenolith reactions, all of which remained essentially unmodified by subsequent processes. Nevertheless, microscopic changes in the distribution of U, Th, La, Ce, Pr, Nd, Sm and Eu in sphene and apatite, can be related directly to recrystallisation during deformation. These occurred only on a local scale (less than that of a whole rock sample) and no significant changes in whole-rock elemental abundances appear to have resulted from progressive deformation.

These conclusions are in accord with previous studies of amphibolite-grade deformation (Kerrich et al., 1980) and metamorphism (Watson et al., 1982) and suggest that closed-system behaviour might be common during amphibolite-grade processes. However, it might be expected that hydrous rocks undergoing active dehydration would show considerable open-system mobility of elements stable in the coexisting fluid. For example, U is known to be mobile during amphibolite-facies processes, especially if substantial grain-boundary or crystal-defect U was originally present (Moorbath et al., 1969; Watson et al., 1982; Dostal and Capedri, 1978 and Ahmed and Wilson, 1982). Further, if the lithological system is saturated by an externally derived fluid with which it is not in

equilibrium, substantial mass transfer might be expected (e.g., Senior and Leake, 1978).

Although the conditions favourable for element mobility can be loosely predicted on the basis of an elementary understanding of probable interactions between a supercritical fluid and the mineral framework of its host rock, there is still a need for more detailed information on the mechanisms by which elements are released and/or fixed from solution. This is perhaps the most promising area for further research into metamorphism at Glen Dessarry. Detailed investigation of the progress of mineral recrystallisation and internal element mobility such as U in sphene documented above might provide a valuable insight into the behaviour of trace elements during deformation and metamorphism. However, magmatism probably offers more immediate and less parochial results - particularly the role of crustal contamination both at source (i.e., does subducted sediment contribute significantly to the primary geochemistry of the melt?) and in situ (was assimilation effectively simple mixing of a Moinian melt with mafic syenite or was some concurrent fractional crystallisation involved as in the popular AFC model for contamination?)

The complementary part of the thesis concerned element mobility in the amphibolite to granulite facies transition, where abundant literature data has indicated that substantial LIL element mobility occurs in diverse lithologies of both sedimentary and igneous origin. The approach used to this topic was to locate and study a prograde Lewisian transition zone of hornblende-granulite sub-facies. Since it has been suggested that the bulk chemistry of the Lewisian complex changes systematically from Scourie (where it is tonalitic) through Gruinard Bay (trondhjemitic) to Torridon (granodioritic; Rollinson, 1978; Rollinson and Fowler, in prep), some time was spent demonstrating the similarity of the Gruinard Bay gneisses in terms of magmagenesis and "immobile" element chemistry with

well-characterised representatives of the amphibolite- and granulite-facies end members. Thence the subsequent purely comparative approach was considered valid, especially when based upon tonalite with tonalite, trondhjemite with trondhjemite, etc.

Literature data have shown that the depletion processes are both "selective" and "differential" but the present study has demonstrated that they are also "progressive" in their operation. The transition takes place in a systematic way, strongly influenced by mineralogy, and is compatible with LILE removal in hydrous fluids generated by progressing dehydration reactions. Testing of the "intracrustal partial melting" model using a hornblende-bearing residuum suggested that it is inappropriate for the genesis of gneisses with the REE patterns documented from Gruinard Bay. Moreover, partition coefficient data for highly silicic melts also argue against the feasibility of granite extraction being the process responsible for radioelement removal on the scale seen in the Lewisian, even when the important minor minerals of the postulated residua are ignored in the calculations.

The significance of mineralogy has been emphasised in other studies of higher-grade metamorphic terrains (Winbrim et al., 1984; Iyer et al., 1982), which have shown that rocks which carry U- and Th-rich minerals that remained stable throughout are less severely depleted than those in which the radioelement-bearing phases became unstable. Indeed, this is applicable to deformation of the Glen Dessarry syenite where many "incompatible" elements remained "locked" in stable minor phases. However, other studies have shown that such strong mineralogical control may not be inviolate (e.g., Watson et al., 1982), especially if recrystallisation accompanies the high-grade event.

The varied responses of apparently similar lithologies to high-grade metamorphism might also suggest that mineralogical controls can be overridden. For example, there is no doubt that the Lewisian meta-igneous

granulitic gneisses are depleted in LILEs with respect to similar lower-grade rocks both from within the Lewisian Complex and elsewhere (e.g., Sheraton and Black, 1982), but low-pressure Polish granulites show no such extensive depletion (Tarney et al., 1977). Further, although Dostal and Capedri (1978), Dupey et al. (1979), Cuney (1981) and Barbey and Cuney (1982) all show that Th is not depleted from metasedimentary rocks and that U loss is variable, the study of Lewisian metasediments (Okeke et al., 1983) suggests that these have lost U and Th in a manner similar to that of their host orthogneisses. These inconsistencies perhaps signal an equal diversity in causative factors. Barbey and Cuney (1982) contend "that there is no metamorphic trend characteristic of granulite-facies terrains", and emphasise the importance of lithology and mineralogy of the protoliths in controlling the nature and extent of element depletion.

Sighnolfi (1971) pointed out the possibly interactive roles played by dehydration and partial melting, although this has been largely neglected recently in favour of simple reliance on one or the other. Many studies of metasedimentary rocks have shown the reality of melt-fluid interaction at high metamorphic grades (e.g., Phillips et al., 1980; Maccarrone et al., 1983), as have more-theoretical studies (Powell, 1983). Similarly, in meta-igneous terrains the amphibolite-granulite boundary is often marked by a complex interplay between partial melting and metasomatism (Friend, 1981; Janardhan et al., 1982), in which the elemental effects of the depletion processes are sometimes obscure (e.g., Allen et al., 1985). Much further work is required to elucidate precisely the relative contributions of both processes to element mobility. Ideally suited to such purposes are relict transitional regions where the processes have been arrested and preserved, as at Gruinard Bay. Also potentially instructive would be a close comparative study of why some granulites are severely depleted and

yet others are not - is there any fundamental relationship with the pressure-temperature regime, or is a vital ingredient missing, such as CO_2-fluxing from a subjacent mantle? In this way, detailed local investigations could be combined with careful regional comparisons to more-closely constrain the causes and mechanisms of the mobility of uranium and other lithophiles during high-grade metamorphism.

REFERENCES

ABBEY, S. 1980. Studies in "standard samples" for use in the general analysis of silicate rocks and minerals. Part 6. 1979 edition of "useable" values. Can. Geol. Surv. Prof. Pap. 80-14, pp1-30.

AHMAD, R. and WILSON, C.J.L. 1981. Uranium and boron distributions related to metamorphic microstructure - evidence for metamorphic fluid activity. Contrib. Mineral. Petrol. 76, 24-32.

ALDERTON, D.H.M., PEARCE, J.A. and POTTS, P.J. 1980. Rare earth element mobility during granite alteration: Evidence from southwest England. Earth Planet. Sci. Lett. 49, 149-165.

ALLEN, P., CONDIE, K.C. AND NARAYANA, B.L. 1985. The geochemistry of prograde and retrograde charnockite-gneiss reactions in southern India. Geochim. Cosmochim. Acta 49, 323-336.

AMIEL, A. 1962. Analytical applications of delayed neutron emission in fissionable elements. Analytical Chemistry 34, 1683-1692.

ANDERSEN, T. 1984. Crystallisation history of a Permian composite monzonite-alkali syenite pluton in the Sande Cauldron, Oslo rift, Southern Norway. Lithos 17, 153-170.

ANDERSON, J.L. 1980. Mineral equilibria and crystallisation conditions in the late Precambrian Wolf River rapakivi massif, Wisconsin. Am. J. Sci. 280, 289-332.

ARTH, J.G. and HANSON, G.N. 1975. Geochemistry and origin of early Precambrian crust of Northeastern Minnesota. Geochim. Cosmochim. Acta 39, 325-362.

ARTH, J.G., BARKER, F., PETERMAN, Z.E. and FRIEDMAN, I. 1978. Geochemistry of the gabbro-diorite-tonalite -trondhjemite suite of southwest Finland and its implications for the origin of tonalitic and trondhjemitic magmas. J. Petrol. 19, 289-316.

ATHERTON, M.P. and BROTHERTON, M.S. 1979. Thorium and uranium in some pelitic rocks from the Dalradian, Scotland. Chem. Geol. 27, 329-342.

BABCOCK, R.S. 1973. Computational models of metasomatic processes. Lithos 6, 279-290.

BAILLIEUL, T.A. and INDELICATO, G.J. 1981. Uranium in the New Jersey and New York Highlands of the Reading Prong. Econ. Geol. 76, 167-171.

BAMFORD, D., NUNN, K., PRODEHL, C. and JACOB, B. 1977. LISPB-III. Upper crustal structure of Northern Britain. J. Geol. Soc. London 133, 481-488.

BARBEY, P. and CUNEY, M. 1982. K, Rb, Sr, Ba, U and Th geochemistry of the Lapland granulites (Fennoscandia). LILE* fractionation controlling factors. Contrib. Mineral. Petrol. 81, 304-316.

BARNICOAT, A.C. 1983. Metamorphism of the Scourian complex, NW Scotland. J. metamorphic Geol. 1, 163-182.

BEACH, A. 1976. The interrelations of fluid transport, deformation, geochemistry and heat flow in early Proterozoic shear zones in the Lewisian complex. Phil. Trans. R. Soc. Lond. A280, 569-604.

BEACH, A. and TARNEY, J. 1978. Major and trace element patterns established during retrogressive metamorphism of granulite-facies gneisses, NW Scotland. Precambrian Res. 7, 325-348.

BENDER, J.F., HANSON, G.N. and BENCE, A.E. 1984. Cortlandt Complex: differentiation and contamination in plutons of alkali basalt affinity. Am. J. Sci. 284, 1-57.

BEN OTHMAN, D., POLVE, M. and ALLEGRE, C.J. 1984. Nd-Sr istopic composition of granulites and constraints on the evolution of the lower continental crust. Nature 307, 510-515.

BESWICK, A.E. 1973. An experimental study of alkali metal distributions in feldspars and micas. Geochim. Cosmochim. Acta 37, 183-208.

BICKLE, M.J., BETTENAY, L.F., BARLEY, M.E., CHAPMAN, H.J., GROVES, D.I., CAMPBELL, I.H. and De LAETER, J.R. 1983. A 3500 Ma plutonic and volcanic calc-alkaline province in the Archaean East Pilbara Block. Contrib. Mineral. Petrol. 84, 25-35.

BINNS, R.A. 1969. Ferromagnesian minerals in high-grade metamorphic rocks. Geol. Soc. Austr. Spec. Publs. 2, 323-332.

BIRCH, F., ROY, R.F. and DECKER, E.R. 1968. Heatflow and thermal history in New England and New York. In: Studies of Appalachian Geology. E. An-Zen (ed.) Interscience, New York, pp 437-451.

BLATTNER, P. and BLACK, P.M. 1980. Apatite and scapolite as petrogenetic indicators in granolites of Milford Sound, New Zealand. Contrib. Mineral. Petrol. 74, 339-348.

BLAXLAND, A.B., AFTALION, M. and VAN BREEMEN, O. 1979. Pb isotopic composition of feldspars from Scottish Caledonian granites, and the nature of the underlying crust. Scott. J. Geol. 15, 139-151.

BOWIE, S.H.U., SIMPSON, P.R. and RICE, C.M. 1973. Application of fission-track and neutron activation methods to geochemical exploration. In: Geochemical Exploration 1972 (proc. 4th Int. geochem. exploration symp., London, 1972). M.J. Jones (ed.), Instn. Min. Metal., London, pp 359-372.

BOWDEN, P. 1966. Zirconium in younger granites of northern Nigeria. Geochim. Cosmochim. Acta 30, 985-993.

BRITISH GEOLOGICAL SURVEY. In press. Geochemical Atlas of Great Britain: Great Glen. Brit. Geol. Surv., Keyworth.

BROGGER, W.C. 1921. Die eruptivgesteine des kristianiagebietes, IV: Das fengebiet in Telemark. Nor. Vidensk. Skr. I, Mat. Naturv. Kl. 9, 1-408

BROWN, G.C., THORPE, R.S. and WEBB, P.C. 1984. The geochemical characteristics of granitoids in contrasting arcs and comments on magma sources. J. Geol. Soc. London 141, 413-426.

BUNTEBARTH, G. 1976. Distribution of uranium in intrusive bodies due to combined migration and diffusion. Earth Planet. Sci. Lett. 32, 84-90.

BURNETT, D.S. and WOOLUM, D.S. 1983. In situ trace element microanalysis. Ann. Rev. Earth Planet. Sci. 11, 329-358.

CHIVAS, A.R., ANDREW, A.S., SINHA, A.K. and O'NEIL, J.R. 1982. Geochemistry of a Plio-Pleistocene oceanic-arc plutonic complex, Guadalcanal. Nature 300, 139-143.

CLAYBURN, J.A.P., HARMON, R.S., PANKHURST, R.J. and BROWN, J.F. 1983. Sr, O, and Pb isotope evidence for origin and evolution of Etive Igneous Complex, Scotland. Nature 303, 492-497.

CLAYTON, R.N. and MAYEDA, T.K. 1963. The use of bromine pentafluoride in the extraction of oxygen from oxides and silicates for isotopic analysis. Geochim. Cosmochim. Acta 27, 43-52.

COLEMAN, M., COX, M. and TAYLOR, R. 1982. Isotopic evidence for the extent of fluid involvement in metasomatism of the St. Lawrence Granite. Internal Report, Isotope Geology Unit, British Geological Survey.

COLLERSON, K.D. and FRYER, B.J. 1978. The role of fluids in the formation and subsequent development of early continental crust. Contrib. Mineral. Petrol. 67, 151-167.

CONDIE, K.C. 1976. Trace element geochemistry of Archaean greenstone belts. Earth Sci. Rev. 12, 393-417.

CONDIE, K.C., ALLEN, P. and NARAYANA, B.L. 1982. Geochemistry of the Archaean low- to high-grade transition zone, southern India. Contrib. Mineral. Petrol. 81, 157-167.

COOLEN, J.J.M.M.M., 1982. Carbonic fluid inclusions in granulites from Tanzania - A comparison of geobarometric methods based on fluid density and mineral chemistry. In: Current Research on Fluid Inclusions. R. Kreulen and J. Touret (eds.) Chem. Geol. 37, 59-77.

CRESSWELL, D. and PARK, R.G., 1973. The metamorphic history of the Lewisian rocks of the Torridon area in relation to that of the remainder of the southern Laxfordian belt. In: The Early Precambrian of Scotland and Related Rocks of Greenland. R.G. Park and J. Tarney (eds.) University of Keele. pp 77-83.

CULLERS, R.L., MEDARIS, L.G. and HASKIN, L.A., 1973. Experimental studies of the distribution of rare earths as trace elements among silicate minerals and liquids and water. Geochim. Cosmochim. Acta 37, 1499-1512.

CURTIS, C.D. and BROWN, P.E. 1969. The metasomatic development of zoned ultrabasic bodies in Unst, Shetland. Contrib. Mineral. Petrol. 24, 275-292.

CURTIS, C.D. and BROWN, P.E. 1971. Trace element behaviour in the zoned metasomatic bodies of Unst, Shetland. Contrib. Mineral. Petrol. 31, 87-93.

DAVIES, F.B. 1977. The Archaean evolution of the Lewisian Complex of Gruinard Bay. Scott. J. Geol. 13, 189-196.

DEARNLEY, R. 1962. An outline of the Lewisian Complex of the Outer Hebrides in relation to that of the Scottish mainland. Q. J. Geol. Soc. London 118, 143-176.

DE WAARD, D. 1966. The biotite-cordierite-almandine subfacies of the hornblende-granulite facies. Can. Mineral. 8, 481-494.

DOSTAL, J. and CAPEDRI, S. 1978. Uranium in metamorphic rocks. Contrib. Mineral. Petrol. 66, 409-414.

DRAKE, M.J. and WEILL, D.F. 1975. Partition of Sr, Ba, Ca, Y, Eu^{2+}, Eu^{3+} and other REE between plagioclase feldspar and magmatic liquid: an experimental study. Geochim. Cosmochim. Acta 39, 689-712.

DRURY, S.A. 1972. The chemistry of some granitic veins from the Lewisian of Coll and Tiree, Argyllshire, Scotland. Chem. Geol. 9, 175-193.

DRURY, S.A. 1973. The geochemistry of Precambrian granulite facies rocks from the Lewisian Complex of Tiree, Inner Hebrides, Scotland. Chem. Geol. 11, 167-188.

DRURY, S.A. 1974. Chemical changes during retrogressive metamorphism of Lewisian granulite facies rocks from Coll and Tiree. Scott. J. Geol. 10, 237-256.

DRURY, S.A. 1978. REE distributions in a high-grade Archaean gneiss complex in Scotland: implications for the genesis of ancient sialic crust. Precambrian Res. 7, 237-257.

DRURY, S.A. 1980. Lewisian pyroxene gneisses from Barra and the geochemistry of the Archaean lower crust. Scott. J. Geol. 16, 199-207.

DUDAS, M.J., SCHMITT, R.A. and HARWARD, M.E. 1971. Trace element partitioning between volcanic plagioclase and dacitic pyroclastic matrix. Earth Planet. Sci. Lett. 11, 440-446.

DUPUY, C., LEYRELOUP, A. and VERNIERES, J. 1979. The lower continental crust of the Massif Central (Bournac, France) - with special references to REE, U and Th composition, evolution, heat flow production. In: Origin and Distribution of the Elements. Pergammon, New York. pp 401-415.

FETTES, D.J. 1979. A metamorphic map of the British and Irish Caledonides. In: The Caledonides of the British Isles - Reviewed. A.L. Harris, C.H. Holland and B.E.Leake (eds.). Spec. Publ. Geol. Soc. London 8, pp 307-321.

FIELD, D. 1978. Granulites at Gruinard Bay. Scott. J. Geol. 14, 359-361.

FLYNN, R.T. and BURNHAM, C.W. 1978. An experimental determination of rare earth partition coefficients between a chloride containing vapor phase and silicate melts. Geochim. Cosmochim. Acta 42, 685-701.

FOLAND, K.A. and FRIEDMAN, I. 1977. Application of Sr and O isotope relations to the petrogenesis of the alkaline rocks of the Red Hill Complex, New Hampshire, USA. Contrib. Mineral. Petrol. 65, 213-225.

FOUNTAIN, D.M. and SALISBURY, M.H. 1981. Exposed cross-sections through the continental crust: implications for crustal structure, petrology and evolution. Earth Planet. Sci. Lett. 56, 263-277.

FOUNTAIN, J.C. and HODGE, D.S. 1981. Incorporation of U and Th into a monzonite pluton, Laramie Range, Wyoming. Econ. Geol. 76, 2253-2256.

FOWLER, M.B. 1981. Uranium content, distribution and migration in the Glendessarry syenite, Inverness-shire. Mineral. Mag. 44, 443-448.

FOWLER, M.B., WILLIAMS, H.R. and WINDLEY, B.F. 1981. The metasomatic development of zoned ultramafic balls from Fiskenaesset, West Greenland. Mineral. Mag. 44, 171-177.

FOWLER, M.B., WILLIAMS, C.T. and HENDERSON, P. 1983. Rare earth element distribution in a metasomatic zoned ultramafic pod from Fiskenaesset, West Greenland. Mineral. Mag. 47, 547-553.

FRIEND, C.R.L. 1981. Charnockite and granite formation and influx of CO_2 at Kabbaldurga. Nature 294, 550-552.

GARSON, M.S., COATS, J.S., ROCK, N.M.S. and DEANS, T. 1984. Fenites, breccia dykes, albitites and carbonatitic veins near the Great Glen Fault, Inverness, Scotland. J. Geol. Soc. London 141, 711-732.

GEOLOGICAL SURVEY OF GREAT BRITAIN. 1957-1962. Summ. Progr. geol. Surv. U.K.

GLASSLEY, W.E. 1983. Deep crustal carbonates as CO_2 fluid sources: evidence from metasomatic reaction zones. Contrib. Mineral. Petrol. 84, 15-24.

GREEN, T.H. and PEARSON, N.J. 1983. Effect of pressure on rare earth element partition coefficients in common magmas. Nature 305, 414-416.

GREEN, D.H. and RINGWOOD, A.E. 1967. An experimental investigation of the gabbro to eclogite transformation and its petrological applications. Geochim. Cosmochim. Acta 31, 767-833.

GRESENS, R.L. 1967. Composition - volume relationships of metasomatism. Chem. Geol. 2, 47-65.

GROMET, L.P. and SILVER, L.T. 1983. Rare earth element distributions among minerals in a granodiorite and their petrogenetic implications. Geochim. Cosmochim. Acta 47, 925-939.

HALLIDAY, A.N. 1984. Coupled Sm-Nd and U-Pb systematics in late Caledonian granites and the basement under northern Britain. Nature 307, 229-233.

HAMILTON, P.J., EVENSEN, N.M., O'NIONS, R.K. and TARNEY, J. 1979. Sm-Nd systematics of Lewisian gneisses: implications for the origin of granulites. Nature 277, 25-28.

HAMILTON, P.J., O'NIONS, R.K. and PANKHURST, R.J. 1980. Isotopic evidence for the provenance of some Caledonian granites. Nature 287, 279-284.

HARRIS, N.B.W., DUYVERMAN, H.J. and ALMOND, D.C. 1983. The trace element and isotope geochemistry of the Sabaloka igneous complex, Sudan. J. Geol. Soc. London 140, 245-256.

HARRISON, T.M. and WATSON, E.B. 1984. The behaviour of apatite during crustal anatexis: equilibrium and kinetic considerations. Geochim. Cosmochim. Acta 48, 1467-1477.

HARRY, W.T. 1951. The migmatites and felspar-porphyroblast rock of Glen Dessary, Inverness-shire. Q. J. Geol. Soc. London 107, 137-158.

HARRY, W.T. 1952. The Glen Dessary marble and its associated calc-silicate rocks. Q. J. Geol. Soc. London 88, 393-403.

HAWKESWORTH, C.J. and MORRISON, M.A. 1978. A reduction in $^{87}Sr/^{86}Sr$ during basalt alteration. Nature 276, 381-383.

HELZ, R.T. 1976. Phase relations of basalts in their melting ranges at PH_2O= 5kb. Part II. Melt compositions. J. Petrol. 17, 139-193.

HENDERSON, P. 1982. Inorganic Geochemistry. Pergamon, Oxford. 353 pp.

HIGUCHI, H. and NAGASAWA, H. 1969. Partition of trace elements between rock-forming minerals and the host volcanic rocks. Earth Planet. Sci. Lett. 7, 281-287.

HINTON, R.W. and LONG, J.V.P. 1979. High-resolution ion-microprobe measurement of lead isotopes: variations within single zircons from Lac Seul, northwestern Ontario. Earth Planet. Sci. Lett. 45, 309-325.

HOEFS, J. and TOURET, J. 1975. Fluid inclusion and carbon isotope study from Bamble granulites (south Norway). A preliminary investigation. Contrib. Mineral. Petrol. 52, 165-174.

HOLDAWAY, M.J. 1971. Stability of andalusite and the aluminium silicate phase diagram. Am. J. Sci. 271, 97-131.

HOLLAND, J.G. and LAMBERT, R.St.J. 1973. Comparative major element geochemistry of the Lewisian of the mainland of Scotland. In: The Early Precambrian of Scotland and Related Rocks of Greenland. R.G. Park and J. Tarney (eds.) University of Keele. pp 51-62.

HOLLAND, J.G. and LAMBERT, R.St.J. 1975. The chemistry and origin of the Lewisian gneisses of the Scotish mainland: the Scourie and Inver assemblages and sub-crustal accretion. Precambrian Res. 2, 161-174.

HOLLOWAY, J.R. and BURNHAM, C.W. 1972. Melting relations of basalt with equilibrium water pressure less than total pressure. J. Petrol. 13, 1-29.

HOLT, R.W. and WIGHTMAN, R.T. 1983. The role of fluids in the development of a granulite facies transition zone in S India. J. Geol. Soc. London 140, 651-656.

HUANG, W.L. and WYLLIE, P.J. 1975. Melting reactions in the system $NaAlSi_3O_8$ - $KAlSi_3O_8$ - SiO_2 to 35 kilobars, dry and with excess water. J. Geol. 83, 737-748.

HUMPHRIS, S.E., MORRISON, M.A. and THOMPSON, R.N. 1978. Influence of rock crystallisation history on subsequent lanthanide mobility during hydrothermal alteration of basalts. Chem. Geol. 23, 125-137.

INSTITUTE OF GEOLOGICAL SCIENCES. 1979. Geochemical Atlas of Great Britain: Caithness and South Orkney. Inst. Geol. Sci., London.

INSTITUTE OF GEOLOGICAL SCIENCES. 1982. Geochemical Atlas of Great Britain: Sutherland. Inst. Geol. Sci., London.

INSTITUTE OF GEOLOGICAL SCIENCES. 1984. Geochemical Atlas of Great Britain: Hebrides. Inst. Geol. Sci., London.

IYER, S.S., CHOUDHURI, A., VASCONCELLOS, M.B.A. and CORDANI, U.G. 1984. Radioactive element distribution in the Archaean granulites of Jequie - Bahia, Brazil. Contrib. Mineral. Petrol. 85, 95-101.

JAHN, B. and ZHANG, Z. 1984. Archaean granulite gneisses from eastern Hebei Province, China: rare earth geochemistry and tectonic implications. Contrib. Mineral. Petrol. 85, 224-243.

JAHN, B.M., GLIKSON, A.Y., DEUCAT, J.J. and HICKMAN, A.H. 1981. REE geochemistry and isotopic data of Archaean silicic volcanics and granitoids from the Pilbara Block, Western Australia: implications for the early crustal evolution. Geochim. Cosmochim. Acta 45, 1633-1652.

JAHN, B., VIDAL, P. and KRONER, A. 1984. Multi-chronometric ages and origin of Archaean tonalitic gneisses in Finnish Lapland: a case for long crustal residence time. Contrib. Mineral. Petrol. 86, 398-408.

JANARDHAN, A.S., NEWTON, R.C. and HANSEN, E.C. 1982. The transformation of amphibolite facies gneiss to charnockite in southern Karnataka and northern Tamil Nadu, India. Contrib. Mineral. Petrol. 79, 130-149.

JAUPART, C., SCLATER, J.G. and SIMMONS, G. 1981. Heat flow studies: constraints on the distribution of uranium, thorium and potassium in the continental crust. Earth Planet. Sci. Lett. 52, 328-344.

JAUPART, C., MANN, J.R. and SIMMONS, G. 1982. A detailed study of the distribution of heat flow and radioactivity in New Hampshire (USA). Earth Planet. Sci. Lett. 59, 267-287.

JONES, A.P. 1984. Mafic silicates from the nepheline syenites of the Motzfeldt centre, south Greenland. Mineral. Mag. 48, 1-12.

KERRICH, R., ALLISON, I., BARNETT, R.L., MOSS,, S. and STARKEY, J. 1980. Microstructural and chemical transformations accompanying deformation of granite in a shear zone at Mieville, Switzerland, with implications for stress corrosion cracking and superplastic flow. Contrib. Mineral. Petrol. 73, 221-242.

KERRICH, R., FYFE, W.S., GORMAN, B.E. and ALLISON, I. 1977. Local modification of rock chemistry by deformation. Contrib. Mineral. Petrol. 65, 183-190.

KITCHEN, D. 1984. Pyrometamorphism and contamination of basaltic magma at Tieveragh, Co. Antrim. J. Geol. Soc. London 41, 733-745.

KOONS, P.O. 1981. A study of natural and experimental metasomatic assemblages in an ultramafic-quartzofeldspathic metasomatic system from the Haast schist, south Island, New Zealand. Contrib. Mineral. Petrol. 78 , 189-195.

KUNO, H. 1938. On the occurrence of a primary cummingtonitic hornblende in some dacites from Japan. Proc. Japan Acad. 14, 221-224.

KYSER, T.K., O'NEIL, J.R. and CARMICHAEL, I.S.E. 1982. Genetic relations among basic lavas and ultramafic nodules: evidence from oxygen isotope compositions. Contrib. Mineral. Petrol. 81, 88-102.

LACHENBRUCH, A.H. 1968. Preliminary geothermal model of the Sierra Nevada. J. Geophys. Res. 73, 6977-6990.

LAMBERT, I.B. and HEIER, K.S. 1967. The vertical distribution of uranium, thorium and potassium in the continental crust. Geochim. Cosmochim. Acta 31, 377-390.

LAMBERT, R.St.J, POOLE, A.B., RICHARDSON, S.W., JOHNSTONE, G.S. and SMITH, D.I. 1964. The Glen Dessary syenite, Inverness-shire. Nature 202, 370-372.

LARSEN, M.L. 1976. Clinopyroxenes and coexisting mafic minerals from the alkaline Ilimaussaq intrusion, South Greenland. J. Petrol. 17, 258-290

LEAKE, B.E. 1978. Nomenclature of amphiboles. Canadian Mineral. 16, 501-520.

LEELANANDUM, C. 1970. Chemical mineralogy of hornblendes and biotites from the charnockitic rocks of Kondapalli, India. J. Petrol. 11, 475-505.

LE MAITRE, R.W. 1979. A new generalised petrological mixing model. Contrib. Mineral. Petrol. 71, 133-137.

LE MAITRE, R.W. 1981. GENMIX - a generalised petrological mixing model program. Comput. Geosci. 7, 229-247.

LOWMAN, P.D. 1984. Formation of the earliest continental crust: inferences from the Scourian Complex of northwest Scotland and geophysical models of the lower continental crust. Precambrian Res. 24, 199-215.

LYON, T.D.B., PIDGEON, R.T., BOWES, D.R. and HOPGOOD, A.M. 1973. Geochronological investigation of the quartzofeldspathic rocks of the Lewisian of Rona, Inner Hebrides. J. Geol. Soc. London 129, 389-404.

MACCARRONE, E., PAGLIONICO, A., PICCARRETA, G. and ROTTURA, A. 1983. Granulite-amphibolite facies metasediments from the Serre (Calabria, southern Italy): their protoliths and the processes controlling their chemistry. Lithos 16, 95-111.

MACDONALD, R., UPTON, B.G.J. and THOMAS, J.E. 1973. Potassium- and fluorine-rich hydrous phase coexisting with peralkaline granite in South Greenland. Earth Planet. Sci. Lett. 18, 217-222.

MACDOUGALL, J.D., FINKEL, R.C., CARLSON, J and KRISHNASWAMI, S. 1979. Isotopic evidence for uranium exchange during low temperature alteration of oceanic basalts. Earth Planet. Sci. Lett. 42, 27-34.

MAHOOD, G. and HILDRETH, W. 1983. Large partition coefficients for trace elements in high-silica rhyolites. Geochim. Cosmochim. Acta 47, 11-30.

MARTIN, R.F., WHITLEY, J.E. and WOOLLEY, A.R. 1978. An investigation of rare-earth mobility: fenitized quartzites, Borralan complex, NW Scotland. Contrib. Mineral. Petrol. 66, 69-73.

MATSUHISA, Y. 1979. Oxygen isotopic compositions of volcanic rocks from the east Japan island arcs and their bearing on petrogenesis. J. Volcan. Geotherm. Res. 5, 271-296.

McCARTHY, T.S. and GROVES, D.I. 1979. The Blue Tier batholith, northeastern Tasmania. A cumulate-like product of fractional crystallisation. Contrib. Mineral. Petrol. 71, 193-209.

McCARTHY, T.S. and HASTY, R.A. 1976. Trace element distribution patterns and their relationship to the crystallisation of granitic melts. Geochim. Cosmochim. Acta 40, 1351-1358.

McKIE, D. 1966. Fenitisation. In: Carbonatites. O.F. Tuttle and J. Gittins (eds.) Wiley, New York. pp 261-294.

METSON, J.B., BANCROFT, G.M., NESBITT, N.W. and JOHASSON, R.G. 1984. Analysis for rare earth elements in accessory minerals by specimen isolated secondary ion mass spectrometry. Nature 307, 347-349.

MICHAEL, P.J. 1983. Chemical differentiation of the Bishop Tuff and other high-silica magmas through crystallisation processes. Geology 1, 31-34.

MICHAEL, P.J. 1984. Chemical differentiation of the Cordillera Paine granite (southern Chile) by in situ fractional crystallisation. Contrib. Mineral. Petrol. 87, 179-195.

MILLER, C.F. 1977. Early alkalic plutonism in the calc-alkalic batholithic belt of California. Geology 5, 685-688.

MILLER, C.F. 1978. Monzonitic plutons, California, and a model for generation of alkali-rich, near silica-saturated magmas. Contrib. Mineral. Petrol. 67, 349-355.

MILLER, C.F. and MITTLEFEHLDT, D.W. 1984. Extreme fractionation in felsic magma chambers: a product of liquid-state diffusion or fractional crystallisation? Earth Planet. Sci. Lett. 68, 151-158.

MITCHELL, R.H. and PLATT, R.G. 1978. Mafic mineralogy of ferroaugite syenite from the Coldwell alkaline complex, Ontario, Canada. J. Petrol. 19, 627-651.

MITCHELL, W.S and AUMENTO, F. 1977. Uranium in oceanic rocks: DSDP Leg 37. Can. J. Earth Sci. 14, 794-808.

MITTLEFEHLDT, D.W. and MILLER, C.F. 1983. Geochemistry of the Sweetwater Wash pluton, California. Implications for anomalous trace element behaviour during differentiation of felsic magmas. Geochim. Cosmochim. Acta 47, 109-124.

MOORBATH, S. and PARK, R.G. 1972. The Lewisian chronology of the southern region of the Scottish mainland. Scott. J. Geol. 8, 51-74.

MOORBATH, S., WELKE, H. and GALE, N.H. 1969. The significance of lead isotope studies in ancient, high-grade metamorphic basement complexes, as exemplified by the Lewisian rocks of NW Scotland. Earth Planet. Sci. Lett. 6, 245-256.

NAGASAWA, H. and WAKITA, H. 1968. Partition of uranium and thorium between augite and host lavas. Geochim. Cosmochim. Acta 32, 917-921.

NAKAMURA, N. 1974. Determination of REE, Ba, Fe, Mg, Na and K in carbonaceous and ordinary chondrites. Geochim. Cosmochim. Acta 38, 757-775.

NEWTON, R.C., SMITH, J.V. and WINDLEY, B.F. 1980. Carbonic metamorphism, granulites and crustal growth. Nature 288, 45-50.

NOCKOLDS, S.R. 1941. The Garabal Hill - Glen Fyne igneous complex. Q. J. Geol. Soc. London 96, 451-511.

O'CONNOR, J.T. 1965. A classification of quartz-rich igneous rocks based on feldspar ratio. U.S. Geol. Surv. Prof. Pap. 525B, 79-84.

O'HARA, M.J. and YARWOOD, G. 1978. High pressure - temperature point on an Archaean geotherm, implied magma genesis by crustal anatexis and consequences for garnet - pyroxene thermometry and barometry. Phil. Trans. R. Soc. Lond. A288, 441-456.

OKEKE, P.O., BORLEY, G.D. and WATSON, J.V. 1983. A geochemical study of Lewisian metasedimentary granulites and gneisses in the Scourie-Laxford area of NW Scotland. Mineral. Mag. 47, 1-9.

O'NIONS, R.K., CARTER, S.R., COHEN, R.S., EVENSON, N.M. and HAMILTON, P.J. 1978. Pb, Nd and Sr isotopes in oceanic ferromagnesian deposits and ocean floor basalts. Nature 273, 435-437.

OTTEN, M.T. 1984. The origin of brown hornblende in the Artfjallet gabbro and dolerites. Contrib. Mineral. Petrol. 86, 189-199.

PANKHURST, R.J. 1979. Isotope and trace element evidence for the origin and evolution of Caledonian granites in the Scottish Highlands. In: Origin of Granite Batholiths: Geochemical Evidence. M.P. Atherton and J. Tarney (eds.) Shiva, Orpington. pp 18-33.

PARK, R.G. 1970. Observations on Lewisian chronology. Scott. J. Geol. 6, 379-399.

PARKER, R.J. 1982. Single pass major element X-ray fluorescence analysis of silicate rock samples using a Philips 1212 spectrometer. X-ray Spectrometry 11, 100-108.

PARSONS, I. 1965. The feldspathic syenites of the Loch Ailsh intrusion, Assynt, Scotland. J. Petrol. 6, 365-394.

PARSONS, I. 1979. The Assynt alkaline suite. In: The Caledonides of the British Isles - reviewed. A.L. Harris, C.H. Holland and B.E. Leake (eds.) Spec. Pub. Geol. Soc. London 8. pp 677-681.

PARSONS, I. 1981. The Klokken gabbro-syenite complex, south Greenland: quantitative interpretation of mineral chemistry. J. Petrol. 22, 233-260.

PEACH, B.N., HORNE, J., GUNN, W., CLOUGH, C.T., HINXMAN, L.W. and TEALL, J.J.H. 1907. The geological structure of the NW Highlands of Scotland. Mem. Geol. Surv. Gt. Britain. 668 pp.

PETO, P. and HAMILTON, D.L. 1976. Partial fusion of basalts and andesites under vapour excess and vapour deficient conditions at 10kb total pressure. In: Progress in Experimental Petrology. Natural Environment Research Council. pp 45-50.

PHILLIPS, G.N. 1980. Water activity changes across an amphibolite-granulite facies transition, Broken Hill, Australia. Contrib. Mineral. Petrol. 75, 377-386.

PIDGEON, R.T. and AFTALION, M. 1972. The geochronological significance of discordant U-Pb ages of oval-shaped zircons from a Lewisian gneiss from Harris, Outer Hebrides. Earth Planet. Sci. Lett. 17, 269-274.

PIDGEON, R.T. and BOWES, D.R. 1972. Zircon U-Pb ages of granulites from the Central Region of the Lewisian, northwestern Scotland. Geol. Mag. 109, 247-248.

PLANT, J.A., BROWN, G.C., SIMPSON, P.R. and SMITH, R.T. 1980. Signatures of metalliferous granites in the Scottish Caledonides. Trans. Instn. Min. Metal. (Sect B: Appl. earth Sci.) 89, B198-B210.

PLANT, J.A., GOODE, G.C. and HERRINGTON, J. 1976. An instrumental neutron activation method for multi-element geochemical mapping. J. Geochem. Explor. 6, 299-319.

PLANT, J.A., SIMPSON, P.R., GREEN, P.M., WATSON, J.V. and FOWLER, M.B. 1983. Metalliferous and mineralised Caledonian granites in relation to regional metamorphism and fracture systems in Northern Scotland. Trans. Instn. Min. Metal. (Sect B: Appl. earth Sci.) 92, B33-B42.

PLANT, J.A., SMITH, R.T., STEVENSON, A.G., FORREST, M.D. and HODGSON, J.F. 1984. Regional geochemical mapping for mineral exploration in northern Scotland. In: Prospecting in Areas of Glaciated Terrain. Instn. Min. Metal. London. pp 103-120.

POLLACK, H.N. 1982. The heat flow from the continents. Ann. Rev. Earth Planet. Sci. 10, 459-481.

POWELL, M. 1978. The crystallisation history of the Igdlerfigssalik nepheline syenite intrusion, Greenland. Lithos 11, 99-120.

POWELL, R. 1983. Fluids and melting under upper amphibolite facies conditions. J. Geol. Soc. London 140, 629-633.

PRIDE, C. and MUECKE, G.K. 1980. Rare earth element geochemistry of the Scourian complex NW Scotland - evidence for the granite-granulite link. Contrib. Mineral. Petrol. 73, 403-412.

PRIDE, C. and MUECKE, G.K. 1981. Rare earth element distributions among co-existing granulite facies minerals, Scourian complex, NW Scotland. Contrib. Mineral. Petrol. 76, 463-471.

PRIDE, C. and MUECKE, G.K. 1982. Geochemistry and origin of granitic rocks, Scourian complex, NW Scotland. Contrib. Mineral. Petrol. 80, 379-385.

RAASE, P 1974. Al and Ti contents of hornblende, indicators of pressure and temperature of regional metamorphism. Contrib. Mineral. Petrol. 45, 231-236.

READ, H.H. 1934. On zoned associations of antigorite, talc, actinolite, chlorite and biotite in Unst, Shetland Islands. Mineral. Mag. 23, 519-540.

RIBBE, P.H. 1980. Titanite. In: Reviews in Mineralogy, vol. 5. Orthosilicates. P.H. Ribbe (ed.) Mineral. Soc. Amer., Michigan. pp 137-154.

RICHARDSON, S.W. 1968. The petrology of the metamorphosed syenite in Glen Dessarry, Inverness-shire. Q. J. Geol. Soc. London 124, 9-51.

ROBERTS, A.M., SMITH, D.I. and HARRIS, A.L. 1984. The structural setting and tectonic significance of the Glen Dessary syenite, Inverness-shire. J. Geol. Soc. London 141, 1033-1042.

ROBERTSON, R.C.R. and PARSONS, I. 1974. The Loch Loyal syenites. Scott. J. Geol. 10, 129-146.

ROCK, N.M.S. 1982. Chemical mineralogy of the Monchique alkaline complex, southern Portugal. Contrib. Mineral. Petrol. 81, 64-78.

ROCK, N.M.S. 1976. Fenitisation around the Monchique alkaline complex, Portugal. Lithos 9, 263-279.

ROLLINSON, H.R. 1978. Geochemical studies on the Scourian complex, NW Scotland. Unpubl. PhD thesis, University of Leicester.

ROLLINSON, H.R. 1979. Ilmenite-magnetite geothermometry in trondhjemites from the Scourian complex of NW Scotland. Mineral. Mag. 43, 165-170.

ROLLINSON, H.R. 1980. Iron-titanium oxides as an indicator of the role of the fluid phase during the cooling of granites metamorphosed to granulite grade. Mineral. Mag. 43, 623-631.

ROLLINSON, H.R. 1981. Garnet-pyroxene thermometry and barometry in the Scourie granulites, NW Scotland. Lithos 14, 225-238.

ROLLINSON, H.R. 1982. Evidence from feldspar compositions of high temperatures in granite sheets in the Scourian complex, NW Scotland. Mineral. Mag. 46, 73-76.

ROLLINSON. H.R. and FOWLER, M.B. In prep. The geochemistry and origin of Archaean trondhjemites from the Lewisian complex, Gruinard Bay, NW Scotland.

ROLLINSON, H.R. and WINDLEY, B.F. 1980. Selective elemental depletion during metamorphism of Archaean granulites, Scourie, NW Scotland. Contrib. Mineral. Petrol. 72, 257-263.

ROLLINSON, H.R. and WINDLEY, B.F. 1980. An Archaean granulite-grade tonalite-trondhjemite-granite suite from Scourie, NW Scotland: geochemistry and origin. Contrib. Mineral. Petrol. 72, 265-281.

RUBIE, D.C. 1982. Mass transfer and volume change during alkali metasomatism at Kisingiri, western Kenya. Lithos 15, 99-109.

SANFORD, R.F. 1982. Growth of ultramafic reaction zones in greenschist to amphibolite facies metamorphism. Am. J. Sci. 282, 543-616.

SAUNDERS, A.D., TARNEY, J. and WEAVER, S.D. 1980. Transverse geochemical variations across the Antarctic Peninsula: implications for the genesis of calc-alkaline magmas. Earth Planet. Sci. Lett. 46, 344-366.

SAWKA, W.N., CHAPPELL, B.W. and NORRISH, K. 1984. Light-rare-earth-element zoning in sphene and allanite during granitoid fractionation. Geology 12, 131-134.

SENIOR, A. and LEAKE, B.E. 1980. Regional metasomatism and the geochemistry of the Dalradian metasediments of Connemara, western Ireland. J. Petrol. 19, 585-625.

SHERATON, J.W. 1970. The origin of the Lewisian gneisses of NW Scotland, with particular reference to the Drumbeg area, Sutherland. Earth Planet. Sci. Lett. 8, 301-310.

SHERATON, J.W. and BLACK, L.P. 1983. Geochemistry of Precambrian gneisses: relevance for the evolution of the East Antarctic shield. Lithos 16, 273-296.

SHERATON, J.W. and COLLERSON, K.D. 1984. Geochemical evolution of Archaean granulite-facies gneisses in the Vestfold Block and comparisons with other Archaean gneiss complexes in the East Antarctic shield. Contrib. Mineral. Petrol. 87, 51-64.

SHERATON, J.W., SKINNER, A.C. and TARNEY, J. 1973. The geochemistry of the Scourian gneisses of the Assynt district. In: The Early Precambrian of Scotland and Related Rocks of Greenland. R.G. Park and J. Tarney (eds.) University of Keele. pp 13-30.

SIGHINOLFI, G.P. 1971. Investigations into deep crustal levels: fractionating effects and geochemical trends related to high-grade metamorphism. Geochim. Cosmochim. Acta 35, 1005-1021.

SILLS, J.D. 1983. Mineralogical changes occurring during the retrogression of Archaean gneisses from the Lewisian Complex of NW Scotland. Lithos 16, 113-124.

SILLS, J.D., SAVAGE, D., WATSON, J.V. and WINDLEY, B.F. 1982. Layered ultramafic-gabbro bodies in the Lewisian of NW Scotland: geochemistry and petrogenesis. Earth Planet. Sci. Lett. 58, 345-360.

SIMMONS, E.C. and HEDGE, C.E. 1978. Minor-element and Sr-isotope geochemistry of Tertiary stocks, Colorado mineral belt. Contrib. Mineral. Petrol. 67, 379-396.

SIMPSON, P.R., BROWN, G.C., PLANT, J.A. and OSTLE, D. 1979. Uranium mineralisation and granite magmatism in the British Isles. Phil. Trans. R. Soc. Lond. A291, 385-412.

SIMPSON, P.R., PLANT, J.A., WATSON, J.V., GREEN, P.M. and FOWLER, M.B. 1982. The role of metalliferous and mineralised uranium granites in the formation of uranium provinces. In: Uranium exploration methods. IAEA/NEA, Paris. pp 157-170.

SISSON, V.B., CRAWFORD, M.L. and THOMPSON, P.H. 1981. CO_2-brine immiscibility at high temperatures, evidence from calcareous metasedimentary rocks. Contrib. Mineral. Petrol. 78, 371-378.

SMALLEY, P.C., FIELD, D., LAMB, R.C. and CLOUGH, P.W.L. 1983. Rare earth, Th-Hf-Ta and large ion lithophile element variations in metabasites from the Proterozoic amphibolite-granulite transition zone at Arendal, South Norway. Earth Planet. Sci. Lett. 63, 446-458.

SPEAR, F.S. 1976. Ca-amphibole composition as a function of temperature, fluid pressure, and oxygen fugacity in a basaltic system. Carnegie Inst. Washington Yearbook 75, 775-779.

SPULBER, S.D. and RUTHERFORD, M.J. 1983. The origin of rhyolite and plagiogranite in oceanic crust: an experimental study. J. Petrol. 24, 1-25.

STEPHENSON. D. 1972. Alkali clinopyroxenes from nepheline syenites of the South Qoroq Centre, south Greenland. Lithos 5, 187-201.

STEPHENSON, D. and UPTON, B.G.J. 1982. Ferromagnesian silicates in a differentiated alkaline complex: Kungnat Fjeld, south Greenland. Mineral. Mag. 46, 283-300.

STEPHENSON, N.C.N. 1977. Coexisting hornblendes and biotites from Precambrian gneisses of the south coast of Western Australia. Lithos 10, 9-27.

STERN, C.R. 1974. Melting products of olivine tholeiite basalts in subduction zones. Geology 2, 227-230.

STERN, C.R., HUANG, W.L. and WYLLIE, P.J. 1975. Basalt-andesite-rhyolite-H_2O: crystallisation intervals with excess H_2O and H_2O undersaturated liquidus surfaces to 35 kilobars, with implications for magma genesis. Earth Planet. Sci. Lett. 28, 189-196.

SUTHERLAND, D.S. 1982. Alkaline intrusions of north-western Scotland. In: Igneous rocks of the British Isles. D.S. Sutherland (ed). Wiley, London. pp 203-214.

SUTTON, J. and WATSON, J. 1951. The Pre-Torridonian metamorphic history of the Loch Torridon and Scourie areas in the NW Highlands, and its bearing on the chronological classification of the Lewisian. Q. J. Geol. Soc. London 106, 241-307.

SYLVESTER, A.G., MILLER, C.F. and NELSON, A. 1978. Monzonites of the White-Inyo Range, California, and their relation to the calc-alkalic Sierra Nevada batholith. Bull. Geol. Soc. Amer. 89, 1677-1687.

SYLVESTER, A.G., OERTEL, G., NELSON, C.A. and CHRISTIE, J.M. 1978. Papoose Flat pluton: a granitic blister in the Inyo Mountains, California. Bull. Geol. Soc. Amer. 89, 1205-1219.

TARNEY, J. 1963. Assynt dykes and their metamorphism. Nature 199, 672-674.

TARNEY, J., SKINNER, A.C. and SHERATON, J.W. 1972. A geochemical comparison of major Archaean gneiss units from NW Scotland and East Greenland. 24th IGC Section 1, 162-174.

TARNEY, J., WEAVER, B.L. and DRURY, S.A. 1979. Geochemistry of Archaean trondhjemitic and tonalitic gneisses from Scotland and East Greenland. In: Trondhjemites, Dacites and Related Rocks. F. Barker (ed.) Elsevier. pp 275-299.

TARNEY, J. and WINDLEY, B.F. 1977. Chemistry, thermal gradients and evolution of the lower continental crust. J. Geol. Soc. London 134, 153-172.

TAYLOR, H.P. and EPSTEIN, S. 1962. Relationships between O^{18}/O^{16} ratios in coexisting minerals of igneous and metamorphic rocks. Part 2. Application to petrologic problems. Bull. Geol. Soc. Amer. 73, 675-694.

TAYLOR, H.P. and FORESTER, R.W. 1971. Low-O^{18} igneous rocks from the intrusive complexes of Skye, Mull and Ardnamurchan, western Scotland. J. Petrol. 12, 465-497.

TAYLOR, H.P., GIANNETTI, B. and TURI, B. 1979. Oxygen isotope geochemistry of the potassic igneous rocks from Roccamonfina volcano, Roman Comagmatic Region. Earth Planet. Sci. Lett. 46, 81-106.

TAYLOR, H.P., TURI, B. and CUNDARI, A. 1984. $^{18}O/^{16}O$ and chemical relationships in K-rich volcanic rocks from Australia, East Africa, Antarctica and San Venanzo-Cupaello, Italy. Earth Planet. Sci. Lett. 69, 263-276.

TAYLOR, R.P., STRONG, D.F. and FRYER, B.J. 1981. Volatile control of contrasting trace element distributions in peralkaline granitic and volcanic rocks. Contrib. Mineral. Petrol. 77, 267-271.

THIRLWALL, M.F. 1981. Implications for Caledonian plate tectonic models of chemical data from volcanic rocks of the British Old Red Sandstone. J. Geol. Soc. London 138, 123-138.

THIRLWALL, M.F. 1982. Systematic variation in chemistry and Nd-Sr isotopes across a Caledonian calc-alkaline volcanic arc: implications for source materials. Earth Planet. Sci. Lett. 58, 27-50.

THOMPSON, R.N. 1982. Magmatism of the British Tertiary volcanic province. Scott. J. Geol. 18, 49-107.

THOMPSON, R.N. and FOWLER, M.B. in prep. Ordovician-Silurian syenites adjacent to the Lewisian foreland in the Scottish Caledonides: products of subduction-related shoshonitic to ultrapotassic magmatism.

THOMPSON, R.N., MORRISON, M.A., HENDRY, G.L. and PARRY, S.J. 1984. An assessment of the relative roles of crust and mantle in magma genesis: an elemental approach. In: The Relative Contributions of Mantle, Oceanic Crust and Continental Crust to Magma Genesis. R. Soc. London. pp 111-152.

TIEH, T.T. and LEDGER, E.B. 1981. Fission track study of uranium in two granites of Central Texas. Contrib. Mineral. Petrol. 76, 12-16.

TINDLE, A.G. and PEARCE, J.A. 1981. Petrogenetic modelling of in situ frctional crystallisation in the zoned Loch Doon pluton, Scotland. Contrib. Mineral. Petrol. 78, 196-207.

TINDLE, A.G. and PEARCE, J.A. 1983. Assimilation and partial melting of continental crust: evidence from the mineralogy and geochemistry of autoliths and xenoliths. Lithos 16, 185-202.

TOURET, J. 1971. Le facies granulite en Norvege Meridionale II: les inclusions fluides. Lithos 4, 423-436.

TOURET, J. and DIETVORST, P. 1983. Fluid inclusions in high-grade anatectic metamorphites. J. Geol. Soc. London 140, 635-649.

TURI, B. and TAYLOR, H.P. 1976. Oxygen isotope studies of volcanic rocks of the Roman Province, central Italy. Contrib. Mineral. Petrol. 55, 4-31.

TURNER, F.J. 1968. Metamorphic Petrology. McGraw-Hill, New York.

VALLEY, J.W., McLELLAND, J., ESSENE, E.J. and LAMB, W. 1983. Metamorphic fluids in the deep crust: evidence from the Adirondacks. Nature 301, 226-228.

VALLEY, J.W. and O'NEIL, J.R. 1984. Fluid heterogeneity during granulite facies metamorphism in the Adirondacks: stable isotope evidence. Contrib. Mineral. Petrol. 85, 158-173.

VAN BREEMEN, O., AFTALION, M., PANKHURST, R.J. and RICHARDSON, S.W. 1979. Age of the Glen Dessary syenite, Inverness-shire: diachronous Palaeozoic metamorphism across the Great Glen. Scott. J. Geol. 15, 49-62.

VAN BREEMEN, O., AFTALION, M. and JOHNSON, M.R.W. 1979. Age of the Loch Borrolan complex, Assynt, and later movement along the Moine thrust zone. J. Geol. Soc. London 136, 489-495.

VILLEMANT, B., JAFFREZIC, H., JORON, J-L and TREUIL, M. 1981. Distribution coefficients of major and trace elements, fractional crystallisation in the alkali basalt series of Chaine des Puys (Massif Central, France). Geochim. Cosmochim. Acta 45, 1997-2016.

WALSH, J.N., BUCKLEY, F. and BARKER, J. 1981. The simultaneous determination of rare earth elements in rocks using inductively coupled plasma source spectrometry. Chem. Geol. 33, 141-153.

WALTHER, J.V. and ORVILLE, P.M. 1982. Volatile production and transport in regional metamorphism. Contrib. Mineral. Petrol. 79, 252-257.

WATSON, E.B. 1976. Two-liquid partition coefficients: experimental data and geochemical implications. Contrib. Mineral. Petrol. 56, 119-134.

WATSON, J.V., FOWLER, M.B., PLANT, J.A. and SIMPSON, P.R. In press. Variscan-Caledonian comparisons: late orogenic granites. Proc. Ussher Soc.

WATSON, J.V., FOWLER, M.B., PLANT, J.A., SIMPSON, P.R. and GREEN, P.M. 1982. Uranium provinces in relation to metamorphic grade and regional geochemistry. In: Uranium exploration methods. IAEA/NEA, Paris. pp 235-248.

WATSON, J.V. and PLANT, J.A. 1979. Regional geochemistry of uranium as a guide to deposit formation. Phil. Trans. R. Soc. Lond. A291, 321-338.

WEAVER, B.L. 1980. Rare-earth element geochemistry of Madras granulites. Contrib. Mineral. Petrol. 71, 271-279.

WEAVER, B.L. and TARNEY, J. 1980. Continental crust composition and nature of the lower crust: constraints from mantle Nd-Sr isotope correlation. Nature 286, 342-346.

WEAVER, B.L. and TARNEY, J. 1980. Rare earth geochemistry of Lewisian granulite-facies gneisses, NW Scotland: implications for the petrogenesis of the Archaean lower continental crust. Earth Planet. Sci. Lett. 51, 279-296.

WEAVER, B.L. and TARNEY, J. 1981. Lewisian gneiss geochemistry and Archaean crustal development models. Earth Planet. Sci. Lett. 55, 171-180.

WEAVER, B.L. and TARNEY, J. 1981. The Scourie dyke suite: petrogenesis and geochemical nature of the Proterozoic sub-continental mantle. Contrib. Mineral. Petrol. 78, 175-188.

WEAVER, B.L. and TARNEY, J. 1984. Empirical approach to estimating the composition of the continental crust. Nature 310, 575-577.

WELLS, P.R.A. 1977. Pyroxene thermometry in simple and complex systems. Contrib. Mineral. Petrol. 62, 129-139.

WENDLANDT, R.F. and HARRISON, W.J. 1979. Rare earth partitioning between immiscible carbonate and silicate liquids and CO_2 vapour: results and implications for the formation of light rare earth enriched rocks. Contrib. Mineral. Petrol. 69, 409-419.

WILLIAMS, C.T. 1978. Uranium enriched minerals in mesostasis areas of the Rhum layered pluton. Contrib. Mineral. Petrol. 66, 29-39.

WILLIAMS, C.T. and FLOYD, P.A. 1981. The localised distribution of U and other incompatible elements in spilitic pillow lavas. Contrib. Mineral. Petrol. 78, 111-117.

WILSON, A.F. and BAKSI, A.K. 1984. Oxygen isotope fractionation and disequilibrium displayed by some granulite facies rocks from the Fraser Ridge, Western Australia. Geochim. Cosmochim. Acta 48, 423-432.

WILSON, J.R., ESBENSEN, K.H. and THY, P. 1981. Igneous petrology of the synorogenic Fongen-Hyllingen layered basic complex, south central Scandinavian Caledonides. J. Petrol. 22, 584-627.

WINCHESTER, J.A., LAMBERT, R. St. J. and HOLLAND, J.G. 1981. Geochemistry of the western part of the Moinian assemblage. Scott. J. Geol. 17, 281-294.

WINDLEY, B.F. 1982. Igneous rocks of the Lewisian Complex. In: Igneous Rocks of the British Isles. D.S. Sutherland (ed.) Wiley, London. pp 9-18.

WOLFF, J.A. 1984. Variation in Nb/Ta during differentiation of phonolitic magma, Tenerife, Canary Islands. Geochim. Cosmochim. Acta 48, 1345-1348.

WONES, D.R. and GILBERT, M.C. 1981. Amphiboles in the igneous environment. In: Reviews in Mineralogy, Vol. 9B. Amphiboles: Petrology and Experimental Phase Relations. D. Veblen (ed.) Mineral. Soc. Amer., Michigan. pp 355-390.

WOOD, B.J. 1977. The activity of components in chinopyroxene and garnet solid solutions and their application to rocks. Phil. Trans. R. Soc. London A 286, 331-342.

WOOD, B.J. and BANNO, S. 1973. Garnet-orthopyroxene and orthopyroxene-chinopyroxene relationships in simple and complex systems. Contrib. Mineral. Petrol. 42, 109-124.

WOOD, D.A. 1979. A variably veined suboceanic upper mantle - genetic significance for mid-ocean ridge basalts from geochemical evidence. Geology 7, 499-503.

WOOLLEY, A.R., SYMES, R.F. and ELLIOTT, C.J. 1972. Metasomatized (fenitized) quartzites from the Borrolan complex, Scotland. Mineral. Mag. 38, 819-836.

WORNER, G., BEUSEN, J.M., DUCHATEAU, N., GIJBELS, R. and SCHMINCKE, H.U. 1983. Trace element abundances and mineral/melt distribution coefficients in phonolites from the Laacher See volcano (Germany). Contrib. Mineral. Petrol. 84, 152-173.

WYLLIE, P.J. 1977. Crustal anatexis: an experimental review. Tectonophysics 43, 41-71.

YERMOLAYEV, N.P. 1971. Processes of redistribution and extraction of uranium in progressive metamorphism. Geochem. Internat. 8, 599-609.

ZEILINSKI, R.A. 1979. Uranium mobility during interaction of rhyolitic obsidian, perlite and felsite with alkaline carbonate solution, T = 120°C, P = 210 kg/cm^3. Chem. Geol. 27, 47-63.

ZIELINSKI, R.A. 1982. The mobility of uranium and other elements during alteration of rhyolite ash to montmorillonite: A case study in the Troublesome Formation, Colorado, USA. Chem. Geol. 35, 185-204.

ZIELINSKI, R.A. and FREY, F.A. 1974. An experimental study of the partitioning of rare earth element (Gd) in the system diopside-aqueous vapour. Geochim. Cosmochim. Acta 38, 545-565.

ZEILINSKI, R.A., PETERMAN, Z.E., STUCKLESS, J.S., ROSHOLT, J.N. and NKOMO, I.T. 1981. The chemical and isotopic record of rock-water interaction in the Sherman granite, Wyoming and Colorado. Contrib. Mineral. Petrol. 78, 209-219.

APPENDIX

A.1: WHOLE-ROCK DATA

Sample preparation.

Whole-rock samples (generally about 1 - 2 Kg) were split and crushed using a manual rock splitter, a jaw crusher and an agate tema mill sequentially, to less-than-200-mesh powder. This was used in all major and trace element determinations.

Major element analysis.

The major element oxides SiO_2, TiO_2, Al_2O_3, Fe_2O_3 (total Fe), MnO, MgO, CaO, Na_2O, K_2O and P_2O_5 were determined by X-ray fluorescence spectrometry using a Philips PW1212 spectrometer, following the method of Parker (1982). Briefly, a single pass technique was used with a Cr X-ray tube and three analysing crystals (TlAP, PET and LIF_{220}), erecting a calibration against international standard rocks. The accuracy of the method has been described by Parker (1982), and is summarised in Table A.1, as is its precision, estimated by the replicate analyses of one sample (MJ015). Note that this sample was deliberately chosen to be the coarsest-grained of the analysed suite (feldspars often 2-3cm), such that the data encompass maximum sampling as well as analytical errors. Duplicates were run as a matter of course, approximately every fifth sample, to routinely monitor preparation technique. They are not reported here.

Precision: Replicate analyses of MJ015.

SiO_2	57.44	57.15	56.86	57.05	57.41	57.25	57.10	57.28	57.40
TiO_2	0.86	0.86	0.88	0.84	0.83	0.89	0.89	0.87	0.88
Al_2O_3	16.09	16.04	16.04	16.06	16.10	15.98	15.92	16.14	16.10
Fe_2O_3*	6.31	6.34	6.40	6.13	6.05	6.36	6.42	6.31	6.35
MnO	0.17	0.14	0.19	0.17	0.17	0.17	0.18	0.14	0.12
MgO	2.91	2.99	2.97	2.73	2.79	2.95	3.05	3.02	2.94
CaO	4.70	4.67	4.73	4.58	4.46	4.76	4.71	4.75	4.70
Na_2O	3.60	3.65	3.58	3.66	3.65	3.62	3.58	3.58	3.63
K_2O	6.94	6.98	6.92	6.96	7.07	6.94	6.95	6.90	6.93
P_2O_5	0.57	0.59	0.62	0.58	0.57	0.59	0.62	0.61	0.61
LOI	0.32	0.32	0.30	0.31	0.29	0.28	0.28	0.26	0.26

	X	δ	RSD %	Parker (1982)	
SiO_2	57.22	0.193	0.337	0.30	0.23
TiO_2	0.87	0.021	2.413	0.51	1.09
Al_2O_3	16.05	0.068	0.424	0.57	0.52
Fe_2O_3	6.30	0.124	1.968	1.05	0.71
MnO	0.16	0.023	14.375	23.06	37.87
MgO	2.93	0.105	3.583	3.40	5.80
CaO	4.67	0.096	2.056	0.71	0.77
Na_2O	3.62	0.033	0.912	2.87	7.65
K_2O	6.95	0.049	0.705	0.23	0.48
P_2O_5	0.60	0.020	3.333	3.79	10.63
LOI	0.29	0.023	7.931	2.09	-

Accuracy: (after Parker, 1980).

	JG-1		JB-1	
	Parker	Lit	Parker	Lit
SiO_2	72.34	72.36	52.69	52.62
TiO_2	0.26	0.27	1.30	1.34
Al_2O_3	14.12	14.20	14.61	14.62
Fe_2O_3	2.14	2.16	9.12	9.01
MnO	0.07	0.06	0.16	0.15
MgO	0.61	0.76	7.40	7.76
CaO	2.17	2.17	9.31	9.35
Na_2O	3.24	3.39	2.68	2.79
K_2O	3.98	3.96	1.45	1.42
P_2O_5	0.10	0.09	0.26	0.26

Table A.1: Accuracy and precision of major-element analyses.

Trace element analysis.

Sr, Rb, Nb, Y, and Zr; Ba, Cr, Ni, and V.

These trace elements were analysed by standard X-ray fluorescence techniques at Bedford College, University of London. For the former group (Sr, Rb, Nb, Y and Zr), an Ag X-ray tube was used, and for the latter group (Ba, Cr, Ni and V) a W tube was used. Full mass absorption corrections were applied, and accuracy and precision are estimated at better than 10%. They can be adjudged from the data in Table A.2 (literature values from Abbey, 1980).

Rare earth elements, Th, Hf and Ta.

The REEs have been analysed using two techniques for this thesis. The majority of Lewisian samples were analysed by standard instrumental neutron activation techniques through the internal facilities of the B.G.S., following the method of Plant et al. (1976). All Th, Hf and Ta values were also determined using this technique. Accuracy and precision were monitored internally and are estimated at better than 10%. The majority of the Glen Dessarry samples were analysed for REEs by ion-exchange, followed by inductively-coupled plasma spectrometry, following the method of Walsh et al. (1981). Accuracy and precision are estimated at better than 10%, and can be adjudged by the data in Table A.3 for Kings College internal standards.

Uranium.

All U values were determined by the delayed neutron method (Amiel, 1962; Bowie et al., 1973), through the internal facilities of the B.G.S. Accuracy and precision were monitored internally and are estimated at better than 10% at concentrations in excess of 1ppm, but at low levels these inevitably suffer, perhaps to +/- 20%.

Precision: Replicate analyses of MJ015.

Nb	11	12	11	11	12	11	11
Zr	161	166	165	162	165	153	160
Y	32	33	30	30	33	32	31
Sr	2880	2849	2878	2923	2823	2933	2888
Rb	108	107	110	113	107	110	110
Ba	3340	3291	3338	3358	3255	3264	3242
Cr	57	56	55	53	58	56	56
Ni	34	34	33	34	36	32	33
V	131	131	128	128	136	130	130

	X	δ	RSD %
Nb	11	0.49	4.4
Zr	162	4.46	2.8
Y	32	1.27	4.0
Sr	2882	38.53	1.3
Rb	109	2.14	2.0
Ba	3298	46.80	1.4
Cr	56	1.57	2.8
Ni	34	1.25	3.7
V	131	2.70	2.0

Accuracy:

	G2	GSP	BR	AGV	BCR	W1
Nb	14	27	131	17	13	9
	14		110	15	13	9
Lit	13?	23?	100?	16?	19?	9.5?
Zr	333	547	250	223	176	91
	343		258	229	178	91
Lit	300	500	250	230	185	105
Y	13	31	33	21	38	23
	16		31	22	39	23
Lit	11	29	30	19	40	25
Sr	487	230	1296	651	311	181
	481		1284	644	307	180
Lit	480	240	1300	660	330	190
Rb	169	246	45	65	44	21
	166		45	65	44	21
Lit	170	250	47	67	47	21

Table A.2: Accuracy and precision of trace element analyses.

	KC10		KC11		KC13	
	Lit	MBF	Lit	MBF	Lit	MBF
La	4.3	4.16	23.0	23.02	59.0	59.25
Ce	9.2	9.37	49.0	44.02	120.0	110.18
Pr	1.6	1.46	5.9	5.17	13.0	12.31
Nd	6.8	6.08	26.5	24.19	62.0	55.14
Sm	1.7	1.54	5.2	4.87	14.0	13.40
Eu	0.75	0.83	1.40	1.44	0.57	0.66
Gd	1.9	2.12	5.0	4.64	15.0	15.35
Dy	2.0	2.00	4.45	4.27	18.0	18.04
Er	1.25	1.10	2.7	2.42	11.8	11.36
Yb	1.1	1.08	2.2	2.17	11.2	11.46
Lu	0.16	0.21	0.32	0.34	1.5	1.61

Table A.3: REE standards.

Density determinations.

Density measurements were made using a 50 cm^3 density bottle, following standard techniques with a detergent solution (to aid wetting the powder) of known density. Approximately 1g of rock powder was used for each determination. Pure quartz was used as a reference sample, and values for this are listed in Table A.4 (recommended value = 2.65).

Determination	1	2	3	4	X
Value	2.662	2.671	2.626	2.633	2.648

Table A.4: Replicate determinations of the density of pure quartz.

Oxygen isotope analyses.

Oxygen isotope compositions of samples of the Glen Dessarry syenite were analysed at the laboratories of the B.G.S., Gray's Inn Road, London. Oxygen was extracted by reaction with BrF_5 at 600°C for about 12 hours (Clayton and Mayeda, 1963). Conversion to CO_2 was achieved by passing the extracted oxygen over heated carbon rods. Isotopic measurements were performed on a V.G. MM903 fully automated mass spectrometer. Accuracy and precision are estimated at better than +/- 0.5‰. All data are reported using the standard δ notation relative to SMOW.

Gamma-ray scintillometry.

A gamma-ray scintillometer was used in the field to give an on-the-spot estimate of the total radioelement content (principally K, U and Th) of the rock at outcrop. Care was taken to avoid solid-angle enhancement of true readings. Its careful use facilitated the determination of suitable material for subsequent analysis, but no great significance has been conferred to any radioelement data collected in this way. It is purely a field instrument.

Gruinard Bay gneisses, 50.00 to 59.99% SiO_2.

Sample:	MJ128	MJ171	MJ154	MJ130	MJ156	MJ131	MJ124	MJ037	MJ129
SiO_2	51.22	51.45	51.90	53.39	54.22	54.55	54.94	55.28	55.63
TiO_2	1.22	0.85	0.17	0.73	0.40	0.76	1.57	0.24	0.76
Al_2O_3	17.69	14.00	9.96	16.72	15.66	15.85	18.59	18.49	17.04
Fe_2O_3*	9.52	9.50	9.94	8.59	8.02	8.71	7.41	5.69	7.57
MnO	0.09	0.19	0.22	0.16	0.13	0.13	0.16	0.11	0.14
MgO	4.91	7.84	15.51	4.43	6.49	4.58	2.25	4.91	3.99
CaO	6.83	9.19	7.88	8.44	7.41	7.71	8.69	9.23	7.77
Na_2O	3.25	2.57	1.72	3.83	3.54	3.29	3.94	4.21	4.21
K_2O	2.89	2.09	1.01	1.35	1.65	1.70	0.99	0.87	1.30
P_2O_5	0.36	0.33	0.02	0.28	0.22	0.40	0.10	0.04	0.12
H_2O^-	0.03	0.06	0.12	0.09	0.13	0.08	0.03	0.07	0.05
LOI	1.10	1.20	1.23	0.75	1.80	0.95	0.91	0.60	0.81
Total	99.11	99.32	99.68	98.76	99.67	98.71	99.58	99.74	99.39
CIPW Norms*									
Qz	0.00	0.83	0.10	3.43	3.21	7.34	8.18	2.54	5.27
Co	0.00	0.00	0.00	0.00	0.00	0.00	0.00	0.00	0.00
Or	17.08	12.35	5.97	7.98	9.75	10.05	5.85	5.14	7.68
Pl	52.65	42.24	31.03	56.85	51.92	51.30	63.45	64.61	59.38
(Ab)	27.50	21.75	14.55	32.41	29.95	27.84	33.34	35.62	35.62
(An)	25.15	20.49	16.47	24.44	21.97	23.46	30.11	28.98	23.76
Di	5.12	18.27	17.78	12.55	10.66	9.79	9.94	13.20	11.25
(Wo)	2.67	9.58	9.39	6.51	5.58	5.08	5.15	6.91	5.85
(En)	1.84	6.98	7.23	4.33	3.97	3.41	3.41	4.95	3.95
(Fs)	0.60	1.71	1.17	1.71	1.11	1.30	1.37	1.34	1.45
Hy	13.33	15.63	36.47	9.36	15.60	11.05	3.07	9.25	8.19
(En)	10.04	12.55	31.40	6.71	12.19	8.00	2.19	7.28	5.99
(Fs)	3.29	3.08	5.07	2.65	3.41	3.05	0.88	1.97	2.20
Ol	0.33	0.00	0.00	0.00	0.00	0.00	0.00	0.00	0.00
(Fo)	0.24	-	-	-	-	-	-	-	-
(Fa)	0.09	-	-	-	-	-	-	-	-
Mt	5.77	5.77	6.03	5.22	4.87	5.29	4.49	3.45	4.60
Il	2.32	1.61	0.32	1.39	0.76	1.44	2.98	0.46	1.44
Hm	0.00	0.00	0.00	0.00	0.00	0.00	0.00	0.00	0.00
Ap	0.85	0.78	0.05	0.66	0.52	0.95	0.24	0.09	0.28
Trace elements									
Sr	487	477	154	503	360	475	176	407	520
Ba	1809	804	104	817	737	1075	332	439	827
Rb	53	52	25	22	25	30	20	12	22
U	0.24	0.17	0.11	0.11	0.29	0.23	0.34	0.14	0.07
Th	13.0	2.2	1.5	0.4	3.4	7.8	0.6	0.3	0.3
Zr	103	114	29	81	112	131	143	103	59
Nb	11	6	2	8	4	9	6	5	7
Y	29	19	5	37	24	38	20	<2	25
Cr	111	213	1180	176	314	96	275	228	57
Ni	61	193	523	58	158	103	147	205	47
V	442	179	91	152	112	134	343	61	150

* Total iron expressed as Fe_2O_3; CIPW norms calculated by setting $Fe_2O_3/FeO = 0.8$, after Weaver and Tarney (1980).

Gruinard Bay gneisses, 50.00 to 59.99% SiO_2.

Sample:	MJ168	MJ157	MJ158	MJ181	MJ192	MJ179	MJ165	MJ148
SiO_2	56.50	56.97	57.44	57.64	57.86	58.37	58.39	59.44
TiO_2	0.74	0.67	0.72	1.00	0.45	0.88	0.74	0.32
Al_2O_3	14.80	16.82	15.62	17.79	18.93	17.17	15.74	16.75
Fe_2O_3*	8.87	7.18	7.86	7.05	4.17	6.63	7.70	5.21
MnO	0.14	0.09	0.13	0.10	0.08	0.08	0.11	0.11
MgO	5.00	4.39	4.70	2.24	2.73	1.99	3.05	4.83
CaO	7.11	5.50	5.55	7.18	7.68	6.91	6.82	5.08
Na_2O	2.95	4.65	3.96	4.78	5.38	4.86	2.84	4.34
K_2O	2.06	0.79	1.37	0.98	1.28	0.77	1.88	1.36
P_2O_5	0.24	0.20	0.12	0.27	0.17	0.23	0.13	0.08
H_2O^-	0.09	0.13	0.13	0.07	0.10	0.39	0.09	0.13
LOI	1.08	1.68	1.90	0.65	0.81	0.74	1.75	1.39
Total	99.58	99.07	99.50	99.75	99.64	99.02	99.24	99.04
CIPW Norms*								
Qz	10.13	8.26	10.12	8.90	3.59	10.93	15.99	10.35
Co	0.00	0.00	0.00	0.00	0.00	0.00	0.00	0.00
Or	12.17	4.67	8.10	5.79	7.56	4.55	11.11	8.04
Pl	46.02	62.04	54.31	64.64	69.25	63.88	48.68	58.93
(Ab)	24.96	39.35	33.51	40.45	45.52	41.12	24.03	36.72
(An)	21.06	22.69	20.80	24.19	23.72	22.76	24.65	22.21
Di	10.15	2.63	4.77	7.83	10.60	8.14	6.75	1.97
(Wo)	5.28	1.37	2.48	4.04	5.54	4.18	3.48	1.03
(En)	3.58	0.96	1.71	2.51	3.93	2.54	2.19	0.75
(Fs)	1.29	0.30	0.57	1.29	1.13	1.42	1.07	0.18
Hy	12.07	13.15	13.30	4.66	3.70	3.77	8.05	13.98
(En)	8.87	9.98	9.99	3.07	2.87	2.42	5.40	11.27
(Fs)	3.20	3.17	3.31	1.58	0.83	1.35	2.65	2.71
Ol	0.00	0.00	0.00	0.00	0.00	0.00	0.00	0.00
(Fo)	-	-	-	-	-	-	-	-
(Fa)	-	-	-	-	-	-	-	-
Mt	5.38	4.36	4.77	4.28	2.54	4.03	4.67	3.16
Il	1.41	1.27	1.37	1.90	0.85	1.67	1.41	0.61
Hm	0.00	0.00	0.00	0.00	0.00	0.00	0.00	0.00
Ap	0.57	0.47	0.28	0.64	0.40	0.54	0.31	0.19
Trace elements								
Sr	405	607	467	460	827	449	613	496
Ba	830	251	463	546	532	384	1018	1163
Rb	34	14	21	14	28	12	38	23
U	0.10	0.14	0.09	0.05	0.31	0.04	0.12	0.21
Th	1.0	2.0	2.5	0.2	6.0	0.6	3.2	0.2
Zr	128	74	62	93	147	81	153	276
Nb	9	7	7	8	6	7	9	5
Y	43	13	17	13	22	18	16	6
Cr	164	47	55	13	25	12	104	228
Ni	103	70	70	22	9	29	80	173
V	118	102	126	110	124	95	118	48

* Total iron expressed as Fe_2O_3; CIPW norms calculated by setting $Fe_2O_3/FeO = 0.8$, after Weaver and Tarney (1980).

Gruinard Bay gneisses, 60.00 to 69.99% SiO_2.

Sample:	MJ152	MJ150	MJ126	MJ134	MJ182	MJ166	MJ180	MJ164	MJ195
SiO_2	60.38	61.20	62.14	62.30	62.90	62.91	64.97	65.26	65.43
TiO_2	0.32	0.09	1.13	0.45	0.38	0.54	0.53	0.51	0.49
Al_2O_3	13.66	17.65	16.22	16.01	16.50	15.22	16.13	15.25	16.56
Fe_2O_3*	7.53	4.39	6.13	5.16	4.65	6.15	4.72	4.98	3.60
MnO	0.14	0.09	0.09	0.07	0.06	0.07	0.07	0.12	0.05
MgO	6.56	3.47	2.46	2.62	2.54	2.62	1.71	1.82	1.51
CaO	6.04	5.34	5.32	5.92	6.29	5.13	4.74	4.90	4.32
Na_2O	3.27	5.23	4.88	4.27	4.50	3.11	4.55	3.54	5.06
K_2O	0.78	0.77	1.14	1.25	0.81	1.87	1.30	1.73	1.41
P_2O_5	0.03	0.07	0.11	0.06	0.06	0.12	0.14	0.12	0.21
H_2O^-	0.11	0.10	0.05	0.05	0.05	0.13	0.06	0.09	0.11
LOI	0.71	0.68	0.70	0.72	0.59	1.53	0.74	1.16	0.89
Total	99.53	99.08	100.37	98.88	99.33	99.40	99.66	99.48	99.64
CIPW Norms*									
Qz	16.83	11.56	15.97	17.55	17.91	23.13	21.49	25.36	19.87
Co	0.00	0.00	0.00	0.00	0.00	0.00	0.00	0.00	0.00
Or	4.61	4.55	6.74	7.39	4.79	11.05	7.68	10.22	8.33
Pl	47.96	66.66	60.28	56.96	60.51	48.36	58.25	50.57	61.12
(Ab)	27.67	44.25	41.29	36.13	38.08	26.32	38.50	29.95	42.82
(An)	20.29	22.41	18.99	20.83	22.43	22.05	19.75	20.61	18.31
Di	7.47	2.87	5.23	6.44	6.62	2.07	2.26	2.31	1.38
(Wo)	3.96	1.51	2.79	3.40	3.50	1.09	1.19	1.22	0.73
(En)	3.11	1.16	2.34	2.63	2.71	0.83	0.91	0.90	0.58
(Fs)	0.40	0.19	0.09	0.41	0.41	0.15	0.16	0.19	0.06
Hy	14.93	8.69	3.93	4.51	4.16	6.72	3.95	4.40	3.53
(En)	13.22	7.48	3.78	3.90	3.61	5.69	3.35	3.63	3.18
(Fs)	1.71	1.21	0.15	0.61	0.55	1.03	0.59	0.77	0.35
Ol	0.00	0.00	0.00	0.00	0.00	0.00	0.00	0.00	0.00
(Fo)	-	-	-	-	-	-	-	-	-
(Fa)	-	-	-	-	-	-	-	-	-
Mt	5.89	3.44	4.78	4.03	3.64	4.81	3.68	3.89	2.81
Il	0.61	0.17	2.15	0.85	0.72	1.03	1.01	0.97	0.93
Hm	0.00	0.00	0.00	0.00	0.00	0.00	0.00	0.00	0.00
Ap	0.07	0.17	0.26	0.14	0.14	0.28	0.33	0.28	0.50
Trace elements									
Sr	336	554	560	409	433	566	488	589	485
Ba	586	655	548	567	395	1114	640	914	548
Rb	12	13	22	22	12	38	24	37	31
U	0.22	0.08	0.13	0.04	0.15	0.08	0.11	0.15	0.07
Th	0.4	0.2	0.6	0.1	0.2	3.0	0.4	3.8	1.9
Zr	194	140	108	67	157	210	116	189	94
Nb	3	2	8	3	3	4	4	4	4
Y	21	3	8	12	15	8	4	8	6
Cr	409	69	73	66	33	75	5	47	15
Ni	215	94	35	49	40	55	26	37	21
V	74	22	125	78	62	88	74	78	56

* Total iron expressed as Fe_2O_3; CIPW norms calculated by setting $Fe_2O_3/FeO = 1.2$, after Weaver and Tarney (1980).

Gruinard Bay gneisses, 60.00 to 69.99% SiO_2.

Sample:	MJ178	MJ149	MJ169	MJ125	MJ163
SiO_2	65.69	66.18	66.70	67.62	68.85
TiO_2	0.51	0.06	0.48	0.59	0.32
Al_2O_3	15.26	16.64	15.31	15.45	13.68
Fe_2O_3*	4.55	2.90	4.77	3.23	4.37
MnO	0.06	0.08	0.06	0.04	0.07
MgO	1.66	2.25	1.59	1.00	1.53
CaO	5.03	5.00	4.79	4.16	4.92
Na_2O	4.14	5.00	4.02	5.33	3.44
K_2O	1.07	0.58	1.11	1.02	1.46
P_2O_5	0.15	0.06	0.15	0.15	0.06
H_2O-	0.06	0.09	0.06	0.05	0.08
LOI	0.89	0.47	0.82	1.50	0.84
Total	99.07	99.31	99.86	100.14	99.62
CIPW Norms*					
Qz	25.24	21.22	26.98	23.63	31.55
Co	0.00	0.00	0.00	0.00	0.00
Or	6.32	3.43	6.56	6.03	8.63
Pl	54.93	63.56	54.47	60.32	46.68
(Ab)	35.03	42.31	34.02	45.10	29.11
(An)	19.89	21.25	20.45	15.22	17.57
Di	3.23	2.51	1.85	3.47	5.13
(Wo)	1.70	1.32	0.97	1.85	2.69
(En)	1.30	1.01	0.73	1.54	1.95
(Fs)	0.23	0.17	0.15	0.08	0.50
Hy	3.32	5.38	3.91	0.99	2.34
(En)	2.83	4.59	3.23	0.95	1.86
(Fs)	0.49	0.79	0.68	0.05	0.48
Ol	0.00	0.00	0.00	0.00	0.00
(Fo)	-	-	-	-	-
(Fa)	-	-	-	-	-
Mt	3.55	2.26	3.73	2.52	3.42
Il	0.97	0.11	0.91	1.12	0.61
Hm	0.00	0.00	0.00	0.00	0.00
Ap	0.36	0.14	0.36	0.36	0.14
Trace elements					
Sr	488	537	476	417	583
Ba	496	477	510	506	613
Rb	21	16	23	26	30
U	0.19	0.09	0.08	0.02	0.14
Th	0.6	0.1	0.2	0.2	1.4
Zr	153	142	114	172	136
Nb	3	<2	3	4	5
Y	7	<2	8	3	13
Cr	17	42	24	<2	38
Ni	22	59	21	13	43
V	73	14	78	67	69

* Total iron expressed as Fe_2O_3; CIPW norms calculated by setting $Fe_2O_3/FeO = 1.2$, after Weaver and Tarney (1980).

Gruinard Bay gneisses, greater than 70.00% SiO_2.

Sample:	MJ183	MJ039	MJ116	MJ117	MJ118	MJ115	MJ144
SiO_2	70.35	70.54	70.68	71.07	71.76	71.93	74.59
TiO_2	0.37	0.27	0.47	0.40	0.23	0.43	0.07
Al_2O_3	15.28	14.62	15.16	15.55	15.18	14.23	13.01
Fe_2O_3*	2.81	2.42	2.25	2.28	2.36	3.00	1.36
MnO	0.04	0.04	0.04	0.02	0.02	0.02	0.02
MgO	0.67	1.14	0.69	0.58	0.28	1.12	0.94
CaO	3.31	2.93	2.90	3.82	2.42	3.12	3.81
Na_2O	4.36	4.73	4.62	4.27	4.09	4.28	4.05
K_2O	1.56	1.20	2.03	1.37	3.21	1.14	0.51
P_2O_5	0.11	0.12	0.08	0.06	0.03	0.01	0.05
H_2O^-	0.06	0.15	0.07	0.04	0.05	0.04	0.09
LOI	0.60	1.40	1.24	0.91	0.94	0.70	0.45
Total	99.52	99.56	100.23	100.37	100.57	100.02	98.95
CIPW Norms*							
Qz	31.24	30.80	29.02	32.11	28.28	34.35	40.25
Co	0.66	0.50	0.28	0.24	0.72	0.31	0.00
Or	9.22	7.09	12.00	8.10	19.19	6.71	3.01
Pl	52.60	53.78	52.96	54.69	49.12	51.63	50.08
(Ab)	36.89	40.02	39.09	36.13	37.17	36.22	34.27
(An)	15.70	13.75	13.86	18.56	11.95	15.41	15.81
Di	0.00	0.00	0.00	0.00	0.00	0.00	2.15
(Wo)	-	-	-	-	-	-	1.15
(En)	-	-	-	-	-	-	1.00
(Fs)	-	-	-	-	-	-	0.00
Hy	1.67	2.84	1.72	1.44	0.78	2.79	1.34
(En)	1.67	2.84	1.72	1.44	0.78	2.79	1.34
(Fs)	0.00	0.00	0.00	0.00	0.00	0.00	0.00
Ol	0.00	0.00	0.00	0.00	0.00	0.00	0.00
(Fo)	-	-	-	-	-	-	-
(Fa)	-	-	-	-	-	-	-
Mt	0.77	0.83	0.12	0.29	0.60	0.02	0.70
Il	0.70	0.51	0.89	0.76	0.32	0.82	0.13
Hm	1.69	1.34	1.70	1.60	0.92	1.94	0.60
Ap	0.26	0.28	0.19	0.14	0.06	0.02	0.12
Trace elements							
Sr	436	535	374	534	473	469	463
Ba	772	685	1096	534	2387	752	532
Rb	39	10	46	35	55	29	15
U	0.16	0.03	0.20	0.13	0.14	0.02	0.22
Th	0.2	0.1	6.9	2.5	14.0	0.1	0.2
Zr	142	103	227	201	137	22	433
Nb	3	<2	3	3	<2	2	<2
Y	2	<2	3	2	2	<2	2
Cr	3	14	<2	2	<2	40	30
Ni	6	22	4	3	6	31	37
V	32	37	42	39	58	50	11

* Total iron expressed as Fe_2O_3; CIPW norms calculated by setting $Fe_2O_3/FeO = 4.2$, after Weaver and Tarney (1980).

Gruinard Bay gneisses, "anorthosites".

Sample:	MJ188	MJ193	MJ198	MJ197	MJ199	MJ190
SiO_2	53.32	54.53	56.08	56.67	56.83	58.27
TiO_2	0.60	0.56	0.31	0.28	0.27	0.46
Al_2O_3	21.08	20.17	21.09	21.65	21.36	19.43
Fe_2O_3*	6.44	5.89	3.90	3.39	3.50	3.92
MnO	0.07	0.07	0.03	0.03	0.03	0.07
MgO	2.74	3.15	2.31	1.62	1.96	2.40
CaO	6.70	6.29	6.19	6.25	6.18	7.87
Na_2O	5.57	5.58	5.99	6.54	6.39	5.51
K_2O	1.74	1.68	1.43	1.45	1.43	0.82
P_2O_5	0.36	0.30	0.11	0.11	0.09	0.16
H_2O-	0.08	0.11	0.08	0.09	0.09	0.09
LOI	0.76	1.02	0.76	0.75	0.82	0.55
Total	99.46	99.35	98.28	98.93	98.95	99.55
CIPW Norms*						
Qz	0.00	0.00	0.00	0.00	0.00	4.90
Co	0.00	0.00	0.00	0.00	0.00	0.00
Or	10.28	9.93	8.45	8.57	8.45	4.85
Pl	71.35	72.24	77.12	78.45	79.11	72.49
(Ab)	43.97	47.22	50.69	53.01	53.73	46.62
(An)	27.38	25.03	26.43	25.44	25.38	25.86
Ne	1.71	0.00	0.00	1.26	0.18	0.00
Di	2.83	3.39	2.85	3.91	3.77	9.70
(Wo)	1.47	1.76	1.48	2.03	1.96	5.07
(En)	0.94	1.20	1.02	1.89	1.33	3.57
(Fs)	0.43	0.43	0.34	0.86	0.48	1.06
Hy	0.00	1.70	3.67	0.00	0.00	3.12
(En)	-	1.25	2.74	-	-	2.41
(Fs)	-	0.45	0.93	-	-	0.72
Ol	6.18	5.28	1.91	2.76	3.48	0.00
(Fo)	4.12	3.78	1.39	1.89	2.49	-
(Fa)	2.06	1.50	0.52	0.86	0.99	-
Mt	3.91	3.58	2.36	2.06	2.12	2.38
Il	1.14	1.06	0.59	0.53	0.51	0.87
Ap	0.85	0.71	0.26	0.26	0.21	0.38
Trace elements						
Sr	907	865	949	1011	990	718
Ba	643	555	526	669	546	846
Rb	47	40	28	29	30	17
U	0.22	0.15	0.05	0.05	0.01	0.25
Th	2.2	1.3	0.3	0.3	0.5	3.0
Zr	65	58	70	49	64	206
Nb	5	4	2	<2	<2	5
Y	12	14	13	10	8	20
Cr	26	35	19	11	14	24
Ni	25	31	12	14	12	10
V	148	129	71	71	59	123

* Total iron expressed as Fe_2O_3; CIPW norms calculated by setting $Fe_2O_3/FeO = 0.8$, after Weaver and Tarney (1980).

Central Block granulites, 50.00 to 59.99% SiO_2.

Sample:	MJ080	MJ051	MJ077	MJ053	MJ073	MJ043	MJ082	MJ076
SiO_2	50.23	50.26	50.27	58.11	58.22	58.31	58.69	59.90
TiO_2	0.91	0.79	0.62	0.66	0.78	0.14	0.84	0.58
Al_2O_3	16.42	13.57	12.66	15.23	15.83	17.99	15.31	15.96
Fe_2O_3*	12.02	14.34	13.47	8.54	7.79	4.88	8.24	6.19
MnO	0.23	0.26	0.19	0.14	0.15	0.09	0.13	0.12
MgO	5.58	5.99	9.10	3.41	3.87	3.66	4.17	3.42
CaO	9.82	10.56	9.85	8.16	7.50	7.44	7.74	6.52
Na_2O	3.45	2.32	2.59	4.47	3.99	5.72	4.23	4.28
K_2O	0.64	0.72	0.72	0.82	0.91	0.54	0.67	1.29
P_2O_5	0.10	0.06	0.03	0.12	0.21	0.15	0.18	0.24
H_2O^-	0.15	0.08	0.06	0.08	0.05	0.04	0.07	0.04
LOI	0.68	0.60	0.59	0.36	0.82	0.86	0.34	1.51
Total	100.23	99.55	100.15	100.10	100.12	99.82	100.61	100.05
CIPW Norms*								
Qz	0.21	4.92	0.42	9.18	11.42	3.71	10.99	12.49
Co	0.00	0.00	0.00	0.00	0.00	0.00	0.00	0.00
Or	3.78	4.25	4.25	4.85	5.38	3.19	3.96	7.62
Pl	56.62	44.12	42.71	56.89	56.36	70.22	56.60	56.74
(Ab)	29.19	19.63	21.92	37.82	33.76	48.40	35.79	36.22
(An)	27.43	24.49	20.79	19.07	22.60	21.82	20.81	20.53
Di	16.67	22.32	22.34	16.72	10.65	11.30	13.19	8.23
(Wo)	8.62	11.49	11.64	8.61	5.53	5.89	6.85	4.28
(En)	5.53	7.05	8.01	5.33	3.68	4.09	4.60	2.90
(Fs)	2.52	3.78	2.69	2.78	1.45	1.32	1.74	1.05
Hy	12.17	12.08	19.58	4.81	8.30	6.64	7.97	7.64
(En)	8.36	7.87	14.65	3.16	5.96	5.02	5.78	5.62
(Fs)	3.80	4.22	4.92	1.65	2.34	1.62	2.18	2.03
Ol	0.00	0.00	0.00	0.00	0.00	0.00	0.00	0.00
(Fo)	-	-	-	-	-	-	-	-
(Fa)	-	-	-	-	-	-	-	-
Mt	7.29	8.70	8.18	5.18	4.73	2.96	5.00	3.76
Il	1.73	1.50	1.18	1.25	1.48	0.27	1.60	1.10
Hm	0.00	0.00	0.00	0.00	0.00	0.00	0.00	0.00
Ap	0.24	0.14	0.07	0.28	0.50	0.36	0.43	0.57
Trace elements								
Sr	232	172	116	360	405	783	595	782
Ba	217	169	135	320	407	810	538	1442
Rb	3	10	4	5	7	4	2	6
U	0.09	0.13	0.04	0.09	0.11	0.05	0.07	0.01
Th	0.2	0.2	0.2	0.3	0.4	0.2	0.2	0.2
Zr	61	51	39	84	100	261	167	80
Nb	5	5	5	3	5	<2	5	2
Y	29	27	27	16	17	10	22	12
Cr	382	306	524	89	127	336	185	181
Ni	101	86	117	63	72	101	145	39
V	253	258	271	156	134	63	116	117

* Total iron expressed as Fe_2O_3; CIPW norms calculated by setting $Fe_2O_3/FeO = 0.8$, after Weaver and Tarney (1980).

Central Block granulites, 60.00 to 69.99% SiO_2.

Sample:	MJ045	MJ046	MJ040	MJ070	MJ081	MJ067	MJ042	MJ083	MJ079
SiO_2	60.58	60.62	61.90	62.08	62.08	62.19	63.89	64.97	65.26
TiO_2	0.80	0.28	0.65	0.79	0.39	0.80	0.57	0.59	0.50
Al_2O_3	16.96	17.72	15.94	15.31	13.48	18.00	15.74	16.19	15.97
Fe_2O_3*	6.16	5.34	6.40	6.47	7.41	5.08	5.06	4.74	5.22
MnO	0.08	0.08	0.11	0.12	0.13	0.07	0.10	0.08	0.12
MgO	2.72	2.37	3.41	2.71	4.23	1.39	2.09	1.91	2.06
CaO	5.96	7.12	6.57	6.51	7.31	5.91	5.83	5.08	5.41
Na_2O	5.38	5.14	4.59	4.25	3.68	4.91	4.60	4.47	4.22
K_2O	0.61	0.60	0.26	0.89	0.65	1.00	1.00	1.01	1.24
P_2O_5	0.38	0.14	0.10	0.14	0.09	0.27	0.14	0.19	0.13
H_2O^-	0.05	0.05	0.04	0.10	0.05	0.03	0.04	0.04	0.05
LOI	0.59	0.76	0.29	0.61	0.65	0.68	1.07	0.65	0.27
Total	100.27	100.22	100.26	99.98	100.15	100.33	100.13	99.92	100.45
CIPW Norms*									
Qz	12.65	11.76	16.93	18.37	19.33	16.38	19.58	22.21	22.28
Co	0.00	0.00	0.00	0.00	0.00	0.00	0.00	0.00	0.00
Or	3.60	3.55	1.54	5.26	3.84	5.91	5.91	5.97	7.33
Pl	65.62	67.00	60.96	56.03	49.48	65.67	58.27	58.95	56.68
(Ab)	45.10	43.49	38.84	35.96	31.14	41.55	38.92	37.82	35.71
(An)	20.52	23.51	22.12	20.07	18.34	24.12	19.35	21.13	20.97
Di	5.11	8.67	7.75	8.93	13.73	2.71	6.85	2.24	3.98
(Wo)	2.71	4.55	4.10	4.72	7.24	1.43	3.62	1.18	2.10
(En)	2.16	3.35	3.21	3.68	5.49	1.13	2.78	0.92	1.57
(Fs)	0.24	0.77	0.43	0.52	1.01	0.14	0.45	0.13	0.32
Hy	5.07	3.15	5.99	3.50	5.98	2.61	2.82	4.38	4.29
(En)	4.56	2.56	5.28	3.06	5.05	2.33	2.42	3.83	3.56
(Fs)	0.50	0.59	0.71	0.43	0.93	0.28	0.39	0.55	0.72
Ol	0.00	0.00	0.00	0.00	0.00	0.00	0.00	0.00	0.00
(Fo)	-	-	-	-	-	-	-	-	-
(Fa)	-	-	-	-	-	-	-	-	-
Mt	4.80	4.18	5.00	5.06	5.79	3.97	3.96	3.71	4.07
Il	1.56	0.53	1.23	1.50	0.74	1.52	1.08	1.12	0.95
Hm	0.00	0.00	0.00	0.00	0.00	0.00	0.00	0.00	0.00
Ap	0.92	0.33	0.24	0.33	0.21	0.64	0.33	0.45	0.31
Trace elements									
Sr	931	1276	481	498	431	754	449	660	398
Ba	856	1011	143	467	547	617	648	533	543
Rb	4	3	<2	5	2	3	5	5	7
U	0.20	0.07	0.01	0.08	0.03	0.05	0.11	0.01	0.04
Th	0.5	0.2	0.2	0.4	0.2	0.1	0.1	0.1	0.2
Zr	107	41	87	239	168	143	114	95	105
Nb	6	2	2	5	2	4	4	3	4
Y	17	10	14	17	15	6	11	6	14
Cr	46	71	130	51	281	6	96	23	42
Ni	47	58	110	29	80	19	46	23	31
V	121	95	142	110	99	81	100	82	64

* Total iron expressed as Fe_2O_3; CIPW norms calculated by setting $Fe_2O_3/FeO = 1.2$, after Weaver and Tarney (1980).

Central Block granulites, 60.00 to 69.99% SiO_2.

Sample:	MJ059	MJ055	MJ066	MJ054	MJ062	MJ069	MJ049	MJ060	MJ065
SiO_2	65.32	66.40	66.81	67.31	67.41	67.60	68.06	68.23	68.28
TiO_2	0.71	0.57	0.48	0.46	0.49	0.46	0.43	0.49	0.42
Al_2O_3	14.55	16.57	16.50	16.85	16.12	15.90	16.43	16.18	16.30
Fe_2O_3*	5.86	3.35	3.52	2.64	3.30	3.99	3.07	3.19	3.13
MnO	0.09	0.06	0.05	0.05	0.05	0.05	0.03	0.09	0.05
MgO	2.65	1.05	0.80	0.79	2.12	1.26	1.12	1.84	0.76
CaO	4.06	4.78	4.01	4.62	1.78	5.25	3.87	3.08	3.39
Na_2O	4.54	5.11	5.00	5.26	6.05	4.30	5.04	4.70	5.01
K_2O	0.64	1.17	1.32	1.13	1.03	0.92	1.21	0.78	1.74
P_2O_5	0.21	0.14	0.19	0.12	0.13	0.21	0.18	0.13	0.15
H_2O^-	0.07	0.08	0.04	0.07	0.08	0.05	0.07	0.07	0.03
LOI	1.72	0.89	1.41	0.82	1.89	0.44	0.74	1.42	0.81
Total	100.42	100.17	100.13	100.12	100.45	100.43	100.25	100.20	100.07
CIPW Norms*									
Qz	24.31	21.54	23.24	22.25	21.52	26.98	24.52	28.77	24.32
Co	0.00	0.00	0.01	0.00	2.13	0.00	0.22	2.32	0.37
Or	3.78	6.91	7.80	6.68	6.09	5.44	7.15	4.61	10.28
Pl	55.85	62.06	60.96	63.54	59.17	57.75	60.67	54.20	58.23
(Ab)	38.42	43.24	42.31	44.51	51.19	36.39	42.65	39.77	42.39
(An)	17.43	18.82	18.65	19.03	7.98	21.37	18.02	14.43	15.84
Di	1.05	3.13	0.00	2.44	0.00	2.62	0.00	0.00	0.00
(Wo)	0.56	1.66	-	1.30	-	1.38	-	-	-
(En)	0.44	1.35	-	1.06	-	1.04	-	-	-
(Fs)	0.06	0.12	-	0.09	-	0.20	-	-	-
Hy	6.95	1.38	2.40	0.99	5.61	2.48	3.10	4.94	2.29
(En)	6.16	1.27	1.99	0.91	5.28	2.09	2.79	4.58	1.89
(Fs)	0.79	0.11	0.41	0.08	0.33	0.39	0.31	0.36	0.40
Ol	0.00	0.00	0.00	0.00	0.00	0.00	0.00	0.00	0.00
(Fo)	-	-	-	-	-	-	-	-	-
(Fa)	-	-	-	-	-	-	-	-	-
Mt	4.58	2.62	2.75	2.06	2.58	3.12	2.41	2.49	2.44
Il	1.35	1.08	0.91	0.87	0.93	0.87	0.82	0.93	0.80
Hm	0.00	0.00	0.00	0.00	0.00	0.00	0.00	0.00	0.00
Ap	0.50	0.33	0.45	0.28	0.31	0.50	0.43	0.31	0.36
Trace elements									
Sr	491	677	707	752	604	458	717	477	604
Ba	353	710	717	783	346	589	695	373	826
Rb	6	7	14	6	12	5	10	11	28
U	0.09	0.09	0.11	0.04	0.07	0.05	0.24	0.12	0.07
Th	0.7	0.1	0.1	0.7	0.1	0.1	0.7	0.1	0.1
Zr	205	118	136	129	165	138	119	178	115
Nb	6	4	3	2	2	3	6	2	<2
Y	10	3	5	2	2	8	2	<2	3
Cr	15	24	2	33	13	14	13	19	2
Ni	31	61	5	34	14	21	16	16	5
V	82	59	48	44	47	51	48	57	44

* Total iron expressed as Fe_2O_3; CIPW norms calculated by setting $Fe_2O_3/FeO = 1.2$, after Weaver and Tarney (1980).

Central Block granulites, 60.00 to 69.99% SiO_2.

Sample:	MJ071	MJ047	MJ085	MJ075	MJ044
SiO_2	68.64	68.87	68.95	69.44	69.67
TiO_2	0.48	0.37	0.37	0.38	0.48
Al_2O_3	15.95	15.96	16.30	15.68	15.06
Fe_2O_3*	3.69	3.21	2.59	3.20	3.57
MnO	0.05	0.05	0.06	0.04	0.07
MgO	0.93	1.31	0.75	1.01	1.20
CaO	4.67	3.03	3.68	3.99	4.29
Na_2O	4.18	4.31	4.96	4.32	4.48
K_2O	0.89	1.82	1.03	1.44	0.76
P_2O_5	0.16	0.14	0.11	0.12	0.07
H_2O^-	0.14	0.11	0.06	0.05	0.04
LOI	0.54	0.78	1.23	0.61	0.45
Total	100.32	99.96	100.09	100.28	100.14
CIPW Norms*					
Qz	29.77	28.56	27.32	28.88	30.16
Co	0.00	1.73	0.60	0.05	0.00
Or	5.26	10.75	6.09	8.51	4.49
Pl	57.49	50.59	59.51	55.57	56.65
(Ab)	35.37	36.47	41.97	36.55	37.91
(An)	22.12	14.12	17.54	19.01	18.74
Di	0.00	0.00	0.00	0.00	1.65
(Wo)	-	-	-	-	0.87
(En)	-	-	-	-	0.67
(Fs)	-	-	-	-	0.11
Hy	2.78	3.76	2.18	2.98	2.68
(En)	2.32	3.26	1.87	2.52	2.32
(Fs)	0.47	0.50	0.31	0.46	0.36
Ol	0.00	0.00	0.00	0.00	0.00
(Fo)	-	-	-	-	-
(Fa)	-	-	-	-	-
Mt	2.89	2.50	2.03	2.51	2.78
Il	0.91	0.70	0.70	0.72	0.91
Hm	0.00	0.00	0.00	0.00	0.00
Ap	0.38	0.33	0.26	0.28	0.17
Trace elements					
Sr	407	554	411	377	520
Ba	708	602	1074	743	493
Rb	5	21	8	13	5
U	0.01	0.05	0.03	0.05	0.03
Th	0.1	0.1	0.1	0.1	0.1
Zr	126	111	95	132	75
Nb	2	3	<2	2	4
Y	4	5	<2	6	4
Cr	15	18	7	19	25
Ni	18	17	14	18	23
V	48	51	44	44	73

* Total iron expressed as Fe_2O_3; CIPW norms calculated by setting $Fe_2O_3/FeO = 1.2$, after Weaver and Tarney (1980).

Central Block granulites, greater than 70.00% SiO_2.

Sample:	MJ052	MJ074	MJ056	MJ072	MJ078
SiO_2	70.49	70.62	70.70	71.94	72.57
TiO_2	0.32	0.36	0.29	0.31	0.17
Al_2O_3	15.21	15.56	15.60	14.96	15.91
Fe_2O_3*	2.38	2.89	2.00	2.35	1.24
MnO	0.06	0.04	0.02	0.04	0.05
MgO	0.80	0.94	0.45	0.51	0.26
CaO	2.50	3.33	2.91	3.47	1.87
Na_2O	4.33	4.59	4.65	3.87	5.38
K_2O	3.23	1.22	2.49	2.00	2.43
P_2O_5	0.18	0.12	0.10	0.09	0.03
H_2O^-	0.05	0.05	0.07	0.05	0.03
LOI	0.68	0.74	0.74	0.75	0.55
Total	100.23	100.46	100.02	100.34	100.49
CIPW Norms*					
Qz	26.90	31.05	27.50	33.83	27.67
Co	0.48	0.92	0.20	0.34	1.10
Or	19.09	7.21	14.71	11.82	14.36
Pl	47.87	54.58	53.13	49.37	54.61
(Ab)	36.64	38.84	39.35	32.75	45.52
(An)	11.23	15.74	13.78	16.63	9.08
Di	0.00	0.00	0.00	0.00	0.00
(Wo)	-	-	-	-	-
(En)	-	-	-	-	-
(Fs)	-	-	-	-	-
Hy	1.99	2.34	1.12	1.27	0.65
(En)	1.99	2.34	1.12	1.27	0.65
(Fs)	0.00	0.00	0.00	0.00	0.00
Ol	0.00	0.00	0.00	0.00	0.00
(Fo)	-	-	-	-	-
(Fa)	-	-	-	-	-
Mt	0.72	0.83	0.45	0.65	0.41
Il	0.61	0.68	0.55	0.59	0.32
Hm	1.38	1.72	1.27	1.41	0.70
Ap	0.43	0.28	0.24	0.21	0.07
Trace elements					
Sr	830	400	450	342	569
Ba	774	685	1291	892	947
Rb	42	11	31	17	17
U	0.04	0.12	0.13	0.03	0.01
Th	0.1	0.1	0.2	0.1	0.1
Zr	139	130	83	144	36
Nb	4	3	2	2	<2
Y	7	5	2	3	<2
Cr	3	10	5	2	<2
Ni	3	17	14	13	3
V	35	44	29	29	15

* Total iron expressed as Fe_2O_3; CIPW norms calculated by setting $Fe_2O_3/FeO = 4.2$, after Weaver and Tarney (1980).

Central Block granulites, "anorthosites".

Sample:	MJ058	MJ057
SiO_2	58.21	60.22
TiO_2	0.66	0.06
Al_2O_3	21.46	22.52
Fe_2O_3*	3.32	1.23
MnO	0.06	0.03
MgO	1.59	0.91
CaO	2.55	3.61
Na_2O	7.99	8.03
K_2O	1.79	1.77
P_2O_5	0.14	0.01
H_2O^-	0.08	0.08
LOI	2.32	1.78
Total	100.17	100.25
CIPW Norms*		
Qz	0.00	0.00
Co	2.08	0.85
Or	10.58	10.46
Pl	75.83	81.84
(Ab)	64.09	64.00
(An)	11.74	17.84
Ne	1.91	2.14
Di	0.00	0.00
(Wo)	-	-
(En)	-	-
(Fs)	-	-
Hy	0.00	0.00
(En)	-	-
(Fs)	-	-
Ol	3.60	2.14
(Fo)	2.77	1.59
(Fa)	0.83	0.55
Mt	2.02	0.74
Il	1.25	0.11
Ap	0.33	0.02
Trace elements		
Sr	680	792
Ba	430	599
Rb	19	19
U	0.21	0.02
Th	0.7	0.1
Zr	92	17
Nb	5	<2
Y	2	<2
Cr	36	19
Ni	33	26
V	55	56

* Total iron expressed as Fe_2O_3; CIPW norms calculated by setting $Fe_2O_3/FeO = 0.8$, after Weaver and Tarney (1980).

Glen Dessarry Complex, ultramafics.

Sample:	GD48	GD49
SiO_2	39.80	49.93
TiO_2	2.39	0.77
Al_2O_3	5.52	3.91
Fe_2O_3*	17.75	9.51
MnO	0.28	0.21
MgO	11.43	12.47
CaO	16.99	21.58
Na_2O	0.85	1.31
K_2O	1.75	0.24
P_2O_5	2.12	0.46
H_2O-	0.02	0.03
LOI	0.33	0.21
Total[x]	99.51	100.69
CIPW Norms*		
Qz	0.00	0.00
Co	0.00	0.00
Or	0.00	1.42
Pl	6.08	9.02
(Ab)	-	4.94
(An)	6.08	4.08
Lc	8.11	0.00
Ne	3.90	3.33
Wo	0.00	1.43
Di	51.27	76.35
(Wo)	26.85	40.32
(En)	19.33	31.06
(Fs)	5.09	4.98
Hy	0.00	0.00
(En)	-	-
(Fs)	-	-
Ol	8.26	0.00
(Fo)	6.40	-
(Fa)	1.86	-
Cs	0.02	0.00
Mt	10.77	5.77
Il	4.54	1.46
Ap	5.02	1.09
Trace elements		
Sr	646	419
Ba	1819	118
Rb	67	5
U	2.30	1.30
Th	6.5	5.8
Zr	153	187
Nb	10	4
Y	53	33
Cr	127	121
Ni	117	66
V	391	190

* Total iron expressed as Fe_2O_3; CIPW norms calculated by setting $Fe_2O_3/FeO = 0.8$, after Richardson (1968).
[x] Totals include BaO and SrO.

Glen Dessarry Complex, mafic syenites.

Sample:	GD43	GD42	GD45	MJ012	MJ020	GD44	GD18	GD19	GD31
SiO_2	49.10	51.63	51.80	51.82	51.82	52.60	52.88	53.02	53.32
TiO_2	1.38	1.32	1.23	1.25	1.29	1.15	1.31	1.28	1.18
Al_2O_3	13.47	12.70	14.48	12.00	14.12	14.81	14.24	14.05	14.05
Fe_2O_3*	12.13	10.27	10.16	10.13	10.20	9.55	9.46	9.37	9.42
MnO	0.21	0.19	0.17	0.20	0.21	0.16	0.17	0.18	0.16
MgO	6.11	5.88	4.20	5.84	5.25	3.97	5.00	5.04	4.56
CaO	9.33	8.23	5.96	8.98	7.98	5.58	7.10	6.99	6.99
Na_2O	2.95	3.36	3.98	3.65	3.06	4.02	3.82	3.80	3.49
K_2O	2.25	4.30	4.71	4.20	4.81	4.81	4.50	4.56	4.62
P_2O_5	0.81	0.68	0.97	1.11	0.81	0.91	0.67	0.66	0.70
H_2O-	0.03	0.03	0.04	0.03	0.08	0.05	0.00	0.01	0.02
LOI	0.53	0.49	0.33	0.27	0.28	0.32	0.32	0.30	0.36
Total[x]	98.55	99.49	99.40	100.56	100.55	99.40	99.92	99.71	99.42
CIPW Norms*									
Qz	0.84	0.00	0.00	0.00	0.00	0.00	0.00	0.00	0.00
Co	0.00	0.00	0.00	0.00	0.00	0.00	0.00	0.00	0.00
Or	13.30	25.41	27.83	24.82	28.42	28.42	26.59	26.95	27.30
Pl	41.83	31.80	38.78	28.97	34.54	41.32	37.58	37.26	38.56
(Ab)	24.96	24.93	31.05	25.02	23.95	33.16	29.16	29.44	29.53
(An)	16.87	6.87	7.73	3.96	10.59	8.16	8.42	7.81	9.03
Lc	0.00	0.00	0.00	0.00	0.00	0.00	0.00	0.00	0.00
Ne	0.00	1.90	1.42	3.18	1.05	0.47	1.71	1.47	0.00
Wo	0.00	0.00	0.00	0.00	0.00	0.00	0.00	0.00	0.00
Di	19.02	23.20	12.23	26.23	18.67	10.72	17.62	17.73	16.60
(Wo)	10.07	12.32	6.47	13.92	9.90	5.67	9.36	9.42	8.80
(En)	7.93	9.92	5.05	11.15	7.88	4.42	7.57	7.59	6.98
(Fs)	1.01	0.96	0.72	1.16	0.39	0.63	0.69	0.72	0.82
Hy	8.21	0.00	0.00	0.00	0.00	0.00	0.00	0.00	3.12
(En)	7.28	-	-	-	-	-	-	-	2.79
(Fs)	0.93	-	-	-	-	-	-	-	0.33
Ol	0.00	3.66	4.39	2.65	4.10	4.44	3.77	3.84	1.25
(Fo)	-	3.31	3.79	2.38	3.64	3.83	3.42	3.48	1.11
(Fa)	-	0.35	0.60	0.27	0.46	0.60	0.34	0.36	0.14
Cs	0.00	0.00	0.00	0.00	0.00	0.00	0.00	0.00	0.00
Mt	9.48	8.03	7.95	7.92	7.97	7.47	7.39	7.32	7.37
Il	2.62	2.51	2.34	2.37	2.45	2.18	2.49	2.43	2.24
Ap	1.92	1.61	2.30	2.63	1.92	2.16	1.59	1.56	1.66
Trace elements									
Sr	2648	1719	7078	4686	2948	7393	1957	2039	2626
Ba	2142	1832	4800	4690	2599	5315	1918	1911	2179
Rb	76	106	96	105	109	95	114	117	82
U	6.35	4.45	2.60	1.89	2.95	2.15	4.80	5.00	5.55
Th	28.8	17.7	9.6	9.8	16.2	7.2	19.6	17.7	36.4
Zr	159	345	32	161	197	79	277	289	186
Nb	44	26	17	11	21	14	32	32	34
Y	76	42	35	51	41	29	40	41	39
Cr	150	119	59	118	78	53	91	86	77
Ni	59	48	40	73	44	38	39	38	35
V	259	238	206	209	227	196	206	206	208

* Total iron expressed as Fe_2O_3; CIPW norms calculated by setting $Fe_2O_3/FeO = 1.3$, after Richardson (1968).
[x] Totals include BaO and SrO.

Glen Dessarry Complex, mafic syenites.

Sample:	MJ013	GD20	GD46	GD52	GD27	GD29	MJ026	GD28	MJ015
SiO_2	53.54	53.76	53.77	54.29	56.70	56.88	56.96	57.24	57.28
TiO_2	1.33	1.26	1.25	1.08	0.90	0.86	0.88	0.86	0.87
Al_2O_3	14.50	13.94	14.20	15.58	15.36	15.19	18.74	15.34	16.14
Fe_2O_3*	9.27	9.06	8.75	7.89	6.99	6.84	6.24	6.62	6.31
MnO	0.17	0.17	0.17	0.13	0.15	0.15	0.09	0.20	0.14
MgO	5.12	4.72	4.64	3.96	3.26	3.07	1.49	2.99	3.02
CaO	6.92	6.75	6.48	6.85	5.14	4.79	3.91	4.77	4.75
Na_2O	3.76	3.76	3.96	3.87	3.71	3.08	4.96	3.05	3.58
K_2O	4.61	4.83	5.00	4.44	5.81	7.32	4.99	7.28	6.90
P_2O_5	0.67	0.62	0.62	0.60	0.62	0.58	0.38	0.56	0.61
H_2O^-	0.03	0.02	0.03	0.05	0.04	0.03	0.06	0.03	0.02
LOI	0.34	0.22	0.25	0.47	0.46	0.29	0.19	0.31	0.26
Total[x]	100.70	99.55	99.54	99.76	99.90	99.76	100.26	99.94	100.59
CIPW Norms*									
Qz	0.00	0.00	0.00	0.00	1.19	0.30	0.17	0.94	0.00
Co	0.00	0.00	0.00	0.00	0.00	0.00	0.00	0.00	0.00
Or	27.24	28.54	29.55	26.24	34.33	43.26	29.55	43.02	40.77
Pl	39.34	37.30	35.65	44.77	39.49	32.07	55.75	32.47	37.88
(Ab)	30.27	30.41	29.45	32.75	31.39	26.06	40.87	25.81	30.29
(An)	9.07	6.89	6.20	12.03	8.10	6.00	14.88	6.67	7.59
Lc	0.00	0.00	0.00	0.00	0.00	0.00	0.00	0.00	0.00
Ne	0.84	0.76	2.20	0.00	0.00	0.00	0.00	0.00	0.00
Wo	0.00	0.00	0.00	0.00	0.00	0.00	0.00	0.00	0.00
Di	16.39	17.72	17.20	14.18	10.52	11.02	1.65	10.53	9.44
(Wo)	8.72	9.41	9.14	7.53	5.57	5.83	0.87	5.57	5.01
(En)	7.09	7.59	7.40	6.06	4.40	4.57	0.66	4.35	3.99
(Fs)	0.58	0.72	0.65	0.59	0.54	0.61	0.12	0.61	0.44
Hy	0.00	0.00	0.00	1.99	4.18	3.48	3.66	3.54	1.54
(En)	-	-	-	1.81	3.72	3.07	3.10	3.10	1.39
(Fs)	-	-	-	0.18	0.46	0.41	0.56	0.44	0.15
Ol	4.32	3.22	3.19	1.54	0.00	0.00	0.00	0.00	1.68
(Fo)	3.96	2.92	2.91	1.39	-	-	-	-	1.50
(Fa)	0.36	0.30	0.28	0.15	-	-	-	-	0.18
Cs	0.00	0.00	0.00	0.00	0.00	0.00	0.00	0.00	0.00
Mt	7.25	7.08	6.84	6.16	5.47	5.35	4.87	5.18	4.93
Il	2.53	2.39	2.37	2.05	1.71	1.63	1.67	1.63	1.65
Ap	1.59	1.47	1.47	1.42	1.47	1.37	0.90	1.33	1.44
Trace elements									
Sr	1933	2015	1923	2467	2628	2415	6279	2494	2933
Ba	1933	1795	1717	2320	3993	3492	5582	3562	3264
Rb	117	131	133	103	93	121	83	120	110
U	4.98	4.95	4.85	4.00	1.90	1.70	1.22	1.50	2.04
Th	18.0	15.9	17.6	14.8	8.4	9.2	6.9	9.0	9.3
Zr	308	281	252	385	153	126	71	133	160
Nb	28	28	27	32	14	12	10	14	11
Y	42	37	37	41	37	31	31	34	31
Cr	87	85	81	55	78	67	4	69	56
Ni	42	38	36	23	40	31	10	34	33
V	200	190	188	147	155	146	132	147	130

* Total iron expressed as Fe_2O_3; CIPW norms calculated by setting $Fe_2O_3/FeO = 1.3$, after Richardson (1968).
[x] Totals include BaO and SrO.

Glen Dessarry Complex, mafic syenites.

Sample:	MJ029	GD30	MJ016	MJ024
SiO_2	57.98	59.25	59.31	61.56
TiO_2	0.90	0.62	0.91	0.57
Al_2O_3	16.22	16.28	17.54	17.70
Fe_2O_3*	6.54	5.37	5.82	3.74
MnO	0.11	0.08	0.10	0.07
MgO	2.82	1.75	1.24	0.93
CaO	4.42	3.74	4.02	2.87
Na_2O	4.12	4.27	6.01	5.49
K_2O	5.87	6.47	4.44	5.97
P_2O_5	0.49	0.41	0.31	0.24
H_2O-	0.09	0.03	0.02	0.06
LOI	0.48	0.17	0.07	0.09
Total[x]	100.41	99.60	100.74	100.40
CIPW Norms*				
Qz	1.13	1.91	0.00	1.19
Co	0.00	0.00	0.00	0.00
Or	34.69	38.23	26.24	35.28
Pl	43.29	42.28	58.04	52.48
(Ab)	34.86	36.13	50.27	46.45
(An)	8.43	6.15	7.77	6.02
Lc	0.00	0.00	0.00	0.00
Ne	0.00	0.00	0.32	0.00
Wo	0.00	0.00	0.21	0.00
Di	8.11	7.71	7.63	5.26
(Wo)	4.30	4.06	4.03	2.78
(En)	3.43	3.07	3.09	2.14
(Fs)	0.38	0.58	0.51	0.34
Hy	3.99	1.53	0.00	0.20
(En)	3.60	1.29	-	0.17
(Fs)	0.40	0.24	-	0.03
Ol	0.00	0.00	0.00	0.00
(Fo)	-	-	-	-
(Fa)	-	-	-	-
Cs	0.00	0.00	0.00	0.00
Mt	5.12	4.20	4.55	2.93
Il	1.71	1.18	1.73	1.08
Ap	1.16	0.97	0.73	0.57
Trace elements				
Sr	1694	6097	4887	5373
Ba	1557	3915	3374	4293
Rb	161	99	69	77
U	9.57	1.15	0.90	1.08
Th	34.0	6.1	6.6	5.9
Zr	401	36	88	54
Nb	35	11	15	14
Y	40	27	27	29
Cr	43	24	2	<2
Ni	22	16	7	6
V	109	100	107	74

* Total iron expressed as Fe_2O_3; CIPW norms calculated by setting $Fe_2O_3/FeO = 1.3$, after Richardson (1968).
[x] Totals include BaO and SrO.

Glen Dessarry Complex, leucocratic syenites.

Sample:	IGS 45671	IGS 45670	IGS 42780	MJ001	MJ011	MJ002	IGS 45672	IGS 42778	GD33
SiO_2	58.00	58.88	59.31	59.80	60.08	60.23	60.28	60.61	60.64
TiO_2	0.84	0.72	0.61	0.69	0.59	0.69	0.58	0.67	0.63
Al_2O_3	15.98	16.86	17.42	17.63	16.63	17.83	17.47	17.21	17.13
Fe_2O_3*	6.48	5.72	5.32	4.82	4.58	4.57	4.64	4.98	4.44
MnO	0.13	0.11	0.12	0.10	0.10	0.09	0.09	0.10	0.07
MgO	2.65	1.69	1.39	1.34	1.44	1.32	1.43	1.03	0.81
CaO	4.34	3.52	2.54	2.93	3.34	2.73	3.21	2.98	2.19
Na_2O	3.34	4.04	5.65	4.59	5.06	5.14	5.07	5.26	4.52
K_2O	5.65	5.96	5.68	6.65	6.46	6.36	5.67	6.24	7.69
P_2O_5	0.52	0.41	0.35	0.36	0.42	0.31	0.37	0.28	0.23
H_2O^-	0.05	0.03	0.05	0.03	0.06	0.03	0.03	0.04	0.06
LOI	0.45	0.37	0.36	0.19	0.30	0.20	0.33	0.21	0.19
Total[x]	99.09	99.18	99.66	100.00	100.28	100.38	100.03	100.55	99.51
CIPW Norms*									
Qz	5.79	4.00	0.00	0.84	0.00	0.00	1.75	0.21	0.45
Co	0.00	0.00	0.00	0.00	0.00	0.00	0.00	0.00	0.00
Or	33.39	35.22	33.56	39.30	38.17	37.58	33.51	36.87	45.44
Pl	40.19	44.45	51.94	46.70	45.81	50.29	51.07	49.43	41.99
(Ab)	28.26	34.19	46.54	38.84	42.23	43.49	42.90	44.51	38.25
(An)	11.92	10.27	5.40	7.86	3.58	6.80	8.17	4.92	3.74
Lc	0.00	0.00	0.00	0.00	0.00	0.00	0.00	0.00	0.00
Ne	0.00	0.00	0.69	0.00	0.32	0.00	0.00	0.00	0.00
Wo	0.00	0.00	0.00	0.00	0.00	0.00	0.00	0.00	0.00
Di	4.94	3.62	3.96	3.46	8.20	3.77	4.28	6.49	4.54
(Wo)	2.59	1.89	2.05	1.80	4.28	1.97	2.23	3.35	2.35
(En)	1.90	1.30	1.35	1.25	2.98	1.40	1.55	2.16	1.49
(Fs)	0.45	0.44	0.56	0.40	0.94	0.41	0.50	0.98	0.71
Hy	5.83	3.89	0.00	2.75	0.00	1.16	2.67	0.59	0.78
(En)	4.70	2.91	-	2.08	-	0.90	2.02	0.41	0.53
(Fs)	1.12	0.98	-	0.67	-	0.26	0.66	0.19	0.25
Ol	0.00	0.00	2.17	0.00	0.57	0.92	0.00	0.00	0.00
(Fo)	-	-	1.48	-	0.42	0.70	-	-	-
(Fa)	-	-	0.69	-	0.15	0.22	-	-	-
Cs	0.00	0.00	0.00	0.00	0.00	0.00	0.00	0.00	0.00
Mt	4.67	4.13	3.84	3.48	3.31	3.29	3.35	3.60	3.20
Il	1.60	1.37	1.16	1.31	1.12	1.31	1.10	1.27	1.20
Ap	1.23	0.97	0.83	0.85	0.99	0.73	0.88	0.66	0.54
Trace elements									
Sr	3169	3994	4146	4164	5054	4198	4333	4678	4303
Ba	2543	3544	3269	3383	5524	3434	3110	3508	3551
Rb	92	95	122	106	115	119	116	100	136
U	2.40	1.50	1.10	2.31	2.60	2.03	2.80	1.50	1.45
Th	12.0	12.0	8.4	12.0	11.3	11.3	15.0	8.7	8.3
Zr	134	188	80	222	121	159	104	31	55
Nb	12	24	14	27	18	24	11	20	24
Y	35	28	28	32	34	31	26	32	28
Cr	64	26	10	9	9	6	21	<2	<2
Ni	32	15	13	10	12	11	15	6	7
V	132	118	94	82	97	81	86	79	82

* Total iron expressed as Fe_2O_3; CIPW norms calculated by setting $Fe_2O_3/FeO = 1.1$, after Richardson (1968).
x Totals include BaO and SrO.

Glen Dessarry Complex, leucocratic syenites.

Sample:	MJ010	MJ008	IGS 42774	MJ005	IGS 48474	MJ027	IGS 45660	MJ003	MJ009
SiO_2	60.75	60.78	60.81	61.14	61.19	61.24	61.24	61.28	61.28
TiO_2	0.66	0.61	0.70	0.61	0.62	0.62	0.68	0.60	0.70
Al_2O_3	17.39	17.55	17.44	17.68	17.73	17.78	17.64	17.73	17.38
Fe_2O_3*	4.64	4.18	4.65	4.09	4.46	4.24	4.46	4.03	4.26
MnO	0.08	0.08	0.08	0.08	0.08	0.08	0.06	0.10	0.09
MgO	1.01	1.02	1.00	0.93	0.62	1.03	0.78	0.99	1.08
CaO	2.95	2.77	2.60	2.70	2.46	2.71	2.60	2.96	2.73
Na_2O	5.25	5.39	4.97	5.85	5.00	4.86	4.14	5.59	5.41
K_2O	6.36	6.22	6.14	6.27	6.11	6.25	6.33	6.00	6.05
P_2O_5	0.31	0.30	0.25	0.25	0.20	0.27	0.22	0.26	0.29
H_2O^-	0.02	0.06	0.03	0.02	0.04	0.06	0.04	0.02	0.02
LOI	0.17	0.20	0.17	0.16	0.27	0.12	0.38	0.17	0.16
Total[x]	100.58	100.33	99.85	100.86	99.84	100.52	99.62	100.85	100.42
CIPW Norms*									
Qz	0.08	0.00	2.51	0.00	3.29	2.80	6.56	0.00	1.03
Co	0.00	0.00	0.00	0.00	0.00	0.00	0.00	0.00	0.00
Or	37.58	36.76	36.28	37.05	36.11	36.93	37.41	35.46	35.75
Pl	49.53	50.93	49.20	48.71	50.20	49.36	45.89	52.87	51.05
(Ab)	44.42	45.61	42.05	45.25	42.31	41.12	35.03	47.30	45.78
(An)	5.10	5.32	7.14	3.46	7.89	8.24	10.85	5.57	5.27
Lc	0.00	0.00	0.00	0.00	0.00	0.00	0.00	0.00	0.00
Ne	0.00	0.00	0.00	2.30	0.00	0.00	0.00	0.00	0.00
Wo	0.00	0.00	0.00	0.03	0.00	0.00	0.00	0.00	0.00
Di	6.04	5.18	3.31	6.62	2.45	2.76	0.49	5.96	5.10
(Wo)	3.14	2.70	1.72	3.44	1.26	1.44	0.25	3.10	2.66
(En)	2.08	1.84	1.16	2.32	0.73	0.98	0.16	2.10	1.87
(Fs)	0.83	0.65	0.44	0.36	0.47	0.35	0.07	0.75	0.56
Hy	0.61	0.95	1.84	0.00	1.35	2.15	2.57	0.20	1.06
(En)	0.44	0.70	1.34	-	0.82	1.59	1.78	0.15	0.81
(Fs)	0.18	0.25	0.50	-	0.53	0.56	0.79	0.05	0.24
Ol	0.00	0.00	0.00	0.00	0.00	0.00	0.00	0.21	0.00
(Fo)	-	-	-	-	-	-	-	0.15	-
(Fa)	-	-	-	-	-	-	-	0.06	-
Cs	0.00	0.00	0.00	0.00	0.00	0.00	0.00	0.00	0.00
Mt	3.35	3.02	3.35	2.94	3.22	3.06	3.22	2.90	3.07
Il	1.25	1.16	1.33	1.16	1.18	1.18	1.29	1.14	1.33
Ap	0.73	0.71	0.59	0.59	0.47	0.64	0.52	0.62	0.69
Trace elements									
Sr	4930	5718	5077	5281	5377	5465	5380	5530	4308
Ba	3676	4417	3664	4093	3773	5451	3749	4189	4083
Rb	125	98	98	97	94	79	93	81	120
U	1.85	1.26	1.30	1.27	1.20	1.06	1.30	1.18	1.68
Th	10.0	7.0	8.6	6.3	8.2	7.3	7.4	6.2	7.4
Zr	104	64	42	66	12	60	12	67	82
Nb	20	15	23	15	18	15	20	15	20
Y	27	27	32	27	28	25	32	31	29
Cr	<2	<2	<2	15	<2	<2	<2	<2	<2
Ni	7	6	7	6	5	7	6	6	7
V	79	78	87	81	87	86	95	80	88

* Total iron expressed as Fe_2O_3; CIPW norms calculated by setting $Fe_2O_3/FeO = 1.1$, after Richardson (1968).
[x] Totals include BaO and SrO.

Glen Dessarry Complex, leucocratic syenites.

Sample:	IGS 45662	MJ006	IGS 42781
SiO_2	61.45	61.99	62.05
TiO_2	0.71	0.48	0.59
Al_2O_3	17.40	18.35	18.12
Fe_2O_3*	4.72	3.21	3.26
MnO	0.08	0.06	0.04
MgO	0.87	0.62	0.42
CaO	2.85	2.05	1.70
Na_2O	4.78	5.88	5.31
K_2O	6.18	6.40	6.59
P_2O_5	0.28	0.20	0.12
H_2O^-	0.03	0.01	0.04
LOI	0.34	0.15	0.32
Total[x]	100.56	100.59	99.76
CIPW Norms*			
Qz	3.93	0.00	2.13
Co	0.00	0.00	0.00
Or	36.52	37.82	38.94
Pl	48.22	52.99	51.08
(Ab)	40.45	48.22	44.93
(An)	7.77	4.77	6.14
Lc	0.00	0.00	0.00
Ne	0.00	0.83	0.00
Wo	0.00	0.00	0.00
Di	3.66	3.30	1.21
(Wo)	1.90	1.71	0.63
(En)	1.23	1.11	0.41
(Fs)	0.54	0.48	0.18
Hy	1.35	0.00	0.92
(En)	0.94	-	0.64
(Fs)	0.41	-	0.28
Ol	0.00	0.44	0.00
(Fo)	-	0.30	-
(Fa)	-	0.14	-
Cs	0.00	0.00	0.00
Mt	3.41	2.32	2.35
Il	1.35	0.91	1.12
Ap	0.66	0.47	0.28
Trace elements			
Sr	4073	5933	6190
Ba	3496	4330	4218
Rb	92	101	124
U	1.90	1.31	1.80
Th	9.2	4.9	9.7
Zr	70	46	44
Nb	27	12	27
Y	37	22	28
Cr	<2	<2	<2
Ni	6	3	4
V	95	63	68

* Total iron expressed as Fe_2O_3; CIPW norms calculated by setting $Fe_2O_3/FeO = 1.1$, after Richardson (1968).
[x] Totals include BaO and SrO.

Glen Dessarry Complex, pegmatites.

Sample:	GD13	GD34	GD35	GD32
SiO_2	64.98	67.29	68.43	72.21
TiO_2	0.06	0.02	0.07	0.04
Al_2O_3	19.95	19.51	17.49	15.76
Fe_2O_3*	0.63	0.20	1.13	0.55
MnO	0.00	0.00	0.01	0.00
MgO	0.11	0.00	0.05	0.00
CaO	2.13	1.90	2.04	1.65
Na_2O	7.51	9.35	6.78	5.96
K_2O	3.73	1.01	2.76	3.31
P_2O_5	0.19	0.07	0.10	0.07
H_2O^-	0.05	0.06	0.04	0.02
LOI	0.36	0.23	0.15	0.14
Total[x]	100.15	100.06	99.25	99.87
CIPW Norms*				
Qz	2.55	5.23	13.80	21.56
Co	0.14	0.00	0.00	0.00
Or	22.04	5.97	16.31	19.56
Pl	72.87	87.40	66.51	56.91
(Ab)	63.55	79.12	57.37	50.43
(An)	9.33	8.28	9.14	6.47
Lc	0.00	0.00	0.00	0.00
Ne	0.00	0.00	0.00	0.00
Wo	0.00	0.12	0.00	0.04
Di	0.00	0.36	0.29	1.04
(Wo)	-	0.17	0.14	0.49
(En)	-	0.00	0.01	0.00
(Fs)	-	0.19	0.14	0.55
Hy	0.89	0.00	1.15	0.00
(En)	0.27	-	0.11	-
(Fs)	0.62	-	1.04	-
Ol	0.00	0.00	0.00	0.00
(Fo)	-	-	-	-
(Fa)	-	-	-	-
Cs	0.00	0.00	0.00	0.00
Mt	0.19	0.06	0.35	0.17
Il	0.11	0.04	0.13	0.08
Ap	0.45	0.17	0.24	0.17
Trace elements				
Sr	2530	3318	1038	726
Ba	1373	257	651	630
Rb	83	17	56	78
U	0.60	0.30	0.70	0.70
Th	6.4	0.8	4.8	2.9
Zr	<2	<2	25	28
Nb	2	<2	8	3
Y	14	6	34	13
Cr	<2	<2	<2	<2
Ni	<2	<2	<2	<2
V	7	<2	5	2

* Total iron expressed as Fe_2O_3; CIPW norms calculated by setting $Fe_2O_3/FeO = 0.3$, after Richardson (1968).
[x] Totals include BaO and SrO.

Glen Dessarry Complex, Moine metasediments.

Sample:	GD3	MJ019	GD6	GD1	GD2
SiO_2	68.15	70.39	72.24	73.26	74.31
TiO_2	0.86	0.81	0.74	0.78	0.70
Al_2O_3	14.69	13.65	13.31	12.20	12.01
Fe_2O_3*	4.38	5.73	3.45	3.45	3.01
MnO	0.06	0.11	0.02	0.08	0.05
MgO	1.21	1.55	0.84	0.93	0.92
CaO	1.97	1.66	1.94	1.81	1.18
Na_2O	3.33	2.56	2.56	3.04	2.47
K_2O	4.21	2.81	3.69	3.81	4.66
P_2O_5	0.08	0.08	0.08	0.06	0.05
H_2O-	0.02	0.04	0.04	0.06	0.03
LOI	0.46	1.06	0.73	0.44	0.38
Total	99.42	100.45	99.64	99.92	99.77
CIPW Norms*					
Qz	25.11	36.53	36.72	34.60	37.22
Co	1.26	3.57	1.77	0.00	0.88
Or	24.88	16.61	21.81	22.51	27.54
Pl	37.43	29.37	30.76	34.11	26.43
(Ab)	28.18	21.66	21.66	25.72	20.90
(An)	9.25	7.71	9.10	8.39	5.53
Lc	0.00	0.00	0.00	0.00	0.00
Ne	0.00	0.00	0.00	0.00	0.00
Wo	0.00	0.00	0.00	0.00	0.00
Di	0.00	0.00	0.00	0.16	0.00
(Wo)	-	-	-	0.08	-
(En)	-	-	-	0.04	-
(Fs)	-	-	-	0.05	-
Hy	6.88	9.50	5.00	5.19	4.78
(En)	3.01	3.86	2.09	2.28	2.29
(Fs)	3.86	5.64	2.91	2.91	2.49
Ol	0.00	0.00	0.00	0.00	0.00
(Fo)	-	-	-	-	-
(Fa)	-	-	-	-	-
Cs	0.00	0.00	0.00	0.00	0.00
Mt	1.20	1.58	0.94	0.94	0.83
Il	1.63	1.54	1.41	1.48	1.33
Ap	0.19	0.19	0.19	0.14	0.12
Trace elements					
Sr	296	292	314	291	308
Ba	1039	532	1053	1019	1253
Rb	153	96	127	133	140
U	2.70	2.43	2.00	8.50	2.40
Th	12.6	17.0	10.1	20.3	11.7
Zr	405	360	398	632	570
Nb	17	18	17	19	17
Y	41	51	41	99	32
Cr	39	44	28	29	23
Ni	24	25	12	11	7
V	62	54	50	51	47

* Total iron expressed as Fe_2O_3; CIPW norms calculated by setting $Fe_2O_3/FeO = 0.26$, after Butler (1965).

Glen Dessarry Complex, "fenitised" Moine.

Sample:	MJ018	MJ014	GD7	GD8	GD39	MJ023	GD40	GD41
SiO_2	62.80	63.57	64.12	64.45	64.82	66.12	76.68	79.00
TiO_2	1.67	1.18	0.64	0.72	0.47	1.20	0.73	0.44
Al_2O_3	17.61	16.20	17.93	17.96	17.97	16.50	11.01	10.51
Fe_2O_3*	3.36	6.49	2.26	2.60	1.79	6.26	2.10	1.59
MnO	0.08	0.09	0.03	0.03	0.01	0.08	0.01	0.02
MgO	0.73	1.79	0.34	0.53	0.31	1.66	0.41	0.21
CaO	1.88	1.64	1.08	1.28	0.97	1.24	0.96	0.79
Na_2O	6.43	3.99	6.27	6.82	5.97	2.22	2.27	2.10
K_2O	4.95	4.05	6.14	5.38	6.40	3.54	4.59	4.36
P_2O_5	0.21	0.05	0.13	0.14	0.13	0.06	0.06	0.07
H_2O-	0.08	0.02	0.17	0.03	0.05	0.10	0.06	0.03
LOI	0.45	0.74	0.59	0.30	0.36	1.42	0.35	0.39
Total	100.25	99.81	99.65	100.24	99.25	100.40	99.23	99.51
CIPW Norms*								
Qz	2.04	16.14	1.39	0.80	2.94	32.17	42.82	47.75
Co	0.00	2.39	0.00	0.00	0.00	6.91	0.71	1.07
Or	29.25	23.93	36.28	31.79	37.82	20.92	27.12	25.76
Pl	58.98	41.57	55.70	60.21	53.85	24.54	23.58	21.23
(Ab)	54.41	33.76	53.05	57.71	50.52	18.79	19.21	17.77
(An)	4.57	7.81	2.65	2.50	3.33	5.76	4.37	3.46
Lc	0.00	0.00	0.00	0.00	0.00	0.00	0.00	0.00
Ne	0.00	0.00	0.00	0.00	0.00	0.00	0.00	0.00
Wo	0.00	0.00	0.00	0.00	0.00	0.00	0.00	0.00
Di	2.77	0.00	1.37	2.46	0.53	0.00	0.00	0.00
(Wo)	1.41	-	0.67	1.22	0.26	-	-	-
(En)	0.78	-	0.23	0.50	0.10	-	-	-
(Fs)	0.58	-	0.46	0.74	0.17	-	-	-
Hy	1.82	10.35	1.83	2.04	1.87	9.69	2.31	1.72
(En)	1.04	4.46	0.61	0.82	0.68	4.13	1.02	0.52
(Fs)	0.78	5.89	1.21	1.21	1.20	5.56	1.29	1.19
Ol	0.00	0.00	0.00	0.00	0.00	0.00	0.00	0.00
(Fo)	-	-	-	-	-	-	-	-
(Fa)	-	-	-	-	-	-	-	-
Cs	0.00	0.00	0.00	0.00	0.00	0.00	0.00	0.00
Mt	0.93	1.78	0.62	0.71	0.49	1.73	0.58	0.43
Il	3.17	2.24	1.22	1.37	0.89	2.28	1.39	0.84
Ap	0.50	0.12	0.31	0.33	0.31	0.14	0.14	0.17
Trace elements								
Sr	386	583	630	515	538	375	247	345
Ba	822	977	708	721	723	902	1321	1072
Rb	102	124	102	117	91	78	126	117
U	7.06	8.16	2.15	5.25	1.45	3.35	1.45	1.20
Th	32.0	35.0	8.0	21.1	4.3	10.2	7.1	7.0
Zr	938	647	446	399	96	586	561	323
Nb	89	34	32	65	19	26	17	8
Y	69	53	22	31	16	58	23	32
Cr	11	71	<2	5	<2	89	10	6
Ni	6	26	3	4	2	21	5	4
V	59	179	43	50	40	108	29	20

* Total iron expressed as Fe_2O_3; CIPW norms calculated by setting $Fe_2O_3/FeO = 0.26$, after Butler (1965).

Glen Dessarry Complex, vein/xenolith reaction.

Sample:	GD24	GD22	IGS 45642
SiO_2	56.87	58.27	61.66
TiO_2	0.88	1.00	0.48
Al_2O_3	15.21	13.40	18.73
Fe_2O_3*	6.70	7.56	5.09
MnO	0.13	0.18	0.06
MgO	3.21	4.11	0.84
CaO	4.87	6.39	1.02
Na_2O	3.61	2.48	4.26
K_2O	4.95	4.90	5.60
P_2O_5	0.51	0.66	0.07
H_2O^-	0.26	0.04	0.07
LOI	1.96	0.34	1.02
Total[x]	99.76	99.91	99.42
CIPW Norms*			
Qz	4.92	10.19	11.79
Co	0.00	0.00	3.97
Or	29.25	28.96	33.09
Pl	41.23	31.94	40.65
(Ab)	30.55	20.99	36.05
(An)	10.68	10.96	4.60
Lc	0.00	0.00	0.00
Ne	0.00	0.00	0.00
Wo	0.00	0.00	0.00
Di	7.99	12.93	0.00
(Wo)	4.24	6.86	-
(En)	3.37	5.49	-
(Fs)	0.38	0.58	-
Hy	5.15	5.25	3.02
(En)	4.62	4.75	2.09
(Fs)	0.53	0.50	0.93
Ol	0.00	0.00	0.00
(Fo)	-	-	-
(Fa)	-	-	-
Cs	0.00	0.00	0.00
Mt	5.23	5.92	3.97
Il	1.67	1.90	0.91
Ap	1.21	1.56	0.17
Trace elements			
Sr	2659	2525	2309
Ba	2512	2559	2249
Rb	109	81	113
U	4.80	2.70	7.80
Th	17.8	6.6	138
Zr	305	76	143
Nb	28	21	10
Y	40	54	18
Cr	54	74	7
Ni	30	38	6
V	152	178	57

* Total iron expressed as Fe_2O_3; CIPW norms calculated by setting $Fe_2O_3/FeO = 1.3$, after Richardson (1968).
[x] Totals include BaO and SrO.

Gruinard Bay gneisses, 50.00 to 59.99% SiO_2.

	MJ128	MJ130	MJ131	MJ129	MJ181	MJ179
La	127	64	110	48	29	26
Ce	222	115	218	96	51	49
Nd	79	58	115	49	31	25
Sm	13	16	19	10	4.4	5.7
Eu	3.0	2.1	2.1	1.9	1.2	1.5
Tb	1.2	1.3	1.8	-	-	-
Dy	5.1	6.1	-	3.9	1.6	2.0
Yb	2.0	2.0	2.3	2.2	1.0	1.3
Lu	0.32	0.29	0.35	0.26	0.14	0.18
Hf	3.5	2.2	4.0	1.9	2.6	3.1

Gruinard Bay gneisses, 60.00 to 69.99% SiO_2.

	MJ150	MJ126	MJ134	MJ178	MJ149
La	23	37	29	35	22
Ce	39	59	39	52	33
Nd	12	17	16	15	9.6
Sm	1.3	3.6	-	3.1	1.2
Eu	0.93	1.2	1.1	1.1	0.90
Tb	-	0.42	-	-	-
Dy	0.68	1.9	2.2	1.3	0.52
Yb	0.41	0.63	0.87	0.50	0.30
Lu	-	0.11	0.12	0.08	-
Hf	4.5	3.8	1.6	4.4	3.6

Gruinard Bay gneisses, greater than 70.00% SiO_2.

	MJ183	MJ117	MJ118	MJ115	MJ144
La	24	33	75	19	16
Ce	34	47	107	23	31
Pr	3.2	4.2	9.2	1.8	-
Nd	12	14	31	5.4	11
Sm	1.3	1.3	2.6	0.47	1.1
Eu	0.75	0.90	1.1	0.65	0.65
Gd	0.81	0.80	1.1	0.65	0.65
Dy	0.38	0.35	0.34	0.14	0.34
Er	0.14	0.15	0.12	0.08	-
Yb	0.17	0.20	0.16	0.08	0.39
Lu	0.03	0.04	0.03	0.02	0.07
Hf	4.2	5.6	4.2	0.5	11.5

Gruinard Bay, "anorthosites".

	MJ198	MJ197	MJ199	MJ190
La	20	21	17	44
Ce	-	46	37	88
Nd	18	19	13	37
Sm	4.5	3.9	3.1	7.8
Eu	1.6	1.2	1.4	1.6
Tb	0.44	-	0.28	-
Dy	2.3	1.7	1.3	3.5
Yb	-	0.48	0.76	0.98
Lu	0.14	-	0.10	-

Central Block granulites, 50.00 to 59.99% SiO_2.

	MJ080	MJ053	MJ073
La	21	20	22
Ce	50	48	52
Nd	19	21	23
Sm	4.6	4.2	4.9
Eu	1.4	1.6	1.6
Dy	4.3	2.0	2.8
Yb	3.0	1.2	1.3
Lu	0.44	-	0.20
Hf	1.9	3.1	1.9

Central Block granulites, 60.00 to 60.99% SiO_2.

	MJ040	MJ079	MJ054	MJ075
La	21	20	21	21
Ce	50	42	40	43
Nd	22	18	13	14
Sm	4.4	3.6	1.8	2.6
Eu	1.5	1.2	1.6	1.3
Tb	-	-	0.25	-
Dy	2.3	2.6	-	-
Yb	1.4	-	0.32	0.62
Lu	0.20	0.22	-	-
Hf	2.6	3.7	2.9	3.6

Central Block granulites, greater than 70.00% SiO_2.

	MJ072	MJ078
La	16	7.4
Ce	22	12
Nd	7.0	4.0
Sm	1.3	0.47
Eu	0.8	0.61
Tb	-	-
Dy	-	-
Yb	0.19	0.14
Lu	0.03	-
Hf	3.2	0.47

Glen Dessarry Complex, ultramafics.

	GD48	GD49
La	130	44.4
Ce	246	90.2
Pr	29.2	11.8
Nd	136	58.4
Sm	21.3	10.7
Eu	5.38	2.82
Gd	16.4	8.55
Dy	10.4	6.10
Er	4.81	2.87
Yb	3.93	2.62
Lu	0.58	0.41
Hf	-	5.6
Ta	-	0.3

Glen Dessarry Complex, mafic syenites.

	GD43	GD44	GD31	MJ013	GD46	GD52	GD27
La	83.2	81.6	96.0	86.0	88.0	99.9	100
Ce	162	145	168	180	136	163	180
Pr	20.5	16.9	18.2	-	-	17.3	19.6
Nd	101	75.4	79.2	-	39.0	71.7	84.1
Sm	19.1	11.4	12.7	13.0	14.0	11.0	12.9
Eu	3.53	3.62	3.41	3.80	3.50	2.87	4.06
Gd	16.2	8.38	9.57	-	-	8.50	9.35
Tb	-	-	-	1.10	1.30	-	-
Dy	13.1	5.20	6.54	6.60	5.70	6.38	6.32
Er	6.61	2.38	3.28	-	-	3.40	3.14
Yb	5.48	2.04	3.06	2.30	2.80	3.25	3.08
Lu	0.76	0.29	0.45	-	0.45	0.48	0.46
Hf	5.9	2.7	5.4	7.7	6.6	9.6	4.8
Ta	1.5	0.76	1.2	1.7	1.7	1.2	0.54

	GD28	MJ029	GD30
La	95.4	92.0	86.2
Ce	173	215	157
Pr	18.0	-	17.7
Nd	75.7	-	76.4
Sm	11.4	11.0	11.2
Eu	3.97	3.10	3.35
Gd	8.38	-	7.68
Tb	-	1.40	-
Dy	5.72	5.70	4.75
Er	2.91	-	2.11
Yb	2.84	3.10	1.79
Lu	0.42	-	0.26
Hf	4.7	10.0	2.8
Ta	0.75	1.8	1.1

Glen Dessarry Complex, leucocratic syenites.

	MJ001	MJ002	MJ005	MJ009	MJ006
La	98.1	98.5	87.0	82.1	63.2
Ce	193	186	151	166	114
Pr	20.7	20.0	17.0	18.1	12.8
Nd	87.5	82.9	73.2	77.1	53.7
Sm	13.0	12.4	11.2	11.8	8.21
Eu	3.56	3.42	3.37	3.36	2.75
Gd	9.32	8.56	7.79	8.38	5.76
Dy	5.77	5.28	4.81	5.31	3.63
Er	2.69	2.46	2.24	2.45	1.69
Yb	2.45	2.23	1.84	2.12	1.46
Lu	0.36	0.33	0.26	0.31	0.21
Hf	5.9	4.5	2.2	2.5	1.5
Ta	2.2	1.9	1.4	1.5	1.1

Glen Dessarry Complex, pegmatites.

	GD13	GD34	GD35	GD32
La	52.1	3.97	32.5	8.46
Ce	96.3	7.26	60.3	23.9
Pr	9.80	0.83	6.51	1.95
Nd	39.5	3.67	28.2	8.24
Sm	6.09	0.88	5.45	2.06
Eu	1.28	0.41	1.19	0.51
Gd	4.12	0.95	4.96	1.83
Dy	2.42	1.01	4.75	1.65
Er	0.97	0.54	2.59	0.96
Yb	0.83	0.47	2.31	0.99
Lu	0.12	0.07	0.32	0.15
Hf	0.17	0.11	0.36	0.82
Ta	0.28	0.18	0.38	0.20

Glen Dessarry Complex, Moine metasediments.

	GD3	MJ019	GD1	GD2	GD7	MJ018	GD8
La	50.4	57.0	75.0	42.7	50.0	-	69.4
Ce	103	135	155	83.2	87.0	355	139
Pr	11.2	-	-	9.42	-	-	13.4
Nd	51.8	60.0	-	41.9	32.0	105	54.5
Sm	10.1	11.0	17.0	7.68	6.40	11.0	8.91
Eu	2.10	2.00	2.50	1.72	2.20	4.80	2.33
Gd	8.97	-	-	6.40	-	-	6.35
Tb	-	1.60	2.70	-	-	-	-
Dy	6.76	-	-	5.10	2.80	11.0	4.88
Er	3.09	-	-	2.91	-	-	2.53
Yb	2.58	5.30	11.0	3.02	1.90	-	2.43
Lu	0.40	0.89	1.60	0.50	0.26	0.89	0.35
Hf	11.5	11.0	19.0	16.6	9.1	24.0	9.2
Ta	0.77	0.89	1.7	0.82	1.7	0.89	3.76

Glen Dessarry Complex, Moine metasediments.

	GD39	GD40
La	35.9	24.9
Ce	61.7	50.4
Pr	6.32	5.56
Nd	27.1	25.1
Sm	4.35	4.85
Eu	1.59	1.45
Gd	3.16	4.06
Dy	2.28	3.16
Er	1.13	1.72
Yb	1.07	1.72
Lu	0.17	0.29
Hf	2.1	19.2
Ta	0.77	0.81

Glen Dessarry Complex, Vein/Xenolith Reaction.

	GD24	GD22	IGS 45642
La	96.8	82.4	260
Ce	163	150	490
Pr	17.6	17.8	-
Nd	74.4	82.3	160
Sm	11.2	14.4	26.0
Eu	3.04	3.25	3.40
Gd	8.39	11.7	-
Dy	6.02	8.88	4.40
Er	3.05	4.40	-
Yb	2.91	3.84	0.54
Lu	0.44	0.54	-
Hf	7.3	2.7	3.8
Ta	1.1	0.88	1.9

Oxygen isotopes.

Sample	$\delta^{18}O$	
GD49	+7.1	pyroxenite
GD29	+7.9	
GD46	+7.7	mafic
MJ013	+7.7	syenites
MJ015	+9.1	
GD33	+8.8	leucocratic
MJ001	+8.2	syenites
MJ002	+8.6	
GD34	+8.5	pegmatites
GD35	+9.3	
GD1	+8.1	
GD3	+9.4	Moine
GD7	+9.6	
GD29H	+6.5	amphiboles
MJ015H	+6.2	

Density determinations.

Sample Number	MJ003	MJ005	MJ008	MJ027
Value	2.762	2.745	2.746	2.745

A.2: MINERAL ANALYSES.

Electron probe microanalysis.

The majority of mineral analyses were performed on a Cambridge Instruments Microscan 5 electron probe, fitted with a Link Systems energy dispersive detector. Operating conditions were 15 KV with a specimen current of 4.0 or 3.5 nA, the latter for alkali feldspars to avoid Na loss during analysis. The calibration was erected against a variety of pure metals, metal oxides and end-member minerals. Accuracy and precision were routinely monitored by reference to standard minerals and can be adjudged from the typical standard data listed in Table A.5.

Zirconolite was analysed on a Cambridge Instruments Microscan 9 electron probe at the British Museum (Natural History), using a wavelength dispersive technique. Pure metals or metal oxides were used as standards.

	Peridot					
SiO_2	40.37	40.70	40.64	40.17	40.54	40.85
FeO	8.99	8.89	8.76	8.91	9.19	8.49
MnO	0.19	0.19	0.12	0.22	0.16	0.17
MgO	50.05	50.23	50.08	49.78	49.65	50.18
CaO	0.12	0.03	0.11	0.13	0.13	0.02
Na_2O	0.49	0.37	0.74	0.62	0.03	0.67
NiO	0.35	0.42	0.35	0.32	0.44	0.42
Total	100.56	100.83	100.80	100.15	100.14	100.80
	Jadeite					
SiO_2	59.32	58.91	58.71	58.55	58.79	59.08
Al_2O_3	25.33	24.74	25.27	24.88	24.15	24.45
MgO	0.26	0.36	0.48	0.63	0.68	0.22
CaO	0.19	0.26	0.42	0.49	0.85	0.43
Na_2O	15.38	15.06	15.28	15.16	14.88	14.99
Total	100.48	99.33	100.16	99.71	99.35	99.17

Table A.5: Typical peridot and jadeite probe standard analyses.

Ion probe microanalysis.

Secondary-ion mass spectrometry was used to measure LREE, U and Th concentrations in accessory minerals in the Glen Dessarry syenite. All measurements were made on an A.E.I. IM20 ion probe, incorporating a MS 702R mass spectrometer, at the University of Cambridge (Hinton and Long, 1979).

Variations in count rates were monitored by reference to Ti (sphene) and Ca (apatite) counts. Semi-quantification was acheived merely by using electron probe data for Ce in sphene, and by analysing a sample of allanite (whose LREE content is also known from EPMA) and assuming negligible matrix effects and similar ion-yields for each element.

Fission track analysis.

Fission track analysis was carried out through the internal facilities of the B.G.S. (Bowie et al., 1973). Polished thin sections were taped to discs of Lexan polycarbonate plastic, and loaded in pure aluminium cannisters. These were irradiated at an integrated neutron dose of 5×10^{16} ncm^{-2}, using the HERALD reactor facility at A.W.R.E., Aldermaston. After a suitable cooling period, detector discs were etched in 6N NaOH at 70°C for about 10 minutes.

Glen Dessarry syenite, clinopyroxenes.

	GD48 (ultramafic)							
SiO_2	51.38	50.69	50.88	49.95	49.79	51.07	51.49	50.71
TiO_2	0.69	0.71	0.65	0.79	0.77	0.69	0.55	0.94
Al_2O_3	2.55	2.78	2.55	4.38	4.54	3.28	2.15	3.23
FeO	7.53	7.26	7.55	7.50	7.32	7.94	7.94	8.55
MnO	0.42	0.29	0.26	0.39	0.29	-	0.38	-
MgO	12.99	13.15	13.13	12.69	12.51	13.24	13.32	12.51
CaO	22.61	22.83	22.72	22.36	22.37	22.65	22.72	22.27
Na_2O	1.24	1.37	1.39	1.56	1.41	1.65	1.35	1.61
Total	99.41	99.08	99.13	99.62	99.00	100.52	99.90	99.82
Si	1.930	1.912	1.920	1.875	1.878	1.901	1.930	1.904
Al	0.070	0.088	0.080	0.125	0.122	0.099	0.070	0.096
Al	0.043	0.036	0.033	0.069	0.079	0.044	0.025	0.047
Ti	0.019	0.020	0.018	0.022	0.022	0.019	0.016	0.027
Fe	0.237	0.229	0.238	0.235	0.231	0.247	0.249	0.269
Mg	0.727	0.739	0.738	0.710	0.703	0.734	0.744	0.700
Mn	0.013	0.009	0.008	0.012	0.009	-	0.012	-
Ca	0.910	0.923	0.918	0.899	0.904	0.903	0.912	0.896
Na	0.090	0.100	0.102	0.114	0.103	0.119	0.098	0.117

	GD30 (mafic syenite)							
SiO_2	52.28	51.93	52.47	52.21	51.29	52.26	52.05	51.96
TiO_2	-	-	-	-	-	-	-	-
Al_2O_3	1.07	1.12	1.11	1.13	1.89	0.93	1.65	0.98
FeO	11.24	11.25	10.81	11.16	11.33	10.84	11.57	11.18
MnO	0.59	0.67	0.60	0.54	0.58	0.67	0.59	0.62
MgO	11.19	11.21	11.21	11.40	10.81	11.25	10.58	10.98
CaO	22.50	22.38	22.57	22.27	21.64	22.06	21.69	22.45
Na_2O	1.49	1.59	1.60	1.49	2.04	1.70	1.76	1.32
Total	100.36	100.15	100.37	100.20	99.58	99.71	99.89	99.49
Si	1.978	1.971	1.981	1.976	1.958	1.986	1.978	1.983
Al	0.022	0.029	0.019	0.024	0.042	0.014	0.022	0.017
Al	0.026	0.022	0.031	0.027	0.043	0.028	0.052	0.027
Ti	-	-	-	-	-	-	-	-
Fe	0.356	0.357	0.341	0.353	0.362	0.345	0.368	0.357
Mg	0.631	0.634	0.631	0.643	0.615	0.637	0.599	0.625
Mn	0.019	0.022	0.019	0.017	0.019	0.022	0.019	0.020
Ca	0.912	0.910	0.913	0.903	0.885	0.898	0.883	0.918
Na	0.109	0.117	0.117	0.109	0.151	0.125	0.130	0.098

Glen Dessarry syenite, clinopyroxenes.

	MJ003 (deformed leucocratic syenite)							
SiO_2	51.62	51.24	52.13	51.91	51.71	52.04	51.92	52.22
TiO_2	-	-	-	-	-	0.27	0.14	0.22
Al_2O_3	1.77	1.84	1.87	1.56	1.90	2.23	1.69	2.19
FeO	12.14	12.17	12.01	11.92	11.74	11.28	11.78	12.17
MnO	0.73	0.73	0.60	0.61	0.79	0.64	0.64	0.55
MgO	10.28	10.33	10.69	10.68	10.77	10.51	10.81	10.25
CaO	20.89	20.60	20.60	21.15	21.94	20.94	21.60	20.77
Na_2O	2.24	2.47	2.23	2.29	1.64	2.29	2.23	2.59
Total	99.67	99.38	100.13	100.12	100.49	100.20	100.81	100.96
Si	1.973	1.966	1.976	1.973	1.959	1.967	1.961	1.967
Al	0.027	0.034	0.024	0.027	0.041	0.033	0.039	0.033
Al	0.052	0.049	0.060	0.043	0.043	0.067	0.036	0.064
Ti	-	-	-	-	-	0.008	0.004	0.006
Fe	0.388	0.390	0.381	0.379	0.372	0.357	0.372	0.383
Mg	0.586	0.591	0.604	0.605	0.608	0.592	0.609	0.575
Mn	0.024	0.024	0.019	0.020	0.025	0.020	0.020	0.018
Ca	0.855	0.847	0.837	0.861	0.890	0.848	0.874	0.838
Na	0.166	0.184	0.164	0.169	0.120	0.168	0.163	0.189

	MJ003	MJ008 (undeformed leucocratic syenite)						
SiO_2	51.95	51.33	51.42	51.81	52.37	51.93	51.72	51.12
TiO_2	0.19	-	-	-	-	-	-	0.22
Al_2O_3	1.54	1.47	1.16	0.83	1.00	1.03	1.20	1.39
FeO	11.65	11.92	12.49	11.86	12.28	12.58	12.43	13.48
MnO	0.54	0.78	0.77	0.78	0.72	0.64	0.74	0.78
MgO	10.52	10.61	10.24	10.76	10.79	10.06	10.30	9.55
CaO	21.16	20.93	21.42	22.06	22.10	20.31	21.18	20.20
Na_2O	2.30	2.30	1.71	1.68	1.73	2.48	2.12	2.47
Total	99.85	99.34	99.21	99.78	100.99	99.03	99.69	99.21
Si	1.977	1.970	1.979	1.980	1.978	1.999	1.981	1.976
Al	0.023	0.030	0.021	0.020	0.022	0.001	0.019	0.024
Al	0.046	0.036	0.032	0.018	0.023	0.045	0.035	0.039
Ti	0.005	-	-	-	-	-	-	0.006
Fe	0.371	0.383	0.402	0.379	0.388	0.405	0.398	0.436
Mg	0.597	0.607	0.588	0.613	0.608	0.577	0.588	0.550
Mn	0.017	0.025	0.025	0.025	0.023	0.021	0.024	0.026
Ca	0.863	0.861	0.883	0.903	0.895	0.837	0.869	0.837
Na	0.170	0.171	0.128	0.125	0.127	0.185	0.157	0.185

Glen Dessarry syenite, clinopyroxenes.

	MJ008	IGS 42778 (leucocratic syenite)						
SiO_2	51.85	50.23	50.49	50.50	51.94	50.46	52.29	51.94
TiO_2	-	1.06	1.88	1.94	0.44	0.76	0.26	0.44
Al_2O_3	1.06	2.98	2.99	3.18	3.40	3.45	2.38	3.40
FeO	13.01	10.17	10.04	10.43	10.30	11.71	10.98	10.30
MnO	0.94	0.41	0.42	0.52	0.47	0.55	0.49	0.47
MgO	9.65	10.90	10.81	10.71	10.92	9.70	10.68	10.92
CaO	20.62	20.80	20.96	20.64	20.49	19.53	19.85	20.49
Na_2O	2.24	2.53	2.65	2.72	2.87	3.43	3.19	2.87
Total	99.37	99.08	100.24	100.64	100.83	99.59	100.12	100.83
Si	1.996	1.918	1.905	1.901	1.941	1.927	1.973	1.941
Al	0.004	0.082	0.095	0.099	0.059	0.073	0.027	0.059
Al	0.044	0.052	0.038	0.042	0.090	0.082	0.078	0.090
Ti	-	0.030	0.053	0.055	0.012	0.022	0.007	0.012
Fe	0.419	0.325	0.317	0.328	0.322	0.374	0.346	0.322
Mg	0.554	0.620	0.608	0.601	0.608	0.552	0.600	0.608
Mn	0.031	0.013	0.013	0.017	0.015	0.018	0.016	0.015
Ca	0.850	0.851	0.848	0.832	0.820	0.799	0.802	0.820
Na	0.167	0.187	0.194	0.198	0.208	0.254	0.233	0.208

IGS 42774 (leucocratic syenite)

SiO_2	51.12	51.68	52.16
TiO_2	0.97	-	-
Al_2O_3	3.11	1.00	0.80
FeO	10.56	12.36	11.91
MnO	0.48	0.85	0.86
MgO	10.66	10.40	10.62
CaO	20.39	21.68	21.95
Na_2O	2.89	1.98	1.62
Total	100.19	99.95	99.92
Si	1.929	1.977	1.989
Al	0.071	0.023	0.011
Al	0.068	0.022	0.025
Ti	0.027	-	-
Fe	0.333	0.395	0.380
Mg	0.600	0.593	0.604
Mn	0.015	0.028	0.028
Ca	0.825	0.889	0.897
Na	0.212	0.147	0.120

Lewisian, clinopyroxenes.

	MJ036			
SiO_2	51.62	51.54	52.04	51.92
TiO_2	0.37	0.31	0.15	0.10
Al_2O_3	3.00	3.20	2.63	2.53
FeO	9.28	8.57	8.59	8.61
MnO	0.35	0.25	0.23	0.24
MgO	12.69	12.88	13.11	12.90
CaO	21.92	22.67	22.83	22.64
Na_2O	1.06	1.01	0.92	0.56
Total	100.29	100.43	100.50	99.50
Si	1.929	1.920	1.937	1.948
Al	0.071	0.080	0.063	0.052
Al	0.061	0.061	0.052	0.060
Ti	0.010	0.009	0.004	0.003
Fe	0.290	0.267	0.267	0.270
Mg	0.707	0.715	0.727	0.722
Mn	0.011	0.008	0.007	0.008
Ca	0.877	0.905	0.910	0.910
Na	0.077	0.073	0.066	0.041

	MJ037			
SiO_2	51.84	51.27	51.72	52.29
TiO_2	0.15	0.17	0.17	0.28
Al_2O_3	2.44	2.64	2.64	2.38
FeO	8.34	8.73	9.15	8.83
MnO	0.19	0.36	0.23	0.19
MgO	13.07	12.85	12.90	13.10
CaO	22.72	22.24	22.31	22.29
Na_2O	0.91	0.89	0.78	0.81
Total	99.66	99.15	99.90	100.17
Si	1.943	1.936	1.938	1.949
Al	0.057	0.064	0.062	0.051
Al	0.051	0.053	0.055	0.054
Ti	0.004	0.005	0.005	0.008
Fe	0.261	0.276	0.287	0.275
Mg	0.730	0.723	0.721	0.728
Mn	0.006	0.012	0.007	0.006
Ca	0.912	0.900	0.896	0.890
Na	0.066	0.065	0.057	0.059

Lewisian, orthopyroxenes.

	MJ036				
SiO_2	51.81	52.07	51.97	52.08	51.71
TiO_2	-	-	-	-	-
Al_2O_3	1.30	1.44	1.16	1.36	1.25
FeO	24.81	24.69	24.08	24.46	23.92
MnO	0.49	0.51	0.65	0.55	0.67
MgO	20.49	20.72	20.71	20.65	20.48
CaO	0.50	0.46	0.49	0.39	0.40
Na_2O	0.61	0.48	0.53	0.70	0.54
Total	100.01	100.37	99.59	100.19	98.97
Si	1.958	1.957	1.966	1.961	1.968
Al	0.042	0.043	0.034	0.039	0.032
Al	0.016	0.021	0.018	0.021	0.024
Ti	-	-	-	-	-
Fe	0.784	0.776	0.762	0.770	0.761
Mg	1.154	1.161	1.168	1.159	1.162
Mn	0.016	0.016	0.021	0.018	0.022
Ca	0.020	0.019	0.020	0.016	0.016
Na	0.045	0.035	0.039	0.051	0.040

Glen Dessarry syenite, feldspars.

	Perthite, GD30 (mafic syenite)					
SiO_2	64.44	64.22	64.76	64.02	64.10	64.10
Al_2O_3	19.96	20.15	20.05	20.17	19.73	20.15
CaO	0.80	0.78	0.88	0.68	0.74	0.85
BaO	0.36	0.40	0.35	0.46	0.36	0.36
Na_2O	5.23	5.72	5.63	5.50	5.35	6.56
K_2O	8.82	8.08	8.04	8.68	8.84	7.23
Total	99.61	99.35	99.71	99.51	99.12	99.25
Si	11.725	11.692	11.732	11.674	11.731	11.664
Al	4.275	4.308	4.268	4.326	4.255	4.321
Al	0.005	0.015	0.012	0.008	-	-
Ca	0.156	0.152	0.171	0.133	0.145	0.166
Ba	0.026	0.029	0.025	0.033	0.026	0.026
Na	1.845	2.019	1.977	1.945	1.898	2.314
K	2.047	1.876	1.858	2.019	2.064	1.678
AB	45.29	49.53	49.06	47.09	45.93	55.32
AN	3.83	3.73	4.24	3.22	3.51	3.96
OR	50.88	46.73	46.70	49.69	50.56	40.72

	Perthite, MJ008 (undeformed leucocratic syenite)					
SiO_2	63.58	63.90	63.61	64.09	63.66	63.99
Al_2O_3	19.61	19.92	19.58	19.62	19.62	19.79
CaO	0.46	0.56	0.39	0.50	0.56	0.57
BaO	1.05	0.56	0.68	0.69	0.76	0.59
Na_2O	3.06	4.19	3.58	3.85	3.89	3.99
K_2O	11.77	10.55	11.58	10.98	11.01	10.83
Total	99.53	99.68	99.42	99.73	99.50	99.76
Si	11.746	11.709	11.740	11.758	11.727	11.728
Al	4.254	4.291	4.258	4.242	4.259	4.272
Al	0.015	0.010	-	-	-	0.002
Ca	0.091	0.110	0.077	0.098	0.111	0.112
Ba	0.076	0.040	0.049	0.050	0.055	0.042
Na	1.096	1.489	1.281	1.369	1.389	1.418
K	2.773	2.466	2.726	2.569	2.587	2.532
AB	27.15	36.27	30.99	33.51	33.55	34.55
AN	2.26	2.68	1.87	2.40	2.67	2.73
OR	70.59	61.05	67.14	64.09	63.79	62.72

Glen Dessarry syenite, feldspars.

Plagioclase, MJ003 (deformed leucocratic syenite)

SiO_2	66.21	65.37	66.31	66.14	65.98
Al_2O_3	21.82	20.95	21.52	20.73	21.03
CaO	1.55	1.72	1.52	1.13	1.42
BaO	-	-	-	-	-
Na_2O	10.94	10.34	10.69	10.99	10.75
K_2O	0.32	0.34	0.34	0.32	0.36
Total	100.84	98.72	100.38	99.31	99.54
Si	11.548	11.630	11.603	11.693	11.645
Al	4.452	4.370	4.397	4.307	4.355
Al	0.033	0.022	0.040	0.012	0.018
Ca	0.290	0.328	0.285	0.214	0.269
Ba	-	-	-	-	-
Na	3.699	3.567	3.627	3.767	3.678
K	0.071	0.077	0.076	0.072	0.081
AB	91.11	89.80	90.95	92.94	91.32
AN	7.13	8.26	7.15	5.28	6.67
OR	1.75	1.94	1.90	1.78	2.01

K-Feldspar, MJ003 (deformed leucocratic syenite)

SiO_2	63.15	63.22	63.56	63.50	63.07
Al_2O_3	19.31	19.48	19.06	19.28	19.06
CaO	-	-	-	-	-
BaO	1.20	1.05	1.02	1.13	1.00
Na_2O	1.63	1.59	1.66	1.83	1.69
K_2O	14.37	14.32	14.32	14.17	14.21
Total	99.66	99.66	99.62	99.91	99.03
Si	11.772	11.764	11.827	11.790	11.807
Al	4.228	4.236	4.173	4.210	4.193
Al	0.013	0.035	0.007	0.008	0.011
Ca	-	-	-	-	-
Ba	0.088	0.077	0.074	0.082	0.073
Na	0.589	0.574	0.599	0.659	0.613
K	3.417	3.399	3.399	3.356	3.393
AB	14.39	14.17	14.71	16.08	15.04
AN	-	-	-	-	-
OR	85.61	85.83	85.29	83.92	84.96

Glen Dessarry syenite, feldspars.

Plagioclase, IGS 45671 (leucocratic syenite)

SiO_2	65.62	66.08	65.64	67.52
Al_2O_3	21.41	21.74	21.84	20.46
CaO	2.09	2.02	2.08	0.70
Na_2O	10.71	10.61	10.57	11.23
K_2O	-	-	-	-
Total	99.83	100.45	100.13	99.91
Si	11.555	11.552	11.518	11.816
Al	4.443	4.448	4.482	4.184
Al	-	0.030	0.033	0.036
Ca	0.394	0.378	0.391	0.131
Na	3.657	3.596	3.596	3.810
AB	32.000	32.000	32.000	32.000
AN	90.27	90.48	90.19	96.67
OR	9.73	9.52	9.81	3.33

K-feldspar, IGS 45671 (leucocratic syenite)

SiO_2	64.45	64.49	65.05
A_2O_3	18.94	19.07	19.43
CaO	0.15	0.14	0.16
Na_2O	1.42	1.40	1.58
K_2O	14.59	14.61	14.27
Total	99.55	99.71	100.49
Si	11.905	11.892	11.877
Al	4.095	4.108	4.123
Al	0.028	0.036	0.057
Ca	0.030	0.028	0.031
Na	0.509	0.501	0.559
K	3.437	3.436	3.323
AB	12.79	12.63	14.29
AN	0.75	0.70	0.80
OR	86.46	86.68	84.91

Lewisian, feldspars.

	Plagioclase, MJ037				
SiO_2	57.50	57.43	57.30	57.65	57.90
Al_2O_3	26.36	26.71	26.55	26.56	26.93
CaO	8.78	8.70	8.74	8.70	8.74
Na_2O	6.22	6.60	6.41	6.30	6.75
K_2O	0.16	0.25	0.13	-	0.12
Total	99.02	99.69	99.13	99.21	100.44
Si	10.387	10.326	10.347	10.382	10.328
Al	5.611	5.659	5.650	5.618	5.660
Al	-	-	-	0.018	-
Ca	1.699	1.676	1.691	1.679	1.670
Na	2.178	2.301	2.244	2.200	2.334
K	0.037	0.057	0.030	-	0.027
AB	55.65	57.03	56.60	56.72	57.90
AN	43.41	41.55	42.65	43.28	41.43
OR	0.94	1.42	0.76	-	0.68

Glen Dessarry syenite, biotites.

	GD48 (ultramafic)				
SiO_2	36.70	37.18	36.69	36.18	37.30
TiO_2	2.12	1.87	2.16	2.09	2.08
Al_2O_3	13.99	13.84	14.23	14.87	13.66
FeO	14.89	14.08	14.03	14.61	15.06
MnO	0.30	0.19	0.17	0.24	-
MgO	16.19	16.58	16.39	16.12	16.41
CaO	-	0.25	0.23	0.19	0.15
Na_2O	0.61	0.46	0.62	0.64	0.30
K_2O	10.00	9.76	9.69	9.86	9.80
H_2O	3.95	3.96	3.95	3.96	3.97
Total	98.75	98.17	98.16	98.76	98.73
Si	5.563	5.632	5.562	5.476	5.634
Al	2.437	2.368	2.438	2.524	2.366
Al	0.062	0.102	0.104	0.128	0.066
Ti	0.242	0.213	0.246	0.238	0.236
Fe	1.888	1.784	1.779	1.849	1.902
Mn	0.039	0.024	0.022	0.031	-
Mg	3.658	3.743	3.703	3.636	3.695
Ca	-	0.041	0.037	0.031	0.024
Na	0.179	0.135	0.182	0.188	0.088
K	1.933	1.886	1.874	1.903	1.888

	GD30 (mafic syenite)				
SiO_2	37.02	37.04	37.04	36.99	37.08
TiO_2	2.22	2.11	2.36	2.11	2.41
Al_2O_3	13.91	13.85	13.59	14.01	13.39
FeO	18.92	18.91	19.21	18.95	19.56
MnO	0.29	0.43	0.29	0.33	0.24
MgO	12.64	12.44	12.31	12.36	12.15
CaO	0.32	0.36	-	0.28	0.25
Na_2O	0.77	0.59	0.31	0.53	0.33
K_2O	8.76	8.89	9.20	9.03	8.86
H_2O	3.91	3.90	3.88	3.90	3.88
Total	98.76	98.52	98.19	98.49	98.35
Si	5.673	5.695	5.719	5.689	5.721
Al	2.327	2.305	2.281	2.311	2.279
Al	0.185	0.204	0.191	0.228	0.156
Ti	0.256	0.244	0.274	0.244	0.280
Fe	2.425	2.431	2.480	2.437	2.524
Mn	0.038	0.056	0.038	0.043	0.031
Mg	2.887	2.851	2.833	2.833	2.794
Ca	0.053	0.059	-	0.046	0.074
Na	0.229	0.176	0.093	0.158	0.099
K	1.712	1.743	1.812	1.771	1.744

Glen Dessarry syenite, biotites.

MJ003 (deformed leucocratic syenite)

SiO_2	35.52	35.41	35.56	34.87	36.38	36.04	35.87
TiO_2	2.59	2.15	2.09	2.15	2.25	2.24	2.34
Al_2O_3	13.55	13.71	13.91	13.87	13.28	13.84	13.67
FeO	22.05	21.91	21.11	23.31	21.38	21.61	21.48
MnO	0.33	0.65	0.49	0.47	0.35	0.37	0.56
MgO	11.16	11.05	11.33	12.13	11.08	11.47	11.28
CaO	0.26	0.30	0.24	0.22	0.38	0.26	0.14
Na_2O	0.42	0.65	0.76	0.35	0.31	0.33	0.47
K_2O	8.32	8.51	8.53	7.36	9.37	8.78	8.75
H_2O	3.82	3.81	3.82	3.83	3.84	3.86	3.84
Total	98.02	98.15	97.84	98.56	98.62	98.80	98.40
Si	5.572	5.564	5.578	5.451	5.676	5.599	5.602
Al	2.428	2.436	2.422	2.549	2.324	2.401	2.398
Al	0.077	0.102	0.149	0.005	0.118	0.133	0.118
Ti	0.036	0.254	0.247	0.253	0.264	0.262	0.275
Fe	2.893	2.879	2.769	3.047	2.790	2.808	2.805
Mn	0.044	0.087	0.065	0.062	0.046	0.049	0.074
Mg	2.609	2.588	2.649	2.826	2.577	2.656	2.647
Ca	0.044	0.051	0.040	0.037	0.064	0.043	0.023
Na	0.128	0.198	0.231	0.106	0.094	0.099	0.142
K	1.665	1.705	1.707	1.467	1.865	1.740	1.743

MJ008 (undeformed leucocratic syenite)

SiO_2	36.98	36.67	37.05	36.98	36.74
TiO_2	2.18	2.16	2.12	2.21	2.16
Al_2O_3	12.30	13.68	13.29	13.20	13.20
FeO	18.90	18.83	18.93	19.39	19.34
MnO	0.46	0.52	0.51	0.47	0.48
MgO	12.82	12.75	12.70	12.16	12.25
CaO	-	-	-	-	0.26
Na_2O	0.64	0.35	0.46	0.36	0.48
K_2O	9.73	9.72	9.78	9.98	9.83
H_2O	3.84	3.88	3.89	3.87	3.87
Total	97.85	98.56	98.73	98.62	98.61
Si	5.765	5.661	5.713	5.726	5.695
Al	2.235	2.339	2.287	2.274	2.305
Al	0.025	0.149	0.128	0.135	0.106
Ti	0.256	0.251	0.246	0.257	0.252
Fe	2.464	2.431	2.411	2.511	2.507
Mn	0.061	0.068	0.067	0.062	0.063
Mg	2.979	2.934	2.919	2.806	2.830
Ca	-	-	-	-	0.043
Na	0.193	0.105	0.138	0.108	0.144
K	1.935	1.914	1.924	1.971	1.944

Glen Dessarry syenite, biotites.

IGS 45671 (leucocratic syenite)

SiO_2	36.82	37.19	37.32	36.57	36.55
TiO_2	2.62	2.17	2.46	2.72	2.75
Al_2O_3	14.17	14.09	13.50	13.33	13.55
FeO	19.65	18.92	19.76	19.49	19.75
MnO	0.37	0.47	0.33	0.32	0.44
MgO	11.98	12.83	12.42	12.25	12.00
CaO	-	-	-	-	-
Na_2O	0.24	0.37	0.12	0.51	-
K_2O	9.26	9.61	9.63	9.72	9.25
H_2O	3.90	3.93	3.92	3.88	3.86
Total	99.01	99.58	99.46	98.79	98.15
Si	5.650	5.666	5.710	5.653	5.668
Al	2.350	2.334	2.290	2.347	2.332
Al	0.212	0.196	0.144	0.081	0.144
Ti	0.302	0.249	0.283	0.316	0.321
Fe	2.521	2.411	2.528	2.519	2.561
Mn	0.048	0.061	0.043	0.042	0.058
Mg	2.740	2.914	2.832	2.822	2.774
Ca	-	-	-	-	-
Na	0.071	0.109	0.036	0.153	-
K	1.812	1.868	1.879	1.916	1.830

IGS 42774 (leucocratic syenite)

SiO_2	36.09
TiO_2	2.86
Al_2O_3	13.33
FeO	19.43
MnO	0.59
MgO	12.18
CaO	-
Na_2O	0.64
K_2O	9.13
H_2O	3.85
Total	98.10
Si	5.615
Al	2.385
Al	0.059
Ti	0.335
Fe	2.528
Mn	0.078
Mg	2.825
Ca	-
Na	0.193
K	1.812

Lewisian, biotites.

	MJ037							
SiO_2	36.49	36.13	36.59	36.97	36.72	36.81	36.89	37.21
TiO_2	4.39	4.32	4.48	3.71	3.71	4.34	4.29	3.70
Al_2O_3	14.53	14.51	14.46	14.27	14.72	14.43	14.50	15.20
FeO	16.04	16.47	16.37	16.37	16.70	16.55	16.28	15.32
MnO	0.17	0.13	0.13	-	0.18	-	0.20	0
MgO	13.05	12.71	13.03	13.44	12.86	12.57	12.52	14.02
CaO	-	-	-	-	-	-	-	-
Na_2O	0.26	0.52	0.33	0.33	0.33	0.15	0.22	0.31
K_2O	9.90	9.74	9.78	9.96	9.54	10.07	9.63	9.95
H_2O	3.94	3.92	3.96	3.95	3.94	3.94	3.94	4.01
Total	98.77	98.45	99.13	99.00	98.70	98.86	98.63	99.72
Si	5.542	5.521	5.541	5.603	5.581	5.592	5.603	5.561
Al	2.458	2.479	2.459	2.397	2.419	2.408	2.397	2.439
Al	0.142	0.134	0.122	0.152	0.218	0.176	0.198	0.237
Ti	0.501	0.496	0.510	0.423	0.424	0.496	0.490	0.416
Fe	2.037	2.105	2.073	2.075	2.123	2.103	2.068	1.915
Mn	0.022	0.017	0.017	-	0.023	-	0.026	-
Mg	2.954	2.895	2.941	3.036	2.913	2.846	2.834	3.123
Ca	-	-	-	-	-	-	0.026	-
Na	0.077	0.154	0.097	0.097	0.097	0.044	0.065	0.090
K	1.918	1.898	1.889	1.925	1.849	1.951	1.866	1.896

	MJ036	
SiO_2	36.91	37.06
TiO_2	3.16	3.21
Al_2O_3	14.72	14.98
FeO	15.76	15.85
MnO	-	0.18
MgO	14.05	14.02
CaO	0.27	0.19
Na_2O	0.48	0.31
K_2O	9.30	9.55
H_2O	3.96	3.99
Total	98.61	99.34
Si	5.584	5.571
Al	2.416	2.429
Al	0.209	0.225
Ti	0.360	0.363
Fe	1.994	1.993
Mn	-	0.023
Mg	3.168	3.142
Ca	0.044	0.031
Na	0.141	0.090
K	1.795	1.831

Glen Dessarry syenite, amphiboles.

	GD48 (ultramafic)				
SiO_2	42.21	45.71	45.98	47.68	45.57
Al_2O_3	10.86	7.88	8.20	6.68	8.10
FeO	11.90	11.35	10.12	10.04	11.11
Fe_2O_3	2.90	2.09	3.27	1.90	2.11
MgO	12.43	14.09	14.60	15.31	13.89
MnO	0.31	0.36	0.38	0.26	0.39
TiO_2	1.28	0.60	0.34	0.33	0.46
CaO	11.82	11.80	11.89	12.02	11.83
Na_2O	2.25	2.22	2.18	1.78	2.06
K_2O	1.24	0.78	0.81	0.68	0.73
Total	97.20	96.88	97.78	96.68	96.25
Si	6.337	6.796	6.754	7.017	6.806
Al	1.663	1.204	1.246	0.983	1.194
Al	0.259	0.177	0.174	0.176	0.232
Ti	0.145	0.067	0.038	0.037	0.052
Fe^3	0.328	0.234	0.361	0.211	0.237
Mg	2.781	3.122	3.196	3.358	3.092
Fe^2	1.487	1.400	1.231	1.219	1.387
Fe^2	0.007	0.011	0.013	0.016	0.000
Mn	-	-	-	-	-
Mn	0.039	0.045	0.047	0.032	0.049
Ca	1.901	1.880	1.872	1.895	1.893
Na	0.053	0.064	0.069	0.056	0.057
Na	0.602	0.576	0.552	0.452	0.539
K	0.238	0.148	0.152	0.128	0.139

	GD30 (mafic syenite)							
SiO_2	43.82	43.86	43.79	43.14	42.90	42.43	42.48	43.31
Al_2O_3	8.39	8.99	8.61	9.70	9.19	9.66	9.28	9.08
FeO	16.18	15.82	15.98	16.47	15.46	16.45	17.00	16.47
Fe_2O_3	2.93	3.24	3.21	2.94	3.97	2.88	2.62	2.88
MgO	10.22	10.30	10.23	10.04	10.15	9.84	9.58	9.86
MnO	0.55	0.48	0.46	0.32	0.51	0.42	0.59	0.51
TiO_2	0.53	0.58	0.54	0.70	0.56	0.56	0.71	0.56
CaO	11.83	11.64	11.56	11.38	11.13	11.24	10.96	10.70
Na_2O	1.84	1.71	1.77	2.18	2.03	2.22	2.28	2.29
K_2O	1.18	1.20	1.20	1.21	1.23	1.39	1.43	1.31
Total	97.28	98.11	97.34	98.09	97.13	97.09	96.93	96.97
Si	6.683	6.622	6.666	6.532	6.554	6.511	6.546	6.633
Al	1.318	1.378	1.335	1.468	1.446	1.490	1.454	1.368
Al	0.191	0.222	0.211	0.264	0.210	0.258	0.232	0.272
Ti	0.061	0.066	0.062	0.078	0.064	0.065	0.082	0.065
Fe^3	0.336	0.369	0.367	0.335	0.456	0.332	0.304	0.331
Mg	2.323	2.318	2.321	2.266	2.311	2.250	2.200	2.250
Fe^2	2.064	1.998	2.034	2.056	1.958	2.095	2.182	2.082
Fe^2	-	-	-	0.031	0.017	0.016	0.009	0.028
Mn	0.025	0.028	0.006	-	-	-	-	-
Mn	0.046	0.033	0.053	0.041	0.066	0.055	0.077	0.066
Ca	1.902	1.928	1.885	1.846	1.822	1.848	1.810	1.756
Na	0.052	0.038	0.061	0.082	0.095	0.081	0.104	0.150
Na	0.492	0.462	0.461	0.558	0.506	0.579	0.577	0.530
K	0.230	0.231	0.233	0.234	0.240	0.272	0.281	0.256

Glen Dessarry syenite, amphiboles.

	MJ003 (deformed leucocratic syenite)							
SiO_2	43.35	44.73	41.61	41.69	41.09	42.45	40.23	40.91
Al_2O_3	8.65	7.86	9.81	9.65	9.75	8.97	10.00	10.49
FeO	17.57	17.20	17.91	18.12	17.21	18.02	17.52	18.99
Fe_2O_3	1.80	2.47	3.49	3.51	4.31	2.95	4.71	2.58
MgO	9.37	9.82	8.62	8.34	8.84	8.73	8.06	7.79
MnO	0.63	0.52	0.73	0.64	0.59	0.63	0.68	0.52
TiO_2	0.58	0.50	0.69	0.57	0.69	0.62	0.83	0.76
CaO	11.16	11.09	11.08	10.96	11.02	10.87	10.79	11.18
Na_2O	2.18	1.86	2.36	2.19	2.48	2.18	2.16	2.13
K_2O	1.11	0.98	1.44	1.39	1.31	1.21	1.60	1.61
Total	96.40	97.03	97.74	97.06	97.28	96.63	96.58	96.96
Si	6.697	6.828	6.420	6.473	6.367	6.590	6.310	6.382
Al	1.303	1.172	1.580	1.528	1.633	1.411	1.690	1.618
Al	0.273	0.243	0.205	0.239	0.148	0.231	0.160	0.312
Ti	0.067	0.057	0.080	0.067	0.080	0.072	0.098	0.089
Fe^3	0.210	0.284	0.406	0.410	0.502	0.344	0.556	0.303
Mg	2.157	2.234	1.982	1.930	2.041	2.020	1.884	1.811
Fe^2	2.270	2.182	2.311	2.353	2.228	2.333	2.298	2.477
Fe^2	-	0.013	-	-	0.002	0.007	-	-
Mn	0.023	-	0.017	0.002	-	-	0.004	0.008
Mn	0.060	0.067	0.078	0.082	0.077	0.083	0.087	0.061
Ca	1.847	1.814	1.832	1.823	1.830	1.808	1.814	1.869
Na	0.093	0.106	0.090	0.095	0.091	0.103	0.100	0.070
Na	0.560	0.445	0.616	0.565	0.654	0.554	0.557	0.574
K	0.219	0.191	0.284	0.275	0.259	0.240	0.320	0.320

	MJ008 (undeformed leucocratic syenite)							
SiO_2	42.32	42.51	42.41	42.56	42.62	42.21	42.52	40.93
Al_2O_3	9.52	9.01	9.04	9.57	9.34	9.18	8.87	10.11
FeO	16.87	17.57	16.37	16.92	17.90	17.43	16.65	17.62
Fe_2O_3	2.75	1.96	3.37	2.99	1.60	2.06	3.77	4.37
MgO	9.40	9.24	9.46	9.37	8.99	9.27	9.32	8.31
MnO	0.74	0.70	0.80	0.75	0.71	0.72	0.63	0.66
TiO_2	0.73	0.61	0.62	0.50	0.43	0.64	0.49	0.71
CaO	10.72	11.33	10.97	10.87	11.30	10.99	11.44	10.93
Na_2O	2.42	2.14	2.04	2.34	2.17	2.38	1.88	2.23
K_2O	1.45	1.35	1.35	1.27	1.33	1.45	1.31	1.52
Total	96.92	96.42	96.43	97.14	96.39	96.33	96.89	97.39
Si	6.525	6.597	6.564	6.541	6.613	6.562	6.564	6.350
Al	1.475	1.403	1.436	1.459	1.387	1.438	1.436	1.651
Al	0.255	0.245	0.214	0.275	0.321	0.244	0.178	0.199
Ti	0.085	0.071	0.072	0.058	0.050	0.075	0.057	0.083
Fe^3	0.319	0.228	0.392	0.346	0.186	0.241	0.439	0.511
Mg	2.160	2.137	2.182	2.146	2.079	2.148	2.144	1.921
Fe^2	2.175	2.280	2.119	2.175	2.323	2.266	2.150	2.285
Fe^2	0.006	-	-	-	-	-	-	-
Mn	-	0.038	0.021	-	0.040	0.026	0.032	0.002
Mn	0.090	0.054	0.084	0.098	0.053	0.068	0.050	0.085
Ca	1.771	1.884	1.819	1.790	1.879	1.831	1.892	1.817
Na	0.139	0.062	0.097	0.112	0.068	0.101	0.058	0.098
Na	0.585	0.582	0.516	0.585	0.584	0.617	0.505	0.573
K	0.285	0.267	0.267	0.249	0.263	0.288	0.258	0.301

Glen Dessarry syenite, amphiboles.

	IGS 45671 (leucocratic syenite)					
SiO_2	44.50	44.66	45.00	44.43	45.63	43.95
Al_2O_3	8.59	8.10	8.40	8.28	6.95	8.46
FeO	17.13	16.22	16.23	16.31	15.50	16.51
Fe_2O_3	2.17	2.41	2.90	2.32	2.01	2.16
MgO	9.93	10.55	10.29	10.28	11.22	10.05
MnO	0.56	0.37	0.41	0.43	0.54	0.53
TiO_2	0.65	0.66	0.69	0.59	0.71	0.98
CaO	11.23	11.41	10.99	11.15	11.27	11.26
Na_2O	1.95	1.71	1.74	1.75	1.84	1.69
K_2O	1.27	1.16	1.17	1.22	0.83	1.22
Total	97.98	97.25	97.51	96.75	96.50	96.81
Si	6.736	6.776	6.797	6.779	6.931	6.717
Al	1.264	1.224	1.203	1.221	1.069	1.283
Al	0.269	0.225	0.292	0.268	0.176	0.242
Ti	0.074	0.075	0.078	0.068	0.081	0.113
Fe^3	0.247	0.275	0.295	0.266	0.230	0.248
Mg	2.240	2.386	2.316	2.338	2.540	2.289
Fe^2	2.169	2.039	2.018	2.061	1.970	2.108
Fe^2	-	0.020	0.031	0.020	-	0.002
Mn	0.002	-	-	-	0.004	-
Mn	0.070	0.048	0.053	0.056	0.065	0.069
Ca	1.821	1.855	1.779	1.823	1.834	1.844
Na	0.109	0.078	0.138	0.102	0.101	0.086
Na	0.464	0.426	0.372	0.416	0.441	0.415
K	0.245	0.225	0.225	0.238	0.161	0.238
	Leucocratic syenite					
SiO_2	42.25	42.73	42.60	44.10	42.57	43.27
Al_2O_3	7.77	10.06	10.12	8.51	9.75	9.96
FeO	15.82	18.27	17.73	16.63	17.45	17.60
Fe_2O_3	3.42	1.80	1.49	2.67	1.83	2.12
MgO	10.51	8.94	9.08	9.76	9.43	9.38
MnO	0.51	0.40	0.49	0.34	0.41	0.29
TiO_2	0.87	0.83	0.76	0.48	0.72	0.66
CaO	11.38	11.25	11.17	11.43	11.41	11.24
Na_2O	1.73	2.21	2.30	1.56	2.06	2.06
K_2O	1.08	1.47	1.45	1.04	1.48	1.43
Total	97.33	97.96	97.19	96.52	97.10	98.01
Si	6.727	6.526	6.540	6.755	6.541	6.572
Al	1.273	1.475	1.460	1.245	1.459	1.428
Al	0.120	0.337	0.372	0.292	0.307	0.355
Ti	0.100	0.095	0.088	0.055	0.083	0.075
Fe^3	0.391	0.207	0.172	0.308	0.211	0.243
Mg	2.381	2.035	2.077	2.228	2.159	2.123
Fe^2	2.009	2.326	2.277	2.117	2.239	2.204
Fe^2	0.002	0.007	-	0.014	0.003	0.032
Mn	-	-	0.015	-	-	-
Mn	0.066	0.052	0.049	0.044	0.053	0.037
Ca	1.854	1.841	1.837	1.876	1.879	1.829
Na	0.078	0.100	0.114	0.066	0.065	0.102
Na	0.432	0.554	0.571	0.397	0.549	0.505
K	0.210	0.286	0.284	0.203	0.290	0.277

Lewisian, amphiboles.

MJ182 (amphibole-quartz symplectites)

SiO_2	44.69	45.03	44.78	44.29	44.74	44.85	44.73	45.20
Al_2O_3	10.61	10.78	10.71	10.71	10.39	10.37	10.26	10.83
FeO	12.82	13.80	13.17	12.90	12.74	12.88	13.09	13.35
Fe_2O_3	2.97	2.16	3.21	2.69	2.74	3.14	2.80	2.23
MgO	11.62	11.42	11.46	11.33	11.47	11.25	11.33	11.40
MnO	0.22	0.27	0.24	0.33	0.46	0.20	0.22	0.28
TiO_2	0.27	0.25	0.23	0.29	0.10	0.31	0.22	0.22
CaO	11.99	12.02	12.07	11.91	11.90	11.62	11.81	11.72
Na_2O	1.50	1.69	1.59	1.55	1.48	1.26	1.45	1.51
K_2O	0.79	0.79	0.73	0.66	0.71	0.63	0.60	0.72
Total	97.48	98.21	98.18	96.66	96.74	96.50	96.51	97.45
Si	6.634	6.650	6.615	6.631	6.687	6.706	6.700	6.696
Al	1.366	1.350	1.385	1.369	1.313	1.294	1.300	1.304
Al	0.491	0.527	0.480	0.521	0.518	0.534	0.512	0.587
Ti	0.030	0.028	0.026	0.033	0.011	0.035	0.025	0.025
Fe^3	0.332	0.240	0.356	0.303	0.309	0.353	0.315	0.248
Mg_2	2.571	2.513	2.523	2.528	2.555	2.507	2.529	2.517
Fe^2	1.576	1.692	1.615	1.616	1.593	1.572	1.619	1.624
Fe^2	0.016	0.012	0.012	-	-	0.039	0.021	0.030
Mn	-	-	-	-	0.014	-	-	-
Mn	0.028	0.034	0.030	0.042	0.044	0.025	0.028	0.035
Ca	1.907	1.902	1.911	1.911	1.906	1.862	1.895	1.860
Na	0.050	0.052	0.048	0.048	0.050	0.074	0.056	0.075
Na	0.382	0.432	0.408	0.402	0.379	0.291	0.365	0.359
K	0.150	0.149	0.138	0.126	0.135	0.120	0.115	0.136

MJ182 (amphibole-quartz symplectites)

SiO_2	45.14	44.61
Al_2O_3	9.84	11.78
FeO	14.38	13.31
Fe_2O_3	0.71	3.13
MgO	11.42	11.35
MnO	0.19	0.21
TiO_2	0.32	0.23
CaO	12.04	12.12
Na_2O	1.64	1.63
K_2O	0.79	0.68
Total	96.47	98.05
Si	6.778	6.603
Al	1.222	1.397
Al	0.520	0.484
Ti	0.036	0.026
Fe^3	0.080	0.349
Mg_2	2.556	2.504
Fe^2	1.806	1.638
Fe^2	-	0.010
Mn	0.001	-
Mn	0.023	0.026
Ca	1.937	1.922
Na	0.040	0.042
Na	0.438	0.426
K	0.151	0.128

Lewisian, amphiboles.

MJ182 ("platy" amphibole)

SiO_2	44.07	43.79	43.39	43.49	44.68	44.56	43.41	43.78
Al_2O_3	11.48	11.02	11.85	10.99	10.06	10.82	11.12	11.48
FeO	14.63	14.22	15.09	14.07	14.18	15.16	14.53	15.27
Fe_2O_3	2.20	2.76	1.20	2.26	1.71	1.00	1.94	1.50
MgO	10.50	10.49	9.81	10.56	10.92	10.69	10.43	10.13
MnO	0.31	0.42	0.44	0.36	0.31	0.37	0.33	0.36
TiO_2	0.44	0.54	0.27	0.39	0.48	0.55	0.58	0.59
CaO	12.01	11.89	12.30	11.73	11.86	12.09	11.79	11.87
Na_2O	1.62	1.53	1.57	1.67	1.48	1.71	1.67	1.71
K_2O	0.89	0.89	0.68	0.80	0.59	0.81	0.89	0.81
Total	98.14	97.55	96.60	96.33	94.27	97.76	96.70	97.50
Si	6.551	6.554	6.555	6.578	6.729	6.644	6.554	6.560
Al	1.449	1.446	1.445	1.422	1.271	1.356	1.446	1.441
Al	0.563	0.499	0.666	0.538	0.515	0.546	0.533	0.587
Ti	0.049	0.061	0.031	0.044	0.054	0.062	0.066	0.067
Fe^3	0.246	0.311	0.136	0.258	0.194	0.111	0.221	0.170
Mg	2.326	2.340	2.209	2.380	2.451	2.375	2.347	2.262
Fe^2	1.817	1.780	1.907	1.780	1.786	1.891	1.834	1.913
Fe^2	0.002	-	-	-	0.001	-	0.001	-
Mn	-	0.010	0.052	-	-	0.015	-	0.002
Mn	0.039	0.043	0.004	0.046	0.040	0.032	0.042	0.044
Ca	1.913	1.907	1.991	1.901	1.914	1.932	1.907	1.906
Na	0.047	0.050	0.005	0.053	0.046	0.037	0.050	0.050
Na	0.420	0.394	0.455	0.437	0.386	0.458	0.439	0.466
K	0.169	0.170	0.131	0.154	0.113	0.154	0.171	0.155

MJ182 ("platy" amphibole)

SiO_2	42.80	43.42
Al_2O_3	11.67	11.13
FeO	13.85	14.49
Fe_2O_3	3.57	2.56
MgO	10.11	10.43
MnO	0.39	0.25
TiO_2	0.48	0.65
CaO	11.78	11.97
Na_2O	1.58	1.59
K_2O	0.83	0.91
Total	97.06	97.40
Si	6.449	6.518
Al	1.551	1.482
Al	0.522	0.488
Ti	0.054	0.073
Fe^3	0.405	0.289
Mg	2.270	2.334
Fe^2	1.745	1.816
Fe^2	-	0.003
Mn	0.004	-
Mn	0.046	0.032
Ca	1.902	1.925
Na	0.052	0.040
Na	0.409	0.423
K	0.160	0.174

Lewisian, amphiboles.

	MJ036						
SiO_2	42.78	42.91	43.35	43.20	43.78	42.96	43.18
Al_2O_3	11.28	11.29	11.39	11.72	11.35	11.14	11.19
FeO	13.14	12.20	12.99	12.56	13.70	12.62	13.41
Fe_2O_3	0.79	1.21	1.13	1.16	0.26	0.66	0.00
MgO	11.40	11.95	11.70	11.69	11.50	11.96	11.81
MnO	0.13	0.32	0.12	0.08	0.00	0.05	0.00
TiO_2	1.92	1.94	1.84	1.48	1.99	2.02	2.09
CaO	11.39	11.33	11.66	11.50	11.75	11.52	11.74
Na_2O	1.59	1.71	1.41	1.47	1.46	1.66	1.80
K_2O	1.72	1.71	1.69	1.69	1.72	1.67	1.68
Total	96.14	96.57	97.27	96.56	97.51	96.26	96.90
Si	6.464	6.440	6.465	6.474	6.513	6.465	6.470
Al	1.536	1.560	1.535	1.527	1.487	1.535	1.530
Al	0.437	0.438	0.468	0.544	0.503	0.441	0.446
Ti	0.218	0.219	0.206	0.167	0.223	0.229	0.236
Fe^3	0.090	0.137	0.127	0.131	0.029	0.074	0.000
Mg	2.567	2.673	2.601	2.611	2.550	2.682	2.637
Fe^2	1.652	1.531	1.599	1.547	1.696	1.574	1.680
Fe^2	0.009	-	0.021	0.028	0.008	0.001	-
Mn	-	0.002	-	-	-	-	-
Mn	0.017	0.039	0.015	0.010	0.000	0.006	0.000
Ca	1.844	1.822	1.863	1.847	1.873	1.858	1.885
Na	0.130	0.139	0.101	0.116	0.119	0.121	0.115
Na	0.335	0.359	0.307	0.311	0.302	0.363	0.408
K	0.332	0.327	0.322	0.323	0.326	0.321	0.321

	MJ037		
SiO_2	42.52	42.48	42.03
Al_2O_3	12.00	12.52	12.03
FeO	14.38	14.09	14.17
Fe_2O_3	0.00	0.42	0.54
MgO	10.88	10.72	10.73
MnO	0.07	0.24	0.29
TiO_2	2.07	1.45	1.97
CaO	12.14	12.24	11.94
Na_2O	1.46	1.21	1.38
K_2O	1.67	1.64	1.81
Total	97.19	96.99	96.88
Si	6.385	6.385	6.348
Al	1.615	1.615	1.652
Al	0.510	0.603	0.491
Ti	0.234	0.164	0.224
Fe^3	0.000	0.048	0.061
Mg	2.435	2.397	2.415
Fe^2	1.806	1.771	1.790
Fe^2	-	-	-
Mn	-	0.017	0.020
Mn	0.009	0.014	0.017
Ca	1.953	1.971	1.932
Na	0.047	0.015	0.050
Na	0.379	0.337	0.354
K	0.320	0.315	0.349

Glen Dessarry syenite, allanites.

	GD27 (mafic syenite, primary)							
SiO_2	34.00	33.65	34.61	34.35	32.51	32.00	33.05	32.96
TiO_2	0.24	0.32	0.42	0.28	0.67	0.92	0.50	0.37
Al_2O_3	17.73	17.95	18.75	18.39	17.90	17.23	17.68	18.11
La_2O_3	4.95	4.92	4.27	4.69	6.70	6.78	5.73	5.55
Ce_2O_3	7.15	7.03	6.99	7.12	9.52	10.10	8.78	7.51
Nd_2O_3	0.75	0.71	0.45	0.66	0.56	0.68	0.23	0.87
FeO	14.18	14.08	13.51	13.68	15.43	15.57	15.35	15.50
MgO	0.51	0.92	0.85	0.67	0.86	0.98	0.76	0.69
CaO	16.19	16.21	16.69	16.38	11.67	11.81	13.96	14.43
H_2O	1.64	1.64	1.68	1.66	1.60	1.59	1.62	1.62
Total	97.34	97.43	98.22	97.88	97.42	97.66	97.66	97.61

	GD16 (mafic syenite, secondary)					
SiO_2	33.65	34.38	34.53	34.34	34.43	35.06
TiO_2	0.23	0.42	-	0.23	0.18	0.21
Al_2O_3	17.24	18.26	18.82	18.22	18.74	19.35
La_2O_3	2.89	3.06	3.35	3.02	2.42	1.75
Ce_2O_3	6.49	7.21	6.24	7.10	6.20	5.30
Nd_2O_3	1.70	1.89	1.53	2.05	2.47	2.50
FeO	14.76	14.62	14.56	14.43	14.18	13.91
MgO	0.67	0.75	0.69	0.82	0.59	0.60
CaO	17.55	16.65	16.87	16.21	17.43	17.69
H_2O	1.63	1.67	1.67	1.66	1.67	1.69
Total	96.81	98.91	98.26	98.08	98.31	98.06

	IGS 42791 (leucocratic syenite)				
	primary			secondary	
SiO_2	32.44	32.94	33.05	34.71	36.07
TiO_2	0.56	0.55	0.61	0.29	0.26
Al_2O_3	14.99	15.13	14.90	17.70	18.08
La_2O_3	7.49	7.20	7.22	3.20	3.31
Ce_2O_3	8.89	8.93	8.79	5.83	5.76
Nd_2O_3	1.51	1.17	1.12	1.54	1.67
FeO	15.35	15.44	15.30	14.58	14.49
MnO	0.50	0.41	0.47	0.56	0.56
MgO	0.85	0.84	0.91	0.51	0.43
CaO	13.33	13.33	13.22	15.54	15.09
H_2O	1.57	1.58	1.58	1.64	1.68
Total	97.48	97.62	97.11	96.10	97.40

	GD34 (pegmatite)		
SiO_2	35.09	35.70	36.53
TiO_2	0.31	0.71	0.53
Al_2O_3	15.35	14.30	15.96
La_2O_3	4.01	4.02	3.86
Ce_2O_3	9.51	10.01	8.46
Nd_2O_3	2.42	1.61	1.86
FeO	14.75	14.90	15.64
MgO	0.45	1.60	0.43
CaO	13.38	12.03	14.16
H_2O	1.60	1.61	1.66
Total	96.87	96.49	99.09

Lewisian, allanites.

	MJ036			
SiO_2	33.51	33.60	33.65	34.42
TiO_2	0.64	1.46	0.60	0.58
Al_2O_3	18.05	17.20	17.38	16.28
La_2O_3	4.35	4.69	4.33	4.36
Ce_2O_3	10.31	9.99	10.45	10.12
Nd_2O_3	2.37	2.49	2.92	2.91
FeO	11.48	12.00	11.89	11.81
MgO	2.14	2.80	2.34	3.15
CaO	12.13	11.83	11.94	10.49
H_2O	1.62	1.63	1.62	1.60
Total	96.97	97.69	97.12	95.72

Glen Dessarry syenite, other accessory minerals.

Monazites

La_2O_3	15.57	17.29	14.40	15.09
Ce_2O_3	27.29	28.14	26.07	26.22
Pr_2O_3	2.96	3.05	2.81	2.38
Nd_2O_3	8.73	8.48	9.80	9.43
Gd_2O_3	0.16	-	0.59	0.35
Y_2O_3	1.77	1.02	1.44	1.55
ThO_2	9.58	10.16	12.19	11.21
UO_2	1.04	0.19	0.66	1.28
CaO	1.85	1.37	2.00	1.85
P_2O_5	30.19	29.25	29.36	30.26
Total	99.14	98.95	99.32	99.62

Sphenes

SiO_2	29.38	29.67	29.58	29.75	29.97	29.99
TiO_2	35.51	35.56	35.70	35.94	35.86	35.78
CaO	27.10	27.17	27.29	27.77	27.63	28.30
Ce_2O_3	2.09	1.75	1.45	1.39	1.30	0.81
Nd_2O_3	1.02	1.13	0.78	0.70	0.49	0.36
Al_2O_3	1.35	0.97	0.99	1.01	1.23	1.53
FeO	1.71	1.99	2.15	2.07	2.03	1.76
Na_2O	0.32	0.22	0.18	0.13	0.16	0.19
Total	98.48	98.46	98.12	98.76	98.67	98.72

Zirconolites

ZrO_2	32.52	31.87	32.17	29.53
TiO_2	29.09	28.50	28.56	29.05
CaO	9.27	8.98	9.30	8.67
FeO	7.53	7.46	7.89	7.91
ThO_2	7.85	8.22	7.57	9.21
UO_2	2.86	2.68	2.26	3.64
La_2O_3	1.03	0.77	1.07	0.77
Ce_2O_3	3.66	2.91	3.47	2.94
Pr_2O_3	0.28	0.31	0.26	0.28
Nd_2O_3	1.44	1.28	1.00	1.71
Sm_2O_3	0.34	0.44	0.37	0.39
Eu_2O_3	0.16	0.18	0.06	0.18
Gd_2O_3	0.50	0.61	0.29	0.47
Yb_2O_3	0.18	0.02	-	0.08
Y_2O_3	0.74	0.61	0.53	0.81
Ta_2O_5	0.09	0.31	0.33	0.29
Nb_2O_5	2.63	2.64	3.19	2.38
HfO_2	0.36	0.41	0.40	0.08
PbO_2	0.24	0.21	0.24	0.46
BaO	0.51	0.57	-	0.55
Total	101.28	98.98	98.96	99.40

Apatites

CaO	53.89	54.15	53.97
P_2O_5	40.63	41.48	40.99
SiO_2	0.78	0.49	0.43
Na_2O	0.41	-	0.32
SrO	0.74	1.06	0.93
SO_4	1.15	0.71	0.91
Total	97.60	97.99	97.55

S.I.M.S. Count Rates.

Magmatic sphene.

Analysis	3	4	5	6	7	8
Ti^{46}	841399	931455	1249861	1195137	1119988	1323928
a	1000	1000	1000	1000	1000	1000
La^{139}	30005	28321	24071	47134	35367	49075
a	35.66	30.41	19.26	39.44	31.58	37.07
b	36.02	30.71	19.45	39.83	31.90	37.44
Ce^{140}	73366	63754	51504	117687	96184	120471
a	87.20	68.45	41.21	98.47	85.85	91.00
b	98.54	77.35	46.57	11.27	97.01	102.83
Pr^{141}	14833	11459	8640	23565	18618	22844
a	17.63	12.30	6.91	19.72	16.62	17.25
b	17.63	12.30	6.91	19.72	16.62	17.25
Nd^{143}	8281	5965	4530	13274	10924	11933
a	9.84	6.40	3.62	11.11	9.75	9.01
b	80.59	52.42	29.65	90.99	79.85	73.79
Sm^{147}	2548	1548	1044	3954	3305	3454
a	3.03	1.66	0.84	3.31	2.95	2.61
b	20.30	11.13	5.63	22.18	19.77	17.49
Eu^{151}	2837	1736	1499	4222	3122	3322
a	3.37	1.86	1.20	3.53	2.79	2.51
b	7.04	3.89	2.51	7.38	5.83	5.25
ThO^{249}	2239	2534	886	3200	1840	3871
a	2.66	2.72	0.71	2.68	1.64	2.92
UO^{255}	315	1564	890	781	745	1401
a	0.37	1.68	0.71	0.65	0.67	1.06

6 8 3 7 4 5
centre.....edge

a = counts standardised to 1000 Ti
b = counts corrected for isotopic abundance of analysed isotope

Deformed sphene.

Analysis	19	14	13	12	11	15
Ti^{46}	911604	1053945	1368824	1466020	1395200	1243464
a	1000	1000	1000	1000	1000	1000
La^{139}	45318	35574	43830	40335	12975	8702
a	49.71	33.75	32.02	27.51	9.30	7.00
b	49.75	33.78	32.05	27.53	9.31	7.01
Ce^{140}	108564	90401	109685	101446	32783	31484
a	119.09	85.77	80.13	69.20	23.49	25.32
b	134.63	96.96	90.59	78.23	26.55	28.62
Pr^{141}	21070	18258	21826	19733	6626	7701
a	23.11	17.32	15.95	13.46	4.75	6.19
b	23.11	17.32	15.95	13.46	4.75	6.19
Nd^{143}	11336	10070	11904	10788	4084	5067
a	12.44	9.55	8.70	7.36	2.93	4.07
b	101.88	78.21	71.25	60.27	23.99	33.33
Sm^{147}	3162	2996	3467	3151	1229	1738
a	3.47	2.84	2.53	2.15	0.88	1.40
b	23.26	19.03	16.96	14.41	5.90	9.38
Eu^{151}	3166	3095	3488	3508	1745	2742
a	3.47	2.94	2.55	2.39	1.25	2.21
b	7.26	6.15	5.34	5.00	2.62	4.62
ThO^{249}	3535	3042	3289	3482	1332	588
a	3.88	2.89	2.40	2.38	0.95	0.47
UO^{255}	1638	1198	1334	2593	7406	2711
a	1.79	1.14	0.97	1.77	5.31	2.18

19 14 13 12 11 15
centre.....edge high-U

a = counts standardised to 1000 Ti
b = counts corrected for isotopic abundance of analysed isotope

Fractured apatite.

Analysis	9	8	10	5	6	7	12
Ca^{44}	654211	506902	524276	647907	576162	462588	561794
a	1000	1000	1000	1000	1000	1000	1000
La^{139}	1821	1584	1648	2911	252	239	462
a	2.78	3.12	3.14	4.49	0.44	0.52	0.82
b	2.78	3.12	3.14	4.49	0.44	0.52	0.82
Ce^{140}	2451	2279	2797	3544	383	355	669
a	3.88	4.49	5.33	5.47	0.66	0.77	1.19
b	4.39	5.08	6.03	6.19	0.75	0.87	1.35
Pr^{141}	438	389	621	639	106	80	147
a	0.67	0.77	1.18	0.99	0.18	0.17	0.26
b	0.67	0.77	1.18	0.99	0.18	0.17	0.26
Nd^{143}	664	534	707	773	384	344	408
a	1.01	1.05	1.35	1.19	0.67	0.74	0.73
b	8.27	8.60	11.06	9.75	5.49	6.06	5.98
Sm^{147}	182	159	190	186	106	96	112
a	0.28	0.31	0.36	0.29	0.18	0.21	0.20
b	1.88	2.08	2.41	1.94	1.21	1.41	1.34
Eu^{151}	1245	1019	1011	1314	1008	791	1009
a	1.90	2.01	1.92	2.03	1.75	1.71	1.80
b	3.98	3.58	4.02	4.25	3.67	1.71	3.77
ThO^{249}	110	62	177	124	0.67	-	6.69
a	0.17	0.122	0.34	0.19	1.2×10^{-3}	-	0.012
UO^{255}	18	37	31	61	7.67	8.00	5.46
a	0.028	0.073	0.059	0.094	0.013	0.017	0.0097

9 8 10 5 6 7 12
....high-U.... ..low-U...

a = counts standardised to 1000 Ca
b = counts corrected for isotopic abundance of analysed isotope

A.3: PARTITION COEFFICIENTS

Arth and Hanson (1975).
(used in the REE models for Lewisian gneiss petrogenesis).

	Garnet	Pyroxene	Hornblende
Ce	0.35	0.50	1.52
Nd	0.53	1.11	4.26
Sm	2.66	1.67	7.77
Eu	1.50	1.56	5.14
Gd	10.50	1.85	10.00
Dy	28.60	1.93	13.00
Er	42.80	1.66	12.00
Yb	39.90	1.58	8.38
Lu	29.60	1.54	5.50

Villement et al. (1981).
(used in modelling of fractional crystallisation of the Glen Dessarry syenites).

	Pyroxene	Plagioclase	K-feldspar	Hornblende	Biotite	Sphene
U	0.05	0.06	0.10	0.15	0.13	-
Th	0.04	0.05	0.09	0.11	0.12	-
Rb	0.04	0.13	0.30	1.90	1.90	-
Ba	0.04	0.56	3.60	6.40	10.00	-
Sr	0.16	2.70	10.00	0.30	0.70	-
Hf	0.48	0.05	0.13	0.92	1.80	-
Ta	0.06	0.04	0.08	0.62	0.56	-
Cr	5.30	0.08	0.60	2.90	5.40	-
Ni	2.50	0.04	0.50	-	1.30	-
Ce (approx)	0.18	0.20	-	0.68	0.70	80.00
Yb (approx)	0.53	0.12	-	0.53	0.80	72.00

Bender et al. (1984).
(used in modelling of contamination of Glen Dessarry mafic syenite via Moine partial melting).

	Plagioclase	Biotite
La	0.20	0.34
Ce	0.15	0.32
Nd	0.12	0.29
Sm	0.09	0.26
Eu	0.50	0.24
Gd	0.09	0.28
Dy	0.06	0.29
Er	0.05	0.35
Yb	0.04	0.44
Rb	0.07	3.00
Sr	3.00	-
Ba	0.23	12.00

Data from other sources required to complete the previous sets for the elements of interest.

Worner et al. (1983).

	Sphene	Apatite
Th	8.00	1.20
U	2.10	0.00
Ta	113.0	-
Hf	14.20	-

Mahood and Hildreth (1983).

	Zircon	Allanite
Th	91.20	548.0
U	383.0	17.00
Ta	40.20	4.40
Hf	3742.	28.00
Ce	10.00	2494.
Yb	564.0	37.00

Henderson (1982).

	Apatite
Ce	31.00
Yb	21.00

Estimate from data produced for this study.

	Zirconolite
Th	8000
U	15000
Ta	1500
Hf	1000
Ce	150
Yb	400

ENCLOSURES

1) FOWLER, M.B. 1981. Uranium content, distribution and migration in the Glendessarry syenite, Inverness-shire. Mineral. Mag. 44, 443-448.

2) WATSON, J.V., FOWLER, M.B., PLANT, J.A., SIMPSON, P.R. and GREEN, P.M. 1982. Uranium provinces in relation to metamorphic grade and regional geochemistry. In: Uranium Exploration Methods. IAEA/NEA, Paris. pp 235-248.

3) FOWLER, M.B., WILLIAMS, C.T. and HENDERSON, P. 1983. Rare earth element distribution in a metasomatic zoned ultramafic pod from Fiskenaesset, West Greenland. Mineral. Mag. 44, 171-177.

MINERALOGICAL MAGAZINE, DECEMBER 1981, VOL. 44, PP. 443-8

Uranium content, distribution, and migration in the Glendessarry syenite, Inverness-shire

M. B. FOWLER

Department of Geology, Imperial College, London SW7 2BP

ABSTRACT. The distribution of uranium in a suite of variably deformed and metamorphosed rocks from the leucocratic member of the Glendessarry syenite has been determined using the fission track method. The uranium content of the magma increased during crystallization and uranium was concentrated in accessory minerals such as monazite, zircon, sphene, allanite, apatite, and micro-inclusions of a Zr- and Ti-rich phase. Contamination of the magma by pelitic metasediment enhanced the uranium content and monazite and zircon formed instead of sphene, allanite, and apatite.

Evidence of subsolidus uranium mobility in late stage magmatic or metamorphic fluids is presented here and shows: (*a*) Intracrystalline redistribution of uranium, especially in grains of sphene. (*b*) Intergranular mobility in a fluid phase, which affected the uraniferous accessory minerals in several ways.

STUDIES of the behaviour of uranium during high-grade metamorphism have recently gained importance and large-ion lithophile element depletion in some granulite-facies terrains is relatively well established (e.g. Lambert and Heier, 1967); however, the processes responsible for uranium mobility are still under discussion (Collerson and Fryer, 1978; Fyfe, 1973). The interest in high-grade metamorphic terrains in genetic studies of ore-forming processes concerns their role as a source region for upper crustal uranium deposits (e.g. Kostov, 1977), and their influence on the formation and subsequent evolution of U-provinces.

The Glendessarry syenite is suitable for detailed studies for the following reasons: (*a*) It is a product of deep-seated processes. (*b*) Intrusion occurred at a low crustal level. (*c*) Amphibolite-facies metamorphism contemporaneous with intrusion affected the complex to varying degrees. (*d*) Uranium is concentrated in a limited number of accessory minerals, some of which commonly occur in the lower crust.

A comparative investigation of metamorphosed and non-metamorphosed phases of the complex was undertaken in relation to studies of uraniferous accessory minerals. Johnstone *et al.* (1969) described the regional setting of the syenite (fig. 1) and its emplacement in high-grade psammitic and pelitic Moinian metasediments. Lambert *et al.* (1964) established the magmatic origin and syn- or slightly pretectonic timing of the intrusion and Van Breeman *et al.* (1979) reported a U-Pb isotopic age of 456 ± 5 Ma and proposed a mantle origin. A detailed petrological study was carried out by Richardson (1968), who ascribed mineralogical changes (summarized in Table I) to an influx of H_2-rich, reducing fluids from sediments during amphibolite-facies deformation.

A suite of twelve samples of the leucosyenite was selected to represent different stages of metamorphism/deformation. Polished thin sections were used for induced fission track analysis of ^{235}U (Bowie *et al.*, 1973) with a neutron dose of 5×10^{16}n cm^{-2}, undertaken at the HERALD reactor AWRE, Aldermaston. Lexan polycarbonate plastic is the preferred detector because of its low uranium content; the detector discs were etched in 6*N* NaOH at 75 °C for four minutes. Rock powders were analysed by the delayed neutron method (Bowie *et al.*, 1973).

Results

General

Most of the uranium is located in accessory minerals, which in decreasing order of U content are: Zr/Ti rich inclusions in perthite; monazite-

TABLE I. *Summary of relevant mineralogical changes in the syenite due to amphibolite facies-metamorphism. After Richardson (1968)*

Original Mineralogy	Effects of metamorphism
Alkali feldspar phenocrysts	Granular orthoclase and sodic plagioclase
Pyroxene-biotite intergrowths	Hydration to ultimately pyroxene-free, hornblende-biotite associations
Accessory calcite	Calcite absent
Euhedral sphene	Recrystallization and loss of crystal outlines
Coarse-grained igneous texture	Development of well-defined fabric and diminution of grain size

© *Copyright the Mineralogical Society*

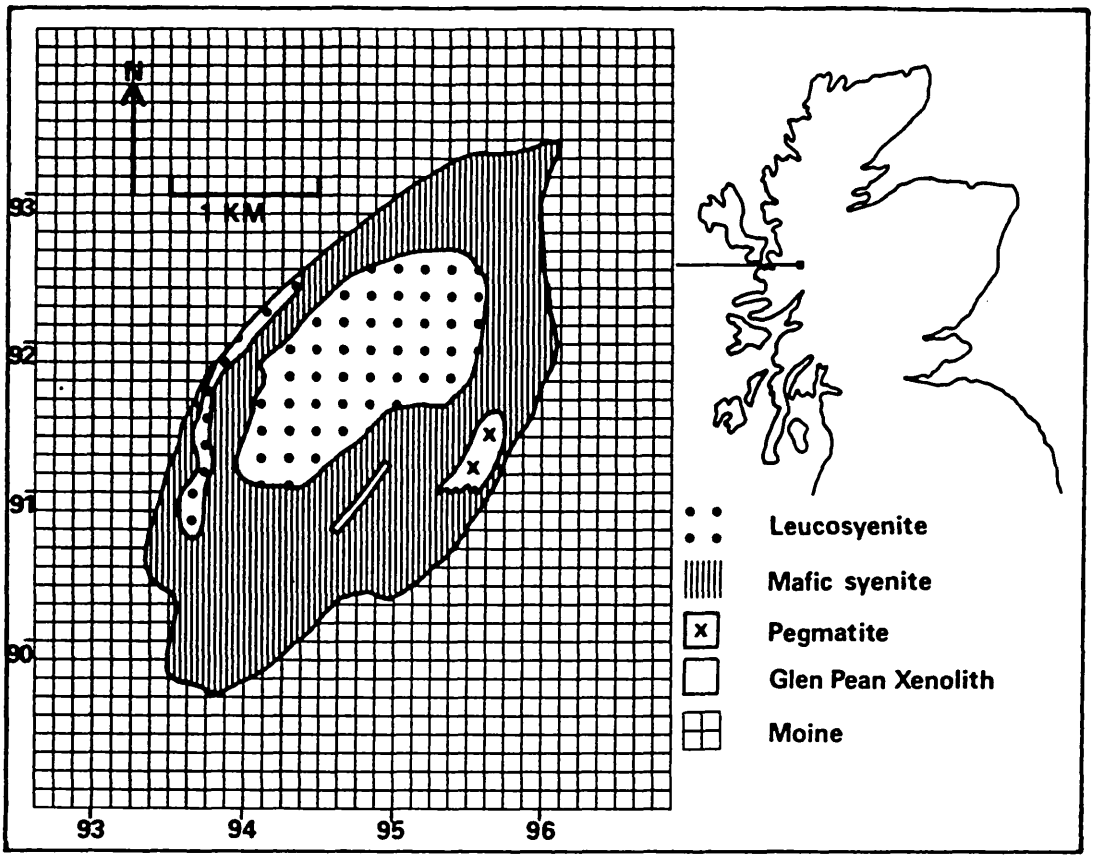


FIG. 1. Geological map of the Glendessarry syenite, Inverness-shire.

zircon; sphene-allanite; and apatite, which is in general agreement with previously published data (Rogers and Adams, 1969). Uranium is not significantly associated with the primary rock-forming minerals or absorbed on grain boundaries.

The primary uranium distribution

All the leucocratic rocks at Glendessarry exhibit some metamorphic/deformation effects. However, samples from the centre of the leucosyenite mass show least post-magmatic recrystallization and the distribution of uranium in relict euhedral minerals from this phase is thought to be relatively unmodified by secondary processes. In these rocks uranium is associated with the Zr/Ti rich inclusions, zircon, sphene, allanite, and apatite. Its distribution in the latter three principal uraniferous minerals is shown in fig. 2*A*. Most sphene and apatite crystals have uniform fission track distributions, but the track density varies between crystals. Since other sphene grains show an increase in uranium concentration towards the edges (fig. 2*B*), those uniform crystals with greater abundance are considered to have formed later indicating increased uranium concentration in the residual magma, as recorded by other workers (e.g. Bohse *et al.*, 1974). Both uniform and regularly zoned U distributions indicate solid solution of uranium within the crystal lattice.

In a vein intruded into the Glen Pean Xenolith (fig. 1), zircon occurs with monazite and together they contain a high proportion of the whole-rock uranium (fig. 2*C*) of 7.8 ppm. This rock, composed of perthite associated with biotite, muscovite, and quartz, with minor pyrite indicative of more reducing conditions of crystallization than the leucosyenites in which primary hematite formed (Richardson, 1968), may be the product of contamination of the magma by country-rock metasediment.

Secondary uranium redistribution

Redistribution of uranium within the syenites, sometimes directly related to the hornblende-rich, foliated members of the suite, is interpreted below

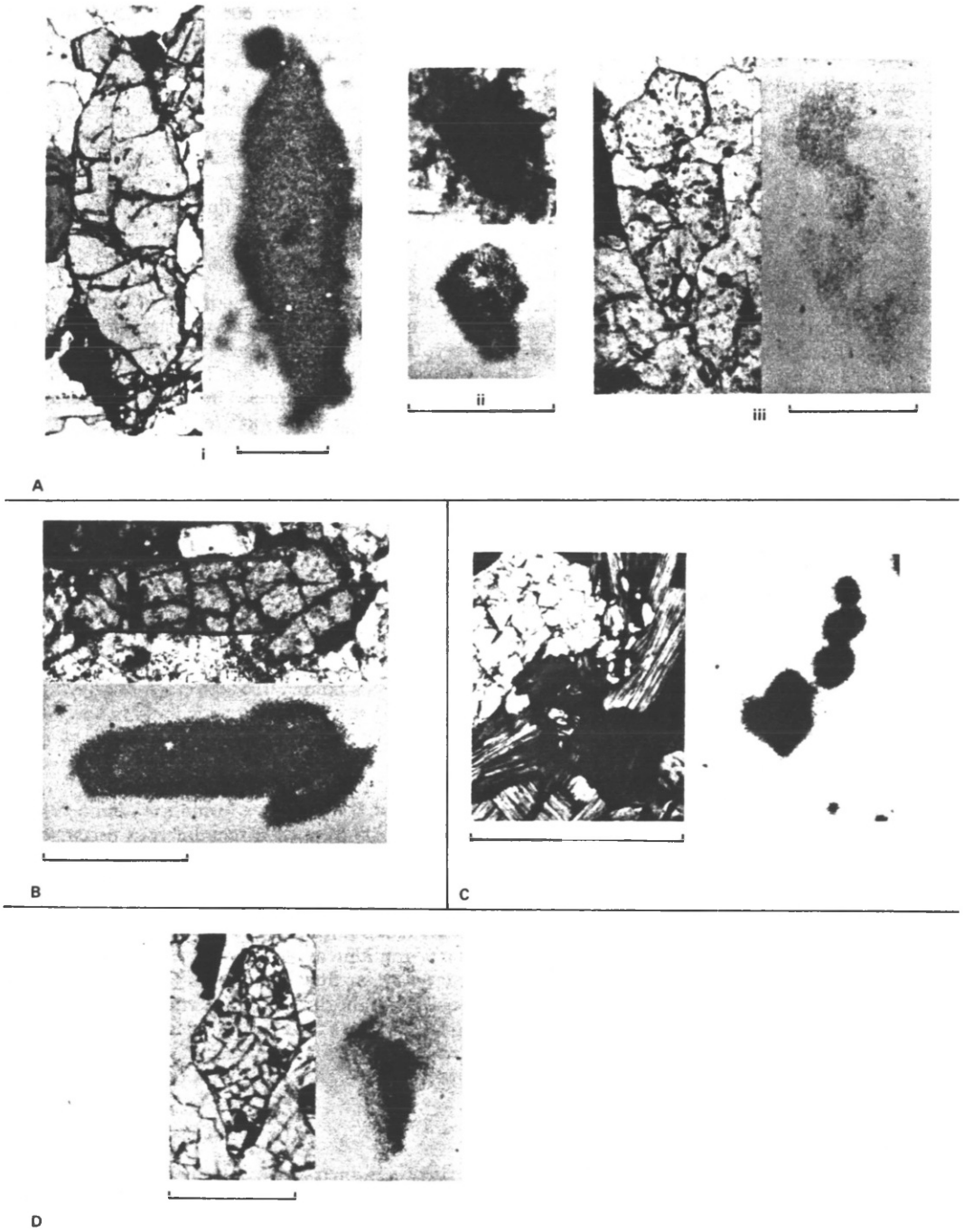


FIG. 2. Photomicrograph–Lexan plastic overlay pairs showing: *A*. i. Sphene, ii. Allanite, iii. Apatite. *B*. Sphene with regular zoning of uranium. *C*. Uraniferous accessories in syenitic vein intruded into the Glen Pean xenolith–zircon and monazite in biotite associated with feldspar. *D*. Apatite grain with an irregular, U-rich core. Scale bar = 0.5 mm.

in the light of three possibilities (cf. Clark *et al.*, 1979). (i) New mineral growth associated with addition of U. (ii) U addition or loss with no new mineral growth. (iii) Internal U mobility and concentration.

The uranium-bearing accessory minerals are described below in relation to uranium redistribution:

Apatite. A cluster of apatite, sphene, allanite, and biotite crystals in alkali feldspar is shown in fig. 3*A*. The corresponding fission track distribution contains linear areas with lower track density (relative to the host apatites) which correspond to intergrain boundaries. Other apatites are irregularly zoned (fig. 2*D*) with uranium-poor rims—the inverse of the expected magmatic trend. The simplest interpretation of both these features involves uranium scavenging by an intergranular fluid phase.

Sphene. Large (up to 1 cm), euhedral grains of sphene respond to deformation by loss of their crystal outlines and diminution of grain size, associated with recrystallization and rotation into concordance with the developing fabric. Some grains thus affected possess zones with high uranium concentration as indicated by the variable track density (fig. 3*B*). Isochemical recrystallization accompanied by internal uranium mobility may have been accompanied by addition of uranium from an intergranular fluid. The development of a heterogeneous uranium distribution in sphene associated with an elevated whole-rock uranium content (Table II) suggests that such late addition of uranium may be responsible for the variation shown.

Sphene in recrystallized samples forms overgrowths on iron oxide as a result of its interaction with plagioclase feldspar. Since neither precursor is uraniferous and the overgrowths are significantly enriched in uranium (fig. 3*C*), the presence of a subsolidus fluid phase capable of uranium transport may again be inferred.

Allanite. In the least deformed members of the suite, allanite is rare but has a euhedral habit sometimes associated with strong colour zoning. It is more abundant in the hornblende-rich leucosyenite where secondary allanite is usually more uraniferous than its primary analogue, and may also have an inhomogeneous uranium distribution (fig. 3*D*). Allanite also occurs as reaction rims on apatite, probably related to the circulation of uranium and *RE*-bearing fluids within the syenite.

TABLE II. *Relationship of whole-rock uranium content to its occurrence in sphene*

Field no.	U (ppm)	Uranium distribution in sphene grains
42774	1.3	uniform or regular zonation (magmatic)
42778	1.5	
42780	1.1	
42781	1.8	
45660	1.3	
45670	1.5	
48474	1.2	
42791	1.9	zones of high uranium content in one or more grains
45662	1.9	
45671	2.4	
45672	2.8	

Discussion

Although the uranium content of these rocks is concentrated in the accessory magmatic minerals, there is substantial evidence for its transport during sub-solidus fluid migration. The uraniferous phases reacted to this process in different ways: for example, uranium was leached from apatite although there is evidence for its concentration in sphene; most allanite is secondary, fixing formerly mobile uranium, but zircon has embayments (Van Breeman *et al.*, 1979) indicative of corrosion and uranium release. Such varying responses may be due to fundamental differences resulting from the physico-chemical nature of the minerals themselves, or to chemical evolution of the fluid. Although Richardson (1968) documented the interaction of the syenite with H_2-rich, reducing country-rock fluids, late-stage magmatic fluids may also have been involved, particularly in view of the syntectonic nature of the syenites. Redistributive processes may be similar to the incipient stages of the model proposed by Simpson *et al.* (1979) and Plant *et al.* (1980) for the formation of mineralized granites (*s.l.*) from their metalliferous precursors.

Questions raised by this study include: (i) The extent to which processes demonstrated by fission track radiography result directly from amphibolite-facies metamorphism. (ii) The source of the secondary uranium and its possible transport by an intergranular fluid phase. (iii) The chemical composition of the fluid and speciation of the uranium. (iv) The extent to which the development of high uranium zones in sphene was an iso-chemical process.

Conclusions

Features of the primary uranium distribution are preserved in the least-deformed syenites, and these suggest that the magmatic uranium content increased during crystallization. Most of the uranium present in these rocks is concentrated in six minor or accessory minerals: Zr/Ti-rich inclusions, monazite, zircon, sphene, allanite, and apatite. Metasediment contamination at the magmatic stage produced a different suite of urani-

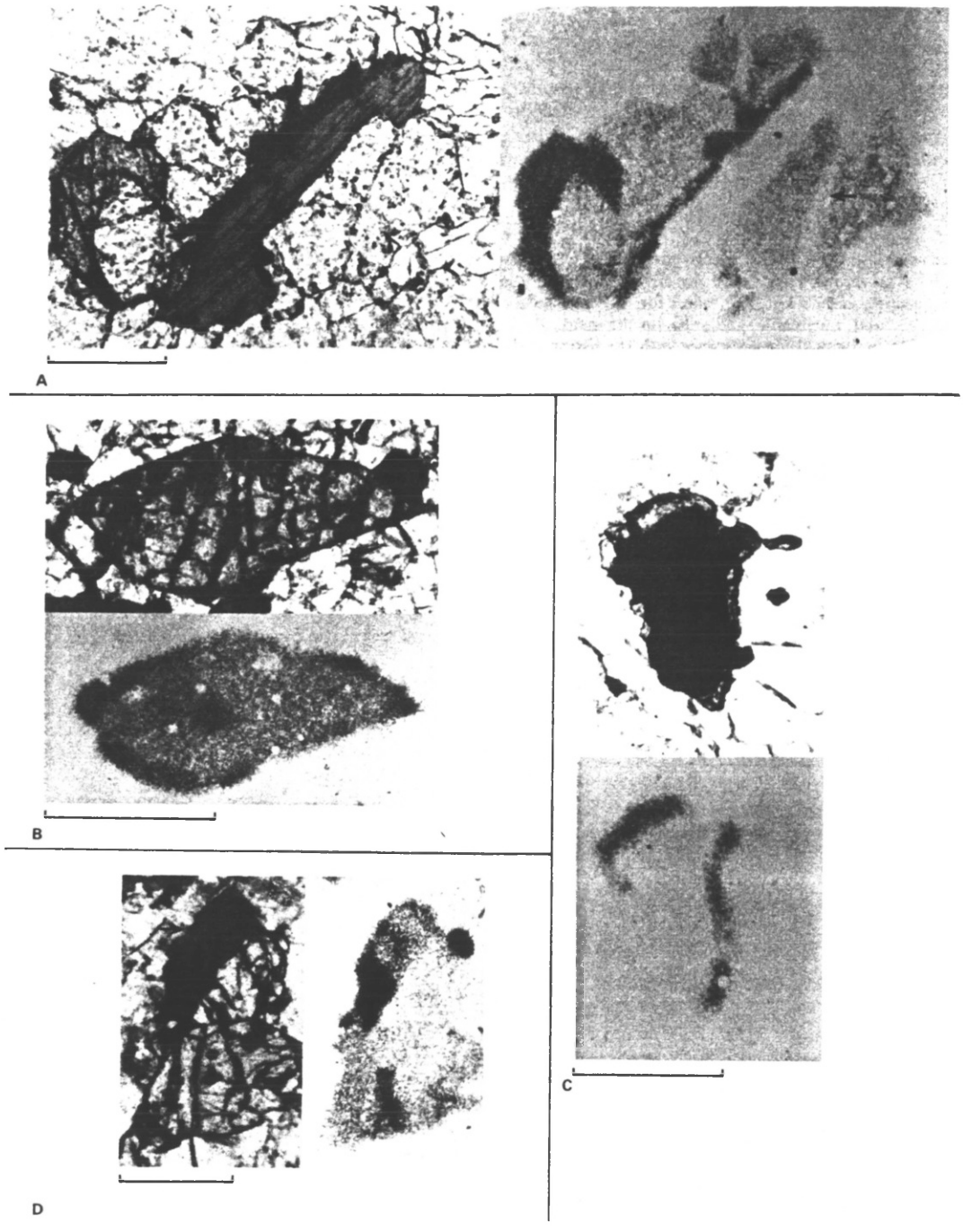


FIG. 3. Photomicrograph–Lexan plastic overlay pairs showing: *A*. Areas of low fission track density (arrowed) associated with grain boundaries in apatite. *B*. High fission track density indicating local uranium concentrations in sphene. *C*. Secondary, U-bearing sphene reaction rims on iron oxide phase enclosed in feldspar. *D*. Allanite (arrowed) with variable track density associated with apatite. Sphene in lower half of the photograph and U-rich zircon (top right) are also present. Scale bar = 0.5 mm.

ferous accessories and a higher whole-rock uranium content. Secondary uranium mobility has occurred on at least two scales: (*a*) Intracrystalline movement of uranium which produced zones of high uranium content and general variation in uranium distribution. (*b*) Uranium movement in solution causing depletion of uranium in apatite and precipitation of secondary uranium bearing mineral phases, such as allanite.

Acknowledgements. Many thanks are due to Professor J. V. Watson and Dr J. Plant for critically reading the manuscript, and to Dr D. I. Smith for provision of the samples and invaluable guidance in the field. P. R. Simpson is thanked for assistance with the fission track method which was carried out using facilities at the Institute of Geological Sciences and AWRE Aldermaston. The NERC is gratefully acknowledged for the provision of a Research Studentship.

REFERENCES

Bohse, H., Rose-Hansen, J., Sorensen, H., Steenfelt, A., Lovborg, L., and Kunzendorf, H. (1974). In *Formation of uranium deposits*, IAEA Vienna, 49-60.

Bowie, S. H. U., Simpson, P. R., and Rice, C. M. (1973). In *Geochemical exploration 1972*, ed. M. J. Jones, pp. 359-72. London: Institution of Mining and Metallurgy.

Clark, G. J., Gulson, B. L., and Cookson, J. A. (1979). *Geochim. Cosmochim. Acta*, **43**, 905-18.

Collerson, K. D. and Fryer, B. J. (1978). *Contrib. Mineral. Petrol.* **67**, 151-67.

Fyfe, W. S. (1973). *Phil. Trans. R. Soc. Lond.* **A273**, 457-61.

Johnstone, G. S., Smith, D. I., and Harris, A. L. (1969). In Kay, M. (ed.), *North Atlantic—Geology and Continental Drift*, a symposium, Am. Assoc. Petrol. Geol. Mem. 12, 159-80.

Kostov, I. (1977). In *Recognition and evaluation of uraniferous areas*. IAEA Vienna, 15-33.

Lambert, I. B. and Heier, K. S. (1967). *Geochim. Cosmochim. Acta*, **31**, 377-90.

Lambert, R. St. J., Poole, A. B., Richardson, S. W., Johnstone, G. S., and Smith, D. I. (1964). *Nature*, **202**, 370-2.

Plant, J. A., Brown, G. C., Simpson, P. R., and Smith, R. T. (1980). *Trans. Inst. Mining Metall.* **B89**, 198-210.

Richardson, S. W. (1968). *Q. J. Geol. Soc.* **124**, 9-51.

Rogers, J. J. W. and Adams, J. A. S. (1969). In Wedepohl, K. H. (ed.), *Handbook of geochemistry*, 11-17. Springer, Berlin.

Simpson, P. R., Brown, G. C., Plant, J. A., and Ostle, D. (1979). *Phil. Trans. R. Soc. Lond.* **A291**, 385-412.

Van Breeman, O., Aftalion, M., Pankhurst, R. J., and Richardson, S. W. (1979). *Scott. J. Geol.* **15**, 49-62.

[*Revised manuscript received 11 August 1981*]

URANIUM PROVINCES IN RELATION TO METAMORPHIC GRADE AND REGIONAL GEOCHEMISTRY

Janet Watson*, M. B. Fowler*, Jane Plant**, P. R. Simpson**, P. M. Green**

* Dept Geology, Imperial College, London SW7 2BP
** Institute of Geological Sciences, London WC1X 8NG

ABSTRACT

Uranium concentration/mineralisation occurs in the northern province of the British Caledonides in association with late tectonic granites and Old Red Sandstone molasse facies sediments. Regional geochemical maps are used to investigate variations in uranium levels in the metamorphic basement complex of the province in relation to the original composition, metamorphic grade and migmatisation in lower-middle crustal conditions (granulite-amphibolite-greenschist facies). Particular attention is paid to the relationship between uranium content, calculated heat production and metamorphic grade and correlations between the behaviour of U, LIL, HFS and other trace and major elements are discussed.

The primary rock composition up to and including upper amphibolite facies, appears to control uranium distribution on the regional scale. However, large scale regional depletion of uranium occurs in the Archaean basement complex of the Caledonian Province at the upper amphibolite/granulite boundary. The factors controlling uranium depletion at high grades are investigated by detailed whole rock geochemical and mineralogical studies. The results are discussed in relation to the variable uranium content of zircon from different metamorphic grades as shown by other workers. The relative importance of partial melting and fluid phase infiltration to the migration of uranium in metamorphic environments is discussed with particular reference to the identification of uranium provinces.

INTRODUCTION

Much of the available literature relating to U deposit genesis concerns the role of processes associated with acid plutonism or volcanism, or that of processes in surficial environments where pH and redox potential fluctuations occur at low P, T. However, the recognition that some economic U deposits may derive directly or indirectly from regional metamorphism and its concomitant dehydration/decarbonation reactions [1], lends a degree of importance to detailed studies of metamorphic terrains. Information relating the microchemical behaviour of U during metamorphic reactions to ore-forming processes is somewhat sparse, yet may be of increasing relevance to exploration needs as currently viable sources are exhausted and lower-grade ore-bodies are actively sought.

The first part of this paper presents a review of the regional geochemical framework applicable to the investigation of metamorphic areas, based on the example of Northern Scotland and using the data from the regional stream sediment geochemical survey undertaken by the IGS [2, 3, 4, 5, 6]. This area is ideally suited to such a study since it includes representatives of all metamorphic grades from greenschist to granulite facies, in geological settings where metamorphism can be related to contemporary tectonic and magmatic events. The second part of the paper concerns the results of more detailed lithogeochemical studies of areas selected on the basis of the regional data for their relevance to the understanding of processes influencing the mobility of U in metamorphic environments. Finally, the relative importance of fluid- and magma-dominated processes is assessed with respect to their ability to mobilise and concentrate U. Geochemical criteria are developed to facilitate recognition of metamorphic U mobility, which may then be applied to the exploration of metamorphic terrains elsewhere in relation to the genesis of U provinces.

GEOLOGICAL SETTING

The distribution of the major geological units within the portion of N Scotland which has been covered by the stream sediment survey to date, is shown in Figure 1. A brief review of the geology will facilitate interpretation of the geochemical maps discussed below.

The Hebridean Craton exposed in the far NW represents an old, deeply eroded terrain. It comprises the Lewisian basement complex of dominantly granodioritic-tonalitic gneisses, with older basic-ultrabasic units and sparse metasediments which were metamorphosed at ~ 2900 Ma in conditions of upper amphibolite or granulite facies. Subsequent metamorphic and tectonic reworking at lower grade continued periodically until about 1800 Ma, spanning the intrusion of the mafic Scourie Dyke suite at ~2400 Ma. Overlying this basement complex is the undisturbed, largely fluviatile Torridonian Formation (late Proterozoic), together with younger formations. The Hebridean Craton is bounded in the east by the eastward-dipping Moine Thrust Zone, which marks the front of the Caledonian orogenic belt. Reworked Lewisian probably continues at depth as far south as the Southern Uplands Fault [7] underlying the metamorphosed sediments and associated intrusive masses of the Caledonian cycle. During this cycle the late Proterozoic to lower Palaeozoic cover units of the Moine and Dalradian groups were folded, metamorphosed and invaded by a variety of igneous rocks, including the well-developed Caledonian granite suites whose origin is currently under discussion. The metamorphic grade reached in the metasediments varies regionally from lower greenschist facies in the west and south, to upper amphibolite facies in parts of the interior. Migmatites are associated with the highest metamorphic grades. The areal distribution of the metamorphic zones is relatively well-established [8], so the consideration of regional geochemical trends may be directly related to the metamorphic grade. Late- and post-orogenic uplift at the end of the Caledonian cycle resulted in rapid erosion and deposition of a second fluviatile and lacustrine sequence in fault-bounded troughs and basins - the Old Red Sandstone (Devonian). Thus an interesting comparison may be drawn between the essentially barren Torridonian succession and the locally mineralised ORS [9].

REGIONAL DISTRIBUTION OF URANIUM IN RELATION TO METAMORPHIC GRADE

The basis for the following discussion is stream sediment geochemical data which may be used to relate the regional distribution of U to that of selected other elements, to heat production, and to K/Rb and U/Zr ratios. This approach should help identify the geochemical associations with which U is mobile and simplify the development of regional geochemical criteria pertinent to the requirements for exploration in metamorphic terrains.

Pre-Caledonian basement

The essential features of U distribution in the Lewisian basement were established by the Archaean 'Badcallian' metamorphism. Evidence from Pb-isotope systematics [10] implies a widespread phase of variable U loss. This is clearly demonstrated on the U map (Figure 2) which records very low U values over the whole Lewisian outcrop. However, values are not uniform and in accord with detailed lithogeochemical investigations [e.g. 11], two extreme end-members may be recognised on the basis of U abundance. In general, regions with the lowest U correspond to high pressure granulite facies Badcallian metamorphism while those with (relatively) high U represent areas which did not exceed amphibolite facies during the metamorphic event. This correlation extends to the lithophile elements Th, Rb, K, Be, Li which show a very similar distribution. Regional U depletion during granulite grade metamorphism may therefore be monitored using a variety of elements which do not require access to a reactor for analytical purposes at low concentrations. Further refinement of the simple amphibolite/granulite distinction is possible by examination of a transition zone identified on the west coast of the mainland. Values of U in sediment around the type granulite area near Scourie (Figure 1) are mostly below 1 ppm, equivalent to whole rock concentrations of 0.05-0.07 ppm average([12] and below). The higher values recorded for amphibolite-facies metamorphism (e.g. at Rhiconich, Figure 1) fall between 3 and 5 ppm in sediments, which is equivalent to $\sim$3 ppm in whole rock samples [11]. However, the area around Gruinard Bay at the southern margin of the granulite terrain (Figure 1) exhibits sediment U values of 1-3 ppm, intermediate between the above extremes. The transitional nature of this marginal tract identifies the area as suitable for a detailed lithogeochemical investigation into the processes responsible for lower crustal element depletion, and the microchemical mechanisms by which it takes place (see below).

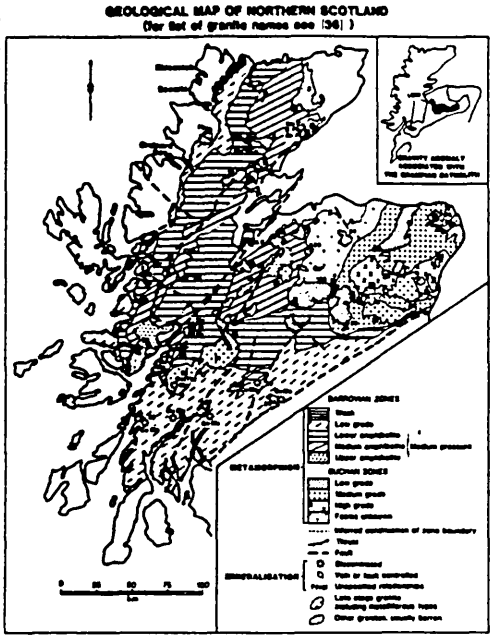
Regional purging of about 98% of the total U budget of granulite facies basement gneisses must release large quantities of the element, making it available for subsequent concentration during redeposition in higher crustal levels. An order of magnitude estimate of the tonnage of U released may be derived from approximate dimensions of the granulite block (50 x 20 x 5 km); an assumed density of 2.8 $g.cm^{-3}$; and an estimated pervasive removal of $\sim$3 ppm U from the rocks. This gives a total in the order of 10^{10} kg liberated by the high pressure granulite-facies metamorphic event. Interestingly, although the bulk of the Lewisian complex is undoubtedly U-poor, local concentrations are found which may be more numerous than is at first apparent (Watson, Plant and Fowler, unpublished scintillometer information), especially in areas of abundant basic-ultrabasic material around which culminations in U content have been recorded. Although part of the overall U budget may thus be merely redistributed during metamorphism, data from heat flow measurement through the continental crust [13] place severe constraints on the actual proportion represented by this fraction. Genetic models proposed to explain the low lithophile concentrations in the lower crust may be conveniently grouped into the following categories:

(a) They are a primary feature of lower crustal rocks.
(b) They are due to partial melt abstraction from amphibolite-facies mid-crustal gneisses.
(c) They are due to CO_2-rich fluid infiltration of the lower crust causing dehydration and associated granulite generation.

Most of the evidence from the Lewisian complex is consistent with model (c), notably (i) the lack of depletion in some typical lithophile elements such

Table I. Relationship between metamorphic facies and U content of Lewisian zircon

Metamorphic facies	U content of zircon in ppm [ref.]
Amphibolite	659-780 [35] 382-452 [36]
Granulite	44.3-56.9 [33] 33.3-55.3 [33]



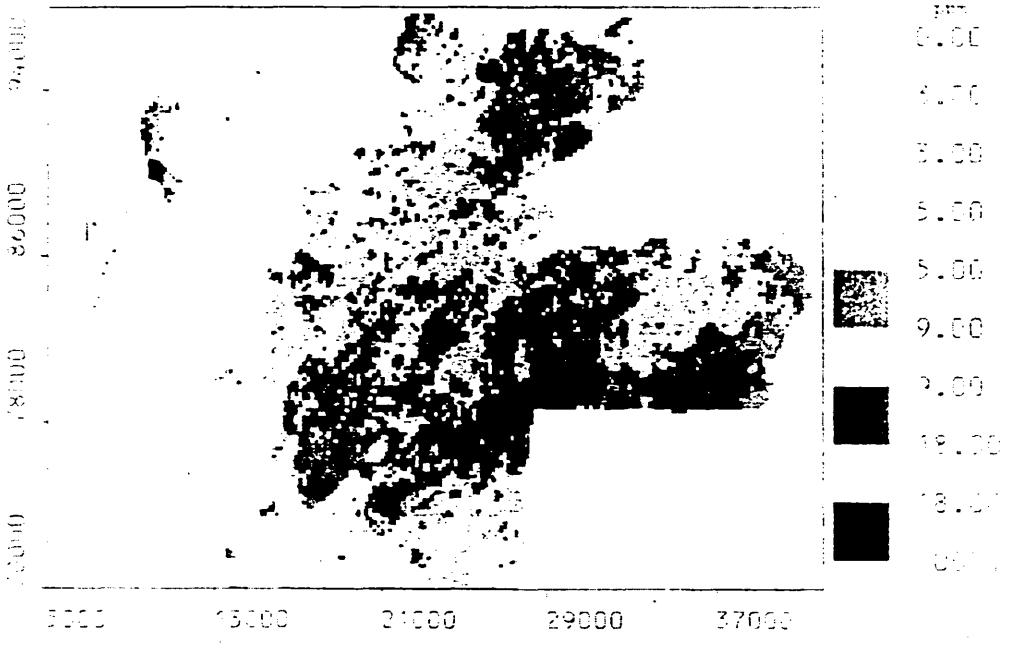


Figure 2. Distribution of Uranium in Stream Sediments, Northern Scotland.

as Ba, Zr which would be expected to enter a melt phase; (ii) the consistently low levels of the lithophile elements U, Th, Rb, K in rocks of diverse (basic to acid) compositions which have differing susceptibility to partial melting; (iii) the lack of field evidence for a widespread partial melting event; (iv) the low levels of Th, Rb, K in intercalated tracts of quartz-rich metasediments [14]. The fluid responsible for depletion may have been derived directly from the underlying mantle, causing a front of granulite formation and U loss as it rose into the lower crust [e.g. 15]. It may be significant that the Lewisian granulites are of high pressure type and are thought to have been formed at pressures of 10-14 kb [16, 17]. It is also well-established in the literature that the K:Rb ratio is a sensitive indicator of high-grade metamorphism and its associated U mobilisation. The type Scourie granulites show K:Rb ratios of $>$ 500 [12] while in amphibolite facies gneiss regions the ratio is usually $<$300. Interestingly, Gruinard Bay again lies in between these end-member values ([18] and below).

Tectonic and metamorphic reworking of the Lewisian granulites and gneisses continued sporadically during the period 2700-1800 Ma, resulting in widespread retrogression to amphibolite facies. The H_2O-dominated fluid activity associated with retrogression caused only limited chemical changes, the depleted geochemical signatures being widely preserved in retrogressed granulites [e.g.19]. No widespread re-introduction of U appears to have taken place at this time [19]. However, local anomalies of U and other lithophiles are recorded; firstly, in association with late Lewisian pegmatites ($\sim$1700 Ma), some of which carry accessory U- and Th-bearing minerals [20]; and secondly, in the vicinity of steep shear zones formed during the tectonic evolution of the basement.

The Laxford front which separates granulites of the Scourie area from less depleted gneisses to the north (Figure 1) is a steep NW-SE shear-zone of this type, characterised by strongly foliated schists and gneisses. A linear zone of U enrichment seen on the regional map (Figure 2) appears to relate partly to the presence of several granite sheets emplaced in the foliation and partly to the effects of metasomatic reactions around pods and layers of ultramafic or mafic rock in the retrogressed granulites. Biotite enrichment at felsic-ultramafic contacts is locally associated with increases in total radioactivity. These relationships suggest that ductile shear zones such as the Laxford front, with their strong planar fabrics, could act as channels for active fluids as well as for the ascent of magma from the lower crust or mantle.

Caledonian metamorphic complexes

The outcrops of the major cover units of Moine and Dalradian metasediments in the Caledonian province (Figure 1) are ideally suited to the study of regional U distribution in relation to the P-T conditions of metamorphic grades ranging from greenschist to amphibolite facies. The highest grades attained are restricted to certain areas in the interior of the orogen, surrounded to the west and south by progressively lower-grade assemblages (Figure 1). It is clear from the regional U map (Figure 2) that no systematic regional trends exist which may be directly attributed to the influence of metamorphic grade. The influence of original lithology is illustrated by low U values over areas where tectonic slices of Lewisian basement are interleaved with the Moinian [21], and by a tendency for U values over Dalradian terrains to be lower than those over the Moinian: low LIL and heat-producing elements in Dalradian areas are consistent with derivation of the Dalradian sediments from immature sourcelands. These characteristics persist along strike, across the metamorphic isograds. This supports views expressed in the literature [e.g. 22] and suggests that in metamorphic assemblages below granulite facies, variations in U content may be inherited from the parent rocks. A similar conclusion has been reached for the Dalradian on the basis of whole-rock determinations [23]. Although this does not preclude local U redistribution within specific geochemical environments, it does limit the degree to which ore-forming fluids may have been generated. The K:Rb ratios of the Moine and Dalradian terrains which are generally $<$ 300

reflect their upper crustal affinities, thus extending the relationship with regional U mobility. Two processes acting within the higher P-T regime of the amphibolite facies are worthy of particular comment:

(i) Extensive tracts of the metasedimentary formations which fall in the higher (kyanite, sillimanite) grades of Barrovian or Buchan metamorphism are characterised by an abundance of gneissose lithologies infused with granitic and pegmatitic veins and permeations. These regional migmatite complexes show a broad correlation with high U values in stream sediments, allowing the tentative inference of a regional influx of U during the migmatisation event, probably as a result of metasomatic processes.

(ii) Local partial melting at or close to the time of the metamorphic climax gave rise to a number of unequivocally 'S'-type granite magmas [24] which were subsequently intruded into the developing orogen as small plutons, often partially foliated. Interestingly, these show no discernible U enrichment and in this and many other geochemical and geophysical respects they merge with the host metasediments [24, 25]. Thus, for whatever reason, melting of crustal source rocks during metamorphism apparently has not radically fractionated U or the other LIL elements into the melt (Figure 2). In contrast, the later suite of metalliferous intrusions (including Cairngorm, Etive, etc.: [24]) contains concentrations well above the background levels for U and other incompatible trace elements. Substantial subcrustal involvement in their genesis has been invoked [26]. Evidence that the metamorphic grade of the host rocks plays an important part in the development of U and other mineralisation associated with such metalliferous intrusions is presented in Simpson et al. (this volume).

Although not directly of metamorphic origin, the local U mineralisation in parts of the Old Red Sandstone should be mentioned because it was formed when the metamorphic complex was undergoing rapid erosion. The general U abundance of the grey, lacustrine facies of the Middle ORS is high, and U concentrations have been found associated with bioturbation features [27]. It is also enriched in dark, phosphatic horizons rich in organic matter [21], and both these associations are consistent with an origin penecontemporaneous with deposition. Evidence for remobilisation of U during fracturing has been recorded, resulting in levels of up to 740 ppm in a calcitic fault breccia. Although the enhancement of U abundance in the ORS molasse-type sedimentary environment is related to surficial processes and pH/redox conditions, the original source may well have been the Moine/Dalradian metasediments and the Caledonian granites. Lithologically rather similar Torridonian sediments which incorporate detritus from the strongly depleted Lewisian complex are essentially barren. This difference may relate to the original U content and distribution in their respective source lithologies, as well as the effectiveness of syngenetic U concentration processes.

LITHOGEOCHEMISTRY

From the preceding discussion it is apparent that regional U mobilisation during high-grade (essentially granulite facies) metamorphism is potentially the most important feature from the exploration standpoint, since it resulted in the transfer of large amounts of U to the upper crust. Clearly, in order to predict the environments in which deposition and perhaps concentration of U might take place in connection with such a transfer, more detailed knowledge of the depletion process and of the nature and chemistry of the phase responsible (melt or fluid) is essential.

To date, detailed chemical studies of the U-poor Lewisian basement have concentrated on amphibolite and granulite facies end-members of the high-grade metamorphic continuum: that is, either rocks unaffected by lithophile depletion or those in which the process has progressed to completion. Thus, although the chemical effects of high-grade metamorphism are well documented, they are open to the various genetic interpretations documented above. Study of a geochemical transition zone in which the depletion process has been arrested before completion may provide further information for consideration in relation to these models. It

has been shown above that the Gruinard Bay area may fulfil the requirements for such a zone, so whole-rock samples have been chosen for more detailed geochemical study.

Representative samples were selected from a suite of ~60 Lewisian gneisses currently under investigation for comparison with published chemical data from amphibolite- and granulite-facies regions [11, 28]. These have been analysed for selected HFS and LIL elements using a combination of XRF, INAA and INA techniques. A fission track study [27] of the microdistribution of U was also undertaken in order to provide the mineralogical basis for a discussion of U depletion.

The histogram of sample U concentrations for the whole suite from the transition zone (Figure 3) indicates that these rocks contain an average of ~3 x the background U level recorded for granulite-facies gneisses [12] with a few ranging up to 7 x this abundance. However, even these higher values represent an 85% depletion relative to average crustal values and some rocks have lost all their 'depletable' U (based on average figures recorded in Figure 4). It may therefore be inferred that the gneisses from Gruinard Bay have been arrested in the final stages of U removal. In contrast, the average K:Rb ratio for gneisses from Gruinard Bay is approximately 400 [18], representing only ~50% of the total amphibolite-facies to granulite-facies increment [11]. This implies that the process responsible for the selective depletion of lithophiles has not operated in a wholly uniform way, since expulsion of U has been carried a stage further than that of Rb.

The REES are often referred to in petrogenetic discussion and since most available evidence suggests that they are not significantly mobile under the metamorphic conditions in question [29], they represent the most reliable group on which to base an inter-facies comparison, combined of course with comparable major element data. Figure 4 presents trace element information in the form of a rock/primordial mantle plot [30], facilitating direct comparison with amphibolite and granulite facies counterparts from Scourie and Rhiconich for which the data of Weaver and Tarney [11, 28] can be used. This figure provides a convenient encapsulation of the sum of the depletion processes and its details confirm that, whatever their overall nature, lithophile removal proceeded in a differential manner. The essential relevant feature is the marked drop in the more lithophilic elements (with the important exception of Ba), in granulites compared to amphibolite-facies rocks. Under the particular conditions attained within the transitional tonalitic gneisses at Gruinard Bay, U reached ~97% depletion; Th~95%; K~89%, and Rb ~77%. Clearly, any genetic model which requires gradual and uniform depletion of all lithophiles becomes untenable, in favour of a rather complex, perhaps multi-stage process partially dependent upon original rock mineralogy.

The removal of U will be particularly sensitive to the proportions resident in each distinct site: in solid solution in the rock-forming silicates; in discrete, high-U accessory minerals or on grain boundaries and in crystal defects. Clearly, each fraction will have a different susceptibility to depletion. Fission track analysis of ^{235}U allows determination of its microdistribution, and hence the relative contribution of each site to the total 'depletable' U may be investigated. A previous study of U microdistribution in relation to high-grade metamorphism [31] concluded that depletion is confined to the grain boundary fraction of the U budget. In the Gruinard Bay gneisses, which show an advanced stage of depletion, there are four major uraniferous accessory minerals - monazite, zircon, allanite and apatite - but virtually no grain boundary U. It is conceivable that the earlier, major phase of Scourian U loss was achieved by the removal of U on grain boundaries, perhaps at the onset of dehydration reactions (the Pb-isotope system records some depletion even in amphibolite-facies terrains, [10]) but detailed consideration of the U distribution suggests that this is only part of the story. Since in general whole-rock samples which contain accessory allanite, have higher U abundances than those which do not, the inference that allanite instability in granulite facies conditions - predictable on theoretical grounds - is important in reducing the U concentration to the background

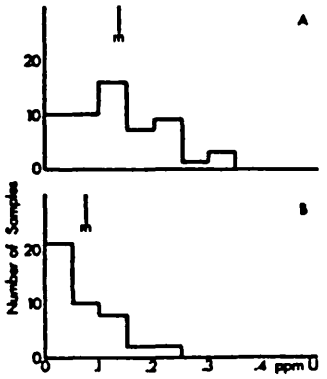


Figure 3. Uranium in whole-rock samples from Gruinard Bay (A) and Scourie (B = granulite facies): M = mean value.

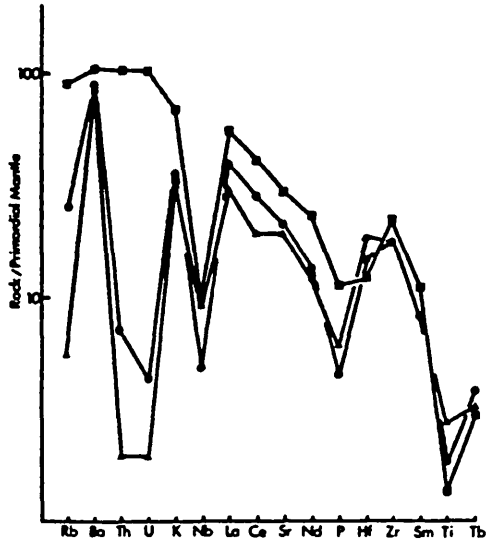


Figure 4. Trace element averages in Lewisian tonalitic gneisses: (triangles = granulite facies; squares = amphibolite facies; circles = Gruinard Bay).

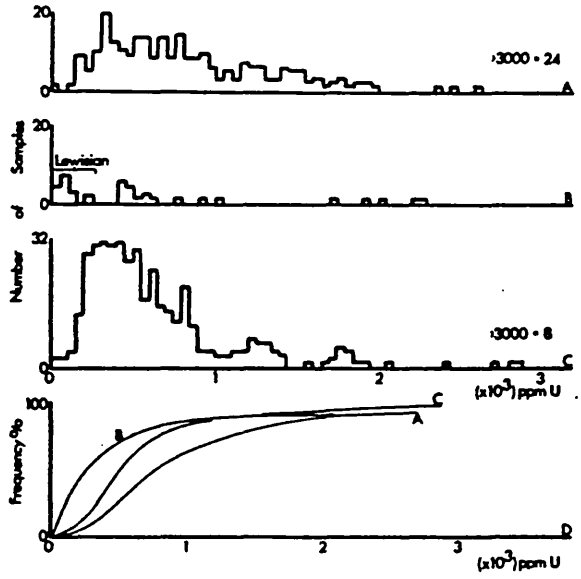


Figure 5. Uranium content of zircons. (A = Unmetamorphosed Felsic Igneous; B = Granulite facies; C = Amphibolite facies; D = Cumulative frequency curves).

granulite levels, seems plausible. Indeed, fresh granulites from the type area (Scourie) contain no allanite. On the other hand, apatite remains stable in granulites from Scourie but contains markedly less U than at Gruinard Bay (MBF, unpublished information). Whether U is leached from the apatite lattice [e.g. 32] or lost during a more complex process of mineral breakdown and reprecipitation, is not yet clear, but a process similar to the latter may be operative in zircon. Table 1 presents published U abundances of Lewisian amphibolite and granulite facies metamorphic zircons, and records approximately an order of magnitude variation between these extremes. The zircons are large and have the typical ovoid habit generated during the high-grade event [33]. The former existence of zircon in the undeformed protoliths is recorded by the presence of sparse U-rich premetamorphic cores. It is therefore inferred that the major phase of U loss from the zircon structure occurred during recrystallisation and new zircon growth at granulite grade, which was accompanied by resetting of the U-Pb isotopic system. The U content of zircon may therefore be a revealing factor for consideration in the assessment of U mobilisation in metamorphic terrains. Accordingly, a study of the U content of zircons from varying metamorphic grades has been undertaken, the data derived from published U-Pb geochronological studies.

Of the common U-bearing accessory minerals in igneous and metamorphic rocks, zircon consistently shows the highest U values. The stability of zircon at all grades of metamorphism and its widespread use for isotopic dating using the U-Pb system, has resulted in the publication of many analyses of the U content of zircons. Figure 5 summarises the range of U values in zircons from

(i) unmetamorphosed felsic igneous rocks (mainly granites, s.l.),
(ii) metamorphic rocks of amphibolite facies, and
(iii) metamorphic rocks of granulite facies.

Assuming that felsic igneous rocks were the principal sources from which zircons in both metasedimentary and metaigneous rocks were derived, these histograms may help elucidate the effects of metamorphic reactions involving U.

The most conspicuous feature of the histogram for unmetamorphosed igneous rocks is the wide range of variation. This feature is apparently primary, since high values are shown mainly by zircons from alkali granites and monzonites; lower (< 800 ppm) values mainly by zircons from granodiorites, tonalites and adamellites. Zircons from amphibolite-facies metamorphic rocks show a similar range of U values, but a better defined peak at 200-700 ppm. The clustering of data in this range suggests that there may have been some U loss from zircons derived from high-U sources but that no general re-equilibration has taken place. The high proportion of samples from which separated fractions (magnetic/nonmagnetic, or distinguished by grain size or habit) have proved to possess very different U content confirms this hypothesis. Although data from granulite-facies terrains are less abundant, certain pertinent observations may be made. The overall range in U content is approximately the same as for the amphibolite facies and granites, suggesting that granulite-facies metamorphism does not necessarily result in U depletion from the zircon lattice. On the other hand, zircons from high-pressure granulites all have very low U contents, approaching that of mantle zircon ($\sim$ 5-40 ppm), and it may be that high confining pressures are required to lower U to this background level. However, the cumulative frequency plot of the histogram data shows that there may be an overall regional trend towards lower levels of U in zircon with increasing metamorphic grade.

Zircon represents perhaps the most important uraniferous minor phase in the granulites of NW Scotland (MBF, unpublished fission-track information). This is reflected in the near coincidence of the average U:Zr ratio for granulite-facies whole-rock samples (data from Figure 4) with that in the zircons derived from granulite-facies rocks. In contrast, a similar comparison using amphibolite-facies samples reveals about an order of magnitude divergence between the respective U:Zr ratios. This is probably related to the increasing importance of the U budget fraction not located in the zircon lattice. Since there is no marked increase in U in water over the amphibolite-facies terrain (at Rhiconich, Figure 1), this is unlikely to be due solely to grain boundary U. More likely, and in accord with the mineralogical studies, is the increased stability of other

U-rich minor phases under these lower-grade conditions. Thus the inferred importance of minor mineral instability in U mobilisation from granulite terrains may be supported on a regional scale.

The regional distribution of U in water relates to its lithological residence site since to be easily leached by meteoric water U must be situated close to the solid/liquid interface [34], i.e., along grain boundaries or in cracks and fracture dislocations in the lattice structure. The uniformly low levels of U in water over the whole of the metamorphic province, bearing little relationship to the metamorphic isograds, suggests that the proportion present in such easily leachable sites may be rather limited, even in the low metamorphic grades. There are a few exceptions, which may generally be rationalised by reference to post-metamorphic hydrothermal processes.

DISCUSSION

It is apparent that the major U mobilisation event in the metamorphic complexes of N Scotland was related to the high-pressure granulite-facies event. The bulk of the evidence from this terrain is compatible with U removal via a pervasive, CO_2-rich fluid phase. Fission-track and mineralogical evidence suggests that such removal was not confined to U on grain boundaries [cf 31], but also involved U lost during destabilisation and/or recrystallisation of uraniferous minor mineral phases. Although the detailed mechanisms by which this process takes place are still under investigation, it is clear that their sum might provide a powerful precursor to an ore-forming event, since it releases very large quantities of U in a form suitable for subsequent concentration. There are indications that conditions required for the latter may be met by chemical or structural discontinuities which cause local perturbations in the fluid chemistry and so alter the solubility of whatever mobile U species is present. Although only minor accumulations of U and selected other elements have been detected in the study area, these do serve to indicate the possibilities of the overall process.

On the other hand, lithologies in which there is unequivocal evidence that crustal partial melts have been formed show no large-scale enrichment of U. For example, the 'S'-type Caledonian granite plutons formed at the acme of the metamorphic episode are noticeably U-poor when compared to other granites with postulated subcrustal genetic involvement [e.g. 5]. Although the regional migmatite terrains show a broad, low-level U enrichment, this may be due to metasomatic introduction rather than directly to partial melting, if indeed the latter is involved in their genesis. Moreover, partial melts such as these formed in a compressive tectonic regime, during or closely following penetrative deformation and with rapid water saturation, are unlikely to move far from their site of formation. The residence of U in the mobile phase is thus transitory, and ore-grade concentrations are unlikely to result. Further, such granites rarely reach the high crustal levels required for effective hydrothermal circulation and associated deposit formation.

In terms of an overall scheme for crustal U mobility and redeposition, three subdivisions of the continental crust may perhaps be postulated. The dominantly granulitic, lower crustal environment may be characterised by high pCO_2, pervasive U removal and a distinctive depleted geochemical signature (low U, Th, K, Rb, Cs, etc.; high K:Rb and low K:Ba, K:Sr). In this region the preliminary requirements of ore formation are met, but structural or chemical traps of a type not present in N Scotland are necessary in order to realise this potential. In the middle crust, partial melting may become more widespread particularly in compressive tectonic regimes,but this process is apparently unlikely to fulfil even the first requirement for deposit formation - the release of large quantities of U in a persistently mobile form. Indeed, in this low-medium metamorphic-grade environment, at which original lithological variation exerts an important control on U distribution, areas where the parent rocks included older U-rich rocks or where pre-metamorphic igneous activity introduced high-U plutons, may provide the only terrains where the metamorphic processes might favour mineralisation. Such conditions were not represented in Scotland.

The more familiar upper crustal regime provides a variety of opportunities for U deposit genesis, ranging from magma-epizonal water convective overturn to sedimentary concentration related to Eh/pH fluctuations. These have been considered at length in the literature and are beyond the scope of this paper. It is, however, worth repeating that whereas the cratonic cover overlying the depleted pre-Caledonian basement of the Hebridean Craton contains no known U mineralisation, the cratonic cover overlying the Caledonian province where U values are somewhat higher and where U-rich granites are present, contains small concentrations of U. Transfer of U from the crystalline basement to the cover by surface and near-surface processes may therefore have taken place.

Published by permission of the Director, Institute of Geological Sciences, London.

REFERENCES

1. Ryan, G. R., 1979. The genesis of Proterozoic uranium deposits in Australia. Phil. Trans. R. Soc. Lond. A 291, 339-353.

2. Institute of Geological Sciences, 1979. Geochemical Atlas of Gt Britain: Caithness and South Orkney. Inst. Geol. Sci. London.

3. Institute of Geological Sciences. In press. Geochemical Atlas of Gt Britain: Sutherland. Inst. Geol. Sci. London.

4. Institute of Geological Sciences. In press. Geochemical Atlas of Gt Britain: Hebrides. Inst. Geol. Sci. London.

5. Institute of Geological Sciences. In prep. Geochemical Atlas of Gt Britain: Great Glen. Inst. Geol. Sci. London.

6. Institute of Geological Sciences. In prep. Geochemical Atlas of Gt Britain: Moray-Buchan, Argyll-Tiree. Inst. Geol. Sci. London.

7. Bamford, D., Nunn, K., Prodehl, C. and Jacob, B., 1978. LISPB-IV. Crustal structure of Northern Britain. Geophys. J.R.Astr.Soc. 52.

8. Fettes, D. J., 1979. A metamorphic map of the British and Irish Caledonides, in: The Caledonides of the British Isles - Reviewed, eds. Harris, A. L., Holland, C. H. and Leake, B. E. (Geol. Soc. London), 307-322.

9. Gallagher, M. J., Michie, U. McL., Smith, R. T. and Haynes, L., 1971. New evidence of uranium and other mineralisation in Scotland. Trans. Instn Min. Metall. (Sect B: Appl. earth sci.) 80, B150-B173.

10. Moorbath, S., Welke, H. and Gale, N. H., 1969. The significance of lead isotope studies in ancient high grade metamorphic basement complexes as exemplified by the Lewisian rocks of northwest Scotland. Earth Planet. Sci. Lett., 6, 245-256.

11. Weaver, B. L. and Tarney, J., 1981. Lewisian gneiss geochemistry and Archaean crustal development models. Earth Planet. Sci. Lett. 55, 171-180.

12. Tarney, J., 1976. Geochemistry of Archaean high-grade gneisses, with implications as to the origin and evolution of the Precambrian crust, in: The Early History of the Earth, ed. Windley, B. F. (Wiley, London), 405-424.

13. Heier, K. S., 1979. The movement of uranium during higher grade metamorphic processes. Phil. Trans. R. Soc. Lond., A291, 413-421.

14. Okeke, P. O., Borley, G. D. and Watson, J., 1982. Geochemistry of metasedimentary gneisses in the Scourie Region, NW Scotland. Mineral. Mag. In press.

15. Newton, R. C., Smith, J. V. and Windley, B. F., 1980. Carbonic metamorphism, granulites and crustal growth. Nature, 288, 45-50.

16. Rollinson, H. R., 1981. Garnet-pyroxene thermometry and barometry in the Scourie granulites, NW Scotland. Lithos, 14, 225-238.

17. O'Hara, M. J., 1977. Thermal history of excavation of Archaean gneisses from the base of the continental crust. J. Geol. Soc. Lond. 134, 185-200.

18. Rollinson, H. R. and Windley, B. F., 1980. Selective Elemental Depletion During Metamorphism of Archaean Granulites, Scourie, NW Scotland. Contrib. Mineral. Petrol. 72, 257-263.

19. Beach, A. and Tarney, J., 1978. Major and trace element patterns established during retrogressive metamorphism of granulite-facies gneisses, NW Scotland. Precambrian Res., 7, 325-348.

20. von Knorring, O. and Dearnley, R., 1959. The Lewisian pegmatites of South Harris, Outer Hebrides. Mineral. Mag., 32, 366-378.

21. Watson, Janet V. and Plant, Jane, 1979. Regional geochemistry of uranium as a guide to deposit formation. Phil. Trans. R. Soc. Lond., A291, 321-338.

22. Bowie, S. H. U., 1979. The Mode of Occurrence and distribution of uranium deposits. Phil. Trans. R. Soc. Lond., A291, 289-300.

23. Atherton, M. P. and Brotherton, M. S., 1979. Thorium and Uranium in some pelitic rocks from the Dalradian, Scotland. Chem. Geol., 27, 329-342.

24. Plant, J., Brown, G. C., Simpson, P. R. and Smith, R. T., 1980. Signatures of metalliferous granites in the Scottish Caledonides. Trans. Instn Min. Metall. (Sect B: Appl. earth sci.), 89, B198-B210.

25. Johnstone, G. S., Plant, Jane and Watson, Janet V., 1979. Regional Geochemistry of the Northern Highlands of Scotland, in: The Caledonides of the British Isles - Reviewed, eds. Harris, A. L., Holland, C. H. and Leake, B. E. (Geol. Soc., London) 117-128.

26. Simpson, P. R., Brown, G. C., Plant, Jane and Ostle, D., 1979. Uranium mineralisation and granite magmatism in the British Isles. Phil. Trans. R. Soc. Lond., A291, 385-412.

27. Bowie, S. H. U., Simpson, P. R. and Rice, C. M., 1973. Application of fission-track and neutron activation methods to geochemical exploration, in: Geochemical Exploration, ed. Jones, M. J. (IMM, London), 359-372.

28. Weaver, B. L. and Tarney, J., 1980. Rare earth geochemistry of Lewisian granulite-facies gneisses, northwest Scotland: Implications for the Petrogenesis of the Archaean Lower Continental Crust. Earth Planet. Sci. Lett., 51, 279-296.

29. Hamilton, P. J., Evensen, N. M., O'Nions, R. K. and Tarney, J., 1979. Sm-Nd systematics of Lewisian gneisses: implications for the origin of granulites. Nature, 277, 25-28.

30. Wood, D. A., Toron, J-L., Treuil, M., Norry, M. and Tarney, J., 1979. Elemental and Sr isotope variations in basic lavas from Iceland and the surrounding ocean floor. Contrib. Mineral. Petrol., 70, 319-339.

31. Dostal, J. and Capedri, S., 1978. Uranium in Metamorphic Rocks. Contrib. Mineral. Petrol., 66, 409-414.

32. Fowler, M. B., 1981. Uranium content, distribution and migration in the Glendessary syenite, Inverness-shire. Mineral. Mag., 44, 443-448.

33. Pidgeon, R. T. and Bowes, P. R., 1972. Zircon U-Pb ages of granulites from the Central Region of the Lewisian, Northwestern Scotland. Geol. Mag., 109, 247-258.

34. Zeilinski, R. A., Peterman, Z. E., Stuckless, J. S., Roaholt, J. N. and Nkomo, I. T., 1981. The Chemical and Isotopic Record of Rock-Water Interaction in the Sherman Granite, Wyoming and Colorado. Contrib. Mineral. Petrol., 78, 209-219.

35. Pidgeon, R. T. and Aftalion, M., 1972. The geochronological significance of discordant U-Pb ages of oval-shaped zircons from a Lewisian gneiss from Harris, Outer Hebrides. Earth Planet. Sci. Lett., 17, 269-274.

36. Lyon, T. D. B., Pidgeon, R. T., Bowes, D. R. and Hopgood, A. M., 1973. Geochronological investigation of the quartzofeldspathic rocks of the Lewisian of Rona, Inner Hebrides. J. Geol. Soc. Lond., 129, 389-404.

37. Plant, J., Watson, J. V., Simpson, P. R., Green, P. M. and Fowler, M. B. Metalliferous and mineralised Caledonian granites in relation to regional metamorphism and fracture systems in Northern Scotland. In prep.

DISCUSSION

B. POTY, France

Did you find in Scotish granulites local high U concentrations ? M. Cuney (thesis 1981) has shown that in Laplands metashales contain up to 16 ppm U with Th/U ratios as low as 1. Thus U and Th may be close to their sedimentary values. This shows again that mobility of uranium during metamorphism depends on a variety of parameters, and that the necessary conditions for U depletion are not always met in granulites.

J. WATSON, United Kingdom

Concentrations of U well above background level have been found in the Lewisian granulites. These are represented by small pegmatitic veins (with granulite mineral assemblages) and by anomalous zones in ultramafic granulites. Both types occur within relatively competent mafic-ultramafic units which may have provided protected sites for the retention of metamorphic fluids. The extreme depletion of Lewisian granulites in LIL elements, may be due to the high pressure (>13 kb ?) nature of the metamorphism.

L.T. SILVER, United States

Can you review any independent evidence that would demonstrate that the protoliths of the Lewisian gneisses were indeed once endowed with higher concentrations of uranium and thorium than they now possess ?

J. WATSON, United Kingdom

The protoliths of Lewisian granulites appear to be the same as those of the adjacent gneisses of high amphibolite facies. The contrasting levels of U and Th characteristic of the granulites and gneisses, and especially the evidence of transitional levels at the granulite/gneiss boundary suggest that the low U and Th levels of the granulites are not primary and that depletion was related to deep metamorphism.

P.A. SABINE, United Kingdom

Although the U in water is low and does not differentiate the metamorphic facies, is it possible to put a time upon the depletion of the uranium ? If it was contemporaneous with the metamorphism, what has been the subsequent history ? The chemistry of Sr is of course different but some isotope studies suggest the involvement of groundwater through geological time in movement of the element.

J. WATSON, United Kingdom

Evidence of Sr mobility in surface water in northwest Scotland is derived mainly from regions in which Cenozoic volcanic centres acted as foci for hydrothermal circulation cells. Outcrops of Lewisian in these regions are small and have not been studied in detail. Elsewhere, there is evidence of limited redistribution of uranium in Lewisian rocks during retrogressive (amphibolite facies) early Proterozoic metamorphism, but U appears to have been essentially immobile since ~1750 Ma.

MINERALOGICAL MAGAZINE, DECEMBER 1983, VOL. 47, PP. 547-53

Rare earth element distribution in a metasomatic zoned ultramafic pod from Fiskenaesset, West Greenland

M. B. FOWLER

Department of Geology, Imperial College, London SW7 2BP

AND

C. T. WILLIAMS AND P. HENDERSON

Department of Mineralogy, British Museum (Natural History), London SW7 5BD

ABSTRACT. The distribution of *REE* in a zoned ultramafic pod formed by incomplete re-equilibration of ultrabasic and quartzofeldspathic reactant compositions has been studied. Transport of the heavy *REE* (*HREE*) as well as the light *REE* (*LREE*) over several metres has occurred during the diffusion-controlled metasomatism of the protolith mineral assemblages. The largest resultant concentration range (Eu) exceeds two orders of magnitude. In general, *REE* abundances increase towards the marginal zones, and differences between the behaviour of *LREE*, middle *REE* (*MREE*) and *HREE* subgroups are observed. *LREE* are least mobile in the aqueous transporting medium. Complexing by carbonate ligands is probably not an important factor in this system, and the final *REE* distribution is thought to be governed largely by the crystal structure of the major zonal minerals.

THE conditions that can give rise to element mobility during processes of rock alteration, metamorphism or metasomatism are of current importance since certain trace elements, including the rare earths, are sometimes used as indicators of a rock's parentage. This use is based on the assumption that the distribution of the elements, at least on the scale of a typical hand specimen, is often unaffected by such secondary processes. There is convincing evidence that in some circumstances, the rare earth elements (*REE*) have not been affected by metasomatism. For example, Muecke *et al.* (1979) report almost unchanging *REE* concentrations across a metabasite-epidosite contact in an amphibolite-facies terrain. On the other hand, significant quantities of *REE*, especially light *REE* (*LREE*), can be introduced during metasomatism (e.g. the significant increase in *LREE* abundances with degree of fenitization of a quartzite as described by Martin *et al.*, 1978), while in other cases (e.g. during boron metasomatism) *REE* may be lost (Alderton *et al.*, 1980).

© *Copyright the Mineralogical Society*

Complexing has long been recognized (e.g. Mineyev, 1963) as a significant factor in *REE* transport, and the importance of pH and the presence of certain ligands (notably F^-, Cl^-, CO_3^{2-}) has become clear. Unfortunately, there is often little direct evidence of which ligand or ligands were involved in a given metasomatic process. Thus, studies of the introduction and removal of trace elements during different types of metasomatism, and of the possible roles that newly-generated minerals may play in fixing these elements, should be helpful.

The purpose of this paper is to present the results of a study of the *REE* distribution after the metasomatic development of a zoned ultramafic pod in order to give further evidence on the types of alteration that lead to element, especially *REE*, redistribution. It is intended also to show the degree of *HREE* mobility, relative to that of the *LREE*, under the prevailing conditions.

Geological setting and relationships of samples

The rocks used in this study are from a zoned ultramafic pod, 6 m in diameter, and its associated rock types set in an Archaean granodioritic to tonalitic orthogneiss complex at SW Akugdlinguit, near Fiskenaesset. The following genetic model is applied throughout this paper.

Tectonic disruption of large, possibly layered ultrabasic protoliths (e.g. Friend and Hughes, 1977) gave rise to sub-spherical ultrabasic inclusions (e.g. GGU 104758) in the host quartzo-feldspathic gneisses (e.g. GGU 68511), between 60 cm and 10 m in diameter. These were subjected to two phases of fluid activity. The first resulted in widespread hydration of the ultrabasic mineral assemblage to

a low-grade association of antigorite + magnesite + iron ore + talc. Remnants of this immediate precursor to the zonal sequence are preserved as unzoned, homogeneous ultramafic masses (e.g. GGU 68549). The second phase was probably initiated during a subsequent prograde metamorphism (Fyfe *et al.*, 1978), and generated the typical zoned pods that form the subject of this investigation [samples GGU 68551, 68552/3(i)–(iv) and 68553(v)] by incomplete re-equilibration of the antigoritic assemblage with the enclosing acid country rocks. Expulsion of MgO and H_2O from the reacting pod produced an impersistent, rather diffuse shell of second-generation antigorite infiltration in the adjacent gneisses (e.g. GGU 68557).

The analysed samples may thus be divided into the groups below, all from SW Akugdlinguit, except GGU 104758, which was necessarily collected away from the region of later intense metasomatism, at Marrardlugtoq.

Parts of the following discussion require a knowledge of the position of the original discontinuity between ultrabasic pod and country rock, with respect to the zonal sequence. Unequivocal statement of its present locus is impossible with the available data since this particular system lacks elemental 'inert markers' (Brady, 1977). However, Fowler *et al.* (1981) suggested on a morphological basis that the discontinuity is probably now represented between the hornblende and chlorite zones. Recent experimental work (Koons, 1981), in addition to studies of other natural occurrences (Koons, 1981; Sanford, 1982), substantiate this inference that the chlorite zone was derived from the granodioritic mass. This interpretation is therefore retained here.

It is not the purpose of the paper to discuss at length the theoretical aspects of zonal metasomatism, since these have received detailed treatment in numerous recent publications (e.g. Brady, 1977; Frantz and Mao, 1976, 1979; Joesten, 1977; Sanford, 1982, Weare *et al.*, 1976). Rather, it is intended to study in particular the behaviour of the *REE* group during zone formation, and thereby to provide data of the type considered to be important by Sanford (1982). The reader is referred to Fowler *et al.* (1981) for further details of the genetic history, mineralogy, and geochemistry of the pod.

Analytical techniques.

Samples were analysed for eleven *REE*, U and Th by instrumental neutron activation analysis using an intrinsic Ge detector coupled to a Nuclear Data 6620 analysing system. 150–200 mg of sample together with multi-element standards were irradiated in a thermal neutron flux of about 10^{12} n cm^{-2} s^{-1} for 24 hours. Details of the procedure are given in Henderson and Williams (1981), but because of the low levels of La in the samples, this element was determined additionally using a Ge(Li) detector for the 487.0 and 1596.2 keV peaks of ^{140}La. U was determined by means of the 106.1 keV peak from ^{239}Np, with 1 μg of U included in the multi-element standard.

The results are given in Table I, together with values for USGS standard rock BCR-1. Correspondence between these values and the 'usable values' of Abbey (1980) are good (Table I). At concentration levels around 1–2 times chondritic abundance (i.e. as in the majority of these samples), the error is estimated at better than $\pm 10\%$ for La, Ce, Sm, Eu, Tb, Yb, and Lu, and 10–20% for Gd, Ho, Tm, and Nd. H_2O and CO_2 were determined with a C-H-N analyser, using the technique described by Din and Jones (1978).

Results and discussion

Chondrite-normalized *REE* plots reveal variations between the zones in the ultramafic pod itself (fig. 1*a*), and between the pod and the other samples studied (fig. 1*b*). The homogeneous ultramafic rock (GGU 68549), which represents the products of the first metasomatic episode, shows an overall enrichment of all the *REE* when compared with its unaltered dunite precursor (fig. 1*b*), together with some fractionation since the *HREE* are enriched over the *LREE* by a factor of 2. Thus, some bulk movement of the *REE* was apparently associated with the initial phase of fluid activity which hydrated the original ultrabasic bodies to the low-grade assemblages observed. The resultant

(i) Original ultrabasic dunite	GGU 104758	from Marrardlugtoq		
(ii) Unzoned, homogeneous ultramafic	GGU 68549	both from the locality of the zoned pod	Reactants	
Unaltered gneiss	GGU 58511			
(iii) Central zone	GGU 68551	all from 6 m diameter zoned pod		
Talc zone	GGU 68552/3(i)			
Inner tremolite	GGU 68552/3(ii)			
Outer tremolite	GGU 68552/3(iii)		Products	
Hornblende	GGU 68552/3(iv)			
Chlorite	GGU 68553(v)			
Altered gneiss	GGU 68557	from immediately adjacent to pod		

(Samples 68552/3(i)–(iv) are averages of samples 68552(i)–(iv) and 68553(i)–(iv) quoted in Fowler *et al.* (1981)).

Table I. Analytical Results

Element (ppm)	GGU 68551	GGU 68553(i)	GGU 68553(ii)	GGU 68553(iii)	GGU 68553(iv)	GGU 68553(v)	GGU 68549	GGU 104758	GGU 68557	GGU 68511	BCR-1 (this work)	BCR-1 (Abbey 1980)
	Central zone	Talc zone	Tremolite zone (Inner)	Tremolite zone (Outer)	Hornblende zone	Chlorite zone	Altered unzoned pod	Unaltered pod	Altered gneiss	Country rock		
	[core					rim]						
La	0.45	0.40	0.43	0.82	2.0	2.0	0.70	0.40	24.9	11.3	26.2	27
Ce	<0.8	0.83	0.83	2.3	7.4	8.2	2.3	1.4	47.5	29.4	53.2	53
Nd	<1.0	<1.0	<1.0	1.8	8.2	9.95	1.2	0.83	9.57	7.60	27.0	26?
Sm	0.06	0.07	0.18	0.75	2.94	3.70	0.33	0.16	0.79	1.25	6.70	6.5
Eu	0.007	0.02	0.06	0.16	0.61	1.16	0.08	0.03	0.30	0.42	2.01	2.0?
Gd	0.1	<0.3	<0.3	0.51	2.2	3.3	<0.3	<0.3	0.74	<0.8	6.9	6.6?
Tb	0.02	0.01	0.04	0.09	0.40	0.57	0.03	<0.02	0.08	0.14	1.12	1.0
Ho	<0.1	<0.1	<0.1	0.1	0.44	0.84	<0.1	<0.1	<0.1	<0.2	1.4	1.2?
Tm	0.02	0.02	0.02	0.07	0.18	0.32	0.02	0.02	0.02	0.07	0.53	0.6?
Yb	0.13	0.05	0.19	0.35	1.20	1.61	0.14	0.04	0.06	0.40	3.33	3.4
Lu	0.02	<0.02	0.03	0.05	0.16	0.20	0.02	<0.01	<0.01	0.05	0.49	0.5?
Th	<0.1	<0.1	<0.1	<0.1	0.14	1.12	0.14	<0.1	3.11	5.5	6.2	6.1
U	<0.1	<0.1	<0.1	<0.1	<0.1	0.21	0.1	<0.1	<0.1	0.5	1.78	1.7
wt% H_2O+	5.61	3.46	3.72	3.09	6.28	12.7	11.6	0.36	5.18	0.66	-	-
wt% CO_2	2.17	0.29	0.20	0.13	0.13	0.35	0.61	0.07	<0.02	0.35	-	-

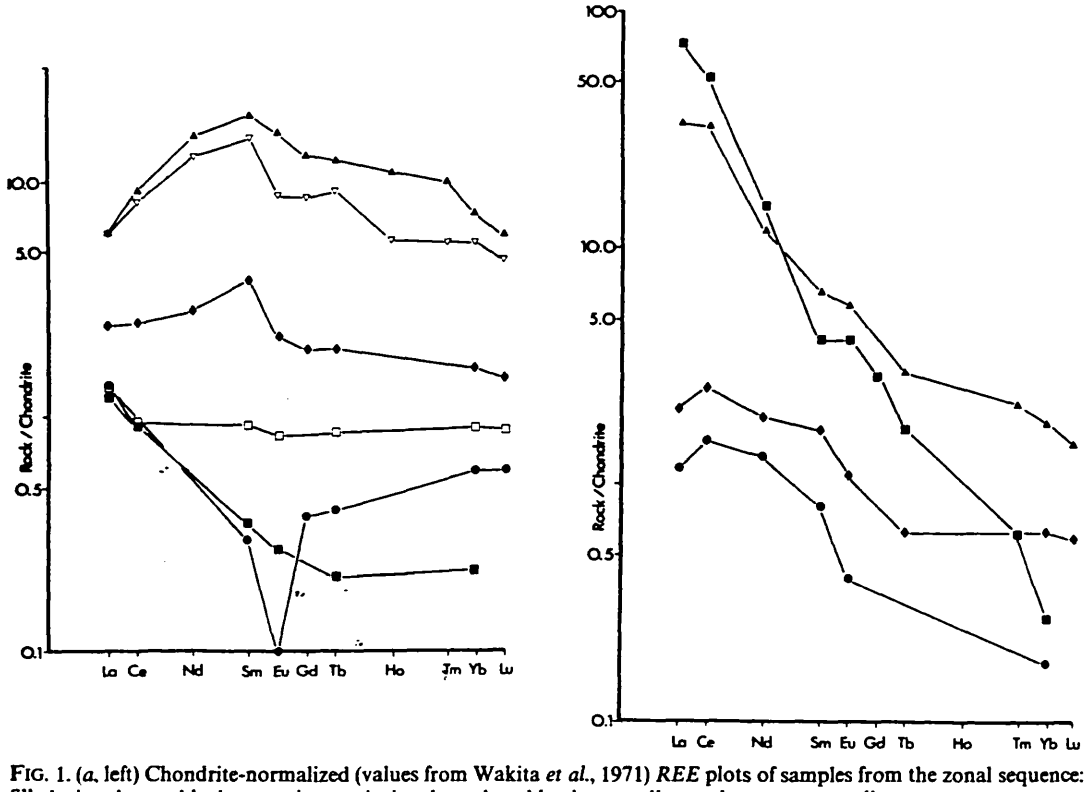


FIG. 1. (*a*, left) Chondrite-normalized (values from Wakita *et al.*, 1971) *REE* plots of samples from the zonal sequence: filled triangles = chlorite zone; inverted triangles = hornblende zone; diamond = outer tremolite zone; open square = inner tremolite zone; filled circle = central zone; filled square = talc zone. (*b*, right) Chondrite-normalized plots of remaining samples: triangles = unaltered gneiss (GGU 68511); squares = altered gneiss (GGU 68557); diamonds = unzoned homogeneous ultramafic (GGU 68549); circles = unaltered dunite (GGU 104758).

REE pattern is slightly *LREE* enriched ($(La/Yb)_{cn}$ = 3.22), has a flat *HREE* section and no significant Eu anomaly. Although the gneissose reactant is also *LREE* enriched (to a greater degree, $(La/Yb)_{cn}$ = 18.3), the pattern is more fractionated and has a steep *HREE* trend.

Zonal sequence. The *REE* distributions in the reaction products (i.e. the mineral zones) produce a series of patterns with regularly varying shape and abundance (fig. 1*a*). This implies substantial *REE* mobility during the metasomatic event, which resulted in increasing *REE* concentrations towards the perimeter of the pod. Some degree of inter-element fractionation is also apparent. *MREE* exhibit a greater interzone concentration range than either the *LREE* or *HREE*, with the maximum variation shown by Eu (greater than two orders of magnitude). It is also apparent that the volume within which *REE* movement occurred was not limited to the zonal sequence itself, since the sample of patchily developed altered gneiss (GGU 68557) adjacent to the pod has a highly fractionated *REE* pattern ($(La/Yb)_{cn}$ > 270), compared with that of the unaltered gneiss ($(La/Yb)_{cn}$ = 18.3).

In discussing the movement of a coherent group of trace elements, such as the *REE*, during an alteration event, it is convenient to normalize to an assumed precursor in order to facilitate a quantitative assessment of concentration changes. For the reasons outlined above, the chlorite zone has been normalized to the values for the unaltered granodioritic gneiss; all other zones have been normalized to the homogeneous ultramafic rock. The assumption is also made that the *REE* were uniformly distributed in the precursor rocks.

With these assumptions, precursor-normalized values for the *REE* were plotted against atomic number (fig. 2). The plots show that substantial *REE* redistribution has occurred within the zonal sequence, particularly of the *MREE* sub-group. Variable depletion in the inner zones is complemented by enrichment in the outer tremolite and hornblende zones. Similarly, the development of a slight positive Eu anomaly in the talc and inner tremolite zones may be partly balanced by larger, negative anomalies in the less voluminous outer tremolite and hornblende zones. A very large, negative Eu anomaly is shown by the central zone. The pattern for the chlorite zone has similar *HREE* and *MREE* characteristics to the amphibole zones, but shows a rapid decrease in those elements lighter than Sm. La and Ce are depleted by factors of 16 and 3.6 respectively relative to the precursor values.

A plot of representative members of the *LREE* (La), *MREE* (Sm), and *HREE* (Yb) against distance

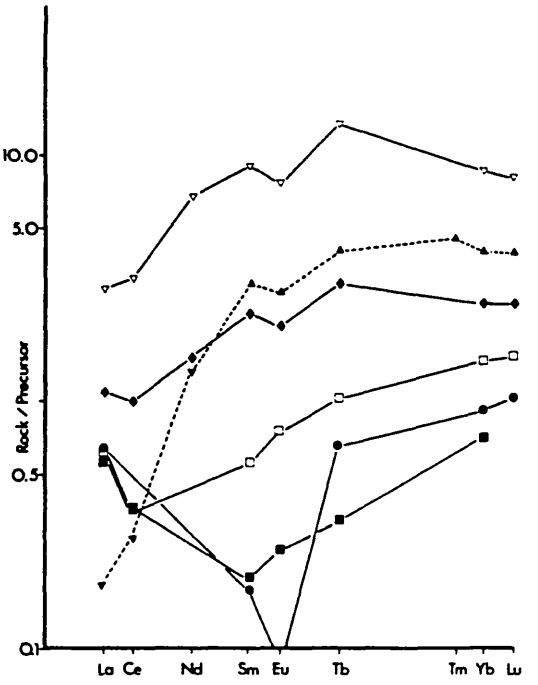


FIG. 2. Precursor-normalized *REE* plots of samples from the zonal sequence, all normalized to GGU 68549 (except chlorite zone, which is normalized to GGU 68511, on the assumption that it was derived from the granodiorite). Symbols as in fig. 1*a*.

(fig. 3) gives an indication of the intra-group variation as concentration profiles. Thus, La varies little in the three inner zones, increases slowly to about three times its assumed original concentration in the outer zones, then rises sharply into the altered gneiss only to fall again to the concentration of the unaltered gneiss. On the other hand, Sm rapidly increases throughout the entire zonal sequence (by a factor of about 50), reaching nine times its original abundance in the hornblende zone. It continues to increase in the chlorite zone, but falls in the altered gneiss to a value lower than that of the unaltered country rock. Yb initially decreases from the central to the talc zones, and then bahaves in a similar manner to Sm.

Mass balance. Several recent studies have considered the importance of volume change in the assessment of mass balance in general (Rubie, 1982) and in zonal metasomatism in particular (Sanford, 1982). Moreover, the latter author points out that significant volume change may occur with only minor variation in linear dimension. Thus, volume changes may be difficult to quantify using linear measurements, but in this particular study no contemporaneous deformation structures were

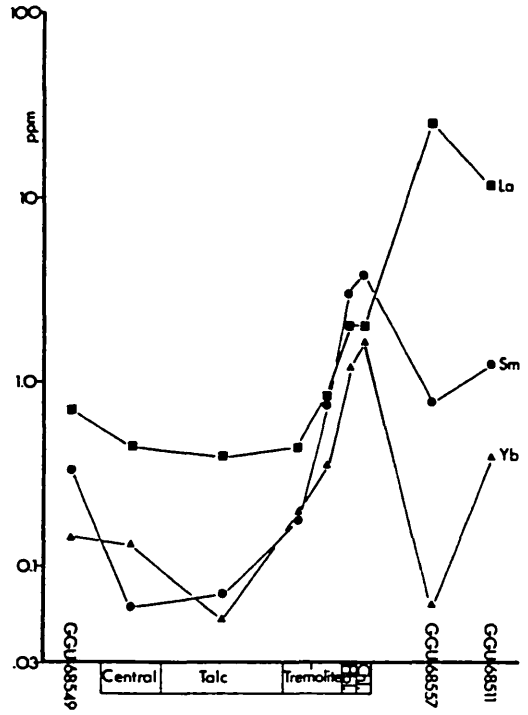


FIG. 3. Element abundance variation diagram for La, Sm, and Yb. (GGU 68549 = ultramafic precursor; GGU 68511 = gneissose precursor; GGU 68557 = altered gneiss; Hbl. = hornblende zone, Chl. = chlorite zone.)

observed in either the pod or the adjacent country rock. Bearing these points in mind, the calculations in Table II are on a constant volume basis. In addition, field observations of the pod showed some zone boundaries to be diffuse and zone widths to vary; the calculations here are based on average zone widths. The mass balance calculations in Table II therefore should be considered only as an indication of trends. They do nevertheless substantiate the differences between the *REE* subgroups discussed above, and imply that Sm and Yb exhibited greater degrees of mobility than did La. It is appropriate also to note that although volume change alone may cause some variation in element abundance, it is not capable of interelement fractionation such as that described here. All *REE* apparently suffered some loss from the pod, indicating some interaction with the surrounding country rock. This information, in conjunction with the profiles in fig. 3, suggests that La was deposited in the altered gneiss surrounding the pod (cf. Allen and Pennell, 1978; and discussion below). However, both Sm and Yb are depleted in the altered gneiss, indicating that mobility of the *MREE* and *HREE* may have continued—indeed, some leaching may have occurred—until deposition at a greater distance from the boundary of the pod.

REE mobility and fixation. Some migration of the REE has clearly occurred during the metasomatic event which produced the zonal sequence. Evidence from comparable sequences described by Allen and Pennell (1978) and Sharpe (1980) suggests that the *REE* redistribution due to metasomatic events of this type may be similar. With *REE* data limited to La and Ce, Sharpe (1980) found that those elements were more abundant in amphibole and chlorite zones than in the others. Allen and Pennell (1978), in describing a zonal sequence produced from serpentinite blocks within a hornblende diorite country rock (Trinity Co., California), found that the *LREE* were lost from the precursor serpentinite, and apparently deposited in a reaction zone around the inclusion. They also found that Sm concentration when plotted against distance, had a sigmoidal pattern similar to that shown in fig. 3. In addition, the chondrite-normalized Eu anomaly changes from negative within the zonal sequence to positive outside it.

TABLE II. *Mass balance calculations for La, Sm, and Yb in the zonal sequence*

Zone	Width (cm)	% mass*	% loss (−) or gain (+) La	Sm	Yb
Central	84.5	2.2	−0.79	−1.79	−0.3
Talc	200	83.0	−35.6	−65.4	−53.3
Inner Tremolite	7	6.5	−2.51	−2.99	+2.26
Outer Tremolite	7	6.8	+1.15	+8.59	+10.1
Hornblende	1	1.0	+1.84	+7.85	+7.51
Total	299.5	—	−34.1	−43.5	−23.1

* Assumes no volume differences between original body and the zones, and ρ = 2.5 throughout, density differences being insignificant compared to other uncertainties.

A preliminary assessment of the relative importance of some of the factors involved in *REE* mobility and fixation may be attempted here. The transporting medium was aqueous, as is indicated by the hydrous mineral assemblage and whole-rock H_2O^+ values (Table I). Carbonate ligands were probably not of significance in *REE* transport as CO_2 contents (Table I) are low and do not correlate with *REE* distribution, and calcite is observed as a trace mineral only in the inner zones. The presence of large Eu anomalies in some of the zones suggests that the oxygen fugacity was sufficiently low to maintain a significant proportion of Eu in the divalent state. Other physico-chemical parameters, including the role of other possible anions (e.g. F^-, Cl^-), are difficult to define because of the complex and changeable nature of the fluid, as reflected in the major and trace element variation profiles presented by Fowler *et al.* (1981).

The presence of *REE*-rich trace or minor minerals may influence the overall *REE* pattern of the rock samples, and for this reason a detailed microscope examination of the minor minerals was undertaken. Sphene was the only observed minor mineral that is capable of accommodating large concentrations of the *REE* (e.g. Staatz *et al.*, 1977). In the pod, it was observed only in the hornblende and chlorite zones where it is developed in grains that are rarely larger than 10 μm across, and at an estimated modal proportion of less than 0.05%. Several grains of sphene from the hornblende zone were analysed by wavelength-dispersive electron probe microanalysis for some of the *REE*. The recorded concentration levels are close to the detection limit and are therefore subject to a large error, but consistent values were obtained for La (0.02%), Ce (0.17%), Gd (0.05%), Dy (0.07%), and Er (0.04%). These data and the estimated modal proportion of sphene, indicate that only 10–15% of the *REE* in the hornblende and chlorite zones is located in this accessory mineral. Thus it is considered that the *REE* patterns observed for the zonal sequence are dominated by those of the major mineral assemblages.

Since the sizes of the avaiable structural sites in talc are too small to allow easy incorporation of any of the *REE*, their observed depletion in the central and talc zones may be readily explained (fig. 2). Interestingly, the depletion is most pronounced for those elements with intermediate ionic radii, suggesting an additional control on the substitution reactions involved. The fact that the central zone is in general less depleted than the talc zone may simply reflect the presence of more relict ultramafic minerals in the former. In amphiboles, Ca^{2+} occupies the approximately 9-fold coordinated M_4 site. Its ionic radius under such conditions is similar to some of the trivalent *REE*, notably Nd^{3+} and Sm^{3+} (Shannon, 1976). Thus, preferential incorporation of these ions in the tremolite and hornblende zones might be one of the more important factors that have led to their convex-upward patterns (figs. 1 and 2). In chlorite, on the other hand, the *REE* are most likely to enter one of the octahedral sites, where the *HREE* and *MREE* (6-fold coordinated Yb^{3+} = 0.868 Å) are better suited to substitute for Fe^{2+} (0.78 Å) than are the larger *LREE* (La^{3+} = 1.03 Å). Hence, in comparison with its country-rock predecessor, the chlorite zone is *HREE*-enriched and substantially *LREE*-depleted (La, Ce).

Thus, within the zonal sequence, crystal-chemical differences between the precursor assemblage and the zonal minerals are a major controlling factor on the final *REE* patterns.

Sphene was also observed in the altered gneiss around the pod, but at a much lower modal abundance than in the hornblende and chlorite zones. Its very low modal abundance and small size precluded a reliable analysis by microprobe. If the *REE* contents of this sphene are similar to those of the sphene in the pod then this mineral has not significantly affected the overall *REE* distribution in the gneiss. However, the major minerals—quartz, feldspar, and stringers of secondary antigorite—cannot be readily correlated with the observed *LREE*-enriched pattern, and it has not been possible to define the major controlling factor(s) on the *REE* pattern of the altered gneiss.

Conclusions

The *REE* were mobilized during metasomatic development of the zoned ultramafic pod. Varying proportions of all the *REE* were apparently lost during zone generation, but the *MREE* and *HREE* showed a greater mobility than did the *LREE*. This is in marked contrast to many other examples of *REE* mobility (notably Martin *et al.*, 1978) where *LREE* have been shown to be the most mobile. The fluid responsible was aqueous, probably not CO_2-rich, and of relatively low oxygen fugacity. The resultant *REE* distribution may have been governed largely by the structural characteristics of the major zonal minerals in the pod.

Acknowledgements. We are gratefeul to Dr B. F. Windley (The University, Leicester) for the provision of the study material and invaluable further information and advice. Professor J. V. Watson (Imperial College, London), Dr J. A. Plant (Institute of Geological Sciences, London), Dr J. E. Chisholm (British Museum, Natural History) and Dr B. F. Windley, are thanked for their constructive criticism of an earlier draft of the manuscript. M.B.F. is indebted to the NERC for a Research Studentship,

during the tenure of which this study was carried out. This paper is published by permission of the Director, Geological Survey of Greenland.

REFERENCES

Abbey, S. (1980) *Paper Geol. Surv. Can.* 80-14, 30 pp. [M.A. 81-3007].

Alderton, D. H. M., Pearce, J. A., and Potts, P. J. (1980). *Earth Planet. Sci. Lett.* **49**, 149-65 [M.A. 81-1516].

Allen, R. O., and Pennell, S. E. (1978) In *Archaeological Chemistry—II* (G. F. Carter, ed.) Advances in Chemistry Series 171, Am. Chem. Soc. 230-57.

Brady, J. B. (1977) *Geochim. Cosmochim. Acta* **41**, 113-25 [M.A. 77-4404].

Din, V. K., and Jones, G. C. (1978) *Chem. Geol.* **23**, 347-52 [M.A. 79-1047].

Fowler, M. B., Williams, H. R., and Windley, B. F. (1981) *Mineral. Mag.* **44**, 171-7 [M.A. 81-3441].

Frantz, J. D., and Meo, H. K. (1976) *Am. J. Sci.* **276**, 817-40 [M.A. 77-4171].

———(1979) Ibid. **279**, 302-23 [M.A. 81-2634].

Friend, C. R. L., and Hughes, D. J. (1977) *Earth Planet. Sci. Lett.* **36**, 157-67 [M.A. 79-935].

Fyfe, W. S., Price, N. J., and Thompson, A. B. (1978) *Fluids in the Earth's Crust.* Elsevier, Amsterdam.

Henderson, P., and Williams, C. T. (1981). *J. Radioanal. Chem.* **67**, 445-52.

Joesten, R. (1977) *Geochim. Cosmochim. Acta*, **41**, 649-70 [M.A. 78-1638].

Koons, P. O. (1981) *Contrib. Mineral. Petrol.* **78**, 189-95 [M.A. 82M-2040].

Martin, R. F., Whitley, J. E., and Wolley, A. R. (1978) Ibid. **66**, 69-73 [M.A. 78-4540].

Mineyev, D. A. (1963) *Geochemistry*, **12**, 1129-49.

Muecke, G. K., Pride, C., and Sarkar, P. (1979) In *Origin and Distribution of the Elements*, (L. H. Ahrens, ed.) Pergamon Press, Oxford, New York, 449-64 [M.A. 81-0541, V1.6].

Rubie, D. C. (1982) *Lithos* **15**, 99-109 [M.A. 83M-1656].

Sanford, R. F. (1982) *Am. J. Sci.* **282**, 543-616.

Shannon, R. C. (1976) *Acta Crystallogr.* **A32**, 751-67.

Sharpe, M. R. (1980) *Bull. Grøn. Geol. Unders.* **135**, 32 pp. [M.A. 80-5180].

Staatz, M. H., Conklin, N. M., and Brownfield, I. K. (1977) *J. Res. U.S. Geol. Surv.* **5**, 623-8 [M.A. 78-760].

Wakita, H., Rey, P., and Schmitt, R. A. (1971) *Proc. Second Lunar Sci. Conf., Geochim. Cosmochim. Acta Suppl.* **2**, 2, 1319-29 [M.A. 73-589].

Weare, J. H., Stephens, J. R., and Eugster, H. P. (1976) *Am. J. Sci.* **276**, 767-816 [M.A. 77-4263].

[*Manuscript received 8 March 1983; revised 15 May 1983*]